2021

EFFECTIVE FIELD THEORY APPLICATIONS: FROM DARK MATTER TO NEUTRINO NUCLEON SCATTERING

Qing Chen
University of Kentucky, qch233@g.uky.edu
Author ORCID Identifier:
https://orcid.org/0000-0003-1058-5324
Digital Object Identifier: https://doi.org/10.13023/etd.2021.241

STUDENT AGREEMENT:

I represent that my thesis or dissertation and abstract are my original work. Proper attribution has been given to all outside sources. I understand that I am solely responsible for obtaining any needed copyright permissions. I have obtained needed written permission statement(s) from the owner(s) of each third-party copyrighted matter to be included in my work, allowing electronic distribution (if such use is not permitted by the fair use doctrine) which will be submitted to UKnowledge as Additional File.

I hereby grant to The University of Kentucky and its agents the irrevocable, non-exclusive, and royalty-free license to archive and make accessible my work in whole or in part in all forms of media, now or hereafter known. I agree that the document mentioned above may be made available immediately for worldwide access unless an embargo applies.

I retain all other ownership rights to the copyright of my work. I also retain the right to use in future works (such as articles or books) all or part of my work. I understand that I am free to register the copyright to my work.

REVIEW, APPROVAL AND ACCEPTANCE

The document mentioned above has been reviewed and accepted by the student's advisor, on behalf of the advisory committee, and by the Director of Graduate Studies (DGS), on behalf of the program; we verify that this is the final, approved version of the student's thesis including all changes required by the advisory committee. The undersigned agree to abide by the statements above.

Qing Chen, Student

Dr. Richard J. Hill, Major Professor

Dr. Christopher Crawford, Director of Graduate Studies

EFFECTIVE FIELD THEORY APPLICATIONS: FROM DARK MATTER TO NEUTRINO NUCLEON SCATTERING

DISSERTATION

A dissertation submitted in partial
fulfillment of the requirements for
the degree of Doctor of Philosophy
in the College of Arts and Sciences
at the University of Kentucky

By
Qing Chen
Lexington, Kentucky

Director: Dr. Richard J. Hill, Professor of Physics and Astronomy
Lexington, Kentucky
2021

https://orcid.org/0000-0003-1058-5324

ABSTRACT OF DISSERTATION

EFFECTIVE FIELD THEORY APPLICATIONS: FROM DARK MATTER TO NEUTRINO NUCLEON SCATTERING

Weakly-interacting-massive-particles (WIMPs) are a large class of viable dark matter candidates. We compute cross sections for electroweak-doublet WIMPs scattering on atomic nuclei, at leading and subleading order using heavy WIMP effective field theory. Neutrino-nucleon charged current elastic scattering is an important process in the detectors of long baseline accelerator neutrino oscillation experiments. We compute QED radiative corrections to this process employing soft-collinear effective field theory.

KEYWORDS: Dark Matter, Heavy WIMP Effective Field Theory, Neutrino oscillations, Radiative corrections, Soft-Collinear Effective Field Theory

Qing Chen

July 8, 2021

EFFECTIVE FIELD THEORY APPLICATIONS: FROM DARK MATTER TO NEUTRINO NUCLEON SCATTERING

By
Qing Chen

Richard J. Hill
Director of Dissertation

Christopher Crawford
Director of Graduate Studies

July 8, 2021

Dedicated to my mother

ACKNOWLEDGMENTS

I am most grateful to my Ph.D. advisor Dr. Richard James Hill, who was willing to take me as his student and has introduced me to the field of effective field theories in particle physics, which becomes the subject of this thesis. Without Dr. Hill, I could have left the current graduate school program three years ago and not to mention accomplishing a thesis at the moment. I have learned most from Dr. Hill's original publications as well as his quantum field theory class, which has built the foundation of my research and this thesis. His ingenious expertise in integral calculations has helped me tremendously. I appreciate that Dr. Hill has been able to take time from his busy schedule answering some of my research questions, which has been very helpful for me to understand my research topics and to figure out ways solving problems that got me stuck. Dr. Hill also gives me all the freedom to choose research projects, work on things that I'm most interested in and encourages me to explore new ideas. So that I could enjoy my thesis project and maintain the motivation when difficulties challenged me. I have been supported as a research assistant the majority of the time when I worked with Dr. Hill, which also provided me more time focusing on my research.

I thank Kevin McFarland and Oleksandr Tomalak for collaborating on a project which is part of this thesis based on.

I appreciate discussions relevant to my research with my colleagues Jun Shi and Xinshuai Yan .

Most of the time, when I have no one to talk to, I heavily rely on reading text books to understand things, and I am particularly thankful to the authors of *An Introduction to Quantum Field Theory*, Michael Peskin and Daniel Schroeder.

I am grateful to my committee professors Susan Gardner, Bradley Plaster and Steve Yates, who have helped me improving my work by our qualifying exam and annual review meetings.

I am indebted to our Director of Graduate Studies Christopher Crawford, who helped me so much in finding an advisor and has been patiently guiding me through all the procedures from qualifying for a Ph.D. candidate to the final thesis defense.

The preparation of this thesis relies on the LaTex class file by Erik Stokes for University of Kentucky Thesis. I also thank Si-Nong Liu for helping me solve some typeset issues.

TABLE OF CONTENTS

LIST OF TABLES

LIST OF FIGURES

Chapter 1 Introduction

Among the most prominent unresolved puzzles in physics are dark matter nature [1] and neutrino mass origin [2, 3] problems. We will briefly introduce these two problems and effective field theories for particles in this chapter. We will employ effective field theory methods to study particle scattering processes relevant to these two problems in the following chapters.

1.1 Introduction of Effective Field Theories

Effective field theories are constructed to describe physics at low energies and long distances where underlying higher energy scale physics can be integrated out. For example, heavy particle effective field theory is useful to study atomic bound states, heavy meson decays [4–7], particularly when we cannot perturbatively solve low energy QCD but could establish an effective theory based on the power counting $\Lambda_{\rm QCD}/m_q \ll 1$ for heavy quark systems.

The idea of integrating out the mass M of a heavy particle can be applied to construct an effective theory at a scale Λ that we are interested in, with $\Lambda/M \ll 1$, when we lack of information from the high energy scale M. We will apply it to compute dark matter nucleon elastic scattering cross section, treating the dark matter particle as a heavy particle compared to any Standard Model particles. So even if we do not know the specific physics beyond Standard Model, we could study its low energy effects by integrating out the high energy scale M. The high energy scale information will be encoded in a small set of parameters (Wilson coefficients), like a multipole expansion of a charge distribution if we measure from a distance.

Soft-collinear effective field theory (SCET) [8–15] like heavy quark effective theory, also originated from heavy meson decays, now has been widely applied to processes with energetic or massless final states, including collider jet events [16–18], electroweak radiative corrections at colliders [19, 20] and in dark matter annihilations [21]. In these problems, the final state energetic particles move along a particular direction (collinear direction). The transverse momentum $p_\perp$ perpendicular to this collinear direction is small compared to the hard scales energy E, heavy particle mass M or momentum transfer Q in the problem. This is an intermediate scale compared to the lowest energy scale in the problem, the soft scale. If we define a power counting small parameter $\kappa \sim p_\perp/E$, then the soft scale is $\sim \kappa^2 E$. The physics can be factorized into soft ($\sim \kappa^2 E$) scale, collinear ($\sim \kappa E$) scale and hard ($\sim E$) scale, three parts [22–28]. When we are interested in lower scale physics, we can integrate out the hard scale and the hard scale physics will serve as Wilson coefficients in the effective soft-collinear theory. SCET allows for perturbative resummation of large logarithms using standard operator methods when fixed order calculations are insufficient. Long baseline accelerator neutrino beams interact with a nucleus target in the detector producing energetic charged leptons. We will apply SCET to compute the radiative correction in this process integrating out the non-perturbative hadronic physics.

1.2 Introduction to Dark Matter

There has been a missing-mass problem in astronomy observations since 1930s when F. Zwicky found that a lot more mass than the luminous mass in the Coma cluster needed to bound the individual galaxies with large velocities [29]. It manifests the need of non-luminous mass to explain the observed curves of rotational velocities versus distance from the core of the rotational galaxies [30] in the framework of Newton's gravity. The existence of the non-luminous mass which we call "dark matter" is further supported by gravitational lensing effects seen in the optical images of clusters and quasars [31–33]. The observation of Bullet clusters collision [34] strongly favors the dark matter existence over the alternative theories such as MOND [35] to modify the Newtonian gravity, since it exhibits a clean separation of electromagnetic-interactive matter and gravitationally-interactive matter, and the latter is evidently the dark matter. From cosmological microwave background (CMB) observation [36], we can determine the abundance of dark matter is about 26.5% of the whole Universe's energy density at current time.

A natural question to ask: what is it? From astronomy evidence, we could infer that it has some basic properties. First, it must be massive instead of massless. Second, it doesn't interact electromagnetically, or could be at most extremely feebly charged. Third, it should be cold, which means it has a small velocity compared to the speed of light in order to form gravitational wells such as dark matter halos around galaxies to hold the luminous matter in. Last, it should be stable and doesn't decay within a Hubble time that we could observe about 10^{16} s.

With the known properties, we still cannot pin-down the exact nature of dark matter. People investigate the nature of it by studying the phenomenology of a certain class of dark matter candidates at a particular mass range usually with some theoretical motivation [37, 38]. It can be as tiny as a fundamental particle, or as large as a macroscopic stellar object and its mass can vary from 10^{-22} eV to 10^{71} eV [38, 39], see Fig. 1.1.

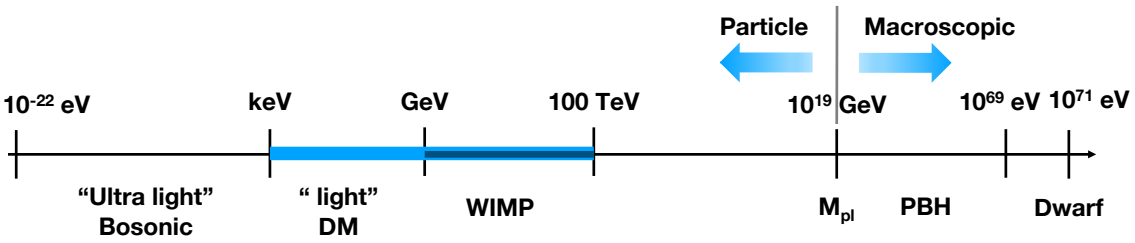

Figure 1.1: Dark matter candidates mass spectrum.

Among all the candidates, the Weakly Interacting Massive Particle (WIMP) has long been considered as a well-motivated dark matter candidate [1, 37, 40–48]. If dark matter is a fundamental particle and was in thermal equilibrium with other particles in the early universe annihilating to each other $\bar{\chi}\chi \Leftrightarrow \bar{\psi}\psi$, we can estimate the thermal average of cross section times the relative velocity $\langle\sigma v\rangle \simeq \frac{\rho_c}{m_\chi n_\chi} 10^{-26}\,\mathrm{cm}^3 s^{-1}$ by solving the thermal equilibrium equation of dark matter particles annihilation-

creation against the expansion of our Universe, see details in Ref. [49], where ρ_c is the critical energy density of the Universe, m_χ is the dark matter particle mass and n_χ is the dark matter number density. The quantity $\frac{\rho_c}{m_\chi n_\chi} = (\Omega_\chi h^2)^{-1}$ can be determined from astronomical observation of CMB, which tells us $\Omega_\chi h^2 \sim 0.12$ [36]. Then we can infer that $\langle \sigma v \rangle \sim 10^{-25}\,\mathrm{cm^3 s^{-1}}$. If the dark matter particle is a WIMP, by definition it interacts with the Standard Model particles via weak gauge bosons by weak coupling $\alpha \sim 0.01$ and yields $\langle \sigma v \rangle \sim \alpha^2 (100\,\mathrm{GeV})^{-2} \sim 10^{-25}\mathrm{cm^3 s^{-1}}$, which coincidentally provides the exact correct order of magnitude for the thermal cross section that we determined before by astronomical observation data. This is called a WIMP miracle.

Thus, there are many experiments searching for WIMPs and mainly three types: collider searches, direct detection experiments and indirect detection experiments. Collider searches look for signals of dark matter production from standard model particles via exchange of Standard Model or beyond Standard Model mediators, or UV-complete models such as supersymmetry or models with rich dark sectors [50]. Indirect detection experiments use astronomy telescopes to detect the stable final products of dark matter annihilation processes, such as Gamma rays, neutrinos or cosmic-ray anti-matter [51–55]. Direct detection experiments are fixed targets waiting for dark matter particles traveling to them and to scatter on them [56–65].

However, with all kinds of experiments going on, WIMPs still remain undetected [66, 67] so far. WIMPs naturally fit in the paradigm of supersymmetric extensions of the Standard Model [49] yet we have not found evidence at the LHC for supersymmetric particles at the electroweak scale [68, 69]. Within the WIMP paradigm, the situation is suggestive that new particles are somewhat heavy compared to the electroweak scale, and in particular, $M_{\mathrm{WIMP}} \gg M_{W^\pm}, M_{Z^0}$. In addition, in order to produce the observed dark matter abundance, the processes of WIMPs annihilating into Standard Model particles thermally in the early universe require the WIMPs' masses to be at TeV scale [70]. In this mass regime, heavy WIMP effective field theory becomes a powerful method to study the universal behavior in low energy WIMP-nucleus scattering processes [71–73], predicting cross sections for dark matter direct detection experiments that are minimally sensitive to unknown ultraviolet (UV) physics. In the following chapter 2, we will use heavy WIMP effective field theory to parameterize the possible interactions of an important class of WIMP candidates with the Standard Model and compute the cross sections in the direct detection experiments.

1.3 Introduction to Neutrino Oscillation

Neutrinos are massless in the Standard Model. However, in the late 1990's and early 2000's, discovery of neutrino flavor changing with time as propagating in space (oscillation) from atmosphere and solar neutrinos experiments [74, 75] provides compelling evidence that they are massive and a certain flavor neutrino is a mixed state of different neutrino mass eigenstates. It stimulates more experiments to measure the neutrino oscillation and determine the parameters of its flavor-mass mixing matrix, Pontecorvo-Maki-Nakagawa-Sakata (PMNS) matrix [76, 77], including long baseline

accelerator experiments [78–84] and reactor experiments [85–89].

Analogous to the quark CKM matrix [90, 91], PMNS matrix is parametrized by mixing-angles and phases in the leptonic sector. For three flavor neutrinos, there are three mixing-angles θ_{12}, θ_{23}, θ_{13} and a CP-violating phase $\delta_{\rm CP}$ in the PMNS matrix,[1]

$$U = \begin{pmatrix} c_{12}\, c_{13} & s_{12}\, c_{13} & s_{13}\, e^{-i\delta_{\rm CP}} \\ -s_{12}\, c_{23} - c_{12}\, s_{13}\, s_{23}\, e^{i\delta_{\rm CP}} & c_{12}\, c_{23} - s_{12}\, s_{13}\, s_{23}\, e^{i\delta_{\rm CP}} & c_{13}\, s_{23} \\ s_{12}\, s_{23} - c_{12}\, s_{13}\, c_{23}\, e^{i\delta_{\rm CP}} & -c_{12}\, c_{23} - s_{12}\, s_{13}\, c_{23}\, e^{i\delta_{\rm CP}} & c_{13}\, c_{23} \end{pmatrix}, \quad (1.1)$$

where $c_{ij} \equiv \cos\theta_{ij}$ and $c_{ij} \equiv \sin\theta_{ij}$, $\theta_{ij} \in [0,\, \pi/2]$ and $\delta_{\rm CP} \in [0,\, 2\pi]$.

According to current experimental data, there could be two types of mass ordering for these three states, normal ordering (NO): $m_1 < m_2 < m_3$ and inverted ordering (IO): $m_3 < m_1 < m_2$. Mass hierarchy is defined by $\Delta m_{ij} \equiv m_i^2 - m_j^2$. The experimental measurement of these parameters has entered a precision era. The parameters θ_{12}, θ_{13}, mass hierarchies Δm^2_{21} and $|\Delta m^2_{32}|$ have been well determined. However, mass ordering is still unknown, θ_{23} and $\delta_{\rm CP}$ have large uncertainties [98]. We yet need to narrow down uncertainty to determine whether there is non-zero CP-violation or not. Precise measurement of neutrino oscillations is crucial for us to understand the physical leptonic sector which is beyond Standard Model. CP-violation information in the leptonic sector also could help us understand matter anti-matter asymmetry in our universe.

We will focus on the long baseline accelerator neutrino oscillation experiments and compute the radiative correction in the detectors. The accelerator neutrino beams are produced by colliding protons into pions and pions decaying into muon neutrinos at the source. After the neutrino beam travels a long distance about kilometer order, we measure the beam at the far detector. The probability of the original muon neutrino oscillating to an electron neutrino is approximately [99]

$$\begin{aligned} P_{\nu_\mu \to \nu_e\,, (\bar\nu_\mu \to \bar\nu_e)} \simeq\; & 4 \sin^2\theta_{13} \sin^2\theta_{23} \frac{\sin^2\Delta}{(1 \mp A)^2} + \left(\frac{\Delta m^2_{21}}{\Delta m^2_{31}}\right)^2 \sin^2 2\theta_{12} \cos^2\theta_{23} \frac{\sin^2 A\Delta}{A^2} \\ & + 8 \frac{\Delta m^2_{21}}{\Delta m^2_{31}} J^{\rm max}_{\rm CP} \cos(\Delta \pm \delta_{\rm CP}) \frac{\sin A\Delta}{A} \frac{\sin(1 \mp A)\Delta}{1 \mp A}\,, \end{aligned} \quad (1.2)$$

where

$$J^{\rm max}_{\rm CP} = c_{12} s_{12} c_{23} s_{23} c^2_{13} s_{13}\,, \quad \Delta \equiv \frac{\Delta m^2_{31} L}{4E_\nu}\,, \quad A \equiv \frac{2E_\nu V}{\Delta m^2_{31}}\,, \quad (1.3)$$

with L being the baseline distance, V being the effective earth matter potential, the upper sign in "$\pm$" or "$\mp$" denoting neutrino process and the lower sign denoting anti-neutrino process.

We measure the muon neutrino and electron neutrino numbers arriving at the far detector by their event rates and compare with the conversion probability Eq. (1.3)

[1] Majorana neutrinos have two other phases in addition to $\delta_{\rm CP}$ compared to Dirac neutrinos, but they don't contribute to the neutrino oscillations [92–97].

to determine the PMNS matrix parameters. In order to obtain precise results from the neutrino oscillation experiments, it is important to compute the cross sections and cross section ratios between different flavors of events correctly, thus obtaining correct fluxes of different flavor neutrinos from their event rates. The charged current neutrino nucleon elastic scattering is the dominant process in the detector for accelerator beam energy at about GeV order. The charged lepton final state particles like electrons radiate and the energetic photons will form a cone around the charged lepton, resulting jet-like events. These jet observables exhibit large logarithms as $\alpha \log^2(E_\nu/m)$ where E_ν is neutrino energy $\sim$ GeV scale and m is electron mass. We will apply soft-collinear effective field theory to separate scales in this problem and evolve from high scale to low scale by renormalization group evolution to account for leading logarithms at all orders, reducing uncertainty of fixed order calculations.

1.4 HQET and SCET Construction

A particle is a representation of our spacetime symmetry Poincaré group. The little group [100] of Poincaré group is the three dimensional rotation group for a massive particle and the two dimensional Euclidean group for a massless particle. It leads to the heavy particle effective theory parametrized by a timelike vector v^μ with $v^2 = 1$ for a massive particle with momentum $p^\mu = Mv^\mu$, and soft-collinear effective field theory parametrized by a lightlike vector n^μ with $n^2 = 0$ for a massless particle with momentum $p^\mu = En^\mu$.

We can construct Lorentz-invariant effective theories on the particle fields transformation properties under their little groups from a bottom-up approach [101] if we do not know the UV theory.

To give a sketch of how these effective theories look like, we provide the following derivation for heavy quark effective Lagrangian (HQET) and collinear fermion effective Lagrangian (SCET) from known relativistic Lagrangians.

For a heavy fermion field ψ with mass M and velocity v, it is useful to do the decomposition

$$\psi = e^{-iMv\cdot x}(\psi_v + \Psi_v)\,, \tag{1.4}$$

with $\not{v}\psi_v = \psi_v$ and $\not{v}\Psi_v = -\Psi_v$, which allows us to expand the Lagrangian in powers of $1/M$.

The relativistic Lagrangian $\mathcal{L} = \bar{\psi}(i\not{D} - M)\psi$, with the covariant derivative $D_\mu = \partial_\mu - igG_\mu^A t^A$ where G_μ is a gauge field, becomes

$$\left(\bar{\psi}_v + \bar{\Psi}_v\right)\left[M(\not{v} - 1) + i\not{D}\right](\psi_v + \Psi_v)\,. \tag{1.5}$$

We decompose the covariant derivative as $D^\mu = v^\mu v\cdot D + D_\perp^\mu$, along and perpendicular to velocity direction, and Eq. (1.5) reduces to

$$\bar{\psi}_v(iv\cdot D)\psi_v + \bar{\psi}_v i\not{D}_\perp \Psi_v + \bar{\Psi}_v i\not{D}_\perp \psi_v - \bar{\Psi}_v(2M + iv\cdot D)\Psi_v\,. \tag{1.6}$$

Equation of motion of $\bar{\Psi}_v$ field yields

$$\Psi_v = \frac{i\not{D}_\perp \psi_v}{2M + iv\cdot D}\,, \tag{1.7}$$

which is suppressed by the heavy mass M.

Taking the solution of Ψ_v Eq. (1.7) back to the Lagrangian Eq. (1.6), we obtain the heavy fermion effective Lagrangian

$$\mathcal{L}_{\rm HQET} = \bar{\psi}_v (iv\cdot D)\psi_v + \bar{\psi}_v i\not{D}_\perp \frac{1}{2M + iv\cdot D} i\not{D}_\perp \psi_v \,. \tag{1.8}$$

In this way, we have integrated out the anti-particle component Ψ, and at $1/M$ order the effective Lagrangian is

$$\bar{\psi}_v \left(iv\cdot D - \frac{\not{D}_\perp^2}{2M} \right) \psi_v \,, \tag{1.9}$$

where $\not{D}_\perp^2 = D_\perp^2 + \frac{g}{2}\sigma_{\mu\nu}F^{\mu\nu}$.

We can work in this low energy effective theory Eq. (1.9) in terms of the field ψ_v and all the high energy M-scale physics will be suppressed by powers of $1/M$.

For a massless particle with momentum p, decomposing it into n-direction with $n^\mu = (1,\, 0,\, 0,\, 1)$, $\bar{n}$-direction with $\bar{n}^\mu = (1,\, 0,\, 0,\, -1)$ and a direction perpendicular to n and $\bar{n}$.

$$p = \frac{1}{2}(\bar{n}\cdot p) n + \frac{1}{2}(n\cdot p)\bar{n} + p_\perp \,, \tag{1.10}$$

where $n^2 = \bar{n}^2 = 0$, $n\cdot\bar{n} = 2$.

We decompose the original field ψ into collinear (n-direction) and anti-collinear ($\bar{n}$-direction) components,

$$\psi = \xi_n + \xi_{\bar{n}} \,, \tag{1.11}$$

where the collinear and anti-collinear fields statisfy

$$\begin{aligned} \frac{\not{n}\not{\bar{n}}}{4}\xi_n &= \xi_n, \quad \not{n}\xi_n = 0 \,, \\ \frac{\not{\bar{n}}\not{n}}{4}\xi_{\bar{n}} &= \xi_{\bar{n}}, \quad \not{\bar{n}}\xi_{\bar{n}} = 0 \,. \end{aligned} \tag{1.12}$$

The Lagrangian becomes

$$\begin{aligned} &\bar{\psi} i\not{D}\psi \\ &= \left(\bar{\xi}_n + \bar{\xi}_{\bar{n}}\right) \left[\frac{\not{\bar{n}}}{2}(n\cdot iD) + \frac{\not{n}}{2}(\bar{n}\cdot iD) + i\not{D}_\perp \right] (\xi_n + \xi_{\bar{n}}) \\ &= \bar{\xi}_n \frac{\not{\bar{n}}}{2}(n\cdot iD)\,\xi_n + \bar{\xi}_{\bar{n}} \left(\frac{\not{n}}{2}\bar{n}\cdot iD \right) \xi_{\bar{n}} + \bar{\xi}_n i\not{D}_\perp \xi_{\bar{n}} + \bar{\xi}_{\bar{n}} i\not{D}_\perp \xi_n \,. \end{aligned} \tag{1.13}$$

Taking equation of motion of $\xi_{\bar{n}}$ from Lagrangian Eq. (1.13), we obtain

$$\frac{\not{n}}{2}\bar{n}\cdot iD\xi_{\bar{n}} = -i\not{D}_\perp \xi_n \,. \tag{1.14}$$

Multiply with $\bar{\not{n}}$ on both sides of Eq. (1.14), and we have the solution of $\xi_{\bar{n}}$ in terms of ξ_n,

$$\xi_{\bar{n}} = -\frac{\bar{\not{n}}}{2}\frac{i\not{D}_\perp}{\bar{n}\cdot iD}\xi_n\,. \tag{1.15}$$

Plug Eq. (1.15) back in Eq. (1.13), we obtain the effective Lagrangian for the collinear field ξ_n,

$$\mathcal{L}_{\rm SCET} = \bar{\xi}_n\left[\frac{\bar{\not{n}}}{2}(n\cdot iD) - i\not{D}_\perp\frac{\bar{\not{n}}}{2\bar{n}\cdot iD}i\not{D}_\perp\right]\xi_n\,. \tag{1.16}$$

We can work in the effective theory Eq. (1.16) for the collinear fermion, and the anti-collinear field has been integrated out. The gauge bosons are also massless and we could also construct an effective collinear Lagrangian for them, which we leave the detailed discussions to Chapter 3.

Chapter 2 Heavy WIMP Nucleus Scattering

2.1 Introduction

As discussed in chapter 1, WIMP is a well-motivated candidate and likely has a heavy mass compared to the electroweak scale. Explicit calculations in heavy WIMP effective theory [72, 73, 102] for WIMP nucleon elastic scattering reveal an amplitude level cancellation [71, 102, 103] that results in cross section predictions for electroweak triplet (Wino-like) and electroweak doublet (Higgsino-like) WIMPs that are below the sensitivity of current direct detection experiment [104]. Such particles thus remain as viable dark matter candidates but it is important to understand whether naively subleading effects could alter the predicted cross section and hence their experimental observability.

To improve the leading order calculation and to compare with next-generation experiments [56–58, 105] approaching the neutrino background which is unavoidable in these direct detection experiments [106], we consider subleading effects from the following sources. First, $1/M$ power corrections in the heavy WIMP expansion depend on the specific representation of electroweak $\mathrm{SU}(2)_W \times \mathrm{U}(1)_Y$ symmetry, and on the detailed UV completion of the WIMP theory. For the case of electroweak triplet, power corrections for the pure Wino-like case were themselves found to exhibit a surprising level of cancellation [107], yielding a cross section prediction for low velocity WIMP-nucleon scattering of $\sigma \sim 10^{-47}\,\mathrm{cm}^2$, for $M \gtrsim 500\,\mathrm{GeV}$. Given that Higgsino-nucleon scattering suffers an even more severe amplitude cancellation compared to the Wino case [73], it is important to study the power corrections in this case. We also explore the consequences of structure beyond the pure Higgsino limit. Second, a complete accounting of nuclear effects can potentially alter the predicted direct detection event rate compared to simple models that apply a nuclear form factor to the single nucleon cross section. Since the cancellation occurs between single nucleon matrix elements of scalar and tensor currents, nuclear effects could be effectively enhanced by impacting the scalar and tensor currents differently. We estimate the impact of such nuclear effects for both triplet and doublet cases, employing a recent model that incorporates constraints of chiral symmetry and multibody interactions [108, 109].

2.2 Heavy WIMP Effective Field Theory

2.2.1 Electroweak Symmetric Heavy WIMP Effective Lagrangian

Heavy WIMPs with mass M large compared to the electroweak scale m_W may be described using an effective theory expanded in powers of $1/M$. Each order is constructed from Lorentz and gauge invariant operators built from Standard Model fields and the heavy WIMP field; the latter transforms as an $\mathrm{SU}(2)_W \times U(1)_\mathrm{Y}$ multiplet and is denoted by χ_v. We consider the WIMP to be a self-conjugate particle here versus

a Dirac fermion which is disfavored by phenomenology. For a heavy self-conjugate particle the Heavy WIMP Effective Theory (HWET) Lagrangian up to $1/M$ order takes the following form in the one-heavy particle sector (cf. Refs. [71, 107]):

$$\mathcal{L}_{\rm HWET} = \bar{\chi}_v \left[iv\cdot D - \delta m - \frac{D_\perp^2}{2M} - \frac{f(H)}{M} - \frac{g(W,B)}{M} + \dots \right] \chi_v \,, \tag{2.1}$$

where v^μ is the heavy WIMP velocity with $v^2 = 1$. The covariant derivative is $D_\mu = \partial_\mu - ig_1 Y B_\mu - ig_2 W_\mu^a t^a$ and $D_\perp^\mu = D^\mu - v^\mu v\cdot D$. Dimension five operators $\bar{\chi}_v f(H)\chi_v$ and $\bar{\chi}_v g(W,B)\chi_v$ describe WIMP interactions with the Higgs field H and with the electroweak field strengths $W_{\mu\nu}$ and $B_{\mu\nu}$, respectively. δm is a residual mass, which can be chosen by different field redefinitions for convenience.

Let us consider a Standard Model extension whose particle content consists of a Dirac fermion WIMP ψ transforming as an SU(2) doublet with hypercharge $Y = 1/2$. This situation may arise in models with supersymmetry [49, 110, 111] and extra dimensions [112]. Related models involve scalars [113, 114].

We anticipate the splitting of mass eigenstates into Majorana components after electroweak symmetry breaking, and construct the higgs interaction term in the Majorana basis. Explicitly, Higgs field H and left-handed Dirac fermion ψ_L are fundamental representations of SU(2) with hyper charge $Y = 1/2$ under U(1) denoted as $(\mathbf{2}, 1/2)$, and ψ_L' is a conjugate representation $(\bar{\mathbf{2}}, -1/2)$. They transform under $\mathrm{SU}(2)_W \times \mathrm{U}(1)_Y$ as follows,

$$\begin{aligned}
&H \to e^{i\boldsymbol{\alpha}\cdot\boldsymbol{\tau}} e^{i\beta Y} H \,, \\
&\psi_L \to e^{i\boldsymbol{\alpha}\cdot\boldsymbol{\tau}} e^{i\beta Y} \psi_L \,, \\
&\psi_L' \to e^{-i\boldsymbol{\alpha}\cdot\boldsymbol{\tau}^*} e^{-i\beta Y} \psi_L' \,, \\
&\psi_R \to e^{i\boldsymbol{\alpha}\cdot\boldsymbol{\tau}} e^{i\beta Y} \psi_R \,, \\
&\psi_R^c \to e^{-i\boldsymbol{\alpha}\cdot\boldsymbol{\tau}^*} e^{-i\beta Y} \psi_R^c \,,
\end{aligned} \tag{2.2}$$

where $\tau^i = \frac{1}{2}\sigma^i$, with σ^i being Pauli matrices, α_i and β are real parameters and we have notation

$$\psi = \begin{pmatrix} \psi_L \\ i\sigma^2 \psi_L'^* \end{pmatrix} , \qquad \psi^c = \begin{pmatrix} \psi_L' \\ i\sigma^2 \psi_L^* \end{pmatrix} , \tag{2.3}$$

and $\psi_R \equiv i\sigma^2 \psi_L'^*$, $\psi_R^c \equiv i\sigma^2 \psi_L^*$. Note that the explicit σ^2 acts as a generator in the Lorentz group, not to be confused with the gauge group generator τ^2.

Thus,

$$\begin{pmatrix} \psi \\ \psi^c \end{pmatrix} \to \begin{pmatrix} e^{i\boldsymbol{\alpha}\cdot\boldsymbol{\tau}} e^{i\beta Y} \otimes 1_{2\times 2} & 0 \\ 0 & e^{-i\boldsymbol{\alpha}\cdot\boldsymbol{\tau}^*} e^{-i\beta Y} \otimes 1_{2\times 2} \end{pmatrix} \begin{pmatrix} \psi \\ \psi^c \end{pmatrix} \equiv U \otimes 1_{2\times 2} \begin{pmatrix} \psi \\ \psi^c \end{pmatrix} , \tag{2.4}$$

where

$$U = \begin{pmatrix} e^{i\boldsymbol{\alpha}\cdot\boldsymbol{\tau}} e^{i\beta Y} & 0 \\ 0 & e^{-i\boldsymbol{\alpha}\cdot\boldsymbol{\tau}^*} e^{-i\beta Y} \end{pmatrix} \tag{2.5}$$

The Higgs $\mathrm{SU}(2)_W \times \mathrm{U}(1)_Y$ gauge- and Lorentz-invariant interaction term should be

$$\begin{aligned}\mathcal{L}_H &= \frac{1}{M}(H^\dagger H)(c_1\psi_R^\dagger\psi_L + c_2\psi_R^{c\dagger}\psi_L') \\ &\quad +\frac{1}{M}\Big[c_3(\psi_R^\dagger H)(H^\dagger\psi_L) + c_4(\psi_R^\dagger H)(H^T\psi_L') \\ &\quad +c_5(\psi_R^{c\dagger}H^*)(H^\dagger\psi_L) + c_6(\psi_R^{c\dagger}H^*)(H^T\psi_L')\Big] \\ &\quad +\text{h.c. terms}\,,\end{aligned} \tag{2.6}$$

where c_1, c_2, c_3, c_4, c_5 and c_6 are complex coefficients.

Express the interaction Lagrangian $\mathcal{L}_H$ in terms of ψ and ψ^c,

$$\mathcal{L}_H = \frac{H^\dagger H}{M}\bar{\psi}(c_1' + ic_2'\gamma^5)\psi + \frac{1}{M}\begin{pmatrix}\bar{\psi} & \bar{\psi^c}\end{pmatrix}\mathbf{A}\begin{pmatrix}\psi \\ \psi^c\end{pmatrix}, \tag{2.7}$$

where the matrix A is

$$\mathbf{A} = \begin{pmatrix}(c_3' + ic_4'\gamma^5)HH^\dagger & (c_5' + c_6'\gamma^5)HH^T \\ (c_5'^* - c_6'^*\gamma^5)H^*H^\dagger & (c_3' + ic_4'\gamma^5)H^*H^T\end{pmatrix}, \tag{2.8}$$

and c_1', c_2', c_3', c_4' are real numbers, c_5' and c_6' are complex coefficients.

Let us introduce two Majorana fermions

$$\chi_1 = \frac{1}{\sqrt{2}}(\psi + \psi^c), \qquad \chi_2 = \frac{i}{\sqrt{2}}(\psi - \psi^c)\,, \tag{2.9}$$

and we have

$$\begin{pmatrix}\psi \\ \psi^c\end{pmatrix} = \frac{1}{\sqrt{2}}\begin{pmatrix}1 & -i \\ 1 & i\end{pmatrix}\begin{pmatrix}\chi_1 \\ \chi_2\end{pmatrix}, \tag{2.10}$$

where $\chi \equiv \begin{pmatrix}\chi_1, & \chi_2\end{pmatrix}^T$ is the relativistic field mapping onto the heavy particle field χ_v in Eq. (2.1).

Note that the original $\mathrm{SU}(2)_W \times \mathrm{U}(1)_Y$ generators T^a in the $(\psi,\, \psi^c)$ basis and the new generators $\hat{T}^a$ in the Majorana $(\chi_1,\, \chi_2)$ basis are related as follows,

$$\frac{1}{\sqrt{2}}\begin{pmatrix}1 & 1 \\ i & -i\end{pmatrix}\begin{pmatrix}\tau^a & 0 \\ 0 & -\tau^{aT}\end{pmatrix}\frac{1}{\sqrt{2}}\begin{pmatrix}1 & -i \\ 1 & i\end{pmatrix} = \frac{1}{2}\begin{pmatrix}\tau^a - \tau^{aT} & -i(\tau^a + \tau^{aT}) \\ i(\tau^a + \tau^{aT}) & \tau^a - \tau^{aT}\end{pmatrix}. \tag{2.11}$$

Define

$$S \equiv \frac{1}{\sqrt{2}}\begin{pmatrix}1 & -i \\ 1 & i\end{pmatrix}, \tag{2.12}$$

$$T^a \equiv \begin{pmatrix}\tau^a & 0 \\ 0 & -\tau^{aT}\end{pmatrix}, \tag{2.13}$$

$$\hat{T}^a \equiv \frac{1}{2}\begin{pmatrix}\tau^a - \tau^{aT} & -i(\tau^a + \tau^{aT}) \\ i(\tau^a + \tau^{aT}) & \tau^a - \tau^{aT}\end{pmatrix}, \tag{2.14}$$

where $a = 0, 1, 2, 3$, $\tau^0 = \frac{1}{2}\mathbf{1}$ and $\tau^i = \frac{1}{2}\sigma^i$, σ^i are Pauli matrices. Note that T^0 is the generator for $\mathrm{U}(1)_Y$ and we combine it with $\mathrm{SU}(2)_W$ generators for compactness of notation.

Then express the Higgs interaction $\mathcal{L}_H$ of Eq. (2.7) in the Majorana basis $\left(\chi_1, \chi_2\right)^T$, and the Higgs interaction term $f(H)$ in Eq. (2.1) takes the form

$$f(H) = \begin{pmatrix} a\mathbf{Re}(HH^\dagger) + \mathbf{Re}(bHH^T) + cH^\dagger H & a\mathbf{Im}(HH^\dagger) - \mathbf{Im}(bHH^T) \\ -a\mathbf{Im}(HH^\dagger) - \mathbf{Im}(bHH^T) & a\mathbf{Re}(HH^\dagger) - \mathbf{Re}(bHH^T) + cH^\dagger H \end{pmatrix}, \tag{2.15}$$

where the real parameters a and c, and the complex parameter b, can be determined by matching with a specific UV theory.

Generally, the gauge invariant and Lorentz invariant Lagrangian for field strength term should be

$$\mathcal{L}_{\mathcal{W}} = \frac{1}{M}[c_{w1}\bar{\chi}W^a_{\mu\nu}\hat{T}^a\sigma^{\mu\nu}\chi + c_{w2}\bar{\chi}\epsilon^{\mu\nu\rho\sigma}W^a_{\mu\nu}\hat{T}^a\sigma_{\rho\sigma}\chi], \tag{2.16}$$

where $W^a_{\mu\nu}\hat{T}^a = i[D_\mu, D_\nu]$ and $D_\mu = \partial_\mu - ig_1W^0_\mu\hat{T}^0 - ig_2W^i_\mu\hat{T}^i$.

It can be checked that for Majorana fields $\bar{\chi}_i\sigma^{\mu\nu}\chi_j = \bar{\chi}^c_i\sigma^{\mu\nu}\chi^c_j = -\bar{\chi}_j\sigma^{\mu\nu}\chi_i$, so the diagonal terms in the first term of Eq.(2.16) vanish, which means we can omit $a = 2$ term that has nonzero diagonal elements. Then the Lagrangian is $\mathcal{C}$-invariant. If we keep $a = 2$ term, by the property of Majorana fields $\bar{\chi}_i\sigma^{\mu\nu}\chi_i = 0$, they still vanish. Meanwhile, we have $\bar{\chi}_i\gamma^5\sigma^{\mu\nu}\chi_j = \bar{\chi}^c_i\gamma^5\sigma^{\mu\nu}\chi^c_j = \bar{\chi}_j\gamma^5\sigma^{\mu\nu}\chi_i$ for the second term of Eq.(2.16), which means the off diagonal terms should vanish so the only surviving terms is $a = 2$ term.

Then explicitly, by charge conjugation invariance, the field strength interaction Lagrangian is

$$\begin{aligned}\mathcal{L}_{\mathcal{W}} &= \frac{1}{M}\left[c_{w1}\bar{\chi}\left(W^0_{\mu\nu}\hat{T}^0 + W^1_{\mu\nu}\hat{T}^1 + W^3_{\mu\nu}\hat{T}^3\right)\sigma^{\mu\nu}\chi + c_{w2}\bar{\chi}\epsilon^{\mu\nu\rho\sigma}W^2_{\mu\nu}\hat{T}^2\sigma_{\rho\sigma}\chi\right] \\ &= \frac{1}{M}\bar{\chi}\Big[c_{w1}\sigma^{\mu\nu}\left(W^0_{\mu\nu}\tau^0 + W^1_{\mu\nu}\tau^1 + W^3_{\mu\nu}\tau^3\right)\otimes\tau^2 \\ &\quad + c_{w2}\epsilon^{\mu\nu\rho\sigma}\sigma_{\rho\sigma}W^2_{\mu\nu}\tau^2\otimes\mathbf{1}\Big]\chi,\end{aligned} \tag{2.17}$$

and the $1/M$ field strength interaction term is

$$g(W, B) = \begin{pmatrix} c_{w2}\epsilon^{\mu\nu\rho\sigma}\sigma_{\rho\sigma}W^2_{\mu\nu}\tau^2 & -ic_{w1}\sigma^{\mu\nu}(W^0_{\mu\nu}\tau^0 + W^1_{\mu\nu}\tau^1 + W^3_{\mu\nu}\tau^3) \\ ic_{w1}\sigma^{\mu\nu}(W^0_{\mu\nu}\tau^0 + W^1_{\mu\nu}\tau^1 + W^3_{\mu\nu}\tau^3) & c_{w2}\epsilon^{\mu\nu\rho\sigma}\sigma_{\rho\sigma}W^2_{\mu\nu}\tau^2 \end{pmatrix}, \tag{2.18}$$

where c_{w1} and c_{w2} are complex coefficients to be determined by UV theory.

The $g(W, B)$ term contains $\sigma_{\mu\nu}$ and therefore contributes to the spin-dependent process of WIMP nucleon scattering. Although the spin-independent amplitude suffers a severe cancellation at leading order in $1/M$ expansion, the spin-dependent

amplitude vanishes at leading order. Since it lacks the coherent enhancement of the spin-independent amplitude, this contribution is expected to remain numerically subdominant in the total direct detection rate. In the following, we focus on the spin-independent process and neglect the field strength interaction term $g(W, B)$, which only contributes to spin-dependent scattering.

2.2.2 Mass and Charge Diagonalization after Electroweak Symmetry Breaking

After electroweak symmetry breaking, the Higgs field acquires its vacuum expectation value

$$\langle H \rangle = \frac{v}{\sqrt{2}} \begin{pmatrix} 0 \\ 1 \end{pmatrix} . \tag{2.19}$$

Let us write down the SU(2) doublet components of the Majorana fields

$$\chi_1 = \begin{pmatrix} \lambda_1 \\ \lambda_0 \end{pmatrix} , \qquad \chi_2 = \begin{pmatrix} \lambda_2 \\ \lambda_0' \end{pmatrix} . \tag{2.20}$$

In the basis of $\chi = \begin{pmatrix} \lambda_1 & \lambda_0 & \lambda_2 & \lambda_0' \end{pmatrix}$, plug Eq. (2.19) into Eq. (2.15) and we obtain the mass matrix

$$\delta M(v) = \delta m + \frac{v^2}{2M} \begin{pmatrix} \begin{pmatrix} c & 0 \\ 0 & c+a+b_1 \end{pmatrix} & \begin{pmatrix} 0 & 0 \\ 0 & -b_2 \end{pmatrix} \\ \begin{pmatrix} 0 & 0 \\ 0 & -b_2 \end{pmatrix} & \begin{pmatrix} c & 0 \\ 0 & c+a-b_1 \end{pmatrix} \end{pmatrix} , \tag{2.21}$$

where we have defined $b \equiv b_1 + ib_2$ and b_1, b_2 are real parameters.

Diagonalize the mass matrix Eq. (2.21) and we get eigenvalues

$$\lambda_{\text{mid}} = \delta m_\psi + \frac{v^2}{2M} c \, , \tag{2.22}$$

$$\lambda_{\text{high, low}} = \lambda_{\text{mid}} + \frac{v^2}{2M} (a \pm |b|) \, , \tag{2.23}$$

and eigenvectors

$$\xi^1_{\text{mid}} = \begin{pmatrix} 1 \\ 0 \\ 0 \\ 0 \end{pmatrix} , \quad \xi^2_{\text{mid}} = \begin{pmatrix} 0 \\ 0 \\ 1 \\ 0 \end{pmatrix} , \quad \xi_{\text{high}} = \begin{pmatrix} 0 \\ -\cos\frac{\theta}{2} \\ 0 \\ \sin\frac{\theta}{2} \end{pmatrix} , \quad \xi_{\text{low}} = \begin{pmatrix} 0 \\ \sin\frac{\theta}{2} \\ 0 \\ \cos\frac{\theta}{2} \end{pmatrix} , \tag{2.24}$$

where we have the parametrization of $b_1 = |b| \cos\theta$ and $b_2 = |b| \sin\theta$.

The diagonalization transformation matrix is

$$P = \begin{pmatrix} \xi^1_{\text{mid}} & \xi_{\text{high}} & \xi^2_{\text{mid}} & \xi_{\text{low}} \end{pmatrix} \tag{2.25}$$

so that

$$P^{-1}[\delta m + f(\langle H\rangle)]P = \mathrm{diag}\,(\lambda_{\rm mid}, \lambda_{\rm high}, \lambda_{\rm mid}, \lambda_{\rm low})\,. \tag{2.26}$$

Then $P^{-1}\chi$ is the mass eigenstate basis. Let's convert it into an electric charge eigenstate basis by transformation

$$\begin{pmatrix}\lambda_1\\ \lambda_2\end{pmatrix} = \frac{1}{\sqrt{2}}\begin{pmatrix}1 & 1\\ i & -i\end{pmatrix}\begin{pmatrix}h_+\\ h_-\end{pmatrix}\,. \tag{2.27}$$

Then the diagonal basis of both mass and charge is

$$h_v = \begin{pmatrix}h_0^{\rm high}\\ h_0^{\rm low}\\ h_+\\ h_-\end{pmatrix}\,, \tag{2.28}$$

where

$$\begin{pmatrix}\lambda_0\\ \lambda_0'\end{pmatrix} = \begin{pmatrix}-\cos\frac{\theta}{2} & \sin\frac{\theta}{2}\\ \sin\frac{\theta}{2} & \cos\frac{\theta}{2}\end{pmatrix}\begin{pmatrix}h_0^{\rm high}\\ h_0^{\rm low}\end{pmatrix}\,. \tag{2.29}$$

Explicitly,

$$\begin{pmatrix}h_0^{\rm high}\\ h_0^{\rm low}\\ h_+\\ h_-\end{pmatrix} = \begin{pmatrix}0 & -\cos\frac{\theta}{2} & 0 & \sin\frac{\theta}{2}\\ 0 & \sin\frac{\theta}{2} & 0 & \cos\frac{\theta}{2}\\ \frac{1}{\sqrt{2}} & 0 & \frac{-i}{\sqrt{2}} & 0\\ \frac{1}{\sqrt{2}} & 0 & \frac{i}{\sqrt{2}} & 0\end{pmatrix}\begin{pmatrix}\lambda_1\\ \lambda_0\\ \lambda_2\\ \lambda_0'\end{pmatrix}\,. \tag{2.30}$$

The Lagrangian of the heavy field χ_v after electroweak symmetry breaking is in the basis h_v

$$\begin{aligned}\mathcal{L} = \bar{h}_v\Big[&iv\cdot\partial + eQv\cdot A + \frac{g_2}{\cos\theta_W}v\cdot Z(\tilde{T}^3 - \sin^2\theta_W Q) + \frac{g_2}{\sqrt{2}}v\cdot(W^+\tilde{T}^+ + W^-\tilde{T}^-)\\ &- \delta M - \frac{\not{D}_\perp^2}{2M} + \frac{f(\phi)}{M} + \frac{g(W,\,Z)}{M} + ...\Big]h_v\,,\end{aligned} \tag{2.31}$$

where v is the velocity.

In the diagonal basis h_v, by field redefinition we could set the residual mass δM for the lightest neutral constituent $h_0^{\rm low}$ to be zero, which will be the WIMP. Then

$$\delta M = \frac{v^2}{2M}\mathrm{diag}\,(2|b|, 0, |b| - a, |b| - a)\,, \tag{2.32}$$

$$Q = \mathrm{diag}\,(0, 0, 1, -1)\,, \tag{2.33}$$

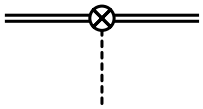

$= i\frac{v}{M}\tilde{c}_H$

Figure 2.1: Feynman rule for 3-point interaction vertex involving the physical Higgs boson h (dashed line) and the lightest electrically neutral Majorana fermion component of the Higgsino field, $h_0^{\rm low}$ (double line). The encircled cross denotes insertion of a $1/M$ effective theory vertex.

$$\tilde{T}^3 - \sin^2\theta_W Q = \frac{1}{2}\begin{pmatrix} 0 & i & 0 & 0 \\ -i & 0 & 0 & 0 \\ 0 & 0 & 1-2\sin^2\theta_W & 0 \\ 0 & 0 & 0 & -1+2\sin^2\theta_W \end{pmatrix}, \tag{2.34}$$

$$\tilde{T}^+ = \frac{e^{i\frac{\theta}{2}}}{\sqrt{2}}\begin{pmatrix} 0 & 0 & 0 & 1 \\ 0 & 0 & 0 & i \\ -1 & -i & 0 & 0 \\ 0 & 0 & 0 & 0 \end{pmatrix}, \tag{2.35}$$

$$\tilde{T}^- = \frac{e^{-i\frac{\theta}{2}}}{\sqrt{2}}\begin{pmatrix} 0 & 0 & -1 & 0 \\ 0 & 0 & i & 0 \\ 0 & 0 & 0 & 0 \\ 1 & -i & 0 & 0 \end{pmatrix}, \tag{2.36}$$

where θ is an arbitrary phase.

Introduce the fluctuations of the Higgs field

$$H = \langle H\rangle + \begin{pmatrix} \frac{1}{\sqrt{2}}(\phi_1 + i\phi_2) \\ \frac{1}{\sqrt{2}}(h + i\phi_3) \end{pmatrix}, \tag{2.37}$$

which we denote their interaction as $f(\phi)$ in Eq. (2.31) and we obtain the interaction between the WIMP and the higgs boson. Particularly, we have the three point interaction in Fig. 2.1, where $\tilde{c}_H \equiv -(a + c - |b|)$.

Loop radiative corrections also modify the tree-level mass matrix Eq. (2.32). We consider one-loop radiative correction Fig. 2.2 to the mass of each mass eigenstate by Feynman rules of effective Lagrangian Eq. (2.31),

$$-i\Sigma_2^j(v\cdot k) = -y_i g_2^2 \int \frac{d^dp}{(2\pi)^d}\bar{h}_v^j \frac{i}{v\cdot(p+k)-\delta+i0}\frac{-i}{p^2-m_i^2+i0}h_v^j$$

Figure 2.2: Electroweak radiative correction self-energy diagram for heavy WIMP mass eigenstates.

$$
\begin{aligned}
&= -iy_i g_2^2 \frac{\Gamma(1+\epsilon)}{(4\pi)^{2-\epsilon}} m_i^{-2\epsilon} \Bigg\{ \frac{-2(\delta - v\cdot k)}{\epsilon} \\
&\quad + 4\sqrt{m_i^2 - (\delta - v\cdot k)^2 - i0} \left[\arctan\left(\frac{\delta - v\cdot k}{\sqrt{m_i^2 - (\delta - v\cdot k)^2 - i0}} \right) - \frac{\pi}{2} \right] \\
&\quad - 4(\delta - v\cdot k) + O(\epsilon) \Bigg\} \cdot \bar{h}_v^j h_v^j \,. \qquad (2.38)
\end{aligned}
$$

where j labels the external particle state, $i = W$, Z, γ labels different gauge bosons and δ is the tree-level residual mass of the internal propagator. The gauge group factor y_i for each type of gauge boson is

$$
\begin{aligned}
y_W &= \left(\frac{1}{\sqrt{2}}\right)^2 \left(\tilde{T}^+\tilde{T}^- + \tilde{T}^-\tilde{T}^+\right) = J(J+1) - Y^2 \,, \\
y_Z &= \frac{1}{\cos^2\theta_W} \left(\tilde{T}^3 - \sin^2\theta_W Q\right)^2 = \frac{1}{\cos^2\theta_W} (Y - \sin^2\theta_W Q)^2 \,, \\
y_\gamma &= \sin^2\theta_W Q^2 \,, \qquad (2.39)
\end{aligned}
$$

where J is the isospin for a certain $\mathrm{SU}(2)_W$ representation and Y is the hyper charge of $\mathrm{U}(1)_Y$. For the Higgsino-like doublet case, $J = 1/2$ and $Y = 1/2$. For the Wino-like triplet case, $J = 1$ and $Y = 0$.

The mass correction Δm_j to a mass eigenstate h_v^j with residual mass δ_j is given by

$$
\Delta m_j \bar{h}_v^j h_v^j = \Sigma_2^j(\delta_j) \,. \qquad (2.40)
$$

Explicitly, for a Higgsino-like particle, evaluating Eq. (2.38), making use of $|\delta - \delta_j| \ll m_{W/Z}$ and we find that the mass correction to the lighter neutral state h_0^{low} is

$$
\begin{aligned}
\Delta m_0^{\mathrm{low}} &= -\frac{\alpha_2}{\pi} \Bigg[\frac{y_W}{2} \left((\delta_\pm - \delta_0^{\mathrm{low}}) \left(-\log\frac{m_W}{M} + 1 \right) + \frac{\pi}{2} m_W \right) \\
&\quad + y_Z \left((\delta_0^{\mathrm{high}} - \delta_0^{\mathrm{low}}) \left(-\log\frac{m_Z}{M} + 1 \right) + \frac{\pi}{2} m_Z \right) \Bigg] \\
&= -\frac{\alpha_2}{\pi} \left[\frac{y_W}{2} (|b| - a) \left(-\log\frac{m_W}{M} + 1 \right) + 2 y_Z |b| \left(-\log\frac{m_Z}{M} + 1 \right) \right] \frac{v^2}{2M}
\end{aligned}
$$

$$- \frac{\alpha_2}{2}(y_W m_W + y_Z m_Z)\,, \tag{2.41}$$

where $y_W = 1/2$ and $y_Z = 1/(4\cos^2\theta_W)$.

The mass correction to the charged states $h_\pm$ is

$$\begin{aligned}\Delta m_\pm &= -\frac{\alpha_2}{\pi}\left[\frac{y_W}{2}(\delta_0^{\rm low} + \delta_0^{\rm high} - 2\delta_\pm)\left(-\log\frac{m_Z}{M} + 1\right)\right] - \frac{\alpha_2}{2}(y_W m_W + y_Z m_Z) \\ &= -\frac{\alpha_2}{\pi} y_W a\left(-\log\frac{m_Z}{M} + 1\right)\frac{v^2}{2M} - \frac{\alpha_2}{2}(y_W m_W + y_Z m_Z)\,,\end{aligned} \tag{2.42}$$

where $y_W = 1/2$ and $y_Z = (1 - 2\sin^2\theta_W)^2/(4\cos^2\theta_W)$.

The mass correction to the heavier neutral state $h_0^{\rm high}$ is

$$\begin{aligned}\Delta m_0^{\rm high} &= -\frac{\alpha_2}{\pi}\left[\frac{y_W}{2}(\delta_\pm - \delta_0^{\rm high})\left(-\log\frac{m_W}{M} + 1\right) + y_Z(\delta_0^{\rm low} - \delta_0^{\rm high})\left(-\log\frac{m_Z}{M} + 1\right)\right] \\ &\quad - \frac{\alpha_2}{2}(y_W m_W + y_Z m_Z) \\ &= \frac{\alpha_2}{\pi}\left[\frac{y_W}{2}(-|b| - a)\left(-\log\frac{m_W}{M} + 1\right) - 2y_Z|b|\left(-\log\frac{m_Z}{M} + 1\right)\right]\frac{v^2}{2M} \\ &\quad - \frac{\alpha_2}{2}(y_W m_W + y_Z m_Z)\,,\end{aligned} \tag{2.43}$$

where $y_W = 1/2$ and $y_Z = 1/(4\cos^2\theta_W)$.

The $1/M$ order terms in the mass corrections Eq. (2.41), Eq. (2.42), Eq. (2.43) are suppressed compared to the gauge boson mass terms and the charged states receive a higher mass correction relative to the neutral states,

$$\Delta^\pm - \Delta^0 = \frac{1}{2}\alpha_2 \sin^2\theta_W m_Z\,, \tag{2.44}$$

and the neutral lightest state remains the lightest state.

Figure 2.3: Electroweak radiative correction self-energy diagram for WIMP mass eigenstates at UV scale.

We can also compute the radiative correction at UV scale before matching onto a low energy effective field theory, which modifies the mass matrix at leading order. These radiative corrections are mainly contributed by electroweak gauge interactions and we compute the self-energy diagram Fig. 2.3. The result is

$$-i\Sigma_2(\not{p}) = -y_i g_2^2 \int \frac{d^d L}{(2\pi)^d} \frac{\gamma^\mu(\not{p} + \not{L} + M)\gamma_\mu}{[(p+L)^2 - M^2 + i0]\,(L^2 - m_i^2 + i0)} \tag{2.45}$$

The mass correction to each state is

$$\Delta m_j = \Sigma_2(M) = -M\frac{\alpha_2}{\pi}\cdot y_i \int_0^1 dx 2(1+x)\log\left[x^2+(1-x)\frac{m_i^2}{M^2}\right]. \tag{2.46}$$

For neutral states,

$$y_W = 1/2\,, \quad y_Z = 1/(4\cos^2\theta_W)\,, \quad y_\gamma = 0\,. \tag{2.47}$$

For charged states,

$$y_W = 1/2\,, \quad y_Z = (1-2\sin^2\theta_W)^2/(4\cos^2\theta_W))\,, \quad y_\gamma = \sin^2\theta_W\,. \tag{2.48}$$

The charged states gain a higher mass correction over the neutral states by

$$\Delta^\pm - \Delta^0 = M\frac{\alpha_2}{\pi}\left[5\sin^2\theta_W + \sin^2\theta_W\int_0^1 dx 2(1+x)\log\left[x^2+(1-x)\frac{m_Z^2}{M^2}\right]\right] > 0\,. \tag{2.49}$$

When $m_Z \ll M$, $\Delta^\pm - \Delta^0$ is positively approaching zero. Since $\Delta^\pm - \Delta^0 \sim \alpha_2 M$, it is still much greater than $1/M$ order tree level correction $(|b|-a)v^2/(2M)$, which is of order $\alpha_2^2 v^2/M$, as we will see in the Section 2.3. Thus, the state h_0^{low} remains the lightest state.

2.3 Illustrative UV Completion

To investigate the impact of additional UV structure from coupling $\tilde{c}_H$, we consider a simple illustration where, in addition to the Dirac doublet ψ of mass M, the Standard Model extension includes another SU(2) multiplet with a mass greater than M [102, 115]. For example, consider an SU(2) triplet Majorana fermion χ' with mass $M' \gg M$. The renormalizable Lagrangian is

$$\mathcal{L}_{\text{UV}} = \mathcal{L}_{\text{SM}} + \bar{\psi}(i\not{D} - M)\psi + \frac{1}{2}\bar{\chi}'(i\not{D} - M')\chi' - \frac{1}{2}\bar{\lambda}F(H)\lambda\,, \tag{2.50}$$

where $\lambda = \begin{pmatrix}\chi', & \chi_1, & \chi_2\end{pmatrix}^T$, with $\chi_1 = (\psi+\psi^c)/\sqrt{2}$ and $\chi_2 = i(\psi-\psi^c)/\sqrt{2}$ and c.f. [72]

$$\begin{aligned} F(H) = &\frac{\kappa_1}{\sqrt{2}}\begin{pmatrix} \mathbf{0}_3 & H^\dagger\boldsymbol{\sigma} - H^T\bar{\boldsymbol{\sigma}} & i(-H^T\bar{\boldsymbol{\sigma}} - H^\dagger\boldsymbol{\sigma}) \\ -\bar{\boldsymbol{\sigma}}H^* + \boldsymbol{\sigma}H & \mathbf{0}_2 & \mathbf{0}_2 \\ i(\boldsymbol{\sigma}H + \bar{\boldsymbol{\sigma}}H^*) & \mathbf{0}_2 & \mathbf{0}_2 \end{pmatrix} \\ &+\frac{\kappa_2}{\sqrt{2}}\begin{pmatrix} \mathbf{0}_3 & i(H^T\bar{\boldsymbol{\sigma}} + H^\dagger\boldsymbol{\sigma}) & H^\dagger\boldsymbol{\sigma} - H^T\bar{\boldsymbol{\sigma}} \\ -i(\boldsymbol{\sigma}H + \bar{\boldsymbol{\sigma}}H^*) & \mathbf{0}_2 & \mathbf{0}_2 \\ -\bar{\boldsymbol{\sigma}}H^* + \boldsymbol{\sigma}H & \mathbf{0}_2 & \mathbf{0}_2 \end{pmatrix}, \end{aligned} \tag{2.51}$$

where $\boldsymbol{\sigma} = (\sigma^1, \sigma^2, \sigma^3)$ and $\bar{\boldsymbol{\sigma}} = -(\sigma^{1T}, \sigma^{2T}, \sigma^{3T})$.

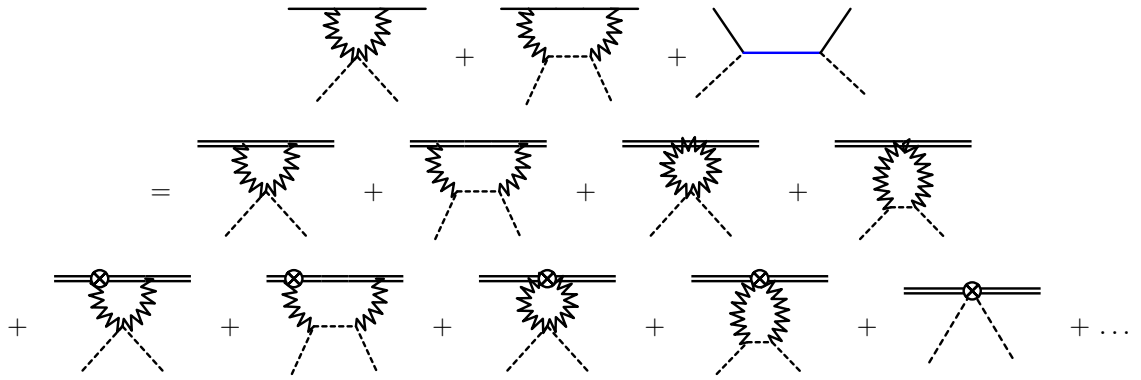

Figure 2.4: Matching condition for the coefficients in the EFT for UV theory consisting of the Standard Model plus $\mathrm{SU}(2)_W$-doublet Majorana fermion χ and another Majorana multiplet χ'. Solid black lines denote χ and blue line denotes χ' (propagator of the third diagram on the L.H.S) , dashed lines denote SM Higgs doublet, zigzag lines denote $\mathrm{SU}(2)_W \times \mathrm{U}(1)_Y$ gauge fields. Matching is performed in the electroweak symmetric theory. Double lines on the R.H.S denote heavy WIMPs χ_v and the encircled cross denotes insertion of a $1/M$ effective theory vertex.

Another interesting case is the Majornana fermion χ' being an SU(2) singlet with interaction

$$F(H) = \frac{\kappa_1}{\sqrt{2}} \begin{pmatrix} 0 & H^\dagger + H^T & i(H^T - H^\dagger) \\ H + H^* & \mathbf{0}_2 & \mathbf{0}_2 \\ i(H - H^*) & \mathbf{0}_2 & \mathbf{0}_2 \end{pmatrix} + \frac{\kappa_2}{\sqrt{2}} \begin{pmatrix} 0 & -i(H^T - H^\dagger) & H^T + H^\dagger \\ -i(H - H^*) & \mathbf{0}_2 & \mathbf{0}_2 \\ H + H^* & \mathbf{0}_2 & \mathbf{0}_2 \end{pmatrix} . \tag{2.52}$$

By matching the UV theory Eq. (2.50) to the effective theory Eq. (2.1) , we can determine the $1/M$ order coefficients in the effective theory. It's convenient to do the matching in the electroweak symmetric phase and we show the matching diagrams in Fig. 2.4 for a singlet χ' case. In the electroweak symmetric phase, we could choose $\delta m = 0$ in Eq. (2.1) and the loop diagrams on the EFT side (RHS) vanish in dimensional regularization since they are scaleless but dimensionful. The only surviving diagram on the EFT side is the last diagram.

Let us do the matching for the operator $\bar{\chi}^m_\alpha \chi^l_\beta H^\dagger_i H_j$, where α, $\beta = 1, 2$ are indices for two Majorana fermions χ_1 or χ_2, m, $l = 1, 2$ are indices for two components of each Majorana fermion χ_α, and i, $j = 1, 2$ are indices for the two components of Higgs doublet. On the L.H.S, when the first diagram contains two W fields exchange, it gives a group factor

$$\left(\tilde{T}^a \tilde{T}^b\right)^{ml}_{\alpha\beta} \left(\tau^a \tau^b + \tau^b \tau^a\right)_{ij} = \frac{1}{2} J(J+1) \delta_{\alpha\beta} \delta_{ml} \delta_{ij} \,, \tag{2.53}$$

where $\tilde{T}^a$ and τ^a are defined in Eq. (2.14), a, $b = 1$, 2, 3.

When the first diagram of L.H.S contains one W and one B exchange, it gives a group factor

$$\begin{aligned}&\left[\left(\tilde{T}^a\tilde{T}^0\right)^{ml}_{\alpha\beta}+\left(\tilde{T}^0\tilde{T}^a\right)^{ml}_{\alpha\beta}\right]\left(\tau^a\tau^0+\tau^0\tau^a\right)_{ij}\\&=\frac{1}{4}\delta_{\alpha\beta}(\sigma^1_{ml}\sigma^1_{ij}+\sigma^3_{ml}\sigma^3_{ij})+\frac{i}{4}\sigma^2_{ij}\sigma^2_{ml}\left(-\delta_{\alpha1}\delta_{\beta2}+\delta_{\alpha2}\delta_{\beta1}\right),\end{aligned}\tag{2.54}$$

where a, $b = 1$, 2, 3.

When the first diagram of L.H.S contains two B fields exchange, it gives a group factor

$$\left(\tilde{T}^0\tilde{T}^0\right)^{ml}_{\alpha\beta}\left(\tau^0\tau^0+\tau^0\tau^0\right)_{ij}=\frac{Y^2}{2}\delta_{\alpha\beta}\delta_{ml}\delta_{ij}\,.\tag{2.55}$$

Thus, working out all the Feynman rules and the first diagram of L.H.S contributes to the operator $\bar{\chi}^m_\alpha\chi^l_\beta H^\dagger_i H_j$ a coefficient

$$\begin{aligned}&-\left[\frac{3}{8}g_2^4\delta_{ml}\delta_{ij}+\frac{1}{4}g_1^2g_2^2(\sigma^1_{ml}\sigma^1_{ij}+\sigma^3_{ml}\sigma^3_{ij})+\frac{1}{8}g_1^4\delta_{ml}\delta_{ij}\right]\delta_{\alpha\beta}I_{\rm loop}\\&-\frac{i}{4}g_1^2g_2^2\sigma^2_{ij}\sigma^2_{ml}\left(-\delta_{\alpha1}\delta_{\beta2}+\delta_{\alpha2}\delta_{\beta1}\right)I_{\rm loop}\,,\end{aligned}\tag{2.56}$$

where $I_{\rm loop}$ is the loop integral for the first diagram on the L.H.S and

$$I_{\rm loop}=\int\frac{d^dp}{(2\pi)^d}\frac{\gamma^\mu(\not{p}+\not{q}+M)\gamma_\mu}{\left[(p+q)^2-M^2+i0\right](p^2+i0)^2}=\frac{i}{(4\pi)^{2-\epsilon}}\frac{\Gamma(1+\epsilon)}{M^{1+2\epsilon}}(3-2\epsilon)\,,\tag{2.57}$$

with $d = 4 - 2\epsilon$.

Similarly, for the second diagram on the L.H.S, we can work out the group factors for different W and B fields exchange cases, but the loop integral for this diagram vanishes, explicitly

$$\begin{aligned}J_{\rm loop}&=\int\frac{d^dp}{(2\pi)^d}\frac{\not{p}(\not{p}+\not{q}+M)\not{p}}{\left[(p+q)^2-M^2+i0\right](p^2+i0)^3}\\&=3\int_0^1dx\int\frac{d^dl}{(2\pi)^d}(1-x)^2\frac{\left[-xM+\frac{2M}{d}(1-x)\right]l^2+x^2(2-x)M^3}{\left[l^2-x^2M^2+i0\right]^4}\\&=\frac{i}{(4\pi)^{2-\epsilon}}\frac{\Gamma(1+\epsilon)}{2}\left[-\left(\frac{5}{2\epsilon}+4\right)\frac{1}{M^{1+2\epsilon}}+\left(\frac{5}{2\epsilon}+4\right)\frac{1}{M^{1+2\epsilon}}\right]\\&=0\,.\end{aligned}\tag{2.58}$$

For the third diagram on the L.H.S, we could fix $\alpha = \beta = 1$ and when χ' is a triplet, this diagram and its crossed diagram (not shown in Fig. 2.4) give a coefficient for $\bar{\chi}^m_1\chi^l_1H^\dagger_iH_j$ operator,

$$\frac{1}{2}(\kappa_1^2+\kappa_2^2)(\bar{\boldsymbol{\sigma}}_{mi}\bar{\boldsymbol{\sigma}}_{jl}+\boldsymbol{\sigma}_{mj}\cdot\boldsymbol{\sigma}_{il})\frac{i}{M'-M}\,,\tag{2.59}$$

and for $\bar{\chi}_2^m \chi_1^l H_i^\dagger H_j$ operator, the coefficient is

$$\frac{1}{2}(\kappa_1^2+\kappa_2^2)(\bar{\boldsymbol{\sigma}}_{mi}\bar{\boldsymbol{\sigma}}_{jl}-\boldsymbol{\sigma}_{mj}\cdot\boldsymbol{\sigma}_{il})\frac{1}{M'-M}\,, \tag{2.60}$$

On the R.H.S for the operator $\bar{\chi}_1^m \chi_1^l H_i^\dagger H_j$, we could choose $m=l=i=j=1$ for simplicity and the coefficient is

$$-\frac{i}{M}(a+c)\,, \tag{2.61}$$

and for the operator $\bar{\chi}_2^m \chi_1^l H_i^\dagger H_j$, the coefficient is

$$\frac{a}{2M}(\delta_{mj}\delta_{il}-\delta_{mi}\delta_{lj}) \tag{2.62}$$

Let us match L.H.S with R.H.S for the operator $\bar{\chi}_1^m \chi_1^l H_i^\dagger H_j$ when $m=l=i=j=1$, considering Eq. (2.56), Eq. (2.59) and Eq. (2.61) and we obtain

$$a+c=\frac{3}{4}\alpha_2^2\left(1+\frac{1}{2\cos^4\theta_W}\right)-(\kappa_1^2+\kappa_2^2)\frac{M}{M'-M}\,, \tag{2.63}$$

where $\alpha_2=g_2^2/(4\pi)$, and θ_W is the weak mixing angle.

Considering Eq. (2.56), Eq. (2.60) and Eq. (2.62), we obtain the matching for $\bar{\chi}_2^m \chi_1^l H_i^\dagger H_j$ when $m=j=1$ and $l=i=2$,

$$a=\frac{3}{2}\alpha_2^2\frac{\sin^2\theta_W}{\cos^2\theta_W}+(\kappa_1^2+\kappa_2^2)\frac{M}{M'-M}\,. \tag{2.64}$$

Then plug Eq. (2.64) into Eq. (2.63) and we obtain

$$c=\frac{3}{4}\alpha_2^2\left(1-2\frac{\sin^2\theta_W}{\cos^2\theta_W}+\frac{1}{2\cos^4\theta_W}\right)-2(\kappa_1^2+\kappa_2^2)\frac{M}{M'-M}\,. \tag{2.65}$$

Now let us consider the matching for another operator $\bar{\chi}_1^m \chi_1^l H_i^T H_j$ to extract the parameter b. The first two diagrams vanish on the L.H.S and the third diagram yields a coefficient

$$\frac{1}{2}(\kappa_2^2-\kappa_1^2+2i\kappa_1\kappa_2)(\boldsymbol{\sigma}_{mi}\bar{\boldsymbol{\sigma}}_{jl}+\boldsymbol{\sigma}_{mj}\bar{\boldsymbol{\sigma}}_{il})\frac{i}{M'-M}\,. \tag{2.66}$$

On the R.H.S, the effective operator yields

$$-\frac{i}{M}\frac{b}{2}(\delta_{mi}\delta_{lj}+\delta_{mj}\delta_{il})\,. \tag{2.67}$$

Identify Eq. (2.66) and Eq. (2.67) and we obtain

$$b=(-\kappa_1^2+\kappa_2^2+2i\kappa_1\kappa_2)\frac{M}{M'-M}\,. \tag{2.68}$$

Thus, after matching we obtain all parameters a, b and c and the relevant coefficient

$$\tilde{c}_H = -(a + c - |b|) = -\frac{3}{4}\alpha_2^2 \left(1 + \frac{1}{2\cos^4\theta_W}\right) + 2\kappa^2 \frac{M}{M' - M}\,. \tag{2.69}$$

We can do the similar matching for the case when χ' is a singlet and the results are

$$\begin{aligned} a &= \frac{3}{2}\alpha_2^2 \left(\frac{1}{\cos^2\theta_W} - 1\right) - (\kappa_1^2 + \kappa_2^2)\frac{M}{M' - M}\,, & (2.70)\\ b &= (-\kappa_1^2 + \kappa_2^2 + 2i\kappa_1\kappa_2)\frac{M}{M' - M}\,, & (2.71)\\ c &= \frac{3}{4}\alpha_2^2 \left(3 - \frac{2}{\cos^2\theta_W} + \frac{1}{2\cos^4\theta_W}\right)\,, & (2.72) \end{aligned}$$

and again

$$\tilde{c}_H = -(a + c - |b|) = -\frac{3}{4}\alpha_2^2 \left(1 + \frac{1}{2\cos^4\theta_W}\right) + 2\kappa^2 \frac{M}{M' - M}\,. \tag{2.73}$$

2.4 Weak Matching

In order to compute the cross section for dark matter direct detection at the nuclear level, we need match and evolve the electroweak scale effective theory of the WIMP specified in Eq. (2.1) to lower energy scales. In a first step we integrate out weak scale particles $W^\pm$, Z^0, h, t and Nambu-Goldstone bosons where we work in the Feynman t'Hooft gauge, and match to an effective theory consisting of five-flavor QCD, and the following effective interactions of the WIMP with quarks and gluons:[1]

$$\mathcal{L} = \bar{h}_0^{\rm low} h_0^{\rm low} \left\{ \sum_{q=u,d,s,c,b} \left[c_q^{(0)} O_q^{(0)} + c_q^{(2)} v_\mu v_\nu O_q^{(2)\mu\nu}\right] + c_g^{(0)} O_g^{(0)} + c_g^{(2)} v_\mu v_\nu O_g^{(2)\mu\nu} \right\}, \tag{2.74}$$

where the spin-0 and spin-2 quark and gluon operators are

$$\begin{aligned} O_q^{(0)} &= m_q \bar{q} q\,, & O_q^{(2)\mu\nu} &= \frac{1}{2}\bar{q}\left(\gamma^{\{\mu} i D_-^{\nu\}} - \frac{g^{\mu\nu}}{d} i\not{D}_-\right) q\,,\\ O_g^{(0)} &= (G_{\mu\nu}^A)^2\,, & O_g^{(2)\mu\nu} &= -G^{A\mu\lambda} G^{A\nu}{}_\lambda + \frac{1}{d} g^{\mu\nu} (G_{\alpha\beta}^A)^2\,. \end{aligned} \tag{2.75}$$

We neglect operators of higher dimension that are suppressed by powers of hadronic scales times $1/m_W$ where m_W is the mass of $W^\pm$ bosons. Here $d = 4 - 2\epsilon$ is the spacetime dimension, $D_- \equiv \overrightarrow{D} - \overleftarrow{D}$, and curly brackets around indices denote symmetrization. We collect the Feynman rules of effective field theory Eq. (2.1) for matching to the five-flavor QCD Eq. (2.74) in Appendix A.

[1] We restrict attention to elastic scattering. Inelastic scattering [116] could be investigated by considering operator structures $\bar{h}_0^{\rm high} h_0^{\rm low}$.

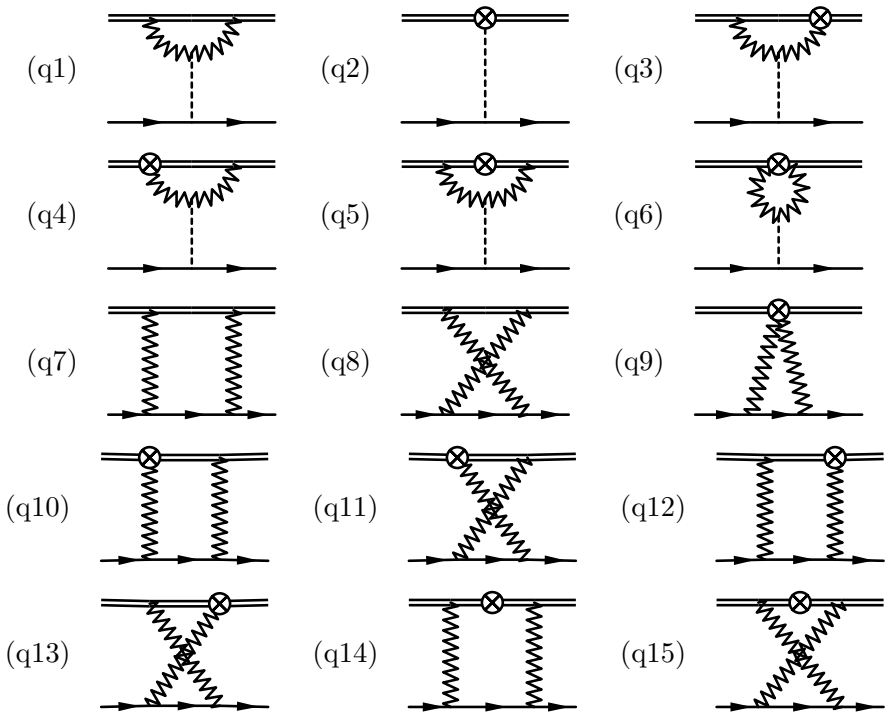

Figure 2.5: Diagrams contributing to up to $1/M$ quark matching, with the same notation as in Fig. 2.4 except that the zigzag lines are symmetry broken gauge bosons.

2.4.1 Quark Operators Matching

The matching diagrams for quark operators are shown in Fig. 2.5. Note that all the diagrams involving Nambu-Goldstone bosons are suppressed compared to the diagrams present in Fig. 2.5. All other particles are treated as massless except the weak scale particles $W^{\pm}$, Z^0, h, t.

Let us compute each diagram of Fig. 2.5 explicitly. First, notice that except for diagram (q2), the other diagrams contain two gauge bosons and they give universal loop integral results with different group factors by different electroweak multiplets (J, Y) with isospin J for $\mathrm{SU}(2)_W$ and Y being hyper charge.

For two $W^{\pm}$ bosons exchange diagrams, the group factor is

$$\left(\tilde{T}^{+}\tilde{T}^{-} + \tilde{T}^{-}\tilde{T}^{+}\right)_{\mathrm{WIMP\,WIMP}} = 2\left(J(J+1) - Y^2\right) \equiv 2f_W\,. \tag{2.76}$$

For two Z^0 bosons exchange diagrams, the group factor is

$$\left(\tilde{T}^3 - \sin^2\theta_W Q\right)^2_{\mathrm{WIMP\,WIMP}} = Y^2 \equiv f_Z\,. \tag{2.77}$$

Particularly, for a Wino-like particle $f_W = 2$, $f_Z = 0$, and for a Higgsino-like particle, $f_W = 1/2$, $f_Z = 1/4$.

We neglect small corrections from $|V_{td}|^2$ and $|V_{ts}|^2$, u and c quarks have the same coefficients, as do d and s quarks through all the weak matching calculations.

The diagram (q1) with two $W^\pm$ bosons yields

$$\begin{aligned}(\mathrm{q1})_{WW} &= 2f_W \int \frac{d^dp}{(2\pi)^d} \bar{h}_0^{\mathrm{low}} \left(\frac{ig_2}{\sqrt{2}} v_\mu \frac{i}{v\cdot p - \delta m^\pm + i0} \frac{ig_2}{\sqrt{2}} v_\nu\right) h_0^{\mathrm{low}} \\ &\quad \left(\frac{-i}{p^2 - m_W^2 + i0}\right)^2 \frac{ig_2^2 v}{2} g^{\mu\nu} \frac{i}{-m_h^2 + i0} \bar{q}\left(-i\frac{m_q}{v}\right) q \\ &= \left(2f_W \frac{-i\alpha_2^2}{4} \frac{\pi}{m_h^2 m_W}\right) \cdot \bar{h}_0^{\mathrm{low}} h_0^{\mathrm{low}} O_q^{(0)} \,. \end{aligned} \tag{2.78}$$

The diagram (q1) with two Z^0 bosons yields

$$\begin{aligned}(\mathrm{q1})_{ZZ} &= f_Z \int \frac{d^dp}{(2\pi)^d} \bar{h}_0^{\mathrm{low}} \left(\frac{ig_2}{\cos\theta_W} v_\mu \frac{i}{v\cdot p - \delta m^{\mathrm{high}} + i0} \frac{ig_2}{\cos\theta_W} v_\nu\right) h_0^{\mathrm{low}} \\ &\quad \left(\frac{-i}{p^2 - m_Z^2 + i0}\right)^2 \frac{ig_2^2 v}{2\cos^2\theta_W} g^{\mu\nu} \frac{i}{-m_h^2 + i0} \bar{q}\left(-i\frac{m_q}{v}\right) q \\ &= \left(f_Z \frac{-i\alpha_2^2}{2\cos^3\theta_W} \frac{\pi}{m_h^2 m_W}\right) \cdot \bar{h}_0^{\mathrm{low}} h_0^{\mathrm{low}} O_q^{(0)} \,. \end{aligned} \tag{2.79}$$

The diagram (q2) is

$$\begin{aligned}(\mathrm{q2}) &= \bar{h}_0^{\mathrm{low}} i \frac{v}{M} \tilde{c}_H h_0^{\mathrm{low}} \frac{i}{-m_h^2 + i0} \bar{q}\left(-i\frac{m_q}{v}\right) q \\ &= \left(-i\frac{\tilde{c}_H}{M m_h^2}\right) \cdot \bar{h}_0^{\mathrm{low}} h_0^{\mathrm{low}} O_q^{(0)} \,. \end{aligned} \tag{2.80}$$

The diagram (q3) with two $W^\pm$ bosons is

$$\begin{aligned}(\mathrm{q3}) &= 2f_W \int \frac{d^dp}{(2\pi)^d} \bar{h}_0^{\mathrm{low}} \left(\frac{ig_2}{\sqrt{2}} \frac{1}{2M} p_\nu (g^{\mu\nu} - v^\mu v^\nu) \frac{i}{v\cdot p - \delta m^\pm + i0} \frac{ig_2}{\sqrt{2}} v_\nu\right) h_0^{\mathrm{low}} \\ &\quad \left(\frac{-i}{p^2 - m_W^2 + i0}\right)^2 \frac{i}{-m_h^2 + i0} \bar{q}\left(-i\frac{m_q}{v}\right) q \\ &= 0 \,, \end{aligned} \tag{2.81}$$

where we used $(g^{\mu\nu} - v^\mu v^\nu) v_\nu = 0$.

Similarly, the diagram (q3) with two Z^0 bosons vanishes. The diagram (q4) vanishes for the same reason.

The diagram (q5) with two $W^\pm$ bosons is

$$\begin{aligned}(\mathrm{q5})_{WW} &= 2f_W \int \frac{d^dp}{(2\pi)^d} \bar{h}_0^{\mathrm{low}} \left[\frac{ig_2}{\sqrt{2}} v^\mu \frac{-i}{2M} \left(\frac{p^2 - (p\cdot v)^2}{(p\cdot v)^2 + i0}\right) \frac{ig_2}{\sqrt{2}} v^\nu\right] h_0^{\mathrm{low}} \\ &\quad \frac{2im_W^2}{v} g_{\mu\nu} \left(\frac{-i}{p^2 - m_W^2 + i0}\right)^2 \frac{i}{-m_h^2 + i0} \bar{q}\left(-i\frac{m_q}{v}\right) q \end{aligned}$$

$$= \left[2f_W \frac{g_2^2 m_W^2}{2Mv^2 m_h^2} \frac{i}{(4\pi)^{2-\epsilon}} \left(\frac{3}{\epsilon} - 2\right) \frac{\Gamma(1+\epsilon)}{m_W^{2\epsilon}}\right] \bar{h}_0^{\rm low} h_0^{\rm low} O_q^{(0)} \tag{2.82}$$

The diagram (q6) with two $W^\pm$ bosons is

$$\begin{aligned}(\text{q6})_{WW} &= 2f_W \int \frac{d^dp}{(2\pi)^d} \bar{h}_0^{\rm low} \frac{i}{2M} \frac{g_2^2}{2} (g^{\mu\nu} - v^\mu v^\nu) h_0^{\rm low} \\ &\left(\frac{-i}{p^2 - m_W^2 + i0}\right)^2 \frac{2im_W^2}{v} g_{\mu\nu} \frac{i}{-m_h^2 + i0} \bar{q} \left(-i\frac{m_q}{v}\right) q \\ &= -\left[2f_W \frac{g_2^2 m_W^2}{2Mv^2 m_h^2} \frac{i}{(4\pi)^{2-\epsilon}} \left(\frac{3}{\epsilon} - 2\right) \frac{\Gamma(1+\epsilon)}{m_W^{2\epsilon}}\right] \bar{h}_0^{\rm low} h_0^{\rm low} O_q^{(0)}\end{aligned} \tag{2.83}$$

Thus, we have $(\text{q5})_{WW} + (\text{q6})_{WW} = 0$, and similarly, $(\text{q5})_{ZZ} + (\text{q6})_{ZZ} = 0$ for two Z^0 bosons diagrams. So diagram (q5) and (q6) cancel each other.

The diagrams (q7) to (q15) contribute to the quark spin-2 operator. Since there is a quark in the loop, we need to distinguish the situations whether the loop quark is top quark or not.

For diagrams (q7) and (q8) with two $W^\pm$ bosons exchange , when the external quark is a bottom quark, the internal quark is a top quark whose mass should be taken into consideration. When the external quark is not a bottom quark, the internal quark is considered massless.

When there is a top quark in the loop,

$$\begin{aligned}(\text{q7})^{\rm top}{}_{WW} = f_W \int \frac{d^dp}{(2\pi)^d} \bar{h}_0^{\rm low} &\left[\frac{ig_2}{\sqrt{2}} v_\mu \frac{i}{v\cdot p + i0} \frac{ig_2}{\sqrt{2}} v_\nu\right] h_0^{\rm low} \left(\frac{-i}{p^2 - m_W^2 + i0}\right)^2 \\ &\bar{q}\left[\frac{ig_2}{2\sqrt{2}} \gamma^\mu (1-\gamma^5) \frac{i}{\not{q} - \not{p} - m_t + i0} \frac{ig_2}{2\sqrt{2}} \gamma^\nu (1-\gamma^5)\right] q\,,\end{aligned} \tag{2.84}$$

and the crossed diagram (q8) with top quark in the loop is

$$\begin{aligned}(\text{q8})^{\rm top}{}_{WW} = f_W \int \frac{d^dp}{(2\pi)^d} \bar{h}_0^{\rm low} &\left[\frac{ig_2}{\sqrt{2}} v_\mu \frac{i}{-v\cdot p + i0} \frac{ig_2}{\sqrt{2}} v_\nu\right] h_0^{\rm low} \left(\frac{-i}{p^2 - m_W^2 + i0}\right)^2 \\ &\bar{q}\left[\frac{ig_2}{2\sqrt{2}} \gamma^\mu (1-\gamma^5) \frac{i}{\not{q} - \not{p} - m_t + i0} \frac{ig_2}{2\sqrt{2}} \gamma^\nu (1-\gamma^5)\right] q\,,\end{aligned} \tag{2.85}$$

and the sum of them after loop integration is

$$\begin{aligned}(\text{q7})^{\rm top}{}_{WW} + (\text{q8})^{\rm top}{}_{WW} = f_W &\frac{ig_2^4}{(4\pi)^{2-\epsilon}} \frac{\pi}{8} \frac{\Gamma(1+\epsilon)}{m_W^{3+2\epsilon}} \left[1 + 2(1-\log 2)\epsilon\right] \bar{h}_0^{\rm low} h_0^{\rm low} \\ &\bar{q}\Bigg\{\frac{4}{3}\frac{(2+3x_t)}{(1+x_t)^3}\left[(v\cdot q)\not{v} - \frac{1}{d}\not{q}\right] - \frac{x_t}{(1+x_t)^3}\not{q} \\ &+ \epsilon\Bigg[-\frac{8}{9}\frac{5 - 18x_t^2 + 4x_t^3 + 9x_t^4 + (9x_t - 21x_t^3)\log x_t}{(x_t^2-1)^3}(v\cdot q)\not{v} \\ &+ \frac{8\,(1 - 18x_t^2 + 8x_t^3 + 9x_t^4 - 24x_t^3 \log x_t) - 9x_t(x_t-1)^3}{18(x_t^2-1)^3}\not{q}\Bigg]\end{aligned}$$

$$\Bigg\}(1-\gamma^5)q\,, \tag{2.86}$$

where we have neglected quadratic suppressed terms $q^2 = m_q^2$ for small external quark mass m_q and define $x_t \equiv m_t/m_W$.

For the diagram without top quark in the loop, we set the top mass m_t to be zero in Eq. (2.84) and Eq. (2.85), and their sum is

$$\begin{aligned}(\mathrm{q7})^{\mathrm{topless}}{}_{WW} + (\mathrm{q8})^{\mathrm{topless}}{}_{WW} = f_W \frac{ig_2^4}{(4\pi)^{2-\epsilon}} \frac{\pi}{8} \frac{\Gamma(1+\epsilon)}{m_W^{3+2\epsilon}} \bar{h}_0^{\mathrm{low}} h_0^{\mathrm{low}} \\ \bar{q}\Bigg\{ \left[\frac{8}{3} + \epsilon\left(\frac{88}{9} - \frac{16}{3}\log 2\right)\right]\left[(v\cdot q)\not{v} - \frac{1}{d}\not{q}\right] \\ + \not{q}\cdot O(\epsilon)\Bigg\}(1-\gamma^5)q\,. \end{aligned} \tag{2.87}$$

Similarly for two Z^0 bosons exchange,

$$\begin{aligned}(\mathrm{q7})_{ZZ} = f_Z \int \frac{d^dp}{(2\pi)^d} \bar{h}_0^{\mathrm{low}} \left[\frac{ig_2}{\cos\theta_W} v_\mu \frac{i}{v\cdot p + i0} \frac{ig_2}{\cos\theta_W} v_\nu\right] h_0^{\mathrm{low}} \left(\frac{-i}{p^2 - m_Z^2 + i0}\right)^2 \\ \bar{q}\left[\frac{ig_2}{4\cos\theta_W}\gamma^\mu(c_V^q - c_A^q\gamma^5) \frac{i}{\not{q} - \not{p} - m_q + i0} \frac{ig_2}{4\cos\theta_W}\gamma^\nu(c_V^q - c_A^q\gamma^5)\right] q\,, \end{aligned} \tag{2.88}$$

and

$$\begin{aligned}(\mathrm{q8})_{ZZ} = f_Z \int \frac{d^dp}{(2\pi)^d} \bar{h}_0^{\mathrm{low}} \left[\frac{ig_2}{\cos\theta_W} v_\mu \frac{i}{-v\cdot p + i0} \frac{ig_2}{\cos\theta_W} v_\nu\right] h_0^{\mathrm{low}} \left(\frac{-i}{p^2 - m_Z^2 + i0}\right)^2 \\ \bar{q}\left[\frac{ig_2}{4\cos\theta_W}\gamma^\mu(c_V^q - c_A^q\gamma^5) \frac{i}{\not{q} - \not{p} - m_q + i0} \frac{ig_2}{4\cos\theta_W}\gamma^\nu(c_V^q - c_A^q\gamma^5)\right] q\,, \end{aligned} \tag{2.89}$$

where $c_V^{(U)} = 1 - \frac{8}{3}\sin^2\theta_W$, $c_V^{(D)} = -1 + \frac{4}{3}\sin^2\theta_W$, $c_A^{(U)} = -1$, $c_A^{(D)} = 1$ with U denoting up-type quarks, D denoting down-type quarks and the sum after loop integration is

$$\begin{aligned}(\mathrm{q7})_{ZZ} + (\mathrm{q8})_{ZZ} = \frac{f_Z}{4} \frac{i\Gamma(1+\epsilon) g_2^4}{(4\pi)^{2-\epsilon}} \frac{\pi}{\cos^4\theta_W m_Z^{3+2\epsilon}} \bar{h}_0^{\mathrm{low}} h_0^{\mathrm{low}} \\ \bar{q}\Bigg\{ \left[\frac{2}{3} + \epsilon\left(\frac{22}{9} - \frac{4}{3}\log 2\right)\right]\left(c_V^{(q)2} + c_A^{(q)2}\right)\left[(v\cdot q)\not{v} - \frac{1}{d}\not{q}\right] \\ + \frac{\not{q}}{2}\left(c_V^{(q)2} - c_A^{(q)2}\right) + O(\epsilon)\not{q}\Bigg\} q\,. \end{aligned} \tag{2.90}$$

The diagram (q9) with two $W^\pm$ bosons and with top quark in the loop is

$$(\mathrm{q9})^{\mathrm{top}}{}_{WW} = 2 f_W \int \frac{d^dp}{(2\pi)^d} \bar{h}_0^{\mathrm{low}} \frac{ig_2^2}{4M}(g_{\mu\nu} - v_\mu v_\nu) h_0^{\mathrm{low}} \left(\frac{-i}{p^2 - m_W^2 + i0}\right)^2$$

$$\bar{q}\left[\frac{ig_2}{2\sqrt{2}}\gamma^\mu(1-\gamma^5)\frac{i}{\not{q}-\not{p}-m_t+i0}\frac{ig_2}{2\sqrt{2}}\gamma^\nu(1-\gamma^5)\right]q\,. \tag{2.91}$$

The diagram (q9) with two $W^\pm$ bosons and without top quark in the loop is equivalent to setting the top quark mass zero in Eq. (2.91) and evaluate the loop integral.

The diagram (q9) with two Z^0 bosons exchange is

$$\begin{aligned}(\mathrm{q9})_{ZZ} = 2f_Z\int\frac{d^dp}{(2\pi)^d}\bar{h}_0^{\mathrm{low}}\frac{ig_2^2}{2M\cos^2\theta_W}(g_{\mu\nu}-v_\mu v_\nu)h_0^{\mathrm{low}}\left(\frac{-i}{p^2-m_Z^2+i0}\right)^2\\ \bar{q}\left[\frac{ig_2}{4\cos\theta_W}\gamma^\mu(c_V^q-c_A^q\gamma^5)\frac{i}{\not{q}-\not{p}-m_q+i0}\frac{ig_2}{4\cos\theta_W}\gamma^\nu(c_V^q-c_A^q\gamma^5)\right]q\,.\end{aligned} \tag{2.92}$$

The diagram (q10) with two $W^\pm$ bosons and with top quark in the loop is

$$\begin{aligned}(\mathrm{q10})^{\mathrm{top}}{}_{WW} = f_W\int\frac{d^dp}{(2\pi)^d}\bar{h}_0^{\mathrm{low}}\left[\frac{ig_2}{\sqrt{2}}v_\mu\frac{i}{-v\cdot p+i0}\frac{ig_2}{2\sqrt{2}M}\left[-p_\nu+(p\cdot v)v_\nu\right]\right]h_0^{\mathrm{low}}\\ \bar{q}\left[\frac{ig_2}{2\sqrt{2}}\gamma^\mu(1-\gamma^5)\frac{i}{\not{q}+\not{p}-m_t+i0}\frac{ig_2}{2\sqrt{2}}\gamma^\nu(1-\gamma^5)\right]q\\ \left(\frac{-i}{p^2-m_W^2+i0}\right)^2.\end{aligned} \tag{2.93}$$

The diagram (q10) with two Z^0 bosons exchange is

$$\begin{aligned}(\mathrm{q10})_{ZZ} = f_Z\int\frac{d^dp}{(2\pi)^d}\bar{h}_0^{\mathrm{low}}\left[\frac{ig_2}{\cos\theta_W}v_\mu\frac{i}{-v\cdot p+i0}\frac{ig_2}{2M\cos\theta_W}\left[-p_\nu+(p\cdot v)v_\nu\right]\right]h_0^{\mathrm{low}}\\ \bar{q}\left[\frac{ig_2}{4\cos\theta_W}\gamma^\mu(c_V^q-c_A^q\gamma^5)\frac{i}{\not{q}+\not{p}-m_q+i0}\frac{ig_2}{4\cos\theta_W}\gamma^\nu(c_V^q-c_A^q\gamma^5)\right]q\\ \left(\frac{-i}{p^2-m_Z^2+i0}\right)^2.\end{aligned} \tag{2.94}$$

The diagram (q11) with two $W^\pm$ bosons and with top quark in the loop is

$$\begin{aligned}(\mathrm{q11})^{\mathrm{top}}{}_{WW} = f_W\int\frac{d^dp}{(2\pi)^d}\bar{h}_0^{\mathrm{low}}\left[\frac{ig_2}{\sqrt{2}}v_\nu\frac{i}{v\cdot p+i0}\frac{ig_2}{2\sqrt{2}M}\left[p_\mu-(p\cdot v)v_\mu\right]\right]h_0^{\mathrm{low}}\\ \left(\frac{-i}{p^2-m_W^2+i0}\right)^2\bar{q}\left[\frac{ig_2}{2\sqrt{2}}\gamma^\mu(1-\gamma^5)\frac{i}{\not{q}+\not{p}-m_t+i0}\right.\\ \left.\frac{ig_2}{2\sqrt{2}}\gamma^\nu(1-\gamma^5)\right]q\,.\end{aligned} \tag{2.95}$$

The diagram (q11) with two Z^0 bosons exchange is

$$(\mathrm{q11})_{ZZ} = f_Z\int\frac{d^dp}{(2\pi)^d}\bar{h}_0^{\mathrm{low}}\left[\frac{ig_2}{\cos\theta_W}v_\mu\frac{i}{v\cdot p+i0}\frac{ig_2}{2M\cos\theta_W}\left[p_\nu-(p\cdot v)v_\nu\right]\right]h_0^{\mathrm{low}}$$

$$\left(\frac{-i}{p^2-m_Z^2+i0}\right)^2 \bar{q}\left[\frac{ig_2}{4\cos\theta_W}\gamma^\nu(c_V^q-c_A^q\gamma^5)\frac{i}{\not{q}+\not{p}-m_q+i0}\right.$$
$$\left.\frac{ig_2}{4\cos\theta_W}\gamma^\mu(c_V^q-c_A^q\gamma^5)\right]q\,. \tag{2.96}$$

The diagram (q12) with two $W^\pm$ bosons and with top quark in the loop is

$$(\mathrm{q12})^{\mathrm{top}}{}_{WW} = f_W\int\frac{d^dp}{(2\pi)^d}\bar{h}_0^{\mathrm{low}}\left[\frac{ig_2}{2\sqrt{2}M}\left[-p_\mu+(p\cdot v)v_\mu\right]\frac{i}{-v\cdot p+i0}\frac{ig_2}{\sqrt{2}}v_\nu\right]h_0^{\mathrm{low}}$$
$$\left(\frac{-i}{p^2-m_W^2+i0}\right)^2\bar{q}\left[\frac{ig_2}{2\sqrt{2}}\gamma^\mu(1-\gamma^5)\frac{i}{\not{q}+\not{p}-m_t+i0}\right.$$
$$\left.\frac{ig_2}{2\sqrt{2}}\gamma^\nu(1-\gamma^5)\right]q\,. \tag{2.97}$$

The diagram (q12) with two Z^0 bosons exchange is

$$(\mathrm{q12})_{ZZ} = f_Z\int\frac{d^dp}{(2\pi)^d}\bar{h}_0^{\mathrm{low}}\left[\frac{ig_2}{2M\cos\theta_W}\left[-p_\mu+(p\cdot v)v_\mu\right]\frac{i}{-v\cdot p+i0}\frac{ig_2}{\cos\theta_W}v_\nu\right]h_0^{\mathrm{low}}$$
$$\left(\frac{-i}{p^2-m_Z^2+i0}\right)^2\bar{q}\left[\frac{ig_2}{4\cos\theta_W}\gamma^\mu(c_V^q-c_A^q\gamma^5)\frac{i}{\not{q}+\not{p}-m_q+i0}\right.$$
$$\left.\frac{ig_2}{4\cos\theta_W}\gamma^\nu(c_V^q-c_A^q\gamma^5)\right]q\,. \tag{2.98}$$

The diagram (q13) with two $W^\pm$ bosons and with top quark in the loop is

$$(\mathrm{q13})^{\mathrm{top}}{}_{WW} = f_W\int\frac{d^dp}{(2\pi)^d}\bar{h}_0^{\mathrm{low}}\left[\frac{ig_2}{2\sqrt{2}M}\left[p_\nu-(p\cdot v)v_\nu\right]\frac{i}{v\cdot p+i0}\frac{ig_2}{\sqrt{2}}v_\mu\right]h_0^{\mathrm{low}}$$
$$\left(\frac{-i}{p^2-m_W^2+i0}\right)^2\bar{q}\left[\frac{ig_2}{2\sqrt{2}}\gamma^\mu(1-\gamma^5)\frac{i}{\not{q}+\not{p}-m_t+i0}\right.$$
$$\left.\frac{ig_2}{2\sqrt{2}}\gamma^\nu(1-\gamma^5)\right]q\,. \tag{2.99}$$

The diagram (q13) with two Z^0 bosons exchange is

$$(\mathrm{q13})_{ZZ} = f_Z\int\frac{d^dp}{(2\pi)^d}\bar{h}_0^{\mathrm{low}}\left[\frac{ig_2}{2M\cos\theta_W}\left[p_\mu-(p\cdot v)v_\mu\right]\frac{i}{v\cdot p+i0}\frac{ig_2}{\cos\theta_W}v_\nu\right]h_0^{\mathrm{low}}$$
$$\left(\frac{-i}{p^2-m_Z^2+i0}\right)^2\bar{q}\left[\frac{ig_2}{4\cos\theta_W}\gamma^\nu(c_V^q-c_A^q\gamma^5)\frac{i}{\not{q}+\not{p}-m_q+i0}\right.$$
$$\left.\frac{ig_2}{4\cos\theta_W}\gamma^\mu(c_V^q-c_A^q\gamma^5)\right]q\,. \tag{2.100}$$

The diagram (q14) with two $W^\pm$ bosons and with top quark in the loop is

$$(\mathrm{q14})^{\mathrm{top}}{}_{WW} = f_W\int\frac{d^dp}{(2\pi)^d}\bar{h}_0^{\mathrm{low}}\left[\frac{ig_2}{\sqrt{2}}v_\mu\frac{-i}{2M}\frac{p^2-(p\cdot v)^2}{(p\cdot v)^2+i0}\frac{ig_2}{\sqrt{2}}v_\nu\right]h_0^{\mathrm{low}}$$

$$\left(\frac{-i}{p^2-m_W^2+i0}\right)^2 \bar{q}\Big[\frac{ig_2}{2\sqrt{2}}\gamma^\mu(1-\gamma^5)\frac{i}{\not{q}-\not{p}-m_t+i0}$$
$$\frac{ig_2}{2\sqrt{2}}\gamma^\nu(1-\gamma^5)\Big]q\,. \tag{2.101}$$

The diagram (q14) with two Z^0 bosons exchange is

$$(\mathrm{q14})_{ZZ} = f_Z\int\frac{d^dp}{(2\pi)^d}\bar{h}_0^{\mathrm{low}}\left[\frac{ig_2}{\cos\theta_W}v_\mu\frac{-i}{2M}\frac{p^2-(p\cdot v)^2}{(p\cdot v)^2+i0}\frac{ig_2}{\cos\theta_W}v_\nu\right]h_0^{\mathrm{low}}$$
$$\left(\frac{-i}{p^2-m_Z^2+i0}\right)^2\bar{q}\Big[\frac{ig_2}{4\cos\theta_W}\gamma^\mu(c_V^q-c_A^q\gamma^5)\frac{i}{\not{q}-\not{p}-m_q+i0}$$
$$\frac{ig_2}{4\cos\theta_W}\gamma^\nu(c_V^q-c_A^q\gamma^5)\Big]q. \tag{2.102}$$

The diagram (q15) with two $W^\pm$ bosons and with top quark in the loop is

$$(\mathrm{q15})^{\mathrm{top}}{}_{WW} = f_W\int\frac{d^dp}{(2\pi)^d}\bar{h}_0^{\mathrm{low}}\left[\frac{ig_2}{\sqrt{2}}v_\mu\frac{-i}{2M}\frac{p^2-(p\cdot v)^2}{(p\cdot v)^2+i0}\frac{ig_2}{\sqrt{2}}v_\nu\right]h_0^{\mathrm{low}}$$
$$\left(\frac{-i}{p^2-m_W^2+i0}\right)^2\bar{q}\Big[\frac{ig_2}{2\sqrt{2}}\gamma^\nu(1-\gamma^5)\frac{i}{\not{q}+\not{p}-m_t+i0}$$
$$\frac{ig_2}{2\sqrt{2}}\gamma^\mu(1-\gamma^5)\Big]q\,. \tag{2.103}$$

The diagram (q15) with two Z^0 bosons exchange is

$$(\mathrm{q15})_{ZZ} = f_Z\int\frac{d^dp}{(2\pi)^d}\bar{h}_0^{\mathrm{low}}\left[\frac{ig_2}{\cos\theta_W}v_\mu\frac{-i}{2M}\frac{p^2-(p\cdot v)^2}{(p\cdot v)^2+i0}\frac{ig_2}{\cos\theta_W}v_\nu\right]h_0^{\mathrm{low}}$$
$$\left(\frac{-i}{p^2-m_Z^2+i0}\right)^2\bar{q}\Big[\frac{ig_2}{4\cos\theta_W}\gamma^\nu(c_V^q-c_A^q\gamma^5)\frac{i}{\not{q}+\not{p}-m_q+i0}$$
$$\frac{ig_2}{4\cos\theta_W}\gamma^\mu(c_V^q-c_A^q\gamma^5)\Big]q\,. \tag{2.104}$$

The sum of (q9) to (q15) with two $W^\pm$ bosons exchange is

$$\sum_{i=9}^{15}(\mathrm{q}i)_{WW} = \frac{f_W}{2}\frac{ig_2^4}{(4\pi)^{2-\epsilon}}\frac{\Gamma(1+\epsilon)}{m_W^{2+2\epsilon}M}\bar{h}_0^{\mathrm{low}}h_0^{\mathrm{low}}\Bigg\{\Bigg[(-2+\epsilon)\int_0^1 dx\frac{(1-x)^2}{(1-x+x_t^2x)^{1+\epsilon}}$$
$$\bar{q}\left((v\cdot q)\not{v}-\frac{1}{d}\not{q}\right)(1-\gamma^5)q+O(\epsilon)m_q\bar{q}q\Big]\delta_{Db}$$
$$-(1-\delta_{Db})\bar{q}\left[(v\cdot q)\not{v}-\frac{1}{d}\not{q}\right](1-\gamma^5)q\Bigg\}$$
$$=\frac{f_W}{8}\frac{ig_2^4}{(4\pi)^{2-\epsilon}}\frac{\Gamma(1+\epsilon)}{m_W^{2+2\epsilon}M}\Bigg\{-4-\frac{\delta_{Db}}{(x_t^2-1)^3}\Big[4x_t^2(1-x_t^4+4x_t^2\log x_t)$$

$$+ 8\epsilon x_t^2(1 - x_t^2 + 2x_t^2 \log x_t - 2x_t^2 \log^2 x_t)\Big]\Big\}$$
$$\bar{h}_0^{\rm low} h_0^{\rm low} \bar{q} \left[(v\cdot q)\not{v} - \frac{1}{d}\not{q}\right](1-\gamma^5)q\,, \tag{2.105}$$

where δ_{Db} is a Kronecker delta to indicate whether the down quark is a bottom quark.

The sum of (q9) to (q15) with two Z^0 bosons exchange is

$$\sum_{i=9}^{15}(\mathrm{q}i)_{ZZ} = -\frac{f_Z}{4}\frac{ig_2^4}{\cos^4\theta_W(4\pi)^{2-\epsilon}}\frac{\Gamma(1+\epsilon)}{m_Z^{2+2\epsilon}M}$$
$$(c_V^{(q)2} + c_A^{(q)2})\bar{h}_0^{\rm low} h_0^{\rm low}\bar{q}\left[(v\cdot q)\not{v} - \frac{1}{d}\not{q}\right](1-\gamma^5)q\,. \tag{2.106}$$

2.4.2 Gluon Operators Matching

The matching for gluon operators are shown in Fig. 2.6. We have gluons attached to quark loop substructure in all these diagrams and this substructure can be separated out as a tensor $\Pi^{\mu\nu}(L)$ with the loop momentum L, shown in Fig. 2.7. This tensor can be calculated in the back-ground gluon field [72, 117], which we review here for comprehensive understanding of the whole matching process.

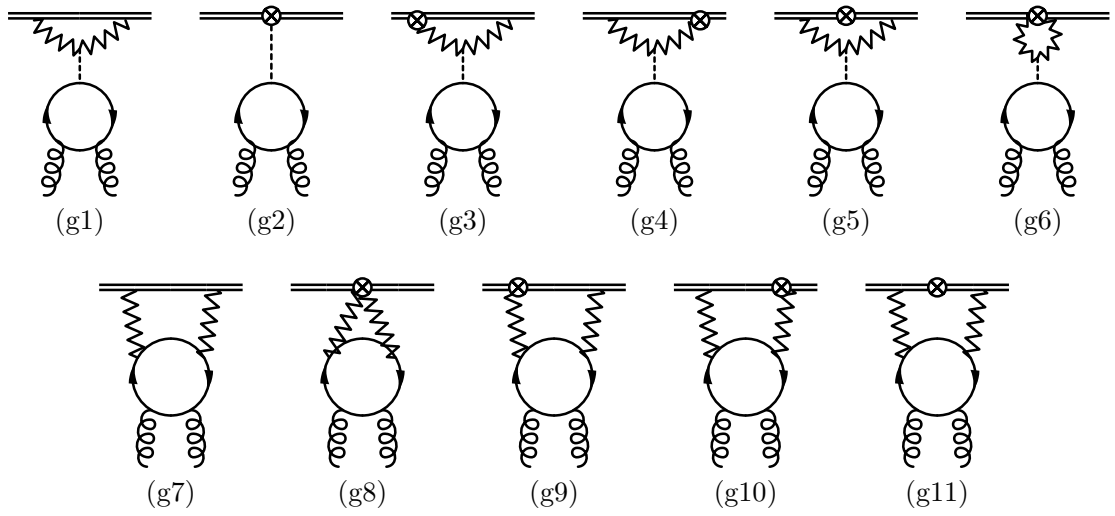

Figure 2.6: Diagrams contributing to up to $1/M$ order gluon matching, with the same notation as in Fig. 2.5 and curly lines denote the gluons. Diagrams with both gluons attached to the upper quark line or with one gluon attached to each of the upper and lower quark lines are not shown.

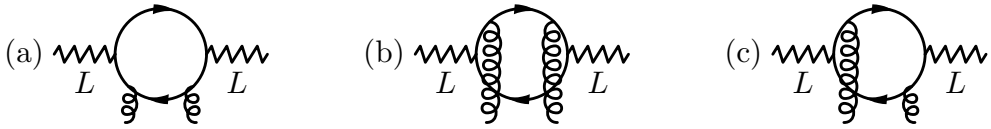

Figure 2.7: Background-field quark loops with three types attachment of two gluons onto the quark loop, (a): both gluons attached to the lower quark line, (b): both gluons attached to the upper quark line, (c): one gluon attached to each of the upper and lower quark lines.

The quark loop with two external sources $J(x)$ and $J'(0)$ is a two-point function and in momentum space, it is

$$\begin{aligned} i\Pi(L) &= -\int d^d x e^{iL\cdot x}\langle T\left\{J(x)J'(0)\right\}\rangle \\ &= -\int d^d x e^{iL\cdot x}\mathrm{Tr}\left\{\Gamma i S^{(q)}(x,0)\Gamma' i S^{(q')}(0,x)\right\}\,, \end{aligned} \tag{2.107}$$

where $iS^{(q)}(x,0) = \langle T\left\{q(x)\bar{q}(0)\right\}\rangle$, and Γ, Γ' are notations for general Dirac structures.

After Fourier Transform, we have

$$\int d^d x e^{ip\cdot x} S^{(q)}(x,0) \equiv S^{(q)}(p)\,, \tag{2.108}$$

$$\int d^d x e^{-ip'\cdot x} \tilde{S}^{(q')}(0,x) \equiv \tilde{S}^{(q')}(p')\,. \tag{2.109}$$

The two-point function tensor can be expressed as

$$i\Pi(L) = -\int \frac{d^d p}{(2\pi)^d}\mathrm{Tr}\left\{\Gamma i S^{(q)}(p)\Gamma' i S^{(q')}(p-L)\right\}\,. \tag{2.110}$$

In momentum space, the fermion propagators in Eq. (2.110) can be perturbatively solved in terms of the background field A with a small coupling g as in Fig. 2.8,

$$\begin{aligned} iS(p) = &\frac{i}{\not p - m} + g\int \frac{d^d q}{(2\pi)^d}\frac{i}{\not p - m} i\not A(q)\frac{i}{\not p - \not q - m} \\ &+ g^2\int \frac{d^d q_1}{(2\pi)^d}\int \frac{d^d q_2}{(2\pi)^d}\frac{i}{\not p - m} i\not A(q_1)\frac{i}{\not p - \not q_1 - m} i\not A(q_2)\frac{i}{\not p - \not q_1 - \not q_2 - m} \\ &+ \dots\,, \end{aligned} \tag{2.111}$$

and

$$i\tilde{S}(p) = \frac{i}{\not p - m} + g\int \frac{d^d q}{(2\pi)^d}\frac{i}{\not p + \not q - m} i\not A(q)\frac{i}{\not p - m}$$

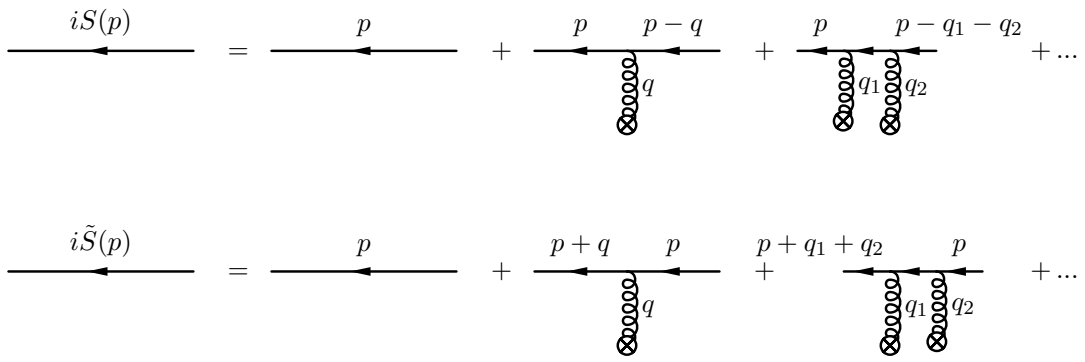

Figure 2.8: Momentum space fermion propagators in a background field, which is denoted by a curly line attached to a circled cross.

$$+ g^2 \int \frac{d^d q_1}{(2\pi)^d} \int \frac{d^d q_2}{(2\pi)^d} \frac{i}{\not p + \not q_1 + \not q_2 - m} i\not A(q_1) \frac{i}{\not p + \not q_2 - m} i\not A(q_2) \frac{i}{\not p - m} + \dots , \tag{2.112}$$

where in Fock-Schwinger gauge $(x-y)A^a_\mu(x) = 0$, and

$$\begin{aligned} A_\mu(q) &= t^a \int d^d x e^{iq\cdot x} A^a_\mu(x) \\ &= t^a \int d^d x e^{iq\cdot x} \left[\frac{1}{2} x^\rho G^a_{\rho\mu}(0) + \dots \right] \\ &= -it^a \frac{(2\pi)^d}{2} G^a_{\rho\mu}(0) \frac{d}{dq_\rho} \delta^{(d)}(q) + \dots , \end{aligned} \tag{2.113}$$

where higher order terms are in the ellipsis and propagators are expressed in terms of derivatives of gauge-invariant field strength $G_{\mu\nu}$ in this way.

Explicitly, for the three types of gluons attachment, we have

$$\begin{aligned} i\Pi_a(L) = &-\frac{g_s^2}{4} \mathrm{Tr}(t^A t^B) G^A_{\rho\alpha}(0) G^B_{\sigma\tau}(0) \int \frac{d^d p}{(2\pi)^d} \frac{\partial}{\partial q_\rho} \frac{\partial}{\partial q'_\sigma} \\ &\mathrm{Tr} \left[\Gamma \frac{1}{\not p - m_1} \gamma^\alpha \frac{1}{\not p - \not q - m_1} \gamma^\tau \frac{1}{\not p - \not q - \not q' - m_1} \Gamma' \frac{1}{\not p - \not L - m_2} \right]_{q=q'=0} , \\ i\Pi_b(L) = &-\frac{g_s^2}{4} \mathrm{Tr}(t^A t^B) G^A_{\rho\alpha}(0) G^B_{\sigma\tau}(0) \int \frac{d^d p}{(2\pi)^d} \frac{\partial}{\partial q_\rho} \frac{\partial}{\partial q'_\sigma} \\ &\mathrm{Tr} \left[\Gamma \frac{1}{\not p - m_1} \Gamma' \frac{1}{\not p - \not L + \not q + \not q' - m_2} \gamma^\alpha \frac{1}{\not p - \not L + \not q' - m_2} \gamma^\tau \frac{1}{\not p - \not L - m_2} \right]_{q=q'=0} , \\ i\Pi_c(L) = &-\frac{g_s^2}{4} \mathrm{Tr}(t^A t^B) G^A_{\rho\alpha}(0) G^B_{\sigma\tau}(0) \int \frac{d^d p}{(2\pi)^d} \frac{\partial}{\partial q_\rho} \frac{\partial}{\partial q'_\sigma} \end{aligned}$$

$$\mathrm{Tr}\left[\Gamma\frac{1}{\not p-m_1}\gamma^\alpha\frac{1}{\not p-\not q-m_1}\Gamma'\frac{1}{\not p-\not L+\not q'-m_2}\gamma^\tau\frac{1}{\not p-\not L-m_2}\right]_{q=q'=0}, \tag{2.114}$$

where t^A is an SU(3) generator, g_s is strong coupling, m_1 and m_2 denote the lower line quark mass and upper line quark mass respectively.

As a special case, the background gluon field quark loops in the first line of Fig. 2.6 can be computed by setting $\Gamma=\Gamma'=1$ and $L=0$,

$$\begin{aligned} i\Pi(0) &= -\frac{g_s^2}{4}\mathrm{Tr}(t^At^B)G^A_{\rho\alpha}(0)G^B_{\sigma\tau}(0)\int\frac{d^dp}{(2\pi)^d}\frac{\partial}{\partial q_\rho}\frac{\partial}{\partial q'_\sigma} \\ &\quad \mathrm{Tr}\left[\frac{1}{\not p-m}\gamma^\alpha\frac{1}{\not p-\not q-m}\gamma^\tau\frac{1}{\not p-\not q-\not q'-m}\right]_{q=q'=0} \\ &= -\frac{g_s^2}{4}\mathrm{Tr}(t^At^B)\left(G^A_{\alpha\beta}(0)\right)^2\frac{i}{(4\pi)^{2-\epsilon}}\frac{16}{3}\frac{6-7\epsilon}{d(d-1)}\frac{\Gamma(1+\epsilon)}{m_t^{1+2\epsilon}} \\ &= -\frac{g_s^2}{3}\frac{i}{(4\pi)^2}\frac{1}{m_t}\left(G^A_{\alpha\beta}(0)\right)^2, \end{aligned} \tag{2.115}$$

and it vanishes when the quark is massless.

Let us make use of this background field quark loop result by inserting it into the full diagrams g(1) to g(6) of Fig. 2.6 and evaluate these diagrams.

The diagram (g1) with two $W^\pm$ and two Z^0 bosons are readily found by plugging in quark diagram (q1) result.

$$\begin{aligned} \mathrm{g}(1) &= \bar h_0^{\mathrm{low}}\left[\left(2f_W\frac{-i\alpha_2^2}{4}\frac{\pi m_t}{m_h^2m_W}\right)+\left(f_Z\frac{-i\alpha_2^2}{2\cos^3\theta_W}\frac{\pi m_t}{m_h^2m_W}\right)\right]h_0^{\mathrm{low}} \\ &\quad \left(-\frac{g_s^2}{3}\right)\frac{1}{(4\pi)^2m_t}\left(G^A_{\alpha\beta}(0)\right)^2 \\ &= i\frac{\alpha_2^2\alpha_s}{24m_W^3x_h^2}\left(f_W+\frac{f_Z}{\cos^3\theta_W}\right)\bar h_0^{\mathrm{low}}h_0^{\mathrm{low}}\left(G^A_{\alpha\beta}(0)\right)^2. \end{aligned} \tag{2.116}$$

The diagram (g2) refers to the quark diagram (q2) and yields,

$$\begin{aligned} \mathrm{g}(2) &= \bar h_0^{\mathrm{low}}\left(-i\frac{m_t\tilde c_H}{Mm_h^2}\right)h_0^{\mathrm{low}}\cdot\left(-\frac{g_s^2}{3}\right)\frac{1}{(4\pi)^2m_t}\left(G^A_{\alpha\beta}(0)\right)^2 \\ &= i\frac{\alpha_s}{12\pi}\frac{\tilde c_H}{Mm_h^2}\bar h_0^{\mathrm{low}}h_0^{\mathrm{low}}\left(G^A_{\alpha\beta}(0)\right)^2. \end{aligned} \tag{2.117}$$

The diagram (g3) and g(4) vanish due to the same reason as vanishing quark diagrams (q3) and (q4). The sum of diagrams (g5) and g(6) vanishes due to the same reason as vanishing sum of quark diagrams (q5) and (q6).

Now we proceed to evaluate (g7) to (g11), which contribute to both spin-0 and spin-2 gluon operators. We project the background gluon field quark loop tensors Eq. (2.114) into spin-0 and spin-2 components,

$$i\Pi_k(L) = -\frac{g_s^2}{8}\left[O_g^{(0)}I_k^{(0)}(L)+O_g^{(2)\mu\nu}I^{(2)}_{k\,\mu\nu}(L)+...\right], \tag{2.118}$$

where $k = a$, b, c and "..." denotes components orthogonal to the spin-0 and spin-2 components, irrelevant for our matching.

To identify $I_k^{(0)}(L)$ and $I_{k\,\mu\nu}^{(0)}(L)$ separately, consider the tensor $G_{\rho\alpha}^A G_{\sigma\tau}^A$, which is symmetric under $\rho \leftrightarrow \sigma$, $\alpha \leftrightarrow \tau$, anti-symmetric under $\rho \leftrightarrow \alpha$ and $\sigma \leftrightarrow \tau$. When it projects to the spin-0 operator $O_g^{(0)}$, it has to be proportional to $(g_{\rho\sigma}g_{\alpha\tau} - g_{\rho\tau}g_{\alpha\sigma})$. By contracting with $g^{\rho\sigma}g^{\alpha\tau}$, we find the proportionality is $1/(d^2-d)$. When it projects to the spin-2 operator $O_g^{(2)\mu\nu}$, it has to be proportional to $(-g_{\rho\sigma}O_{g\,\alpha\tau}^{(2)} + g_{\rho\tau}O_{g\,\alpha\sigma}^{(2)} - g_{\alpha\tau}O_{g\,\rho\sigma}^{(2)}$ $+ g_{\alpha\sigma}O_{g\,\rho\tau}^{(2)})$ and the proportionality is $1/(d-2)$ by contracting with $v^\rho v^\sigma g^{\alpha\tau}$. Thus,

$$\begin{aligned} G_{\rho\alpha}^A G_{\sigma\tau}^A = & \frac{1}{d(d-1)}(g_{\rho\sigma}g_{\alpha\tau} - g_{\rho\tau}g_{\alpha\sigma})O_g^{(0)} \\ & + \frac{1}{d-2}\left(-g_{\rho\sigma}O_{g\,\alpha\tau}^{(2)} + g_{\rho\tau}O_{g\,\alpha\sigma}^{(2)} - g_{\alpha\tau}O_{g\,\rho\sigma}^{(2)} + g_{\alpha\sigma}O_{g\,\rho\tau}^{(2)}\right) \\ & + \dots . \end{aligned} \tag{2.119}$$

We apply the decomposition Eq. (2.119) to contract the loop integral tensor in Eq. (2.114) and obtain the corresponding $I_k^{(0)}(L)$ and $I_{k\,\mu\nu}^{(2)}(L)$, which will be integrals of a Feynman parameter x,

$$\begin{aligned} I_k^{(0)}(L) &= \frac{1}{d(d-1)}\frac{i\Gamma(1+\epsilon)}{(4\pi)^{2-\epsilon}}\int_0^1 dx N_k^{(0)}(L)\,, \\ I_{k\,\mu\nu}^{(2)}(L) &= \frac{1}{d-2}\frac{i\Gamma(1+\epsilon)}{(4\pi)^{2-\epsilon}}\int_0^1 dx N_{k\,\mu\nu}^{(2)}(L)\,. \end{aligned} \tag{2.120}$$

The diagrams in Fig. 2.6 involve two $W^\pm$ or two Z^0 bosons exchange currents entering Γ^α and Γ'^β in Eq. (2.114). We can work out the specific $N_k^{\alpha\beta}$ expressions in Eq. (2.120) for these two currents exchange cases and list them explicitly here,

$$\begin{aligned} N_{a\,(W^+W^+)}^{\alpha\beta\,(0)}(L) &= \frac{(1-x)^3}{3!}64(3-2\epsilon)m_t^2\left[\frac{(1+\epsilon)(1-\epsilon)}{\Delta^{2+\epsilon}}g^{\alpha\beta}\right. \\ &\quad \left. - \frac{(2+\epsilon)(1+\epsilon)}{\Delta^{3+\epsilon}}x(1-x)\left(2L^\alpha L^\beta - L^2 g^{\alpha\beta}\right)\right], \\ N_{b\,(W^+W^+)}^{\alpha\beta\,(0)}(L) &= 0\,, \\ N_{c\,(W^+W^+)}^{\alpha\beta\,(0)}(L) &= x(1-x)64(1-\epsilon)\left[\frac{(1+\epsilon)(3-2\epsilon)}{2\Delta^{1+\epsilon}}g^{\alpha\beta}\right. \\ &\quad \left. + \frac{1+\epsilon}{2}x(1-x)\frac{2(1-2\epsilon)L^\alpha L^\beta + (1+2\epsilon)L^2 g^{\alpha\beta}}{\Delta^{2+\epsilon}}\right], \\ N_{a\,(ZZ)}^{\alpha\beta\,(0)}(L) &= \frac{(1-x)^3}{3!}32(3-2\epsilon)\frac{m_q^2}{\Delta^{3+\epsilon}}\left\{\left(c_V^{(q)2} + c_A^{(q)2}\right)\left[(1-\epsilon)(1+\epsilon)\Delta g^{\alpha\beta}\right.\right. \\ &\quad \left. - (2+3\epsilon)x(1-x)\left(2L^\alpha L^\beta - L^2 g^{\alpha\beta}\right)\right] \\ &\quad \left. - \left(c_V^{(q)2} - c_A^{(q)2}\right)\left[(2-\epsilon)(1+\epsilon)\Delta - (2+3\epsilon)x^2L^2\right]g^{\alpha\beta}\right\}, \end{aligned}$$

$$
\begin{aligned}
N^{\alpha\beta\,(0)}_{b\,(ZZ)}(L) = \frac{x^3}{3!}32(3-2\epsilon)\frac{m_q^2}{\Delta^{3+\epsilon}}\Bigg\{ & \left(c_V^{(q)2}+c_A^{(q)2}\right)\Big[(1-\epsilon)(1+\epsilon)\Delta g^{\alpha\beta} \\
& -(2+3\epsilon)x(1-x)\left(2L^\alpha L^\beta - L^2 g^{\alpha\beta}\right)\Big] \\
& -\left(c_V^{(q)2}-c_A^{(q)2}\right)\left[(2-\epsilon)(1+\epsilon)\Delta-(2+3\epsilon)(1-x)^2L^2\right]g^{\alpha\beta}\Bigg\},
\end{aligned}
$$

$$
\begin{aligned}
N^{\alpha\beta\,(0)}_{c\,(ZZ)}(L) = \frac{32}{\Delta^{3+\epsilon}}x(1-x)\Bigg\{ & \left(c_V^{(q)2}+c_A^{(q)2}\right)(1-\epsilon)\Big[\frac{1}{2}(3-2\epsilon)(1+\epsilon)\Delta^2 g^{\alpha\beta} \\
& +x(1-x)\left[(1-2\epsilon)L^\alpha L^\beta+\frac{1}{2}(1+2\epsilon)L^2 g^{\alpha\beta}\right](1+\epsilon)\Delta\Big] \\
& +\left(c_V^{(q)2}-c_A^{(q)2}\right)\frac{\epsilon}{2}(3-2\epsilon)(1+\epsilon)m_q^2\Delta g^{\alpha\beta}\Bigg\},
\end{aligned}
$$

$$
\begin{aligned}
N^{\alpha\beta\,(2)}_{a\,\mu\nu(W^+W^+)}(L) = \frac{(1-x)^3}{3!}128(1-\epsilon)\Bigg\{ & (2-\epsilon)\frac{1}{2}(\delta^\alpha_\mu\delta^\beta_\nu+\delta^\alpha_\nu\delta^\beta_\mu)\frac{1}{\Delta^{1+\epsilon}} \\
& +\frac{1+\epsilon}{\Delta^{2+\epsilon}}\Big[(m_t^2-x^2L^2)\frac{1}{2}(\delta^\alpha_\mu\delta^\beta_\nu+\delta^\alpha_\nu\delta^\beta_\mu) \\
& +(2-\epsilon)x(1-x)(\delta^\alpha_\mu L^\beta+\delta^\beta_\mu L^\alpha)L_\nu - x(2-x-\epsilon)L_\mu L_\nu g^{\alpha\beta}\Big] \\
& -(3+2\epsilon)x(1-x)\Big[(m_t^2 g^{\alpha\beta}-2x^2L^\alpha L^\beta)L_\mu L_\nu \\
& -(m_t^2-x^2L^2)(\delta^\alpha_\mu L^\beta+\delta^\beta_\mu L^\alpha)L_\nu\Big]\frac{1}{\Delta^{3+\epsilon}}\Bigg\},
\end{aligned}
$$

$$
\begin{aligned}
N^{\alpha\beta\,(2)}_{b\,\mu\nu(W^+W^+)}(L) = \frac{x^3}{3!}128(1-\epsilon)\Bigg\{ & (2-\epsilon)\frac{1}{2}(\delta^\alpha_\mu\delta^\beta_\nu+\delta^\alpha_\nu\delta^\beta_\mu)\frac{1}{\Delta^{1+\epsilon}} \\
& -\frac{1+\epsilon}{\Delta^{2+\epsilon}}(1-x)\Big[(1-x)L^2\frac{1}{2}(\delta^\alpha_\mu\delta^\beta_\nu+\delta^\alpha_\nu\delta^\beta_\mu) \\
& -(2-\epsilon)x(\delta^\alpha_\mu L^\beta+\delta^\beta_\mu L^\alpha)L_\nu+(1+x-\epsilon)L_\mu L_\nu g^{\alpha\beta}\Big] \\
& -\frac{2(2+3\epsilon)}{\Delta^{3+\epsilon}}x(1-x)^3\left[-L^\alpha L^\beta L_\mu L_\nu+L^2\frac{1}{2}(\delta^\alpha_\mu L^\beta+\delta^\beta_\mu L^\alpha)L_\nu\right]\Bigg\},
\end{aligned}
$$

$$
\begin{aligned}
N^{\alpha\beta\,(2)}_{c\,\mu\nu(W^+W^+)}(L) = 128x(1-x)\Bigg\{ & -\frac{1}{2}(1-\epsilon)(1-2\epsilon)\frac{1}{\Delta^{1+\epsilon}}\frac{1}{2}(\delta^\alpha_\mu\delta^\beta_\nu+\delta^\alpha_\nu\delta^\beta_\mu) \\
& +\frac{1+\epsilon}{2}\frac{x(1-x)}{\Delta^{2+\epsilon}}\Big[\epsilon L_\mu L_\nu g^{\alpha\beta} \\
& +(1-2\epsilon)(\delta^\alpha_\mu L^\beta+\delta^\beta_\mu L^\alpha)L_\nu-(1-2\epsilon)L^2\frac{1}{2}(\delta^\alpha_\mu\delta^\beta_\nu+\delta^\alpha_\nu\delta^\beta_\mu)\Big]\Bigg\},
\end{aligned}
$$

$$
\begin{aligned}
N^{\alpha\beta\,(2)}_{a\,\mu\nu(ZZ)}(L) = \frac{(1-x)^3}{3!}64(1-\epsilon)\Bigg\{ & -(2+3\epsilon)\left(c_V^{(q)2}-c_A^{(q)2}\right)x^2m_q^2\frac{L_\mu L_\nu}{\Delta^{3+\epsilon}}g^{\alpha\beta} \\
& +\left(c_V^{(q)2}+c_A^{(q)2}\right)\Bigg[(2-\epsilon)\frac{1}{\Delta^{1+\epsilon}}\frac{1}{2}(\delta^\alpha_\mu\delta^\beta_\nu+\delta^\alpha_\nu\delta^\beta_\mu) \\
& +\frac{1+\epsilon}{\Delta^{2+\epsilon}}\Big[(m_q^2-x^2L^2)\frac{1}{2}(\delta^\alpha_\mu\delta^\beta_\nu+\delta^\alpha_\nu\delta^\beta_\mu) \\
& +(2-\epsilon)x(1-x)(\delta^\alpha_\mu L^\beta+\delta^\beta_\mu L^\alpha)L_\nu+x(2-x-\epsilon)L_\mu L_\nu g^{\alpha\beta}\Big] \\
& -(2+3\epsilon)\frac{x(1-x)}{\Delta^{3+\epsilon}}\Big[\left(m_q^2g^{\alpha\beta}-2x^2L^\alpha L^\beta\right)L_\mu L_\nu \\
& -\left(m_q^2-x^2L^2\right)(\delta^\alpha_\mu L^\beta+\delta^\beta_\mu L^\alpha)L_\nu\Big]\Bigg]\Bigg\}, \\
N^{\alpha\beta\,(2)}_{b\,\mu\nu(ZZ)}(L) = \frac{x^3}{3!}64(1-\epsilon)\Bigg\{ & -(2+3\epsilon)\left(c_V^{(q)2}-c_A^{(q)2}\right)(1-x)^2m_q^2\frac{L_\mu L_\nu}{\Delta^{3+\epsilon}}g^{\alpha\beta} \\
& +\left(c_V^{(q)2}+c_A^{(q)2}\right)\Bigg[(2-\epsilon)\frac{1}{\Delta^{1+\epsilon}}\frac{1}{2}(\delta^\alpha_\mu\delta^\beta_\nu+\delta^\alpha_\nu\delta^\beta_\mu) \\
& +\frac{1+\epsilon}{\Delta^{2+\epsilon}}\Big[(m_q^2-(1-x)^2L^2)\frac{1}{2}(\delta^\alpha_\mu\delta^\beta_\nu+\delta^\alpha_\nu\delta^\beta_\mu) \\
& +(2-\epsilon)x(1-x)(\delta^\alpha_\mu L^\beta+\delta^\beta_\mu L^\alpha)L_\nu+(1-x)(1+x-\epsilon)L_\mu L_\nu g^{\alpha\beta}\Big] \\
& -(2+3\epsilon)\frac{x(1-x)}{\Delta^{3+\epsilon}}\Big[\left(m_q^2g^{\alpha\beta}-2(1-x)^2L^\alpha L^\beta\right)L_\mu L_\nu \\
& -\left(m_q^2-(1-x)^2L^2\right)(\delta^\alpha_\mu L^\beta+\delta^\beta_\mu L^\alpha)L_\nu\Big]\Bigg]\Bigg\}, \\
N^{\alpha\beta\,(2)}_{c\,\mu\nu(ZZ)}(L) = 64x(1-x)\Bigg\{ & -\left(c_V^{(q)2}-c_A^{(q)2}\right)(1+\epsilon)(1-\epsilon)\frac{m_q^2}{\Delta^{2+\epsilon}}\frac{1}{2}(\delta^\alpha_\mu\delta^\beta_\nu+\delta^\alpha_\nu\delta^\beta_\mu) \\
& +\left(c_V^{(q)2}+c_A^{(q)2}\right)\Bigg[-\frac{1}{2}(1-\epsilon)(1-2\epsilon)\frac{1}{\Delta^{1+\epsilon}}\frac{1}{2}(\delta^\alpha_\mu\delta^\beta_\nu+\delta^\alpha_\nu\delta^\beta_\mu) \\
& +\frac{x(1-x)}{2}\Big[\epsilon L_\mu L_\nu g^{\alpha\beta}+(1-2\epsilon)(\delta^\alpha_\mu L^\beta+\delta^\beta_\mu L^\alpha)L_\nu \\
& -(1-2\epsilon)L^2\frac{1}{2}(\delta^\alpha_\mu\delta^\beta_\nu+\delta^\alpha_\nu\delta^\beta_\mu)\Big]\frac{1+\epsilon}{\Delta^{2+\epsilon}}\Bigg]\Bigg\}, \qquad (2.121)
\end{aligned}
$$

where $\Delta=(1-x)m_1^2+xm_2^2-x(1-x)L^2-i0$ and $N^{(S)}_{k\,(W^-W^-)}(L)=N^{(S)}_{k\,(W^+W^+)}(-L)$ with spin $S=0,2$.

The spin-0 gluon matching of the diagram (g7) with W^+W^+ and W^-W^- exchanges is

$$
(\mathrm{g7})^{(0)}_{\mathrm{WW}}=f_W\int\frac{d^dL}{(2\pi)^d}\bar{h}_0^{\mathrm{low}}\frac{ig_2}{\sqrt{2}}v_\alpha\left[\frac{i}{v\cdot L+i0}+\frac{i}{-v\cdot L+i0}\right]\frac{ig_2}{\sqrt{2}}v_\beta h_0^{\mathrm{low}}
$$

$$\left(\frac{ig_2}{2\sqrt{2}}\right)^2\left(\frac{-i}{L^2-m_W^2}\right)^2\left(-\frac{g_s^2}{8}\right)O_g^{(0)}\sum_{k=a,b,c}I^{\alpha\beta\,(0)}_{k\,(W^+W^+)}(L)$$
$$=i\frac{\pi\left[\Gamma(1+\epsilon)\right]g_2^4g_s^2}{(4\pi)^{4-2\epsilon}}\frac{f_W}{12m_W^{3+4\epsilon}}\left[\frac{1}{(1+x_t)^2}+N_l\right]\bar{h}_0^{\rm low}h_0^{\rm low}O_g^{(0)}\,, \qquad (2.122)$$

where $N_l=2$ is the number of massless generations of quarks.

The spin-0 gluon matching of the diagram (g7) with ZZ exchange is

$$(\mathrm{g7})^{(0)}_{\rm ZZ}=f_Z\int\frac{d^dL}{(2\pi)^d}\bar{h}_0^{\rm low}\frac{ig_2}{\cos\theta_W}v_\alpha\left[\frac{i}{v\cdot L+i0}\right]\frac{ig_2}{\cos\theta_W}v_\beta h_0^{\rm low}$$
$$\left(\frac{ig_2}{4\cos\theta_W}\right)^2\left(\frac{-i}{L^2-m_Z^2}\right)^2\left(-\frac{g_s^2}{8}\right)O_g^{(0)}\sum_{k=a,b,c}I^{\alpha\beta\,(0)}_{k\,(ZZ)}(L)$$
$$=i\frac{\pi\left[\Gamma(1+\epsilon)\right]g_2^4g_s^2}{(4\pi)^{4-2\epsilon}}\frac{f_Z}{64\cos^4\theta_W m_Z^{3+4\epsilon}}\Bigg[4(c_V^{(D)2}+c_A^{(D)2})+(c_V^{(U)2}+c_A^{(U)2})\Big[\frac{8}{3}$$
$$+\frac{32y_t^6(8y_t^2-7)}{(4y_t^2-1)^{7/2}}\arctan(\sqrt{4y_t^2-1})-\pi y_t+\frac{4(48y_t^6-2y_t^4+9y_t^2-1)}{3(4y_t^2-1)^3}\Big]$$
$$+(c_V^{(U)2}-c_A^{(U)2})\Big[3\pi y_t-\frac{4(144y_t^6-70y_t^4+9y_t^2-2)}{3(4y_t^2-1)^3}$$
$$-\frac{32y_t^4(24y_t^4-21y_t^2+5)}{(4y_t^2-1)^{7/2}}\arctan(\sqrt{4y_t^2-1})\Big]\Bigg]\bar{h}_0^{\rm low}h_0^{\rm low}O_g^{(0)}\,. \qquad (2.123)$$

The spin-2 gluon matching of the diagram (g7) with W^+W^+ and W^-W^- exchange is

$$(\mathrm{g7})^{(2)}_{\rm WW}=f_W\int\frac{d^dL}{(2\pi)^d}\bar{h}_0^{\rm low}\frac{ig_2}{\sqrt{2}}v_\alpha\left[\frac{i}{v\cdot L+i0}+\frac{i}{-v\cdot L+i0}\right]\frac{ig_2}{\sqrt{2}}v_\beta h_0^{\rm low}$$
$$\left(\frac{ig_2}{2\sqrt{2}}\right)^2\left(\frac{-i}{L^2-m_W^2}\right)^2\left(-\frac{g_s^2}{8}\right)O_g^{(2)\,\mu\nu}\sum_{k=a,b,c}I^{\alpha\beta\,(2)}_{k\,\mu\nu\,(W^+W^+)}(L)$$
$$=i\frac{\pi\left[\Gamma(1+\epsilon)\right]g_2^4g_s^2}{(4\pi)^{4-2\epsilon}}\frac{f_W}{2m_W^{3+4\epsilon}}\Bigg[-\frac{16}{9\epsilon}-\frac{284}{27}+\frac{32}{9}\log 2-\frac{2(3x_t+2)}{9(x_t+1)^3}\frac{1}{\epsilon}$$
$$+\frac{8(6x_t^8-18x_t^6+21x_t^4-3x_t^2-2)}{9(x_t^2-1)^3}\log(x_t+1)$$
$$+\frac{4(3x_t^4-21x_t^3+3x_t^2+9x_t-2)}{9(x_t^2-1)^3}\log 2$$
$$-\frac{4(12x_t^8-36x_t^6+39x_t^4+14x_t^3-9x_t^2-6x_t-2)}{9(x_t^2-1)^3}\log x_t$$
$$-\frac{144x_t^6+72x_t^5-312x_t^4-105x_t^3-40x_t^2+47x_t+98}{27(x_t^2-1)^2(x_t+1)}\Bigg]$$
$$\bar{h}_0^{\rm low}h_0^{\rm low}v_\mu v_\nu O_g^{(2)\,\mu\nu}\,. \qquad (2.124)$$

The spin-2 gluon matching of the diagram (g7) with ZZ exchange is

$$(\mathrm{g7})^{(2)}_{\rm ZZ}=f_Z\int\frac{d^dL}{(2\pi)^d}\bar{h}_0^{\rm low}\frac{ig_2}{\cos\theta_W}v_\alpha\left[\frac{i}{v\cdot L+i0}\right]\frac{ig_2}{\cos\theta_W}v_\beta h_0^{\rm low}$$

$$
\begin{aligned}
&\left(\frac{ig_2}{4\cos\theta_W}\right)^2\left(\frac{-i}{L^2-m_Z^2}\right)^2\left(-\frac{g_s^2}{8}\right)O_g^{(2)\,\mu\nu}\sum_{k=a,b,c}I^{\alpha\beta\,(2)}_{k\,\mu\nu\,(ZZ)}(L)\\
&=i\frac{\pi\left[\Gamma(1+\epsilon)\right]g_2^4g_s^2}{(4\pi)^{4-2\epsilon}}\frac{f_Z m_Z^{-3-4\epsilon}}{64\cos^4\theta_W}\Bigg\{\Big[8(c_V^{(U)2}+c_A^{(U)2})+12(c_V^{(D)2}+c_A^{(D)2})\Big]\Big[-\frac{16}{9\epsilon}\\
&-\frac{284}{27}+\frac{32}{9}\log 2\Big]\\
&+4(c_V^{(U)2}+c_A^{(U)2})\Big[\frac{32(24y_t^8-21y_t^6-4y_t^4+5y_t^2-1)}{9(4y_t^2-1)^{7/2}}\arctan(\sqrt{4y_t^2-1})-\frac{\pi y_t}{3}\\
&+\frac{4(48y_t^6+62y_t^4-47y_t^2+9)}{9(4y_t^2-1)^3}\Big]+4(c_V^{(U)2}-c_A^{(U)2})\Big[\frac{4y_t^2(624y_t^4-538y_t^2+103)}{9(4y_t^2-1)^3}\\
&-\frac{13\pi y_t}{3}+\frac{32y_t^2(104y_t^6-91y_t^4+35y_t^2-5)}{3(4y_t^2-1)^{7/2}}\arctan(\sqrt{4y_t^2-1})\Big]\Bigg\}\\
&\bar h_0^{\rm low}h_0^{\rm low}v_\mu v_\nu O_g^{(2)\,\mu\nu}\,.
\end{aligned}
\tag{2.125}
$$

The spin-S gluon matching of the diagram (g8) with W^+W^+ and W^-W^- exchange is

$$
\begin{aligned}
(\mathrm{g8})^{(S)}_{WW}=f_W\int\frac{d^dL}{(2\pi)^d}\bar h_0^{\rm low}\frac{ig_2^2}{2M}(g_{\alpha\beta}-v_\alpha v_\beta)h_0^{\rm low}\quad&\frac{1}{2}\left(\frac{ig_2}{\sqrt{2}}\right)^2\left(\frac{-i}{L^2-m_W^2}\right)^2\\
\left(-\frac{g_s^2}{8}\right)O_g^{(S)}\sum_{k=a,b,c}I^{\alpha\beta\,(S)}_{k\,(W^+W^+)}(L)\,.&
\end{aligned}
\tag{2.126}
$$

The spin-S gluon matching of the diagram (g8) with ZZ exchange is

$$
\begin{aligned}
(\mathrm{g8})^{(S)}_{ZZ}=f_Z\int\frac{d^dL}{(2\pi)^d}\bar h_0^{\rm low}\frac{ig_2^2}{2M\cos^2\theta_W}(g_{\alpha\beta}-v_\alpha v_\beta)h_0^{\rm low}\left(\frac{-i}{L^2-m_Z^2+i0}\right)^2\\
\left(\frac{ig_2}{4\cos\theta_W}\right)^2\left(-\frac{g_s^2}{8}\right)O_g^{(S)}\sum_{k=a,b,c}I^{\alpha\beta\,(S)}_{k\,(ZZ)}(L)\,.
\end{aligned}
\tag{2.127}
$$

The spin-S gluon matching of the diagram (g9) with W^+W^+ and W^-W^- exchange is

$$
\begin{aligned}
(\mathrm{g9})^{(S)}_{WW}=f_W\int\frac{d^dL}{(2\pi)^d}\bar h_0^{\rm low}\left[\frac{ig_2}{\sqrt{2}}v_\alpha\frac{i}{-v\cdot L+i0}\frac{ig_2}{2\sqrt{2}M}\left[-L_\beta+(L\cdot v)v_\beta\right]\right]h_0^{\rm low}\\
\left(\frac{-i}{L^2-m_W^2+i0}\right)^2\frac{1}{2}\left(\frac{ig_2}{\sqrt{2}}\right)^2\left(-\frac{g_s^2}{8}\right)O_g^{(S)}\sum_{k=a,b,c}I^{\alpha\beta\,(S)}_{k\,(W^+W^+)}(L)\,.
\end{aligned}
\tag{2.128}
$$

The spin-S gluon matching of the diagram (g9) with ZZ exchange is

$$
\begin{aligned}
(\mathrm{g9})^{(S)}_{ZZ}=f_Z\int\frac{d^dL}{(2\pi)^d}\bar h_0^{\rm low}\left[\frac{ig_2}{\cos\theta_W}v_\alpha\frac{i}{-v\cdot L+i0}\frac{ig_2}{2M\cos\theta_W}\left[-L_\beta+(p\cdot v)v_\beta\right]\right]h_0^{\rm low}\\
\left(\frac{-i}{L^2-m_Z^2+i0}\right)^2\left(\frac{ig_2}{4\cos\theta_W}\right)^2\left(-\frac{g_s^2}{8}\right)O_g^{(S)}\sum_{k=a,b,c}I^{\alpha\beta\,(S)}_{k\,(ZZ)}(L)\,.
\end{aligned}
\tag{2.129}
$$

The spin-S gluon matching of the diagram (g10) with W^+W^+ and W^-W^- exchange is

$$(\mathrm{g10})^{(S)}_{WW} = f_W \int \frac{d^dL}{(2\pi)^d} \bar{h}_0^{\mathrm{low}} \left[\frac{ig_2}{2\sqrt{2}M} \left[-L_\alpha + (L\cdot v) v_\alpha \right] \frac{i}{-v\cdot L + i0} \frac{ig_2}{\sqrt{2}} v_\beta \right] h_0^{\mathrm{low}} \left(\frac{-i}{L^2 - m_W^2 + i0} \right)^2 \frac{1}{2} \left(\frac{ig_2}{\sqrt{2}} \right)^2 \left(-\frac{g_s^2}{8} \right) O_g^{(S)} \sum_{k=a,b,c} I^{\alpha\beta\,(S)}_{k\,(W^+W^+)}(L) \,. \quad (2.130)$$

The spin-S gluon matching of the diagram (g10) with ZZ exchange is

$$(\mathrm{g10})^{(S)}_{ZZ} = f_Z \int \frac{d^dL}{(2\pi)^d} \bar{h}_0^{\mathrm{low}} \left[\frac{ig_2}{\cos\theta_W} \left[-L_\alpha + (p\cdot v) v_\alpha \right] \frac{i}{-v\cdot L + i0} \frac{ig_2}{2M\cos\theta_W} v_\beta \right] h_0^{\mathrm{low}} \left(\frac{-i}{L^2 - m_Z^2 + i0} \right)^2 \left(\frac{ig_2}{4\cos\theta_W} \right)^2 \left(-\frac{g_s^2}{8} \right) O_g^{(S)} \sum_{k=a,b,c} I^{\alpha\beta\,(S)}_{k\,(ZZ)}(L) \,. \quad (2.131)$$

The spin-S gluon matching of the diagram (g11) with W^+W^+ and W^-W^- exchange is

$$(\mathrm{g11})^{(S)}_{WW} = f_W \int \frac{d^dL}{(2\pi)^d} \bar{h}_0^{\mathrm{low}} \left[\frac{ig_2}{\sqrt{2}} v_\alpha \frac{-i}{2M} \frac{L^2 - (L\cdot v)^2}{(L\cdot v)^2 + i0} \frac{ig_2}{\sqrt{2}} v_\beta \right] h_0^{\mathrm{low}} \left(\frac{-i}{L^2 - m_W^2 + i0} \right)^2 \left(\frac{ig_2}{\sqrt{2}} \right)^2 \left(-\frac{g_s^2}{8} \right) O_g^{(S)} \sum_{k=a,b,c} I^{\alpha\beta\,(S)}_{k\,(W^+W^+)}(L) \,. \quad (2.132)$$

The spin-S gluon matching of the diagram (g11) with ZZ exchange is

$$(\mathrm{g11})^{(S)}_{ZZ} = f_Z \int \frac{d^dL}{(2\pi)^d} \bar{h}_0^{\mathrm{low}} \left[\frac{ig_2}{\cos\theta_W} v_\alpha \frac{-i}{2M} \frac{L^2 - (L\cdot v)^2}{(L\cdot v)^2 + i0} \frac{ig_2}{\cos\theta_W} v_\beta \right] h_0^{\mathrm{low}} \left(\frac{-i}{L^2 - m_Z^2 + i0} \right)^2 \left(\frac{ig_2}{4\cos\theta_W} \right)^2 \left(-\frac{g_s^2}{8} \right) O_g^{(S)} \sum_{k=a,b,c} I^{\alpha\beta\,(S)}_{k\,(ZZ)}(L) \,. \quad (2.133)$$

The sum of all $1/M$ order spin-0 gluon matching with WW exchanges vanishes as

$$\begin{aligned} &(\mathrm{g8})^{(0)}_{WW} + (\mathrm{g9})^{(0)}_{WW} + (\mathrm{g10})^{(0)}_{WW} + (\mathrm{g11})^{(0)}_{WW} \\ &\propto \left[(v\cdot L) g_{\alpha\beta} - \frac{1}{2}(v_\alpha L_\beta + v_\beta L_\alpha) \right] \sum_{k=a,b,c} I^{\alpha\beta\,(0)}_{k\,(W^+W^+)}(L) = 0 \,. \end{aligned} \quad (2.134)$$

Similarly, the sum of the exchange of ZZ diagrams for $1/M$ order spin-0 gluon matching is zero,

$$\begin{aligned} &(\mathrm{g8})^{(0)}_{ZZ} + (\mathrm{g9})^{(0)}_{ZZ} + (\mathrm{g10})^{(0)}_{ZZ} + (\mathrm{g11})^{(0)}_{ZZ} \\ &\propto \left[(v\cdot L) g_{\alpha\beta} - \frac{1}{2}(v_\alpha L_\beta + v_\beta L_\alpha) \right] \sum_{k=a,b,c} I^{\alpha\beta\,(0)}_{k\,(ZZ)}(L) = 0 \,. \end{aligned} \quad (2.135)$$

So there is no contribution to spin-0 gluon matching from $1/M$ order.

The spin-2 gluon matching of $1/M$ order diagrams with WW exchange is

$$
\begin{aligned}
&(\mathrm{g8})^{(2)}_{WW} + (\mathrm{g9})^{(2)}_{WW} + (\mathrm{g10})^{(2)}_{WW} + (\mathrm{g11})^{(2)}_{WW} \\
&= i\frac{\pi[\Gamma(1+\epsilon)]^2 g_2^4 g^2}{(4\pi)^{4-2\epsilon}} 2 f_W m_W^{-3-4\epsilon} \frac{m_W}{\pi M}\bigg[N_l\Big(\frac{4}{3\epsilon} - \frac{1}{3}\Big) \\
&\quad + \frac{2(-1+4x_t^2-3x_t^4+4x_t^4\log x_t)}{3(x_t^2-1)^3}\frac{1}{\epsilon} + \frac{-1+3x_t^2-8x_t^4}{3(x_t^2-1)^2} + \frac{4}{9}\pi^2 x_t^2 + \frac{16}{3}x_t^2(\log x_t)^2 \\
&\quad - \frac{4}{3}\frac{(1+6x_t^2-18x_t^4+4x_t^6)\log x_t}{(x_t^2-1)^3} + \frac{8x_t^2}{3}(-1+4x_t^2-3x_t^4+x_t^6)\mathrm{Li}_2(1-x_t^2)\bigg] \\
&\quad \bar{h}_0^{\mathrm{low}} h_0^{\mathrm{low}} v_\mu v_\nu O_g^{(2)\,\mu\nu}
\end{aligned}
\tag{2.136}
$$

The spin-2 gluon matching of $1/M$ order diagrams with ZZ exchange is

$$
\begin{aligned}
&(\mathrm{g8})^{(2)}_{ZZ} + (\mathrm{g9})^{(2)}_{ZZ} + (\mathrm{g10})^{(2)}_{ZZ} + (\mathrm{g11})^{(2)}_{ZZ} \\
&= i\frac{\pi[\Gamma(1+\epsilon)]^2 g_2^4 g^2}{(4\pi)^{4-2\epsilon}} f_Z \frac{m_Z^{-3-4\epsilon}}{24 c_W^4}\frac{m_Z}{\pi M}\bigg[\Big[2(c_V^{(U)2}+c_A^{(U)2}) + 3(c_V^{(D)2}+c_A^{(D)2})\Big]\Big(\frac{4}{\epsilon}-1\Big) \\
&\quad - (c_V^{(U)2}+c_A^{(U)2})\Big[\frac{1-18y_t^2+36y_t^4}{(4y_t^2-1)^2} + \frac{8(1-4y_t^2+3y_t^4+18y_t^6)\log y_t}{(4y_t^2-1)^3} \\
&\quad + \frac{16y_t^2(2-13y_t^2+32y_t^4-18y_t^6)}{(4y_t^2-1)^{7/2}}\Big[2\arctan\Big(\frac{1}{\sqrt{4y_t^2-1}}\Big)\log y_t \\
&\quad - \mathrm{Im}\,\mathrm{Li}_2\Big(\frac{1-i\sqrt{4y_t^2-1}}{2y_t^2}\Big)\Big]\Big] \\
&\quad + 4y_t^2(c_V^{(U)2}-c_A^{(U)2})\Big[-\frac{8-59y_t^2+108y_t^4}{(4y_t^2-1)^3} - \frac{(29-128y_t^2+108y_t^4)\log y_t}{(4y_t^2-1)^3} \\
&\quad + \frac{2(-7+38y_t^2-82y_t^4+108y_t^6)}{(4y_t^2-1)^{7/2}}\Big[2\arctan\Big(\frac{1}{\sqrt{4y_t^2-1}}\Big)\log y_t \\
&\quad - \mathrm{Im}\,\mathrm{Li}_2\Big(\frac{1-i\sqrt{4y_t^2-1}}{2y_t^2}\Big)\Big]\Big]\bigg] .
\end{aligned}
\tag{2.137}
$$

For all the gluon operators matching diagrams, we reduce them to integrals with two Feynman parameters x and y, then do the double integrals analytically and check the analytic results by numerical double integrals.

We collect all the results for quark and gluon operators matching and list the bare matching coefficients

$$
\begin{aligned}
c_U^{(0)} &= \frac{\pi\Gamma(1+\epsilon)g_2^4}{(4\pi)^{2-\epsilon}}\bigg\{-\frac{m_W^{-3-2\epsilon}}{2x_h^2}(f_W + \frac{f_Z}{c_W^3}) + \frac{f_Z m_Z^{-3-2\epsilon}}{8c_W^4}(c_V^{(U)2}-c_A^{(U)2}) + O(\epsilon)\bigg\} \\
&\quad - \frac{m_W^{-2}}{M}\frac{\tilde{c}_H}{x_h^2}\,, \\
c_D^{(0)} &= \frac{\pi\Gamma(1+\epsilon)g_2^4}{(4\pi)^{2-\epsilon}}\bigg\{-\frac{m_W^{-3-2\epsilon}}{2x_h^2}(f_W + \frac{f_Z}{c_W^3}) + \frac{f_Z m_Z^{-3-2\epsilon}}{8c_W^4}(c_V^{(D)2}-c_A^{(D)2})
\end{aligned}
\tag{2.138}
$$

$$
\begin{aligned}
&- \delta_{Db} m_W^{-3-2\epsilon} f_W \frac{x_t}{8(x_t+1)^3} + O(\epsilon) \Big\} - \frac{m_W^{-2}}{M} \frac{\tilde{c}_H}{x_h^2}\,, \qquad (2.139)\\
c_g^{(0)} = {}& \frac{\pi[\Gamma(1+\epsilon)]^2 g_2^4 g_s^2}{(4\pi)^{4-2\epsilon}} \Big\{ \frac{m_W^{-3-4\epsilon}}{6} \Big[\frac{1}{x_h^2} \Big(f_W + \frac{f_Z}{c_W^3} - \frac{2}{\alpha_2^2} \frac{m_W}{\pi M} \tilde{c}_H \Big) \\
&+ f_W \left[1 + \frac{1}{2(x_t+1)^2} \right] \Big] + \frac{f_Z m_Z^{-3-2\epsilon}}{16 c_W^4} \Big[(c_V^{(D)2} + c_A^{(D)2}) + \frac{1}{4}(c_V^{(U)2} + c_A^{(U)2}) \Big[\frac{8}{3} \\
&+ \frac{32 y_t^6 (8y_t^2 - 7)}{(4y_t^2-1)^{7/2}} \arctan(\sqrt{4y_t^2-1}) - \pi y_t + \frac{4(48y_t^6 - 2y_t^4 + 9y_t^2 - 1)}{3(4y_t^2-1)^3} \Big] \\
&+ \frac{1}{4}(c_V^{(U)2} - c_A^{(U)2}) \Big[3\pi y_t - \frac{4(144y_t^6 - 70y_t^4 + 9y_t^2 - 2)}{3(4y_t^2-1)^3} \\
&- \frac{32 y_t^4 (24y_t^4 - 21y_t^2 + 5)}{(4y_t^2-1)^{7/2}} \arctan(\sqrt{4y_t^2-1}) \Big] \Big] + O(\epsilon) \Big\}, \qquad (2.140)\\
c_U^{(2)} = {}& \frac{\pi\Gamma(1+\epsilon) g_2^4}{(4\pi)^{2-\epsilon}} \Big\{ \Big[f_W m_W^{-3-2\epsilon} + \frac{f_Z m_Z^{-3-2\epsilon}}{2c_W^4} (c_V^{(U)2} + c_A^{(U)2}) \Big] \Big[\frac{1}{3} + (\frac{11}{9} - \frac{2}{3}\log 2)\epsilon \Big] \\
&- \frac{f_Z m_Z^{-3-2\epsilon}}{4c_W^4} (c_V^{(U)2} + c_A^{(U)2}) \frac{m_Z}{\pi M} - \frac{f_W m_W}{2\pi M} m_W^{-3-2\epsilon} + O(\epsilon^2) \Big\}, \qquad (2.141)\\
c_D^{(2)} = {}& \frac{\pi\Gamma(1+\epsilon) g_2^4}{(4\pi)^{2-\epsilon}} \Big\{ \Big[f_W m_W^{-3-2\epsilon} + \frac{f_Z m_Z^{-3-2\epsilon}}{2c_W^4} (c_V^{(D)2} + c_A^{(D)2}) \Big] \Big[\frac{1}{3} + (\frac{11}{9} - \frac{2}{3}\log 2)\epsilon \Big] \\
&- \frac{f_W m_W}{2\pi M} m_W^{-3-2\epsilon} - \frac{f_Z m_Z^{-3-2\epsilon}}{4c_W^4} (c_V^{(D)2} + c_A^{(D)2}) \frac{m_Z}{\pi M} \\
&+ \delta_{Db} \frac{f_W m_W^{-3-2\epsilon}}{2} \Big[\frac{3x_t+2}{3(x_t+1)^3} - \frac{2}{3} - \frac{m_W}{\pi M} \frac{x_t^2(1 - x_t^4 + 4x_t^2 \log x_t)}{(x_t^2-1)^3} \\
&+ \Big(\frac{2x_t(7x_t^2-3)}{3(x_t^2-1)^3} \log x_t - \frac{2(3x_t+2)}{3(x_t+1)^3} \log 2 - \frac{2(25x_t^2 - 2x_t - 11)}{9(x_t^2-1)^2(x_t+1)} - \frac{22}{9} + \frac{4}{3}\log 2 \\
&- \frac{m_W}{\pi M} \frac{2x_t^2(1 - x_t^2 + 2x_t^2 \log x_t - 2x_t^2 (\log x_t)^2)}{(x_t^2-1)^3} \Big) \epsilon \Big] + O(\epsilon^2) \Big\}, \qquad (2.142)\\
c_g^{(2)} = {}& \frac{\pi[\Gamma(1+\epsilon)]^2 g_2^4 g_s^2}{(4\pi)^{4-2\epsilon}} \Big\{ \frac{f_W m_W^{-3-4\epsilon}}{2} \Big[- \frac{16}{9\epsilon} - \frac{284}{27} + \frac{32}{9}\log 2 - \frac{2(3x_t+2)}{9(x_t+1)^3} \frac{1}{\epsilon} \\
&+ \frac{8(6x_t^8 - 18x_t^6 + 21x_t^4 - 3x_t^2 - 2)}{9(x_t^2-1)^3} \log(x_t+1) \\
&+ \frac{4(3x_t^4 - 21x_t^3 + 3x_t^2 + 9x_t - 2)}{9(x_t^2-1)^3} \log 2 \\
&- \frac{4(12x_t^8 - 36x_t^6 + 39x_t^4 + 14x_t^3 - 9x_t^2 - 6x_t - 2)}{9(x_t^2-1)^3} \log x_t \\
&- \frac{144x_t^6 + 72x_t^5 - 312x_t^4 - 105x_t^3 - 40x_t^2 + 47x_t + 98}{27(x_t^2-1)^2(x_t+1)} \Big] \\
&+ \frac{f_Z m_Z^{-3-2\epsilon}}{16 c_W^4} \Big[\Big[2(c_V^{(U)2} + c_A^{(U)2}) + 3(c_V^{(D)2} + c_A^{(D)2}) \Big] \Big[- \frac{16}{9\epsilon} - \frac{284}{27} + \frac{32}{9}\log 2 \Big]
\end{aligned}
$$

$$
\begin{aligned}
&+ (c_V^{(U)2} + c_A^{(U)2})\Big[\frac{32(24y_t^8 - 21y_t^6 - 4y_t^4 + 5y_t^2 - 1)}{9(4y_t^2-1)^{7/2}} \arctan(\sqrt{4y_t^2-1}) \\
&- \frac{\pi y_t}{3} + \frac{4(48y_t^6 + 62y_t^4 - 47y_t^2 + 9)}{9(4y_t^2-1)^3}\Big] \\
&+ (c_V^{(U)2} - c_A^{(U)2})\Big[\frac{4y_t^2(624y_t^4 - 538y_t^2 + 103)}{9(4y_t^2-1)^3} - \frac{13\pi y_t}{3} \\
&+ \frac{32y_t^2(104y_t^6 - 91y_t^4 + 35y_t^2 - 5)}{3(4y_t^2-1)^{7/2}} \arctan(\sqrt{4y_t^2-1})\Big]\Big] \\
&+ 2f_W m_W^{-3-4\epsilon}\frac{m_W}{\pi M}\Big[N_l\Big(\frac{4}{3\epsilon} - \frac{1}{3}\Big) + \frac{2(-1 + 4x_t^2 - 3x_t^4 + 4x_t^4 \log x_t)}{3(x_t^2-1)^3}\frac{1}{\epsilon} \\
&+ \frac{-1 + 3x_t^2 - 8x_t^4}{3(x_t^2-1)^2} + \frac{4}{9}\pi^2 x_t^2 + \frac{16}{3}x_t^2(\log x_t)^2 \\
&- \frac{4}{3}\frac{(1 + 6x_t^2 - 18x_t^4 + 4x_t^6)\log x_t}{(x_t^2-1)^3} + \frac{8x_t^2}{3}(-1 + 4x_t^2 - 3x_t^4 + x_t^6)\mathrm{Li}_2(1 - x_t^2)\Big] \\
&+ f_Z \frac{m_Z^{-3-4\epsilon}}{24c_W^4}\frac{m_Z}{\pi M}\Big[\Big[2(c_V^{(U)2} + c_A^{(U)2}) + 3(c_V^{(D)2} + c_A^{(D)2})\Big]\Big(\frac{4}{\epsilon} - 1\Big) \\
&- (c_V^{(U)2} + c_A^{(U)2})\Big[\frac{1 - 18y_t^2 + 36y_t^4}{(4y_t^2-1)^2} + \frac{8(1 - 4y_t^2 + 3y_t^4 + 18y_t^6)\log y_t}{(4y_t^2-1)^3} \\
&+ \frac{16y_t^2(2 - 13y_t^2 + 32y_t^4 - 18y_t^6)}{(4y_t^2-1)^{7/2}}\Big[2\arctan\Big(\frac{1}{\sqrt{4y_t^2-1}}\Big)\log y_t \\
&- \mathrm{ImLi}_2\Big(\frac{1 - i\sqrt{4y_t^2-1}}{2y_t^2}\Big)\Big]\Big] \\
&+ 4y_t^2(c_V^{(U)2} - c_A^{(U)2})\Big[-\frac{8 - 59y_t^2 + 108y_t^4}{(4y_t^2-1)^3} - \frac{(29 - 128y_t^2 + 108y_t^4)\log y_t}{(4y_t^2-1)^3} \\
&+ \frac{2(-7 + 38y_t^2 - 82y_t^4 + 108y_t^6)}{(4y_t^2-1)^{7/2}}\Big[2\arctan\Big(\frac{1}{\sqrt{4y_t^2-1}}\Big)\log y_t \\
&- \mathrm{ImLi}_2\Big(\frac{1 - i\sqrt{4y_t^2-1}}{2y_t^2}\Big)\Big]\Big]\Big] + O(\epsilon)\Big\}\,. \qquad (2.143)
\end{aligned}
$$

2.5 Renormalization

The quark and gluon operators will mix through renormalization, and operators belonging to the same spin class will remain closed in that class under renormalization. We review their renormalization and running following procedures in Ref. [73]. For an operator $O_i^{(S)}$ with Wilson coefficient $c_i^{(S)}$ for a certain spin class, we have renormalization matrix $Z^{(S)}$ by

$$
O_i^{(S)\mathrm{bare}} = Z_{ij}^{(S)}(\mu) O_j^{(S)\mathrm{ren}}(\mu)\,, \quad c_i^{(S)\mathrm{ren}}(\mu) = Z_{ji}^{(S)}(\mu) c_j^{(S)\mathrm{bare}}\,, \qquad (2.144)
$$

where $S = 0$, 2 for our purpose here.

We work out the renormalization matrix Z_{ij} in the $\overline{\mathrm{MS}}$ scheme. For spin-0 operators, the renormalization factors can be obtained to all orders in perturbation theory

[118–120] and the result is

$$Z_{qq}^{(0)} = 1\,, \quad Z_{qg}^{(0)} = 0,$$
$$Z_{gq}^{(0)} = \frac{2\gamma_m}{\epsilon}\,, \quad Z_{gg}^{(0)} = 1 - \frac{\beta}{g\epsilon}\,, \tag{2.145}$$

where $\gamma_m = d\log m_q/d\log\mu$ is the anomalous dimension of quark mass, $\beta = dg/d\log\mu$ is the QCD beta function, and detailed perturbative expansion in α_s series are in Appendix B.

Let us compute the spin-2 operators renormalization to 1-loop order.

The quark self-energy diagram result is

$$\begin{aligned} -i\Sigma_2(p) &= \int \frac{d^dL}{(2\pi)^d} igt^a\gamma^\mu \frac{i}{\not{L} - m_q} igt^a\gamma^\nu \frac{-ig_{\mu\nu}}{(p-L)^2} \\ &= \frac{-ig^2C_2(r)}{(4\pi)^{2-\epsilon}}\frac{1}{\epsilon}\int_0^1 dx\left[(1-x)^2m_q^2\right]^{-\epsilon}\left[(2-d)x\not{p} + dm_q\right]\,, \end{aligned} \tag{2.146}$$

where $C_2(r) = 4/3$ for SU(3) .

The quark field strength renormalization factor is

$$Z_q = 1 + \left.\frac{d\Sigma_2(p)}{d\not{p}}\right|_{\not{p}=m_q} = 1 - C_2(r)\frac{g^2}{(4\pi)^2}\frac{1}{\epsilon}\,. \tag{2.147}$$

We use background-field method for gluons and the gluon field strength renormalization factor is

$$Z_A = 1 + \frac{g^2}{(4\pi)^2}\frac{1}{\epsilon}\left[\frac{11}{3}C_2(G) - \frac{4}{3}n_fC(r)\right]\,, \tag{2.148}$$

where $C_2(G) = 3$ and $C(r) = 1/2$ for SU(3) .

Before we compute the spin-2 renormalization factor $Z_{qq}^{(2)}$, let us define a null vector Y for convenience and we compute the scalar quantity $Y_\mu Y_\nu O_i^{(2)\mu\nu}$ instead of the direct tensor quantity $O_i^{(2)\mu\nu}$ for renormalization of spin-2 operators.

The diagrams contributing to renormalization factor $Z_{qq}^{(2)}$ are shown in Fig. 2.9.

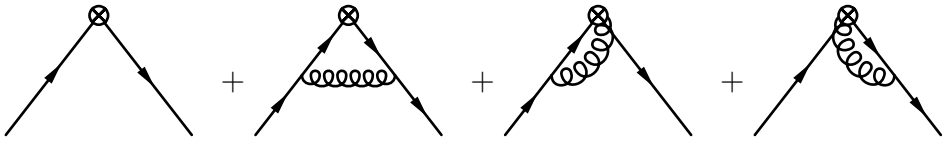

Figure 2.9: Diagrams contributing to renormalization factor $Z_{qq}^{(2)}$.

The first diagram in Fig. 2.9, i.e. $O_q^{(2)\mu\nu}$ contracted by $Y_\mu Y_\nu$ yields

$$Y_\mu Y_\nu \frac{1}{2}\bar{q}\left(\gamma^{\{\mu}iD_-^{\nu\}} - \frac{g^{\mu\nu}}{d}i\not{D}_-\right)q$$

$$= (\bar{q}(Y\cdot q)\not{Y}q)^{\rm bare}\,. \tag{2.149}$$

The second diagram in Fig. 2.9 multiplied with $Y_\mu Y_\nu$ is

$$\begin{aligned}&\int \frac{d^dp}{(2\pi)^d}\bar{q}igt^a\not{Y}Y^\alpha\frac{i}{\not{p}}ig\gamma_\alpha t^a\frac{-ig_{\mu\nu}}{(p-q)^2}q\\ &= C_2(r)\frac{g^2}{(4\pi)^2}\frac{1}{3\epsilon}(\bar{q}(Y\cdot q)\not{Y}q)^{\rm bare}\,.\end{aligned} \tag{2.150}$$

The sum of the third and fourth diagrams in Fig. 2.9 multiplied with $Y_\mu Y_\nu$ is

$$\begin{aligned}&2\int \frac{d^dp}{(2\pi)^d}\bar{q}igt^a\gamma^\mu\frac{i}{\not{p}}(Y\cdot p)\not{Y}\frac{i}{\not{p}}igt^a\gamma_\mu\frac{-ig_{\mu\nu}}{(p-q)^2}q\\ &= -C_2(r)\frac{g^2}{(4\pi)^2}\frac{2}{\epsilon}(\bar{q}(Y\cdot q)\not{Y}q)^{\rm bare}\,.\end{aligned} \tag{2.151}$$

Thus, we have

$$\begin{aligned}Z_{qq}^{(2)} &= Z_q\left[1+\left(\frac{1}{3}-2\right)C_2(r)\frac{g^2}{(4\pi)^2}\frac{1}{\epsilon}\right]\\ &= 1-\frac{8}{3}C_2(r)\frac{g^2}{(4\pi)^2}\frac{1}{\epsilon}\,.\end{aligned} \tag{2.152}$$

The diagram contributing to $Z_{gq}^{(2)}$ is shown in Fig. 2.10. The spin-2 operator $O_g^{(2)\mu\nu}$ contracted by $Y_\mu Y_\nu$ in momentum space is

$$\begin{aligned}Y_\mu Y_\nu O_g^{(2)\mu\nu} &= Y_\mu Y_\nu\left[-G^{a,\mu\alpha}G^{a,\nu\beta}g_{\alpha\beta}+\frac{1}{d}g^{\mu\nu}(G^a_{\rho\sigma})^2\right]\\ &= Y_\mu Y_\nu A^a_\alpha\Big[g^{\alpha\beta}k^\mu k^\nu-\frac{1}{2}\left(g^{\nu\alpha}k^\mu k^\beta+g^{\mu\beta}k^\alpha k^\nu\right)\\ &\quad-\frac{1}{2}\left(g^{\nu\beta}k^\mu k^\alpha+g^{\mu\alpha}k^\beta k^\nu\right)+\frac{k^2}{2}\left(g^{\mu\alpha}g^{\nu\beta}+g^{\mu\beta}g^{\nu\alpha}\right)\Big]A^a_\beta\\ &= -2A^a_\mu\left[g^{\mu\nu}\left(Y\cdot k\right)^2+k^2Y^\mu Y^\nu-\left(k^\mu Y^\nu+Y^\mu k^\nu\right)\left(Y\cdot k\right)\right]A^a_\nu\,.\end{aligned} \tag{2.153}$$

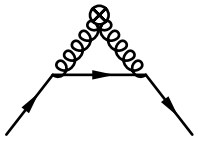

Figure 2.10: The diagram contributing to renormalization factor $Z_{gq}^{(2)}$.

The diagram in Fig. 2.10 is then evaluated as

$$\int\frac{d^dk}{(2\pi)^d}\bar{q}\Bigg\{igt^a\gamma_\mu\frac{i}{\not{q}-\not{k}-m_q}igt^a\gamma_\nu\left(\frac{-i}{k^2}\right)^2$$

$$\cdot(-2)\left[g^{\mu\nu}\left(Y\cdot k\right)^2+k^2Y^\mu Y^\nu-\left(k^\mu Y^\nu+Y^\mu k^\nu\right)\left(Y\cdot k\right)\right]\Bigg\}q$$
$$=\frac{8}{3}C_2(r)\frac{g^2}{(4\pi)^2}\frac{1}{\epsilon}(\bar{q}(Y\cdot q)\not{Y}q)^{\rm bare}\,. \tag{2.154}$$

Thus, combing with Z_q, we obtain

$$Z_{gq}^{(2)}=\frac{8}{3}C_2(r)\frac{g^2}{(4\pi)^2}\frac{1}{\epsilon}\,. \tag{2.155}$$

The diagrams contributing to $Z_{qg}^{(2)}$ are shown in Fig. 2.11. Their sum yields

$$-\int\frac{d^dk}{(2\pi)^d}A_\mu^a{\rm Tr}\left[\left(igt^a\gamma^\mu\frac{i}{\not q+\not k}igt^b\gamma^\nu+igt^b\gamma^\nu\frac{i}{-\not q+\not k}igt^a\gamma^\mu\right)\frac{i}{\not k}\not{Y}(Y\cdot k)\frac{i}{\not k}\right]A_\nu^b$$
$$=\frac{4}{3}C(r)\frac{g^2}{(4\pi)^2}\frac{1}{\epsilon}A_\mu^a\left[-2g^{\mu\nu}\left(Y\cdot k\right)^2-2k^2Y^\mu Y^\nu+2\left(k^\mu Y^\nu+Y^\mu k^\nu\right)\left(Y\cdot k\right)\right]A_\nu^a\,. \tag{2.156}$$

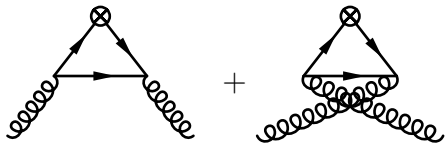

Figure 2.11: Diagrams contributing to renormalization factor $Z_{qg}^{(2)}$.

Thus, we obtain

$$Z_{qg}^{(2)}=\frac{4}{3}C(r)\frac{g^2}{(4\pi)^2}\frac{1}{\epsilon}\,. \tag{2.157}$$

We compute the diagrams in Fig. 2.12 to derive the renormalization factor $Z_{gg}^{(2)}$.

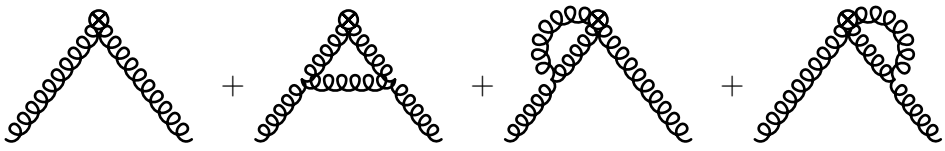

Figure 2.12: Diagrams contributing to renormalization factor $Z_{gg}^{(2)}$.

The fist diagram in Fig. 2.12 contracted by $Y_\mu Y_\nu$ has been calculated in Eq. (2.153).

Table 2.1: Renormalization factors for quark and gluon operators.

Operator	Renormalization factors
$O_q^{(0)},\ O_g^{(0)}$	$Z_{qq'}^{(0)} = \delta_{qq'}\,, \quad Z_{qg}^{(0)} = 0\,,$ $Z_{gq}^{(0)} = \frac{2\gamma_m}{\epsilon}\,, \quad Z_{gg}^{(0)} = 1 - \frac{\beta}{g\epsilon}\,.$
$O_q^{(2)},\ O_g^{(2)}$	$Z_{qq'}^{(2)} = \left(1 - \frac{\alpha_s}{4\pi}\frac{32}{9\epsilon}\right)\delta_{qq'} + O(\alpha_s^2)\,, \quad Z_{qg}^{(2)} = \frac{\alpha_s}{4\pi}\frac{2}{3\epsilon} + O(\alpha_s^2)\,,$ $Z_{gq}^{(2)} = \frac{\alpha_s}{4\pi}\frac{32}{9\epsilon} + O(\alpha_s^2)\,, \quad Z_{gg}^{(2)} = 1 - \frac{\alpha_s}{4\pi}\frac{2n_f}{3\epsilon} + O(\alpha_s^2)\,.$

Employing background-field Feynman rules, the second diagram in Fig. 2.12 yields

$$2C_2(G)\frac{g^2}{(4\pi)^2}\frac{1}{\epsilon}A_\mu^a\left[-\frac{7}{3}g^{\mu\nu}\left(Y\cdot k\right)^2 - \frac{5}{3}k^2Y^\mu Y^\nu + 2\left(k^\mu Y^\nu + Y^\mu k^\nu\right)\left(Y\cdot k\right)\right]A_\nu^a\,. \tag{2.158}$$

The sum of the third and fourth diagram is

$$2C_2(G)\frac{g^2}{(4\pi)^2}\frac{1}{\epsilon}A_\mu^a\left[6g^{\mu\nu}\left(Y\cdot k\right)^2 + \frac{16}{3}k^2Y^\mu Y^\nu - \frac{17}{3}\left(k^\mu Y^\nu + Y^\mu k^\nu\right)\left(Y\cdot k\right)\right]A_\nu^a\,. \tag{2.159}$$

Thus, combining with the gluon Z_A factor Eq. (2.148), the sum of all diagrams in Fig. 2.12 gives the renormalization factor

$$\begin{aligned} Z_{gg}^{(2)} &= \left[1 - \frac{11}{3}C_2(G)\frac{g^2}{(4\pi)^2}\frac{1}{\epsilon}\right]Z_A \\ &= 1 - \frac{4}{3}n_f C(r)\frac{g^2}{(4\pi)^2}\frac{1}{\epsilon}\,. \end{aligned} \tag{2.160}$$

Now we have all the Z factors from Eq. (2.145), Eq. (2.152), Eq. (2.157), Eq. (2.155) and Eq. (2.160) for spin-0 and spin-2 operators in Eq. (2.144), and we list them in Table 2.1.

The renormalized Wilson coefficients for the quark and gluon operators are given by Eq. (2.144), plugging the renormalization factors in Table 2.1 and we obtain

$$\begin{aligned} c_q^{(0)\mathrm{ren}}(\mu) &= c_q^{(0)\mathrm{bare}} + O(\alpha_s^2)\,, \\ c_g^{(0)\mathrm{ren}}(\mu) &= c_g^{(0)\mathrm{bare}} + O(\alpha_s^2)\,, \\ c_q^{(2)\mathrm{ren}}(\mu) &= c_q^{(2)\mathrm{bare}} + O(\alpha_s)\,, \end{aligned}$$

$$c_g^{(2)\mathrm{ren}}(\mu) = \sum_q \frac{1}{\epsilon}\frac{\alpha_s}{6\pi} c_q^{(2)\mathrm{bare}} + c_g^{(2)\mathrm{bare}} + O(\alpha_s^2)\,. \tag{2.161}$$

Explicitly, the renormalized Wilson coefficients are

$$\begin{aligned}
\hat{c}_U^{(0)}(\mu) &= -\frac{1}{2x_h^2}\left(f_W + \frac{f_Z}{c_W^3}\right) + \frac{f_Z}{8c_W}(c_V^{(U)2} - c_A^{(U)2}) - \frac{m_W}{\pi M}\frac{\tilde{c}_H}{\alpha_2^2 x_h^2}\,,\\
\hat{c}_D^{(0)}(\mu) &= -\frac{1}{2x_h^2}\left(f_W + \frac{f_Z}{c_W^3}\right) + \frac{f_Z}{8c_W}(c_V^{(D)2} - c_A^{(D)2}) - \delta_{Db} f_W \frac{x_t}{8(x_t+1)^3} - \frac{m_W}{\pi M}\frac{\tilde{c}_H}{\alpha_2^2 x_h^2}\,,\\
\hat{c}_g^{(0)}(\mu) &= \frac{\alpha_s(\mu)}{4\pi}\Bigg\{\frac{1}{6}\Bigg[\frac{1}{x_h^2}\Big(f_W + \frac{f_Z}{c_W^3}\Big) + f_W\left[\frac{N_l}{2} + \frac{1}{2(x_t+1)^2}\right]\Bigg] + \frac{m_W}{\pi M}\frac{\tilde{c}_H}{3\alpha_2^2 x_h^2}\\
&\quad + \frac{f_Z}{16c_W}\Bigg[(c_V^{(D)2} + c_A^{(D)2}) + \frac{1}{4}(c_V^{(U)2} + c_A^{(U)2})\Big[\frac{4(48y_t^6 - 2y_t^4 + 9y_t^2 - 1)}{3(4y_t^2-1)^3}\\
&\quad + \frac{8}{3} - \pi y_t + \frac{32y_t^6(8y_t^2-7)}{(4y_t^2-1)^{7/2}}\arctan(\sqrt{4y_t^2-1})\Big] + \frac{1}{4}(c_V^{(U)2} - c_A^{(U)2})\Big[3\pi y_t\\
&\quad - \frac{32y_t^4(24y_t^4 - 21y_t^2 + 5)}{(4y_t^2-1)^{7/2}}\arctan(\sqrt{4y_t^2-1})\\
&\quad - \frac{4(144y_t^6 - 70y_t^4 + 9y_t^2 - 2)}{3(4y_t^2-1)^3}\Big]\Bigg]\Bigg\}\,,\\
\hat{c}_U^{(2)}(\mu) &= \frac{f_W}{3} + \frac{f_Z}{6c_W}(c_V^{(U)2} + c_A^{(U)2}) - \frac{f_Z}{4c_W^2}(c_V^{(U)2} + c_A^{(U)2})\frac{m_W}{\pi M} - f_W\frac{m_W}{2\pi M}\,,\\
\hat{c}_D^{(2)}(\mu) &= \frac{f_W}{3} + \frac{f_Z}{6c_W}(c_V^{(D)2} + c_A^{(D)2}) - \frac{f_Z}{4c_W^2}(c_V^{(D)2} + c_A^{(D)2})\frac{m_W}{\pi M} - f_W\frac{m_W}{2\pi M}\\
&\quad + f_W\frac{\delta_{Db}}{2}\Big[\frac{3x_t+2}{3(x_t+1)^3} - \frac{2}{3} - \frac{m_W}{\pi M}\frac{x_t^2(1 - x_t^4 + 4x_t^2\log x_t)}{(x_t^2-1)^3}\Big]\,,\\
\hat{c}_g^{(2)}(\mu) &= \frac{\alpha_s(\mu)}{4\pi}\Bigg\{2f_W\Bigg[N_\ell\left(-\frac{4}{9}\log\frac{\mu}{m_W} - \frac{1}{2}\right) - \frac{(2+3x_t)}{9(1+x_t)^3}\log\frac{\mu}{m_W(1+x_t)}\\
&\quad - \frac{(12x_t^5 - 36x_t^4 + 36x_t^3 - 12x_t^2 + 3x_t - 2)}{9(x_t-1)^3}\log\frac{x_t}{1+x_t}\\
&\quad - \frac{2x_t(-3+7x_t^2)}{9(x_t^2-1)^3}\log 2 - \frac{48x_t^6 + 24x_t^5 - 104x_t^4 - 35x_t^3 + 20x_t^2 + 13x_t + 18}{36(x_t^2-1)^2(1+x_t)}\Bigg]\\
&\quad + f_W\frac{m_W}{2\pi M}\Bigg[N_\ell\left(\frac{8}{3}\log\frac{\mu}{m_W} - \frac{1}{3}\right) + \frac{16x_t^4}{3(x_t^2-1)^3}\log x_t\log\frac{\mu}{m_W}\\
&\quad - \frac{4(3x_t^2-1)}{3(x_t^2-1)^2}\log\frac{\mu}{m_W} + \frac{16x_t^2}{3}\log^2 x_t - \frac{4(4x_t^6 - 16x_t^4 + 6x_t^2 + 1)}{3(x_t^2-1)^3}\log x_t\\
&\quad + \frac{8x_t^2(x_t^6 - 3x_t^4 + 4x_t^2 - 1)}{3(x_t^2-1)^3}\mathrm{Li}_2(1-x_t^2) + \frac{4\pi^2 x_t^2}{9} - \frac{8x_t^4 - 7x_t^2 + 1}{3(x_t^2-1)^2}\Bigg]\\
&\quad + \frac{f_Z}{16c_W}\Bigg[\Big[2(c_V^{(U)2} + c_A^{(U)2}) + 3(c_V^{(D)2} + c_A^{(D)2})\Big]\Big[-\frac{32}{9}\log\frac{\mu}{m_Z} - 4\Big]\\
&\quad + (c_V^{(U)2} + c_A^{(U)2})\Big[\frac{32(24y_t^8 - 21y_t^6 - 4y_t^4 + 5y_t^2 - 1)}{9(4y_t^2-1)^{7/2}}\arctan(\sqrt{4y_t^2-1})
\end{aligned}$$

$$
\begin{aligned}
&- \frac{\pi y_t}{3} + \frac{4(48y_t^6 + 62y_t^4 - 47y_t^2 + 9)}{9(4y_t^2-1)^3}\Big] \\
&+ (c_V^{(U)2} - c_A^{(U)2})\Big[\frac{4y_t^2(624y_t^4 - 538y_t^2 + 103)}{9(4y_t^2-1)^3} \\
&- \frac{13\pi y_t}{3} + \frac{32y_t^2(104y_t^6 - 91y_t^4 + 35y_t^2 - 5)}{3(4y_t^2-1)^{7/2}} \arctan(\sqrt{4y_t^2-1})\Big]\Big] \\
&+ \frac{f_Z}{24c_W^2}\frac{m_W}{\pi M}\Big[\Big[2(c_V^{(U)2} + c_A^{(U)2}) + 3(c_V^{(D)2} + c_A^{(D)2})\Big]\Big(8\log\frac{\mu}{m_Z} - 1\Big) \\
&- (c_V^{(U)2} + c_A^{(U)2})\Big[\frac{1 - 18y_t^2 + 36y_t^4}{(4y_t^2-1)^2} + \frac{8(1 - 4y_t^2 + 3y_t^4 + 18y_t^6)\log y_t}{(4y_t^2-1)^3} \\
&+ \frac{16y_t^2(2 - 13y_t^2 + 32y_t^4 - 18y_t^6)}{(4y_t^2-1)^{7/2}}\Big[2\arctan\Big(\frac{1}{\sqrt{4y_t^2-1}}\Big)\log y_t \\
&- \mathrm{Im}\,\mathrm{Li}_2\Big(\frac{1 - i\sqrt{4y_t^2-1}}{2y_t^2}\Big)\Big]\Big] \\
&+ 4y_t^2(c_V^{(U)2} - c_A^{(U)2})\Big[-\frac{8 - 59y_t^2 + 108y_t^4}{(4y_t^2-1)^3} - \frac{(29 - 128y_t^2 + 108y_t^4)\log y_t}{(4y_t^2-1)^3} \\
&+ \frac{2(-7 + 38y_t^2 - 82y_t^4 + 108y_t^6)}{(4y_t^2-1)^{7/2}}\Big[2\arctan\Big(\frac{1}{\sqrt{4y_t^2-1}}\Big)\log y_t \\
&- \mathrm{Im}\,\mathrm{Li}_2\Big(\frac{1 - i\sqrt{4y_t^2-1}}{2y_t^2}\Big)\Big]\Big]\Big\}, \qquad (2.162)
\end{aligned}
$$

where the reduced coefficients $\hat{c}_i^{(S)}$ are given in terms of the original Wilson coefficients by $c_i^{(S)} \equiv (\pi\alpha_2^2/m_W^3)\hat{c}_i^{(S)}$, where $i = u, d, s, c, b, g$ is the index for quark or gluon and U denotes up-type while D denotes down-type. The strong coupling is denoted by $\alpha_s(\mu)$. The mass ratios are defined as $x_j \equiv m_j/m_W$ and $y_j \equiv m_j/m_Z$ where m_Z is the mass of Z^0 boson, and j is the index of the specific particle, e.g. $j = t$ stands for top quark, $j = h$ for Higgs boson. $\mathrm{Li}_2(z) \equiv \sum_{k=1}^{\infty} z^k/k^2$ is the dilogarithm function. $N_\ell = 2$ is the number of massless Standard Model generations. For electroweak scale matching, light quarks u, d, s, c, b are treated as massless. Also neglecting small corrections from $|V_{td}|^2$ and $|V_{ts}|^2$, u and c quarks have the same coefficients, as do d and s quarks. We note that our results obey the correct formal limit at small top quark mass $m_t \to 0$ for top quark and gluon coefficients relation c.f. Eq. (2.195) and Eq. (2.200):

$$
\begin{aligned}
c_g^{(0)}|_{m_t\to 0} &= c_{g,\,n_f=6}^{(0)} - \frac{\alpha_s}{12\pi}c_{t,\,n_f=6}^{(0)} + O(\alpha_s^2)\,, \\
c_g^{(2)}|_{m_t\to 0} &= c_{g,\,n_f=6}^{(2)} - \frac{\alpha_s}{3\pi}\log\frac{m_t}{\mu}c_{t,\,n_f=6}^{(2)} + O(\alpha_s^2)\,, \qquad (2.163)
\end{aligned}
$$

where $c_{t,\,n_f=6}^{(S)}$ denotes the massless 6-flavor top quark operator coefficient and $c_{g,\,n_f=6}^{(S)}$ for gluon operator coefficient, by setting $N_l = 3$ in Eq. (2.162) and treating top quark as massless in all the loop calculations. Explicitly the reduced 6-flavor coefficients

are

$$\begin{aligned}
\hat{c}^{(0)}_{g,\,n_f=6} &= \frac{\alpha_s(\mu)}{4\pi}\left[f_W\left(\frac{N_l}{2}\right)+\frac{f_Z}{16c_W}\left(c_V^{(D)2}+c_A^{(D)2}+c_V^{(U)2}+c_A^{(U)2}\right)\right],\\
\hat{c}^{(0)}_{t,\,n_f=6} &= -\frac{1}{2x_h^2}\left(f_W+\frac{f_Z}{c_W^3}\right)+\frac{f_Z}{8c_W}(c_V^{(U)2}-c_A^{(U)2})-\frac{m_W}{\pi M}\frac{\tilde{c}_H}{\alpha_2^2 x_h^2},\\
\hat{c}^{(2)}_{g,\,n_f=6} &= \frac{\alpha_s(\mu)}{4\pi}\left[2f_W N_l\left(-\frac{4}{9}\log\frac{\mu}{m_W}-\frac{1}{2}\right)+f_W\frac{m_W}{2\pi M}N_l\left(\frac{8}{3}\log\frac{\mu}{m_W}-\frac{1}{3}\right)\right.\\
&\quad+\frac{f_Z}{16c_W}\left[N_l(c_V^{(U)2}+c_A^{(U)2})+N_l(c_V^{(D)2}+c_A^{(D)2})\right]\left(-\frac{32}{9}\log\frac{\mu}{m_Z}-4\right)\\
&\quad\left.+\frac{f_Z}{24c_W^2}\frac{m_W}{\pi M}\left[N_l(c_V^{(U)2}+c_A^{(U)2})+N_l(c_V^{(D)2}+c_A^{(D)2})\right]\left(8\log\frac{\mu}{m_Z}-1\right)\right],\\
\hat{c}^{(2)}_{t,\,n_f=6} &= \frac{f_W}{3}+\frac{f_Z}{6c_W}(c_V^{(U)2}+c_A^{(U)2})-\frac{f_Z}{4c_W^2}(c_V^{(U)2}+c_A^{(U)2})\frac{m_W}{\pi M}-f_W\frac{m_W}{2\pi M},
\end{aligned}\tag{2.164}$$

where $N_l = 3$.

2.6 Renormalization Group Evolution

Now by taking scale derivatives of Eq. (2.144), we obtain the renormalizaiton group evolution equations in terms of anomalous dimension γ_{ij},

$$\frac{d}{d\log\mu}c_i(\mu) = \gamma_{ji}c_j(\mu)\,,\tag{2.165}$$

where

$$\gamma_{ij} = Z^{-1}_{ik}\frac{d}{d\log\mu}Z_{kj}\,.\tag{2.166}$$

In the $\overline{\rm MS}$ scheme, the anomalous dimension is given by taking coupling derivative of the coefficient of $1/\epsilon$ term in Z_{ij},

$$\gamma_{ij} = -g\frac{\partial}{\partial g}Z^{(1)}_{ij}\,,\quad Z_{ij} = \delta_{ij}+\sum_{n=1}^{\infty}\frac{Z^{(n)}_{ij}}{\epsilon^n}\,.\tag{2.167}$$

and we tabulate the results in Table 2.2.

Let us solve the renormalization group evolution equation Eq. (2.165), for spin-0 coefficients,

$$\frac{dc_q}{d\log\mu} = \gamma_{gq}c_g+\gamma_{qq}c_q = -2\gamma'_m c_g\,,\tag{2.168}$$

$$\frac{dc_g}{d\log\mu} = \gamma_{gg}c_g+\sum_q\gamma_{qg}c_q = \tilde{\beta}'c_g\,,\tag{2.169}$$

where we have defined $\gamma' \equiv \frac{\partial\gamma_m}{\partial\log g}$, $\tilde{\beta} = \beta/g$ and $\tilde{\beta}' \equiv \frac{\partial(\beta/g)}{\partial\log g}$.

Table 2.2: Anomalous dimensions for quark and gluon operators.

Operator	Anomalous dimension
$O_q^{(0)},\ O_g^{(0)}$	$\gamma_{qq'}^{(0)} = 0\,, \quad \gamma_{qg}^{(0)} = 0\,,$ $\gamma_{gq}^{(0)} = -2\frac{\partial\gamma_m}{\partial\log g}\,, \quad \gamma_{gg}^{(0)} = \frac{\partial(\beta/g)}{\partial\log g}\,.$
$O_q^{(2)},\ O_g^{(2)}$	$\gamma_{qq'}^{(2)} = \frac{\alpha_s}{4\pi}\frac{64}{9}\delta_{qq'} + O(\alpha_s^2)\,, \quad \gamma_{qg}^{(2)} = -\frac{\alpha_s}{4\pi}\frac{4}{3} + O(\alpha_s^2)\,,$ $\gamma_{gq}^{(2)} = -\frac{\alpha_s}{4\pi}\frac{64}{9} + O(\alpha_s^2)\,, \quad \gamma_{gg}^{(2)} = \frac{\alpha_s}{4\pi}\frac{4n_f}{3} + O(\alpha_s^2)\,.$

Eq. (2.169) yields

$$\begin{aligned}
\int \frac{dc_g}{c_g} &= \int \frac{d\tilde{\beta}}{d\log g} d\log\mu = \int \frac{\partial\tilde{\beta}}{\partial\log\mu}\frac{\partial\log\mu}{\partial\log g} d\log\mu\,, \\
\Rightarrow \int d\log c_g &= \int \frac{\partial\tilde{\beta}}{\partial\log\mu}\frac{1}{\tilde{\beta}} d\log\mu = \int \log\tilde{\beta}\,, \\
\Rightarrow c_g(\mu_l) &= \frac{\tilde{\beta}(\mu_l)}{\tilde{\beta}(\mu_h)} c_g(\mu_h)\,.
\end{aligned} \tag{2.170}$$

Eq. (2.168) yields

$$\begin{aligned}
\int dc_q &= \int -2\gamma_m' c_g d\log\mu \\
&= \int -2\frac{\partial\gamma_m}{\partial\log\mu}\frac{c_g}{\tilde{\beta}} d\log\mu \\
&= \frac{c_g(\mu_h)}{\tilde{\beta}(\mu_h)} \int -2\frac{\partial\gamma_m}{\partial\log\mu} d\log\mu \\
\Rightarrow c_q(\mu_l) &= c_q(\mu_h) - 2\frac{c_g(\mu_h)}{\tilde{\beta}(\mu_h)}\left[\gamma_m(\mu_l) - \gamma_m(\mu_h)\right]\,.
\end{aligned} \tag{2.171}$$

For spin-2 coefficients,

$$\frac{dc_q}{d\log\mu} = \gamma_{gq}c_g + \gamma_{qq}c_q = -\frac{64}{9}\frac{\alpha_s}{4\pi}c_g + \frac{64}{9}\frac{\alpha_s}{4\pi}c_q\,, \tag{2.172}$$

$$\frac{dc_g}{d\log\mu} = \gamma_{gg}c_g + \sum_q \gamma_{qg}c_q = \frac{4}{3}n_f\frac{\alpha_s}{4\pi}c_g - \frac{4}{3}\frac{\alpha_s}{4\pi}\sum_q c_q\,. \tag{2.173}$$

Summing over all flavors of quarks on both sides of Eq. (2.172) and combining with Eq. (2.173), we obtain

$$\sum_q \frac{dc_q}{d\log\mu} + \frac{16}{3}\frac{dc_g}{d\log\mu} = 0\,. \tag{2.174}$$

Take derivative of $d/d\log\mu$ on both sides of Eq. (2.173), plug in Eq. (2.174) and we obtain

$$\frac{d^2c_g}{d\log\mu^2} = \frac{4}{3}(n_f c_g - \sum_q c_q)\frac{d\alpha_s/4\pi}{d\log\mu} + \left(\frac{4}{3}n_f + \frac{64}{9}\right)\frac{\alpha_s}{4\pi}\frac{dc_g}{d\log\mu}\,. \tag{2.175}$$

Let us denote $dc_g/d\log\mu$ by shorthand notation $f_t(\mu)$ and we solve Eq. (2.175) obtaining

$$\int \frac{df_t(\mu)}{f_t(\mu)} = \int \left[\frac{1}{\alpha_s}\frac{d\alpha_s}{d\log\mu} + \left(\frac{4}{3}n_f + \frac{64}{9}\right)\frac{\alpha_s}{4\pi}\right] d\log\mu\,, \tag{2.176}$$

where

$$\frac{d\alpha_s}{d\log\mu} = \frac{2gdg}{d\log\mu} = 2g\beta = -2\beta_0\alpha_s^2 \Rightarrow \qquad \alpha_s = -\frac{1}{2\beta_0}\frac{d\log\alpha_s}{d\log\mu}\,. \tag{2.177}$$

Plug Eq. (2.177) into Eq. (2.176), and we obtain

$$\log\frac{f_t(\mu_l)}{f_t(\mu_h)} = \left[1 - \frac{1}{2\beta_0}\left(\frac{4}{3}n_f + \frac{64}{9}\right)\right]\log\frac{\alpha_s(\mu_l)}{\alpha_s(\mu_h)}\,. \tag{2.178}$$

Thus, we get

$$\frac{\frac{4}{3}\frac{\alpha_s(\mu_l)}{4\pi}[n_f c_g(\mu_l) - \sum_q c_q(\mu_l)]}{\frac{4}{3}\frac{\alpha_s(\mu_h)}{4\pi}[n_f c_g(\mu_h) - \sum_q c_q(\mu_h)]} = \left[\frac{\alpha_s(\mu_l)}{\alpha_s(\mu_h)}\right]^{1-\frac{1}{2\beta_0}\left(\frac{4}{3}n_f+\frac{64}{9}\right)}\,. \tag{2.179}$$

Combining Eq. (2.179) with solution of Eq. (2.174)

$$\sum_q [c_q(\mu_l) - c_q(\mu_h)] + \frac{16}{3}[c_g(\mu_l) - c_g(\mu_h)] = 0\,, \tag{2.180}$$

we obtain

$$c_q(\mu_l) = \frac{3n_f + 16r(n_f)}{3n_f + 16}c_q(\mu_h) + \frac{16n_f(1-r(n_f))}{16+3n_f}c_g(\mu_h)\,, \tag{2.181}$$

$$c_g(\mu_l) = \frac{3(1-r(n_f))}{3n_f + 16}c_q(\mu_h) + \frac{2n_f r(n_f) + 16}{16+3n_f}c_g(\mu_h)\,, \tag{2.182}$$

where function $r(t) \equiv (\alpha_s(\mu_l)/\alpha_s(\mu_h))^{-\frac{1}{\beta_0}\left(\frac{32}{9}+\frac{2}{3}t\right)}$.

Table 2.3: Renormalization group evolution equation solutions, where $\tilde{\beta} \equiv \beta/g$ and function $r(t) = (\alpha_s(\mu_l)/\alpha_s(\mu_h))^{-\frac{1}{\beta_0}\left(\frac{32}{9}+\frac{2}{3}t\right)}$.

Operator	RG running matrix
$O_q^{(0)},\ O_g^{(0)}$	$R^{(0)}_{qq'} = \delta_{qq'}, \quad R^{(0)}_{qg} = \frac{2}{\tilde{\beta}(\mu_h)}\left[\gamma_m(\mu_h) - \gamma_m(\mu_l)\right],$ $R^{(0)}_{gq} = 0, \quad R^{(0)}_{gg} = \frac{\tilde{\beta}(\mu_l)}{\tilde{\beta}(\mu_h)}.$
$O_q^{(2)},\ O_g^{(2)}$	$R^{(2)}_{qq'} = \frac{1}{n_f}\left[\frac{16r(n_f)+3n_f}{16+3n_f} - r(0)\right] + r(0)\delta_{qq'} + O(\alpha_s^2),$ $R^{(2)}_{qg} = \frac{16\left[1-r(n_f)\right]}{16+3n_f} + O(\alpha_s^2),$ $R^{(2)}_{gq} = \frac{3\left[1-r(n_f)\right]}{16+3n_f} + O(\alpha_s^2), \quad R^{(2)}_{gg} = \frac{16+3n_f r(n_f)}{16+3n_f} + O(\alpha_s^2).$

Thus, we obtain the relation between high-scale μ_h and low-scale μ_l Wilson coefficients

$$c_i(\mu_l) = R_{ij}(\mu_l, \mu_h) c_j(\mu_h), \tag{2.183}$$

and the results are listed in Table 2.3.

In order to make predictions about the low-energy dark matter direct detection experiments, we need to evolve and match the 5-flavor quark and gluon effective field theory with Wilson coefficients Eq. (2.162) at weak scale to another effective field theory at a lower energy. At a first step, We evolve the Wilson coefficients Eq. (2.162) from weak scale about top-quark mass scale $\sim \mu_t$ to the next lower scale about bottom-quark mass scale $\sim \mu_b$ by the running matrix R in Eq. (2.183).

2.7 Heavy Quark Threshold Matching

Now we are at the bottom-quark mass scale with an effective field theory consisting of only quarks and gluons. For the WIMP-nucleus spin-independent scattering, we could simplify the picture by considering the coherent contribution of WIMP-nulceon scattering and leave the nucleus effect discussion to Section. 2.9. Each nucleon could be treated as a combination of light quarks and gluon. We consider the light quarks to be u, d, s three flavors and integrate out the heavy quarks c and b, thus eventually we match the 5-flavor quarks and gluon effective theory to a 3-flavor quarks and gluon effective theory.

When we integrate out a heavy quark with mass m_Q in an (n_f+1)-flavor to an n_f-flavor theory, we do the following matching

$$\sum_{q=q_1}^{q_{n_f+1}} c_q^{\prime(S)}\langle O_q^{\prime(S)}\rangle + c_g^{\prime(S)}\langle O_g^{\prime(S)}\rangle = \sum_{q=q_1}^{q_{n_f}} c_q^{(S)}\langle O_q^{(S)}\rangle + c_g^{(S)}\langle O_g^{(S)}\rangle + O(\frac{1}{m_Q})\,, \quad (2.184)$$

where the bracket $\langle ...\rangle$ represents taking matrix elements over a nucleon state $|N\rangle$.

We can find a solution to Eq. (2.184), expressing n_f-flavor theory in terms of (n_f+1)-flavor theory at the matching scale μ_Q,

$$c_i^{(S)}(\mu_Q) = M_{ij}^{(S)}(\mu_Q)c_j^{\prime(S)}(\mu_Q)\,, \quad \langle O_i^{\prime(S)}(\mu_Q)\rangle = M_{ji}^{(S)}(\mu_Q)\langle O_j^{(S)}(\mu_Q)\rangle\,, \quad (2.185)$$

where $i = q_1, ..., q_{n_f}, g$ and $j = q_1, ..., q_{n_f+1}, g$, so M is an $(n_f+1)\times(n_f+2)$ matrix.

The matrix elements $\langle O_i^{(S)}\rangle$ are constrained by sum rules of QCD energy-momentum tensor $T^{\mu\nu}$. By Noether's theorem, we can derive the energy-momentum tensor,

$$\begin{aligned} T^{\mu\nu} = &\sum_q \frac{1}{2}\bar{q}\gamma^{\{\mu}iD_-^{\nu\}}q - G^{A\,\mu\lambda}G^{A\,\nu}{}_{\lambda} \\ &- g^{\mu\nu}\left[\sum_q \bar{q}\left(\frac{i}{2}\not{D}_- - m_q\right)q - \frac{1}{4}G^A_{\alpha\beta}G^{A\,\alpha\beta}\right]\,, \end{aligned} \quad (2.186)$$

and

$$\begin{aligned} \langle T^{\mu\nu}\rangle = &g^{\mu\nu}\left[\sum_q \frac{1}{d}\langle O_q^{(0)}\rangle + \left(\frac{1}{4}-\frac{1}{d}\right)\langle O_g^{(0)}\rangle\right] \\ &+ \sum_q \langle O_q^{(2)\mu\nu}\rangle + \langle O_g^{(2)\mu\nu}\rangle. \end{aligned} \quad (2.187)$$

Particularly, after renormalization of Eq. (2.187), the trace of energy-momentum tensor constrains the spin-0 matrix elements as

$$\langle T_\mu^\mu\rangle = \sum_q (1-\gamma_m)\langle O_q^{(0)}\rangle + \frac{\tilde{\beta}}{2}\langle O_g^{(0)}\rangle\,, \quad (2.188)$$

and

$$\begin{aligned} &\sum_q^{n_f}\left(1-\gamma_m^{(n_f)}\right)\langle O_q^{(0)}\rangle + \frac{\tilde{\beta}^{(n_f)}}{2}\langle O_g^{(0)}\rangle \\ &= \sum_q^{n_f+1}\left(1-\gamma_m^{(n_f+1)}\right)\langle O_q^{\prime(0)}\rangle + \frac{\tilde{\beta}^{(n_f+1)}}{2}\langle O_g^{\prime(0)}\rangle\,. \end{aligned} \quad (2.189)$$

The traceless part of the renormalized energy-momentum tensor Eq. (2.187) relates the spin-2 matrix elements of n_f- and (n_f+1)- flavor theory as

$$\sum_q^{n_f}\langle O_q^{(2)\mu\nu}\rangle + \langle O_g^{(2)\mu\nu}\rangle = \sum_q^{n_f+1}\langle O_q^{\prime(2)\mu\nu}\rangle + \langle O_g^{\prime(2)\mu\nu}\rangle\,. \quad (2.190)$$

Combining Eq. (2.185) and Eq. (2.189), we obtain the constraints among entries of the spin-0 matching matrix $M^{(0)}$,

$$
\begin{aligned}
&1-\gamma_m^{(n_f)}-\left(1-\gamma_m^{(n_f+1)}\right)\left[\left((2-n_f)\delta_{qq'}+n_f-1\right)M^{(0)}_{qq'}+M^{(0)}_{qQ}\right]-\frac{\tilde{\beta}^{(n_f+1)}}{2}M^{(0)}_{qg}=0\,,\\
&\frac{\tilde{\beta}^{(n_f)}}{2}-\left(1-\gamma_m^{(n_f+1)}\right)\left(n_f M^{(0)}_{gq}+M^{(0)}_{gQ}\right)-\frac{\tilde{\beta}^{(n_f+1)}}{2}M^{(0)}_{gg}=0\,,
\end{aligned}
\tag{2.191}
$$

where the subscript "Q" denotes the (n_f+1)-th heavy quark and "q" denotes a light quark.

Combining Eq. (2.185) and Eq. (2.190), we obtain the constraints among entries of the spin-2 matching matrix $M^{(2)}$,

$$
\begin{aligned}
&1-\left[(2-n_f)\delta_{qq'}+n_f-1\right]M^{(2)}_{qq'}-M^{(2)}_{qQ}-M^{(2)}_{qg}=0\,,\\
&1-n_f M^{(2)}_{gq}-M^{(2)}_{gQ}-M^{(2)}_{gg}=0\,.
\end{aligned}
\tag{2.192}
$$

The matching matrix M can be expanded as a series of strong couping α_s at heavy quark scale μ_Q,

$$
M^{(S)}=\sum_{n=0}^{\infty}\left(\frac{\alpha_s^{(n_f+1)}(\mu_Q)}{\pi}\right)^n M^{(S)}_n\,,
\tag{2.193}
$$

and we can solve Eq. (2.185) order by order through this expansion.

At leading order, we have solution to Eq. (2.185),

$$
\begin{aligned}
&M^{(S)}_{qq'}=\delta_{qq'}\,,\quad M^{(S)}_{gg}=1\,,\\
&M^{(S)}_{qQ}=M^{(S)}_{qg}=M^{(S)}_{gq}=M^{(S)}_{gQ}=0\,.
\end{aligned}
\tag{2.194}
$$

We take higer order results for $M^{(0)}_{qQ}$ and $M^{(0)}_{gQ}$ from Ref. [121], applying constraints from Eq. (2.191) and we obtain the following $M^{(0)}$ matrix at NNNLO,

$$
\begin{aligned}
M^{(0)}_{qq'}&=\delta_{qq'}\,,\\
M^{(0)}_{qg}&=\left(\frac{\alpha_s^{(n_f+1)}(\mu_Q)}{\pi}\right)^2\left[-\frac{89}{54}+\frac{20}{9}\log\left(\frac{\mu_Q}{m_Q}\right)-\frac{8}{3}\log^2\left(\frac{\mu_Q}{m_Q}\right)\right]\,,\\
M^{(0)}_{gq}&=0\,,\\
M^{(0)}_{gQ}&=-\frac{\alpha_s^{(n_f+1)}(\mu_Q)}{12\pi}-\left(\frac{\alpha_s^{(n_f+1)}(\mu_Q)}{\pi}\right)^2\left[\frac{11}{48}-\frac{1}{36}\log\left(\frac{\mu_Q}{m_Q}\right)\right]\\
&\quad-\left(\frac{\alpha_s^{(n_f+1)}(\mu_Q)}{\pi}\right)^3\frac{1}{12}\left[\frac{2821}{288}-\frac{3}{8}\log\left(\frac{\mu_Q}{m_Q}\right)+\frac{1}{9}\log^2\left(\frac{\mu_Q}{m_Q}\right)\right.\\
&\quad\left.+n_f\left[-\frac{67}{96}+\frac{2}{3}\log\left(\frac{\mu_Q}{m_Q}\right)\right]\right]\,,
\end{aligned}
$$

$$
\begin{aligned}
M_{qQ}^{(0)} &= \left(\frac{\alpha_s^{(n_f+1)}(\mu_Q)}{\pi}\right)^2 \left[\frac{5}{18} - \frac{2}{3}\log\left(\frac{\mu_Q}{m_Q}\right)\right] \\
&+ \left(\frac{\alpha_s^{(n_f+1)}(\mu_Q)}{\pi}\right)^3 \left[\frac{311}{1296} + \frac{5}{3}\zeta(3) - \frac{175}{54}\log\left(\frac{\mu_Q}{m_Q}\right) - \frac{29}{9}\log^2\left(\frac{\mu_Q}{m_Q}\right)\right. \\
&\left. + n_f\left[\frac{53}{216} + \frac{2}{90}\log^2\left(\frac{\mu_Q}{m_Q}\right)\right]\right], \\
M_{gg}^{(0)} &= 1 - \frac{\alpha_s^{(n_f+1)}(\mu_Q)}{3\pi}\log\left(\frac{\mu_Q}{m_Q}\right) \\
&+ \left(\frac{\alpha_s^{(n_f+1)}(\mu_Q)}{\pi}\right)^2 \left[\frac{11}{36} - \frac{11}{6}\log\left(\frac{\mu_Q}{m_Q}\right) + \frac{1}{9}\log^2\left(\frac{\mu_Q}{m_Q}\right)\right] \\
&+ \left(\frac{\alpha_s^{(n_f+1)}(\mu_Q)}{\pi}\right)^3 \left[\frac{564731}{41472} - \frac{2821}{288}\log\left(\frac{\mu_Q}{m_Q}\right) + \frac{3}{16}\log^2\left(\frac{\mu_Q}{m_Q}\right)\right. \\
&- \frac{1}{27}\log^3\left(\frac{\mu_Q}{m_Q}\right) - \frac{82043}{9216}\zeta(3) + n_f\left[-\frac{2633}{10368} + \frac{67}{96}\log\left(\frac{\mu_Q}{m_Q}\right)\right. \\
&\left.\left. - \frac{1}{3}\log^2\left(\frac{\mu_Q}{m_Q}\right)\right]\right],
\end{aligned}
\tag{2.195}
$$

where $\zeta(s) = \sum_{n=1}^{\infty} n^{-s}$ is the Riemann zeta function.

For spin-2 matching matrix $M^{(2)}$, we could consider the heavy quark to be an inactive quark and integrate it out in loops of $n_f + 1$-theory to obtain an n_f-theory with n_f active quarks. Matching for $M_{gQ}^{(2)}$ is shown in Fig. 2.13.

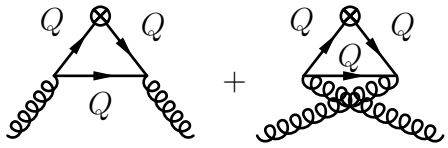

Figure 2.13: Diagrams contributing to matching matrix element $M_{gQ}^{(2)}$, with "Q" denotes the heavy quark.

The diagrams in Fig. (2.13) yield the same loop integrals as that by Fig. (2.11) and the result is

$$
\frac{2}{3}\frac{\alpha_s}{4\pi}\log\frac{\mu^2}{m_Q^2}O_g^{\prime(2)\mu\nu}. \tag{2.196}
$$

The matching from $n_f + 1$-theory to n_f-theory is

$$
c_g^{(2)\mu\nu} = c_g^{\prime(2)\mu\nu} + \frac{2}{3}\frac{\alpha_s}{4\pi}\log\frac{\mu^2}{m_Q^2}c_Q^{\prime(2)\mu\nu}\,. \tag{2.197}
$$

Matching for $M_{gg}^{(2)}$ is obtained by integrating out the heavy quark Q loop in the external gluon line, shown in Fig. 2.14.

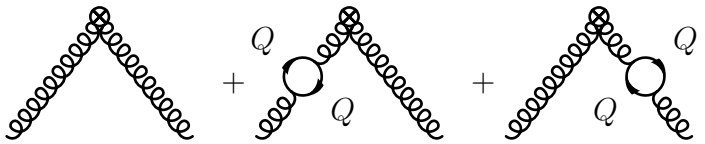

Figure 2.14: Diagrams contributing to matching matrix element $M_{gg}^{(2)}$, with "Q" denotes the heavy quark.

The loop diagrams in Fig. 2.14 yield the same loop integral as the quark loop integral computation for the background-field gluon field strength renormalization factor Z_A Eq. (2.148) and the result is

$$-\frac{2}{3}\frac{\alpha_s}{4\pi}\log\frac{\mu^2}{m_Q^2}O_g'^{(2)\mu\nu}. \tag{2.198}$$

The matching from n_f+1-theory to n_f-theory is

$$c_g^{(2)\mu\nu} = \left(1-\frac{2}{3}\frac{\alpha_s}{4\pi}\log\frac{\mu^2}{m_Q^2}\right)c_g'^{(2)\mu\nu}\,. \tag{2.199}$$

Thus, we obtain the NLO results for spin-2 matching matrix $M^{(2)}$, which also satisfy the constraint Eq. (2.192).

$$\begin{aligned}
&M_{qq'}^{(2)} = \delta_{qq'}\,, \quad M_{gg}^{(2)} = 1-\frac{\alpha_s^{(n_f+1)}(\mu_Q)}{3\pi}\log\left(\frac{\mu_Q}{m_Q}\right),\\
&M_{gQ}^{(2)} = \frac{\alpha_s^{(n_f+1)}(\mu_Q)}{3\pi}\log\left(\frac{\mu_Q}{m_Q}\right),\\
&M_{qg}^{(2)} = M_{gq}^{(2)} = M_{qQ}^{(2)} = 0\,.
\end{aligned} \tag{2.200}$$

2.8 WIMP Nucleon Elastic Scattering Cross Section

To compute the cross section for WIMP nucleon scattering from the 3-flavor quarks and gluon effective theory, we need the Wilson coefficients and nucleon matrix elements for the operators. The nucleon matrix elements are non-perturbative at GeV scale, and we will take results from Lattice QCD calculation. The 3-flavor effective theory Wilson coefficients are obtained by renormalization group evolution and heavy quark matching from the 5-flavor quarks and gluon effective theory Wilson coefficents Eq. (2.162).

2.8.1 Light Flavors Effective Theory

We use the R-matrix Table 2.3 to evolve the coefficients from a high scale to a low scale and the M-matrix Eq. (2.195) and Eq. (2.200) to integrate the heavy quarks at a threshold scale. The low energy 3-flavor effective theory Wilson coefficients are

$$c_j(\mu_0) = [R(\mu_0,\, \mu_c)M(\mu_c)R(\mu_c,\, \mu_b)M(\mu_b)R(\mu_b,\, \mu_t)]_{ji}\, c_i(\mu_t)\,, \tag{2.201}$$

where μ_0 is about GeV scale, μ_q is a scale about the quark mass scale m_q, $i = u,\, d,\, s,\, c,\, b,\, g,\ j = u,\, d,\, s,\, g,$ and $R(\mu_b,\, \mu_t)$ is a 6×6 matrix, $M(\mu_b)$ is a 5×6 matrix, $R(\mu_c,\, \mu_b)$ is a 5×5 matrix, $M(\mu_c)$ is a 4×5 matrix, $R(\mu_0,\, \mu_c)$ is a 4×4 matrix. Specifically, we take $\mu_t = (m_t + m_W)/2 = 126$ GeV, $\mu_b = 4.75$ GeV, $\mu_c = 1.4$ GeV, and $\mu_0 = 1.2$ GeV, as in Refs. [73, 107].

To evaluate Eq. (2.201) and obtain $c_j(\mu_0)$ numerically, we expand the β-function and mass anomalous dimension γ_m in series of $\alpha_s(\mu, n_f)$ in Appendix B. Here we illustrate how we evaluate $\alpha_s(\mu, n_f)$ at 4-loop order by an iterative method from Ref. [121],

$$\begin{aligned}\alpha_s(\mu, n_f, \Lambda) = 4\pi\Bigg\{ & \frac{1}{\beta_0 L} - \frac{b_1 \log L}{(\beta_0 L)^2} + \frac{1}{(\beta_0 L)^3}\left[b_1^2(\log^2 L - \log L - 1) + b_2\right] \\ & + \frac{1}{(\beta_0 L)^4}\Bigg[b_1^3\left(-\log^3 L + \frac{5}{2}\log^2 L + 2\log L - \frac{1}{2}\right) \\ & - 3b_1 b_2 \log L + \frac{b_3}{2}\Bigg]\Bigg\}\,,\end{aligned} \tag{2.202}$$

where $L = \log(\mu^2/\Lambda^2)$, $b_n = \beta_n/\beta_0$ and β_n can be found in Appendix B.

In order to determine the scale Λ in Eq. (2.202), we match the 5-flavor α_s to its value at Z^0 boson mass scale which is 0.118, and solve equation

$$\alpha_s(m_Z,\, 5, \Lambda) = 0.118\,, \tag{2.203}$$

which provides a solution for 5-flavor scale $\Lambda_5 = 0.208365$, $\alpha_s(m_t,\, 5, \Lambda_5) = 0.107688$.

Then for 4-flavor scale Λ_4 is obtained by solving

$$\alpha_s(m_b,\, 5, \Lambda_5) = \alpha_s(m_b,\, 4, \Lambda_4)\,, \tag{2.204}$$

and $\Lambda_4 = 0.292968$, $\alpha_s(m_b,\, 4, \Lambda_4) = 0.216634$.

Similarly, for 3-flavor scale Λ_3, we solve

$$\alpha_s(m_c,\, 4, \Lambda_4) = \alpha_s(m_c,\, 3, \Lambda_3)\,, \tag{2.205}$$

and $\Lambda_3 = 0.337109$, $\alpha_s(m_c,\, 3, \Lambda_3) = 0.371843$.

We obtain $\alpha_s(\mu, n_f, \Lambda_{n_f})$ for n_f-flavor theory at a scale μ by plugging in Λ_{n_f} that has been determined and evaluating Eq. (2.202).

2.8.2 Nucleon Matrix Elements

Now that we have 3-flavor theory Wilson coefficients Eq. (2.201) at $\mu_0 \sim$ GeV scale, in order to compute the scattering cross section, we need the nucleon matrix elements for the corresponding operators.

For spin-0 quarks and gluon operators, we have nucleon matrix elements at zero momentum transfer definitions, c.f. Ref. [73]

$$\begin{aligned} m_N f_{q,N}^{(0)} &\equiv \frac{E_k}{m_N} \langle N(k)|O_q^{(0)}|N(k)\rangle \,, \\ m_N f_{g,N}^{(0)} &\equiv -\frac{9\alpha_s(\mu)}{8\pi} \frac{E_k}{m_N} \langle N(k)|O_g^{(0)}|N(k)\rangle \,, \end{aligned} \tag{2.206}$$

where $q = u$, d, s, and $|N(k)\rangle$ is a nucleon (proton or neutron) state, $N = p$, n, normalized by $\bar{u}_N(k)u_N(k) = m_N/E_k$, and $-9\alpha_s(\mu)/(8\pi)$ is a convention by definition.

We usually determine the scalar nucleon matrix elements $f_{u,N}^{(0)}$ and $f_{d,N}^{(0)}$ from scale-invariant quantities,

$$\begin{aligned} \Sigma_{\pi N} &= \frac{m_u + m_d}{2} \langle N|\bar{u}u + \bar{d}d|N\rangle \,, \\ \Sigma_- &= (m_d - m_u)\langle N|\bar{u}u - \bar{d}d|N\rangle \,. \end{aligned} \tag{2.207}$$

Solving Eq. (2.207) in a parametric way, we obtain the scalar matrix elements for u and d quarks,

$$\begin{aligned} f_{u,N}^{(0)} &= (1+\xi)\frac{R_{ud}}{1+R_{ud}}\frac{\Sigma_{\pi N}}{m_N} \,, \quad f_{d,N}^{(0)} = (1-\xi)\frac{1}{1+R_{ud}}\frac{\Sigma_{\pi N}}{m_N} \,, \\ \xi &= \frac{1+R_{ud}}{1-R_{ud}}\frac{\Sigma_-}{2\Sigma_{\pi N}} \,, \end{aligned} \tag{2.208}$$

where $R_{ud} \equiv m_u/m_d$.

In practice, we take $\Sigma_{\pi N} = 40(4)$ MeV and $R_{ud} = 0.49(2)$ from lattice results in Ref. [122] averaged from Refs. [123–127]. [2] We take $\Sigma_- = 2(2)$ MeV for proton, and $\Sigma_- = -2(2)$ MeV for neutron from Ref. [131]. For the s-quark scalar matrix element, we take $f_{s,N}^{(0)} = 0.056(8)$ from Ref. [122]. We tabulate the spin-0 quark matrix elements $f_{q,N}^{(0)}$ in Table 2.4.

Recall the constraint among quarks and gluon scalar matrix elements from Eq. (2.188), and we derive the gluon spin-0 matrix element by quarks scalar matrix elements,

$$f_{g,N}^{(0)} = -\frac{\alpha_s}{4\pi}\frac{9}{\tilde{\beta}}\left[1 - (1-\gamma_m)\sum_{q=u,\,d,\,s} f_{q,N}^{(0)}\right] , \tag{2.209}$$

where α_s and $\tilde{\beta}$ are taken at $\mu_0 \sim$ GeV scale and for $n_f = 3$ theory.

[2] There is tension between the lattice result [122] $\Sigma_{\pi N} = 40(4)$ MeV, and phenomenological extractions $\Sigma_{\pi N} = 59.1(3.5)$ MeV and $\Sigma_{\pi N} = 58(5)$ MeV from pionic atoms [128] and low energy pion-nucleon scattering [129], see also Ref. [130], which found $\Sigma_{\pi N} = 59(7)$ MeV. Since the scalar matrix elements of u and d quarks represent a small contribution to the total cross section [71], our results would be essentially unchanged if a larger value, $\Sigma_{\pi N} \approx 60\,\text{MeV}$, were used.

Table 2.4: Scale independent spin-0 nucleon matrix elements for proton and neutron for light quarks u, d, s. The first,second and third uncertainties are from $\Sigma_{\pi N}$, R_{ud} and Σ_- respectively for u and d quarks.

q	$f_{q,p}^{(0)}$	$f_{q,n}^{(0)}$
u	0.0150(14)(10)(4)	0.0130(14)(10)(3)
d	0.0265(29)(21)(4)	0.0307(29)(21)(3)
s	0.056(8)	0.056(8)

Table 2.5: Spin-2 nucleon matrix elements from lattice QCD calculation at different renormalization scales.

Scale μ (GeV)	$f_{u,p}^{(2)}(\mu)$	$f_{d,p}^{(2)}(\mu)$	$f_{s,p}^{(2)}(\mu)$	$f_{g,p}^{(2)}(\mu)$
1	0.404(9)	0.217(8)	0.024(4)	0.356(29)
1.2	0.383(8)	0.208(8)	0.027(4)	0.381(25)
1.4	0.370(8)	0.202(7)	0.030(4)	0.398(23)
2	0.346(7)	0.192(6)	0.034(3)	0.419(19)

For spin-2 quarks and gluon operators, we have nucleon matrix elements definitions,

$$\begin{aligned}
\frac{E_k}{m_N}\langle N(k)|O_q^{(2)\mu\nu}|N(k)\rangle &\equiv \left(k^\mu k^\nu - \frac{g^{\mu\nu}}{4}m_N^2\right) f_{q,N}^{(2)}\,, \\
\frac{E_k}{m_N}\langle N(k)|O_g^{(2)\mu\nu}|N(k)\rangle &\equiv \left(k^\mu k^\nu - \frac{g^{\mu\nu}}{4}m_N^2\right) f_{g,N}^{(2)}\,,
\end{aligned} \tag{2.210}$$

The energy momentum conservation constraint Eq. (2.190) requires

$$\sum_{q=u,\,d,\,s} f_{q,N}^{(2)} + f_{g,N}^{(2)} = 1\,. \tag{2.211}$$

We take lattice calculation results from Ref. [132] for spin-2 matrix elements as in Ref. [73] and list them in Table 2.5 for relevant renormalization scales. Shown in Table 2.5 are for proton matrix elements. For neutron matrix elements, neglecting iso-spin breaking, we have $f_{u,n}^{(2)} = f_{d,p}^{(2)}$, $f_{u,n}^{(2)} = f_{d,p}^{(2)}$, and $f_{s,n}^{(2)} = f_{s,p}^{(2)}$.

2.8.3 Nucleon Level Cross Section

Let us compute the low-velocity limit of the WIMP-nucleon spin-independent scattering cross section, as a standard benchmark process. The cross section is c.f. [133]

$$\begin{aligned}
\frac{d\sigma}{d\Omega} &= \frac{\sum_{\text{spins}}|\mathcal{M}|^2}{2E_A 2E_B|v_A - v_B|}\frac{|\mathbf{p}|}{(2\pi)^2 4E_{\text{cm}}} \\
&= \frac{4M^2 4m_N^2|\mathcal{M}_N^{(0)} + \mathcal{M}_N^{(2)}|^2}{2M 2m_N v}\frac{m_r v}{(2\pi)^2 4(M+m_N)}
\end{aligned}$$

$$= \frac{m_r^2}{4\pi^2}|\mathcal{M}_N^{(0)} + \mathcal{M}_N^{(2)}|^2 \,. \tag{2.212}$$

Thus, we have

$$\sigma_N = \frac{m_r^2}{\pi}|\mathcal{M}_N^{(0)} + \mathcal{M}_N^{(2)}|^2 \,, \tag{2.213}$$

where $N = n, p$ is a nucleon, $m_r = m_N M/(m_N + M) \approx m_N$ is the reduced mass of the WIMP-nucleon system, and the scattering amplitude is

$$\mathcal{M}_N^{(S)} = \sum_{i=q,g} c_i^{(S)}(\mu_0)\langle N|O_i^{(S)}(\mu_0)|N\rangle \,, \tag{2.214}$$

where $S = 0, 2$.

For our default matching scales μ_t, μ_b, μ_c and μ_0, and with the central values of all nucleon matrix elements at scale μ_0, we find the spin-0 and spin-2 amplitudes for Higgsino-like WIMP-proton scattering are (normalized by spin-2 amplitude $\mathcal{M}_p^{(2)}|_{M\to\infty} = 1$)

$$\mathcal{M}_p^{(0)} = -1.05 - 0.50\frac{\tilde{c}_H}{\alpha_2^2}\frac{m_W}{M} \,, \qquad \mathcal{M}_p^{(2)} = 1 - 0.54\frac{m_W}{M} \,. \tag{2.215}$$

At $M \to \infty$, Eq. (2.215) exhibits a remarkable cancellation at the level of $\sim 5\%$ (compared to $\sim 20\%$ in the triplet case [107]). At order $1/M$, the pure Wino case also exhibited a strong cancellation between the power corrections of spin-0 and spin-2 amplitudes [107]. For the pure Higgsino case we have $\tilde{c}_H = -(3\alpha_2^2/4)[1 + 1/(2c_W^4)]$, and $\mathcal{M}_p^{(0)} = -1.05 + 0.69\, m_W/M$. Owing to the severity of the leading order cancellation, the total $1/M$ correction can compete with the leading order for moderate M. These features can be seen in the central value curve of Fig. 2.15. The sign of the power correction relative to leading power further suppresses the cross section as M decreases from the heavy WIMP limit.

As usual when evaluating the nucleon-level amplitude, we have two sources of uncertainties: Wilson coefficients and hadronic matrix elements. Perturbative uncertainty in the matching coefficients is estimated by varying the matching scales within the ranges $m_W^2/2 \le \mu_t^2 \le 2m_t^2$, $m_b^2/2 \le \mu_b^2 \le 2m_b^2$, $m_c^2/2 \le \mu_c^2 \le 2m_c^2$, and $1.0\,\text{GeV} \le \mu_0 \le 1.4\,\text{GeV}$, as in Ref. [73, 107]. Uncertainties from neglected $1/M^2$ and higher order power corrections are estimated by shifting $\mathcal{M}_p^{(2)} \to \mathcal{M}_p^{(2)}|_{M\to\infty}[1 \pm (m_W/M)^2]$ as in Refs. [73, 107]. Uncertainties from nucleon matrix elements are propagated to the observable cross section [73, 123, 127, 131, 132]. We add in quadrature the errors from different sources for each of the spin-0 and spin-2 amplitudes. Then the maximum and minimum of all possible values of the combination $|\mathcal{M}_p^{(0)} + \mathcal{M}_p^{(2)}|$ sets the boundaries of the cross section curves depicted in Fig. 2.15.[3] Also shown n Fig. 2.15 are current dark matter direct detection experimental exclusion limits (solid lines) [59, 104, 134],

[3]We combined errors in this way at the amplitude level since the cross section can be zero for some parameter values.

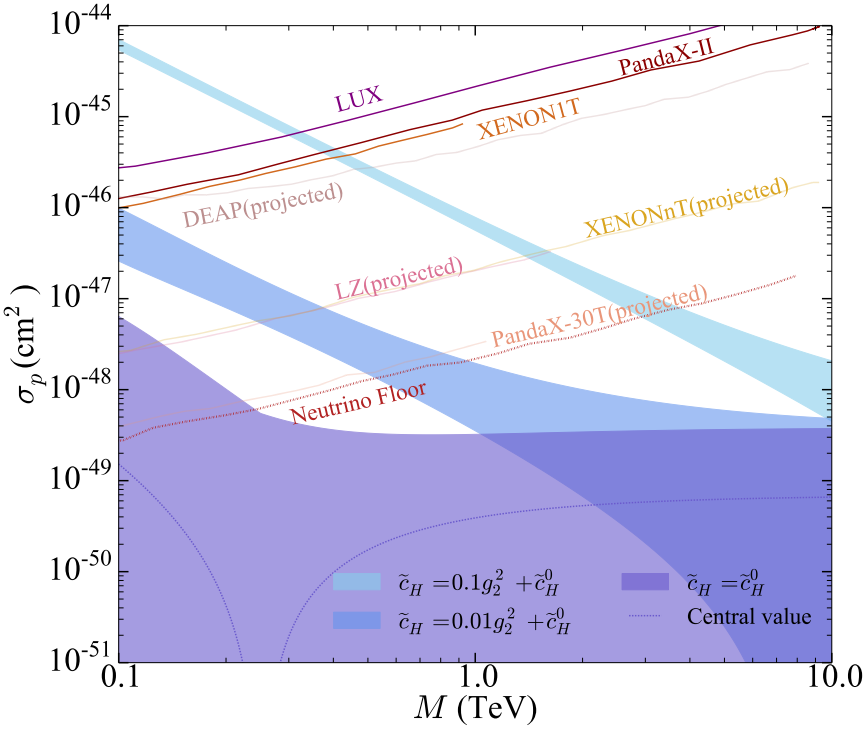

Figure 2.15: Scattering cross section for Majorana SU(2) doublet (Higgsino-like) WIMP on proton. Corrections to this limit are parameterized by dimensionless Higgs coupling $\tilde{c}_H$ as discussed in the text. The pure Higgsino limit ($\tilde{c}_H = -(3\alpha_2^2/4)[1 + 1/(2c_W^4)] \equiv \tilde{c}_H^0$) is shown as the lower violet band and dashed central value curve. The impact of non-decoupled states in the UV completion are illustrated with $\tilde{c}_H = \tilde{c}_H^0 + 0.01\, g_2^2$ (middle, dark blue band) and $\tilde{c}_H = \tilde{c}_H^0 + 0.1\, g_2^2$ (upper, light blue band).

future projected detectors' sensitivities (dotted lines) [56–58, 105], and neutrino floor (dash-dotted line) for Xenon detectors [106].

For the lower, violet colored, region in Fig. 2.15, the limit $M' \gg M$ has been taken to decouple heavier states in the pure Higgsino limit for the coefficient $\tilde{c}_H$ in Eq. (2.215). Before taking this limit, we may use Eq. (2.69) to investigate the impact of non-decoupled states in the UV completion. Away from the pure-state limit, we have $\tilde{c}_H \approx 2\kappa^2 M/(M' - M)$. For weakly coupled theories we consider a range of values $\tilde{c}_H/g_2^2 = 0.01 - 0.1$ in Fig. 2.15. For TeV mass WIMPs, the cross section is within the detectable range of next generation detectors [56, 57, 105] when $\tilde{c}_H/g_2^2 \approx 0.1$, and is close to the neutrino floor when $\tilde{c}_H/g_2^2 \approx 0.01$. In the pure Higgsino limit, the cross section upper limit remains at or below $10^{-48}\,\mathrm{cm}^2$ for masses above a few hundred GeV.

2.9 Nuclear Effect

Finally, we note that the actual scattering process in experimental searches takes place on compound nuclei versus on isolated nucleons. A standard practice for treating nuclear modifications is to apply a nuclear form factor to the free-nucleon result [135, 136]. At the same time, a distribution in WIMP velocities is assumed present in our local galactic halo, and the event rate ansatz is a convolution of halo velocity profile, nuclear form factor, and single nucleon cross section [136].

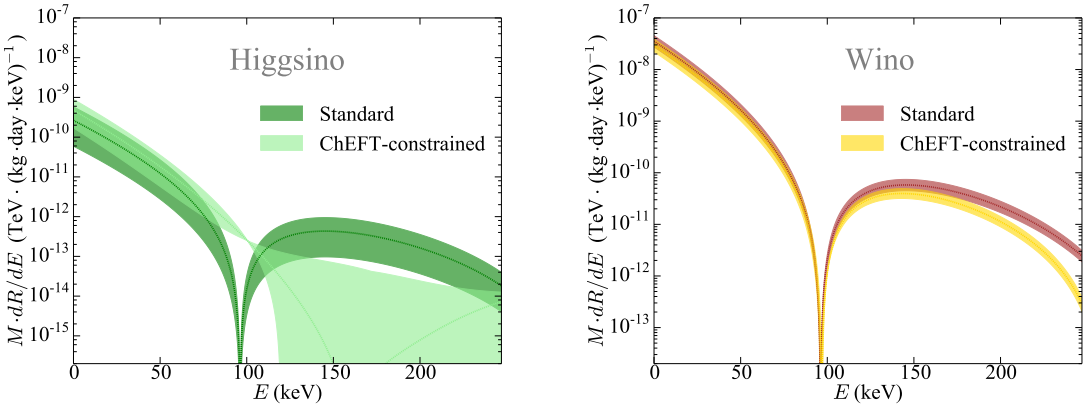

Figure 2.16: Event rate (times WIMP mass) versus recoil energy for Xenon target, for Higgsino-like (left panel) and Wino-like (right panel) WIMP. The "Standard" rate uses the standard halo model, dark matter velocity distribution and Helm nuclear form factor [136]. The "ChEFT constrained" rate replaces the Helm form factor by the model of Refs. [108, 109]. Dashed curves are central values and shaded regions represent perturbative matching uncertainty. Nucleon matrix element uncertainties are not displayed.

The severe cancellation in the single-nucleon cross section, cf. Eq. (2.215), suggests that nuclear corrections could potentially have a larger than expected impact. We investigate this possibility here, using the model presented in Refs. [108, 109] which includes effects from multi-nucleon interactions. In general, the differential event rate versus recoil energy takes the form

$$\frac{dR}{dE} = \frac{\rho}{2\pi M}|\mathcal{F}(q^2)|^2 \int_{v_{min}(E)}^{\infty} \frac{f(\mathbf{v})}{v} d^3v \,, \tag{2.216}$$

where $\rho \approx 0.3\,\mathrm{GeV}\cdot\mathrm{cm}^{-3}$ [136] is the dark matter mass density, $q = (2m_N E)^{1/2}$ is the momentum transfer with E being recoil energy, $\mathcal{F}(q^2)$ is the nuclear structure factor [108, 109] and $f(\mathbf{v})$ is the WIMP velocity distribution function. Explicitly, the velocity distribution function is [136],

$$f(\mathbf{v}) = (\pi^{3/2} v_0^3 k)^{-1} e^{-\frac{(\mathbf{v}+\mathbf{v_E})^2}{v_0^2}} \theta\left(v_{\mathrm{esc}} - |\mathbf{v}+\mathbf{v_E}|\right) \,, \quad k \equiv \mathrm{erf}(z) - \frac{2z}{\sqrt{\pi}} e^{-z^2} \,, \tag{2.217}$$

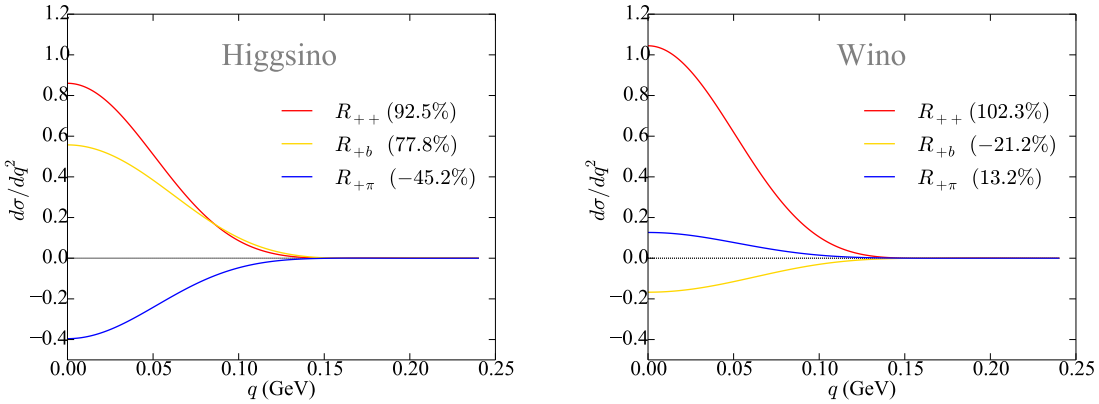

Figure 2.17: Different nuclear response channels contributing to $d\sigma/dq^2$ versus momentum transfer q, for Higgsino-like (left panel) and Wino-like (right panel) WIMPs of velocity $v/c = 10^{-3}$ scattering on a Xenon nucleus. Curves are normalized to unity for the sum of all contributions at $q = 0$. R_{++} denotes the one-body isoscalar response (denoted $(c_+^M \mathcal{F}_+^M)^2$ in Ref. [108]). R_{+b} and $R_{+\pi}$ denote one-body/two-body interference terms (denoted $2\, c_+^M c_b \mathcal{F}_+^M \mathcal{F}_b$ and $2\, c_+^M c_\pi \mathcal{F}_+^M \mathcal{F}_\pi$ in Ref. [108]). Numbers in parentheses are the percentage contribution for each nuclear response channel to the total integrated cross section. Other subdominant channels are not displayed.

where $z = v_{\rm esc}/v_0$, $v_0 \approx 220$ km/s is the galactic rotation velocity for a galaxy with a flat rotation curve, $v_{\rm esc} \approx 600$ km/s is the local galactic escape velocity, $\mathbf{v}$ is dark matter velocity onto the target, $v_E \approx 232$ km/s is Earth's velocity relative to the dark matter.

Equation (2.216) reduces to the "Standard" treatment under the replacement $|\mathcal{F}(q^2)|^2 \to A^2 |F(q^2)|^2 \pi \sigma_N M/m_r^2$, where

$$F(q^2) = 3 \frac{j_1(q r_n)}{q r_n} e^{-\frac{(qs)^2}{2}} , \tag{2.218}$$

is the Helm form factor [135, 136], $j_1(x)$ is the first-order spherical Bessel function, r_n is an effective nuclear radius with $r_n^2 = (1.23 A^{1/3} - 0.6)^2 + 7\pi^2 a^2/3 - 5s^2$, $a \sim 0.52$ fm, $s \sim 1$ fm [137] is a measure of the nuclear skin thickness and A is the mass number of the nucleus. Figure 2.16 compares the event rate for Xenon detectors (^{132}Xe) from our "Standard" computation, to the "ChEFT constrained" computation with nuclear model from Refs. [108, 109]. For discussion of nuclear corrections see also Refs. [138, 139].

The rate is multiplied by the WIMP mass to make the curves on the plot independent of WIMP mass. For the purpose of illustrating nuclear effects, we focus on the heavy WIMP limit, neglecting small corrections to both curves when $m_W/M \neq 0$. In order to perform an "apples to apples" comparison in Fig. 2.16, we have employed the same input values for nucleon-level matrix elements in our "Standard" nuclear model as in Ref. [109], except for the spin-0 gluon matrix element, which was evaluated in Ref. [109] using a leading order perturbative QCD relation. Higher order perturbative

Table 2.6: Spin-0 nucleon matrix elements used for nuclear effect analyses.

q	$f_{q,p}^{(0)}$	$f_{q,n}^{(0)}$
u	0.0208	0.0189
d	0.0411	0.0451
s	0.037	0.037

Table 2.7: Spin-2 nucleon matrix elements used for nuclear effect analyses.

i	$f_{i,p}^{(0)}$	$f_{i,n}^{(0)}$
u	0.346	0.192
d	0.192	0.346
s	0.034	0.034
g	0.419	0.419

Table 2.8: A table of different channels' contributions to the total cross section with percentage greater than 1%, Higgsino case, normalized to a single nucleon.

Channel	$(c_+^M F_+)^2$	$2\, c_+^M c_b F_+ F_b$	$2\, c_+^M c_\pi F_+ F_\pi$	$2\, c_b c_\pi F_b F_\pi$
Percent	86.0%	55.7%	-39.6%	-12.8%
Channel	$(c_b F_b)^2$	$(c_\pi F_\pi)^2$	$2\, c_+^M c_-^M F_+ F_-$	
Percent	9.0%	4.6%	-2.7%	

QCD corrections turn out to be significant [102, 140], and we have included corrections through NNNLO by Eq. (2.209) in both "Standard" and "ChEFT-constrained" analyses. We tabulate the nucleon matrix elements central values from Ref. [109] explicitly in Table 2.6 and Table 2.7.

We have also implemented the "ChEFT constrained" nuclear model for the triplet case studied in Ref. [107]. For both doublet and triplet cases, a breakdown of $d\sigma/dq^2$ into separate nuclear response channels is displayed in Fig. 2.17 for an illustrative WIMP velocity $v/c = 10^{-3}$. Considering up to two nucleons interaction, the differential cross section $d\sigma/dq^2$ for our Majorana WIMP-nucleus spin-independent scattering takes the form in the notation of Refs. [108, 109] ,

$$\frac{d\sigma}{dq^2} = \frac{1}{4\pi v^2} \Big| \sum_{I=\pm} \left(c_I^M - \frac{q^2}{m_N^2} \dot{c}_I^M \right) \mathcal{F}_I^M(q^2) + c_\pi \mathcal{F}_\pi(q^2) + c_b \mathcal{F}_b(q^2) \Big|^2 . \tag{2.219}$$

Converting the notations of Refs. [108, 109] to ours, we have the following relations

$$c_\pm^M = \frac{1}{2} \left[f_p \pm f_n + \frac{3}{4} \left(f_p^{(2)} \pm f_n^{(2)} \right) \right] ,$$
$$\dot{c}_\pm^M = \frac{m_N^2}{2} (\dot{f}_p + \dot{f}_n) ,$$

Table 2.9: A table of different channels' contributions to the total cross section with percentage greater than 1%, Wino case, normalized to a single nucleon.

Channel	$(c_+^M F_+)^2$	$2\, c_+^M c_b F_+ F_b$	$2\, c_+^M c_\pi F_+ F_\pi$	$2\, c_b c_\pi F_b F_\pi$
Percent	104.0%	-16.7%	12.7%	-1.0%

Table 2.10: A table of different channels' contributions to the total cross section with percentage greater than 1%, Higgsino case, for Xenon.

Channel	$(c_+^M F_+)^2$	$2\, c_+^M \dot{c}_+^M F_+^2$	$2\, c_+^M c_b F_+ F_b$	$2\, c_+^M c_\pi F_+ F_\pi$
Percent	92.5%	-23.6%	77.8%	-45.2%
Channel	$2\, c_b c_\pi F_b F_\pi$	$(c_b F_b)^2$	$(\dot{c}_+^M F_+)^2$	$2\, \dot{c}_+^M c_b F_+ F_b$
Percent	-19.7%	17.9%	3.2%	-12.0%
Channel	$2\, \dot{c}_+^M c_\pi F_+ F_\pi$	$(c_\pi F_\pi)^2$	$2\, c_+^M c_-^M F_+ F_-$	
Percent	6.0%	5.6%	-2.4%	

Table 2.11: A table of different channels' contributions to the total cross section with percentage greater than 1%, Wino case, for Xenon.

Channel	$(c_+^M F_+)^2$	$2\, c_+^M c_b F_+ F_b$	$2\, c_+^M c_\pi F_+ F_\pi$	$2\, c_b c_\pi F_b F_\pi$	$2\, c_+^M \dot{c}_+^M F_+^2$	$(c_b F_b)^2$
Percent	102.3%	-21.2%	13.2%	-1.4%	6.1%	1.2%

$$
\begin{aligned}
c_\pi &= f_\pi + 2 f_\pi^\theta - \frac{1}{2} f_\pi^{(2)} \,, \\
c_b &= f_\pi^\theta + \frac{1}{4} f_\pi^{(2)} \,,
\end{aligned}
\tag{2.220}
$$

where

$$
\begin{aligned}
f_N &\equiv m_N \left[\sum_{q=u,d,s} c_q^{(0)} f_{q,N}^{(0)} - \frac{8\pi}{9\alpha_s} c_g^{(0)} f_{g,N}^{(0)} \right] , \\
\dot{f}_N &\equiv c_u^{(0)} \frac{1-r}{2} \dot{\sigma} + c_d^{(0)} \frac{1+r}{2} \dot{\sigma} + c_s^{(0)} \dot{\sigma}_s \,, \\
f_N^{(2)} &\equiv m_N \left[\sum_{q=u,d,s} c_q^{(2)} f_{q,N}^{(2)} + c_g^{(2)} f_{g,N}^{(2)} \right] , \\
f_\pi &\equiv m_\pi \sum_{q=u,d} \left(c_q^{(0)} + \frac{8\pi}{9\alpha_s} c_g^{(0)} \right) f_{q,\pi}^{(0)} \,, \\
f_\pi^{(2)} &\equiv m_\pi \left[\sum_{q=u,d} c_q^{(2)} f_{q,\pi}^{(2)} + c_g^{(2)} f_{g,\pi}^{(2)} \right] , \\
f_\pi^\theta &\equiv -m_\pi \frac{8\pi}{9\alpha_s} c_g^{(0)} \,.
\end{aligned}
\tag{2.221}
$$

Table 2.12: Pion matrix elements for light quarks used for nuclear effect analyses.

q	$f_{q,\pi}^{(0)}$	$f_{q,\pi}^{(2)}$
u	0.32	0.298
d	0.68	0.298
s	0	0.055
g	0	0.341

where $N = n, p$ for neutron or proton, $r = (m_d - m_u)/(m_d + m_u) = 0.37(3)$, $\dot{\sigma} = 0.27(1)\,\mathrm{GeV}^{-1}$, $\dot{\sigma}_s = 0.3(2)\,\mathrm{GeV}^{-1}$, the pion matrix element $f_{i,\pi}^{(S)}$ are listed in Table 2.12.

Contributions to the total integrated cross section from different channels are tabulated in Table 2.8 ,Table 2.9 , Table 2.10 and Table 2.11. In the terminology of Ref. [108], isoscalar one-body scattering (corresponding to the "Standard" nuclear form factor treatment) remains the dominant contribution to the direct detection rate. As the comparison of Higgsino-like and Wino-like cases in the figure illustrates, the more severe cancellation of the Higgsino one-body amplitude, Eq. (2.215), leads to an effective enhancement of one-body/two-body interference terms in the Higgsino-like cross section. An interesting feature of these plots is a partial cancellation between the different two-body contributions, R_{+b} and $R_{+\pi}$. This cancellation is not directly related to the cancellation between spin-0 and spin-2 one body amplitudes (2.215). The ratio of the relevant two-body nuclear response coefficients can be expressed in our basis as

$$\frac{c_\pi}{c_b} = \frac{\sum_{q=u,d} c_q^{(0)} f_{q,\pi}^{(0)} - 8\pi c_g^{(0)}/(9\alpha_s) - (1/2)\sum_{i=u,d,s,g} c_i^{(2)} f_{i,\pi}^{(2)}}{-8\pi c_g^{(0)}/(9\alpha_s) + (1/4)\sum_{i=u,d,s,g} c_i^{(2)} f_{i,\pi}^{(2)}}\,. \tag{2.222}$$

Coefficients $c_i^{(0)}$ and $c_i^{(2)}$ enter with different weights in the two-body responses, compared to the one-body response which involves $c_+^M \propto \frac{1}{2}\sum_{N=p,n}\sum_{i=u,d,s,g}[c_i^{(0)} f_{i,N}^{(0)} + \frac{3}{4} c_i^{(2)} f_{i,N}^{(2)}]$.

However, for both doublet and triplet cases, the considered nuclear modifications do not qualitatively impact the cross section, and are comparable in magnitude to other sources of uncertainty.

2.10 Summary

We have computed subleading corrections to the cross sections for Wino-like and Higgsino-like WIMP particles scattering on nuclear targets. The doublet result shows that order $1/M$ corrections do not significantly enhance the small leading order cross section. The upper limit for the pure doublet is less than $10^{-48}\,\mathrm{cm}^2$ in the TeV mass regime, consistent with the leading order estimate [73, 102], and lower than the estimated Xenon neutrino floor [106]. We also investigated the impact of nuclear effects by employing a modern EFT-based model in place of the standard nuclear

form factor. Although individual nuclear response channels have significant contributions, cancellations occur in the total nuclear response. The overall effect of the new nuclear model is comparable to other uncertainties for both Wino-like and Higgsino-like WIMP candidates, leaving the TeV scale pure Wino within striking distance of next generation experiments, and the pure Higgsino well below the neutrino floor. The small cross section in the pure Higgsino limit can be modified by non-decoupled states in the UV completion. For WIMP masses of order $M = 500$ GeV, current experiments constrain the dimensionless Higgs-WIMP-WIMP coupling as $\tilde{c}_H \lesssim 0.04$.

Chapter 3 Radiative Correction to Neutrino-Nucleon Elastic Scattering

3.1 Introduction

The accelerator neutrino oscillation experiments [78, 80, 82–84] have entered a precision stage to determine the mixing parameters of different neutrino mass eigenstates and the ordering of neutrino masses. For the accelerator neutrino beams with energy about $\sim$ GeV scale, the neutrino nucleon charged current elastic scattering in Standard Model is an important process in the detector contributing to the measurement signals of muon neutrinos (ν_μ) oscillating into electron neutrinos (ν_e) and anti-muon neutrinos ($\bar{\nu}_\mu$) to anti-electron neutrinos ($\bar{\nu}_e$).

The radiative corrections to this charged current elastic scattering process for different lepton flavors could be different due to the differences in muon and electron masses. It is imperative to compute this radiative correction and obtain the correct cross sections corresponding to the measured event rates in order to determine the precise fluxes of muon neutrinos and electron neutrinos incident on the far detector, comparing with the flux of muon neutrinos at the near detector. Compared to other works [141, 142], we base on the factorization theorem to compute the radiatively corrected cross section which is a product of hard, collinear and soft scales physics up to $O(\kappa)$ corrections, with a small parameter $\kappa \sim m^2/\Lambda^2$, where m is the charged lepton mass and Λ is a hard scale. The hard scale physics is hadronic model-dependent but insensitive to the lepton masses and its effect would be largely canceled out when we take ratio of the electron and muon processes cross sections, and the ratio is what we need to determine the oscillation. By integrating out the hard scale physics, we obtain a soft-collinear effective field theory (SCET) with the hard function serving as a matching coefficient. The lepton mass-dependent soft and collinear functions, which contribute to the main cross section bias between electron and muon flavors, can be computed perturbatively. There appear large logarithms in this perturbation calculation, which we will employ renormalization group (RG) evolution to resum and estimate a reliable radiative corrected cross section result. We use a physical tree level amplitude with dipole form factors fitted from the experimental data and the radiative corrected cross sections ratio is the physical one for factorizable jet-like observables.

In the experiments, there could also occur non-factorizable observables containing non-collinear hard photons emission . Therefore, instead of ignoring the hard function contribution to the radiative corrected cross sections ratio, an illustrative hadronic model is considered [143], with the nucleon form factors taken from experimental data fits. For the non-factorizable observables with non-collinear hard photons emission, we focus on a simplified case here, which is the heavy nucleon mass limit, and the hadronic physics only depend on vector and axial vector coefficients c_V and c_A and can be computed analytically. It provides a prototype for computing the radiative corrections for inclusive observables in a more sophisticated setting as [143], and an estimate for the size of the radiative correction in real experiments.

3.2 Tree Level

The tree level (anti)neutrino-nucleon quasi-elastic scattering processes involve:

$$\nu_l(k) + n(p) \to l^-(k') + p(p') \tag{3.1}$$
$$\bar{\nu}_l(k) + p(p) \to l^+(k') + n(p') \tag{3.2}$$

as shown in Fig. 3.1.

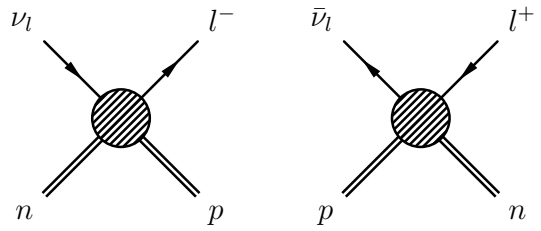

Figure 3.1: Neutrino neutron scattering and antineutrino proton scattering at tree level.

The amplitudes for neutrino neutron scattering and antineutrino proton scattering are

$$i\mathcal{M}_\nu = c_F \langle l^-(k')|j^-_\mu(0)|\nu_l(k)\rangle \langle p(p')|J^{+\mu}(0)|n(p)\rangle \,, \tag{3.3}$$
$$i\mathcal{M}_{\bar{\nu}} = c_F \langle \bar{\nu}_l(k)|j^+_\mu(0)|l^+(k')\rangle \langle n(p')|J^{-\mu}(0)|p(p)\rangle \,. \tag{3.4}$$

where c_F is a coupling and the leptonic currents matrix elements are

$$\langle l^-(k')|j^-_\mu(0)|\nu_l(k)\rangle = \bar{u}_{l^-}(k')\gamma_\mu(1-\gamma^5)u_{\nu_l}(k) \equiv \bar{u}_{l^-}(k')\Gamma_{l\mu}u_{\nu_l}(k) \,, \tag{3.5}$$
$$\langle \bar{\nu}_l(k)|j^+_\mu(0)|l^+(k')\rangle = \bar{v}_{\bar{\nu}_l}(k)\gamma_\mu(1-\gamma^5)v_{l^+}(k') \equiv \bar{v}_{\bar{\nu}_l}(k)\Gamma_{l\mu}v_{l^+}(k') \,. \tag{3.6}$$

The hadronic currents matrix elements may be formally written as

$$\langle p(p')|J^{+\mu}(0)|n(p)\rangle = \bar{u}_p(p')\Gamma^\mu_h u_n(p) \,, \tag{3.7}$$
$$\langle n(p')|J^{-\mu}(0)|p(p)\rangle = \bar{u}_n(p')\Gamma^\mu_h u_p(p) \,. \tag{3.8}$$

Thus, the amplitudes can be expressed as

$$i\mathcal{M}_\nu = c_F \bar{u}_{l^-}(k')\Gamma_{l\mu}u_{\nu_l}(k) \otimes \bar{u}_p(p')\Gamma^\mu_h u_n(p) \,, \tag{3.9}$$
$$i\mathcal{M}_{\bar{\nu}} = c_F \bar{v}_{\bar{\nu}_l}(k)\Gamma_{l\mu}v_{l^+}(k') \otimes \bar{u}_n(p')\Gamma^\mu_h u_p(p) \,. \tag{3.10}$$

We know the leptonic Γ_l basis is $\{\gamma^\mu,\, \gamma^\mu\gamma^5\}$, and by Lorentz-invariance, the hadronic Γ_h should be a Lorentz-vector or pseudo-vector. Then all the possible vector and pseudo-vector ingredients in this problem form a basis

$$\left\{\gamma^\mu,\, \gamma^\mu\gamma^5,\, \frac{P^\mu}{M},\, \frac{P^\mu}{M}\gamma^5,\, \frac{q^\mu}{M},\, \frac{q^\mu}{M}\gamma^5\right\}$$

, where M is nucleon mass, $P \equiv p + p'$ and $q \equiv p' - p$. Along with the Γ_l basis $\{\gamma^\mu,\, \gamma^\mu\gamma^5\}$. The combination basis for $\Gamma_l \otimes \Gamma_h$ is

$$\Big\{\gamma^\mu \otimes \gamma_\mu,\, \gamma^\mu \otimes \gamma_\mu\gamma^5,\, \frac{\not{P}}{M} \otimes \mathbf{1},\, \frac{\not{P}}{M} \otimes \gamma^5,\, \frac{\not{q}}{M} \otimes \mathbf{1},\, \frac{\not{q}}{M} \otimes \gamma^5,\, \gamma^\mu\gamma^5 \otimes \gamma_\mu,$$
$$\gamma^\mu\gamma^5 \otimes \gamma_\mu\gamma^5,\, \frac{\not{P}}{M}\gamma^5 \otimes \mathbf{1},\, \frac{\not{P}}{M}\gamma^5 \otimes \gamma^5,\, \frac{\not{q}}{M}\gamma^5 \otimes \mathbf{1},\, \frac{\not{q}}{M}\gamma^5 \otimes \gamma^5 \Big\}, \tag{3.11}$$

The six operators in the hadronic basis Γ_h correspond to the general hadronic six form factors structure in notation by Llewellyn-Smith [144],

$$\begin{aligned}\Gamma_h^\mu &= \gamma^\mu F_V^1(q^2) + i\frac{\sigma^{\mu\nu}q_\nu}{2M}F_V^2(q^2) + \frac{q^\mu}{M}F_V^3(q^2) + \gamma^\mu\gamma^5 F_A(q^2) + \frac{q^\mu\gamma^5}{M}F_P(q^2) \\ &\quad + \frac{P^\mu\gamma^5}{M}F_A^3(q^2)\,,\end{aligned} \tag{3.12}$$

where for on-shell Dirac particle, identity $i\sigma^{\mu\nu}q_\nu = 2M\gamma^\mu - P^\mu$ has been applied and the pure P^μ in the hadronic basis has been replaced by combination of $\sigma^{\mu\nu}q_\nu$ and γ^μ.

The spin-averaged squared amplitude for neutrino neutron scattering is

$$\begin{aligned}&\frac{1}{2}\sum_{spins}|\mathcal{M}_\nu|^2 \\ &= \frac{c_F^2}{2}\sum_{spins}\Big[\bar{u}_{l^-}(k')\Gamma_l u_{\nu_l}(k) \otimes \bar{u}_p(p')\Gamma_h u_n(p)\Big]^*\Big[\bar{u}_{l^-}(k')\Gamma_l u_{\nu_l}(k) \otimes \bar{u}_p(p')\Gamma_h u_n(p)\Big] \\ &= \frac{c_F^2}{2}\left[A - B\cdot\frac{s-u}{M^2} + C\cdot\frac{(s-u)^2}{M^4}\right],\end{aligned} \tag{3.13}$$

where Mandelstam variables expression $s - u = 4ME_\nu + q^2 - m^2$ in the laboratory frame with E_ν being neutrino energy, m being the final state charged lepton mass and A, B, C are functions of momentum transfer q^2 [144],

$$\begin{aligned}A &= 8(m^2 - q^2)M^2\Bigg\{\left(4 - \frac{q^2}{M^2}\right)|F_A|^2 - \left(4 + \frac{q^2}{M^2}\right)|F_V^1|^2 - \frac{q^2}{M^2}\left(1 + \frac{q^2}{4M^2}\right)|F_V^2|^2 \\ &\quad - \frac{4q^2}{M^2}\mathbf{Re}\Big(F_V^{1*}F_V^2\Big) + \frac{q^2}{M^2}\left(4 - \frac{q^2}{M^2}\right)|F_A^3|^2 - \frac{m^2}{M^2}\Bigg[|F_V^1 + F_V^2|^2 + |F_A + 2F_P|^2 \\ &\quad + \left(\frac{q^2}{M^2} - 4\right)\left(|F_V^3|^2 + |F_P|^2\right)\Bigg]\Bigg\},\end{aligned} \tag{3.14}$$

$$\begin{aligned}B &= 32M^4\Bigg\{-\frac{q^2}{M^2}\mathbf{Re}\Big[F_A^*\Big(F_V^1 + F_V^2\Big)\Big] + \frac{m^2}{M^2}\Bigg[\mathbf{Re}\left(\left(F_A^* + \frac{q^2F_P^*}{2M^2}\right)F_A^3\right) \\ &\quad - \mathbf{Re}\left(\left(F_V^{1*} + \frac{q^2F_V^{2*}}{4M^2}\right)F_V^3\right)\Bigg]\Bigg\},\end{aligned} \tag{3.15}$$

$$C = 8M^4 \left\{ |F_V^1|^2 + |F_A|^2 - \frac{q^2}{4M^2}|F_V^2|^2 - \frac{q^2}{M^2}|F_A^3|^2 \right\}. \tag{3.16}$$

Similarly, the spin-averaged squared amplitude for antineutrino proton scattering is

$$\begin{aligned}
&\frac{1}{2}\sum_{spins} |\mathcal{M}_{\bar{\nu}}|^2 \\
&= \frac{c_F^2}{2}\sum_{spins} \left[\bar{v}_{\bar{\nu}_l}(k)\Gamma_l v_{l^+}(k') \otimes \bar{u}_n(p')\Gamma_h u_p(p) \right]^* \left[\bar{v}_{\bar{\nu}_l}(k)\Gamma_l v_{l^+}(k') \otimes \bar{u}_n(p')\Gamma_h u_p(p) \right] \\
&= \frac{c_F^2}{2}\left[A + B\cdot\frac{s-u}{M^2} + C\cdot\frac{(s-u)^2}{M^4} \right].
\end{aligned} \tag{3.17}$$

Combing with the phase space integration in Appendix D Eq.(D.2) to Eq.(D.3), the differential cross section is

$$\frac{d\sigma_{\nu(\bar{\nu})}}{d|q^2|} = \frac{1}{4E_\nu M}\cdot\frac{1}{16\pi E_\nu M}\cdot\frac{c_F^2}{2}\left[A \mp B\cdot\frac{s-u}{M^2} + C\cdot\frac{(s-u)^2}{M^4} \right]. \tag{3.18}$$

3.3 Virtual Radiative Correction

Let us consider the heavy nucleon limit situation, when we have $m_l \ll E_\nu \ll M$. In this limit, we treat nucleon as a point-like Dirac particle and proton has a unit of positive charge $+e$, neutron being neutral. The effective Lagrangian for the heavy nucleon in the electromagnetic sector is c.f. Eq. (1.9)

$$\mathcal{L}_{heavy} = \bar{h}_v \left(iV\cdot\partial + QV\cdot A \right) h_v \tag{3.19}$$

where $Q = +e$ for proton and $Q = 0$ for neutron.

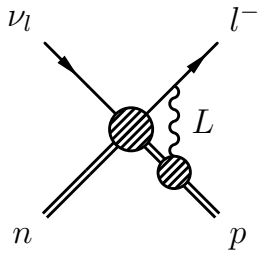

Figure 3.2: Virtual radiation correction to neutrino neutron scattering.

For one-loop virtual radiative correction, wre work in Feynman gauge and we have the bare result

$$\begin{aligned}
i\mathcal{M}_{vir}^{\nu} &= c_F \int \frac{d^dL}{(2\pi)^d}\bar{u}_{l^-}(k')iQ_l\gamma_\alpha \frac{i}{-\not{L}+\not{k}'-m+i0}\gamma_\mu(1-\gamma^5)u_{\nu_l}(k)\frac{-i}{L^2-\lambda^2+i0} \\
&\quad \otimes \bar{u}_p(p')iQ_pV^\alpha\frac{i}{V\cdot L+i0}\Gamma_h^\mu u_n(p)
\end{aligned}$$

$$= c_F \frac{\alpha}{4\pi}\left[\frac{1}{\epsilon} + 2 + \frac{5\pi^2}{3} + 4\log\frac{\lambda}{m}\log\left(\frac{2V\cdot k'}{m}\right) - 2\log^2\left(\frac{2V\cdot k'}{m}\right)\right.$$
$$\left.+4\log\left(\frac{2V\cdot k'}{m}\right) - 2\log\left(\frac{2V\cdot k'}{\mu}\right)\right]\bar{u}_l(k')\Gamma_l u_{l_\nu}(k)\otimes\bar{u}_p(p')\Gamma_h u_n(p)\,, \tag{3.20}$$

where $V = p'/M$, λ is photon mass as an IR regulator, α is QED coupling at renormalization scale μ, we drop the imaginary part which doesn't contribute at $O(\alpha)$ and $V\cdot k' = E_\nu - m^2/(2M)$.

Combining with the tree level diagram, the bare result is

$$\left(\int d\Pi \sum |\mathcal{M}_\nu|^2\right)_{tree}\left\{1 + 2\frac{\alpha}{4\pi}\left[\frac{1}{\epsilon} + 2 + \frac{5\pi^2}{3} + 4\log\frac{\lambda}{m}\log\left(\frac{2E_\nu}{m} - \frac{m}{M}\right)\right.\right.$$
$$\left.\left.-2\log^2\left(\frac{2E_\nu}{m} - \frac{m}{M}\right) + 4\log\left(\frac{2E_\nu}{m} - \frac{m}{M}\right) - 2\log\left(\frac{2E_\nu}{\mu} - \frac{m^2}{\mu M}\right)\right]\right\}. \tag{3.21}$$

Consider the field strength renormalization of the charged lepton and proton c.f. Appendix C,

$$Z_l = 1 + \frac{\alpha}{4\pi}\left(-\frac{1}{\epsilon} + 2\log\frac{m^2}{\lambda^2} + \log\frac{m^2}{\mu^2} - 4\right), \tag{3.22}$$

and

$$Z_p = 1 + \frac{\alpha}{4\pi}\left(\frac{2}{\epsilon} + 2\log\frac{\mu^2}{\lambda^2}\right). \tag{3.23}$$

The renormalized virtual radiation corrected result is

$$\left(\int d\Pi \sum |\mathcal{M}_\nu|^2\right)_{virtual} = \left(\int d\Pi \sum |\mathcal{M}_\nu|^2\right)_{tree}\frac{\alpha}{4\pi}\left[\frac{3}{\epsilon} + \frac{10\pi^2}{3}\right.$$
$$-4\log^2\left(\frac{2E_\nu}{m} - \frac{m}{M}\right) + 8\log\frac{\lambda}{m}\left[\log\left(\frac{2E_\nu}{m} - \frac{m}{M}\right) - 1\right] + 4\log\left(\frac{2E_\nu}{m} - \frac{m}{M}\right)$$
$$\left.-6\log\frac{m}{\mu}\right], \tag{3.24}$$

where UV divergence $1/\epsilon$ is expected to be cancelled by coefficients in the hadronic part.

Specifically, in the heavy nucleon limit, the hadronic structure reduces to

$$\Gamma_h^\mu = c_V\gamma^\mu + c_A\gamma^\mu\gamma^5\,, \tag{3.25}$$

and plug it into loop diagram calculation Eq. (3.20), combining with the field strength renormalization factors $\sqrt{Z_l Z_p}$, and we obtain

$$c_i^{\rm ren} = \left(1 + \frac{\alpha}{4\pi}\frac{1}{\epsilon}\right)\sqrt{Z_l Z_p}c_i^{\rm bare}$$

$$= \left(1 + \frac{3}{2}\frac{\alpha}{4\pi}\frac{1}{\epsilon}\right) c_i^{\rm bare}\,, \tag{3.26}$$

where $i = V, A$ and so c_V and c_A have anomalous dimension

$$-g\frac{\partial}{\partial g} g\left(\frac{3}{2}\frac{\alpha}{4\pi}\right) = -\frac{3\alpha}{4\pi}\,, \tag{3.27}$$

which will cancel the divergence in eq.(3.24), and explicitly they evolve as

$$\frac{dc_V}{d\log\mu} = \left(-3\frac{\alpha}{4\pi} + \mathcal{O}(\alpha^2)\right) c_V\,, \tag{3.28}$$

$$\frac{dc_A}{d\log\mu} = \left(-3\frac{\alpha}{4\pi} + \mathcal{O}(\alpha^2)\right) c_A\,. \tag{3.29}$$

Finally the total of tree level and one-loop virtual correction to neutrino neutron scattering is

$$\int d\Pi \sum |\mathcal{M}_\nu(\mu)|^2_{tree} \Bigg\{ 1 + \frac{\alpha}{4\pi}\left[\frac{10\pi^2}{3} - 6\log\frac{m}{\mu} + 4\log\left(\frac{2E_\nu}{m} - \frac{m}{M}\right)\right.$$
$$\left. -4\log^2\left(\frac{2E_\nu}{m} - \frac{m}{M}\right) + 8\log\frac{\lambda}{m}\left[\log\left(\frac{2E_\nu}{m} - \frac{m}{M}\right) - 1\right]\right]\Bigg\}\,, \tag{3.30}$$

where $c_V(\mu)$ and $c_A(\mu)$ are hadronic coefficients in the tree amplitude, and in the heavy nucleon limit, the tree level amplitude is

$$\sum |\mathcal{M}_\nu(\mu)|^2_{tree} = \frac{c_F^2}{2} 128\left[c_V^2(\mu) + c_A^2(\mu)\right] M^2 E_\nu^2 \left[1 + \frac{c_A^2(\mu) - c_V^2(\mu)}{c_V^2(\mu) + c_A^2(\mu)}\frac{m^2 + Q^2}{4E_\nu^2}\right], \tag{3.31}$$

where $Q^2 = -q^2$ is the momentum transfer and the total tree level cross section is

$$\begin{aligned}\sigma_{tree} &= \int_{Q^2_{\rm min}}^{Q^2_{\rm max}} \frac{dQ^2}{16\pi E_\nu M}\frac{\sum |\mathcal{M}_\nu(\mu)|^2_{tree}}{4E_\nu M} \\ &= \frac{c_F^2}{2}\frac{8}{\pi}E_\nu^2(c_V^2 + c_A^2)\left(1 + \frac{1}{2}\frac{c_A^2 - c_V^2}{c_V^2 + c_A^2}\right)\,,\end{aligned} \tag{3.32}$$

where

$$Q^2_{\rm min} = \frac{E_\nu^2}{1 + 2E_\nu/M}\left[2 - \frac{m^2}{E_\nu^2}\left(1 + \frac{E_\nu}{M}\right) - 2\sqrt{\left(1 - \frac{m^2}{2E_\nu M}\right)^2 - \frac{m^2}{E_\nu^2}}\right]\,,$$

$$Q^2_{\rm max} = \frac{E_\nu^2}{1 + 2E_\nu/M}\left[2 - \frac{m^2}{E_\nu^2}\left(1 + \frac{E_\nu}{M}\right) + 2\sqrt{\left(1 - \frac{m^2}{2E_\nu M}\right)^2 - \frac{m^2}{E_\nu^2}}\right]\,, \tag{3.33}$$

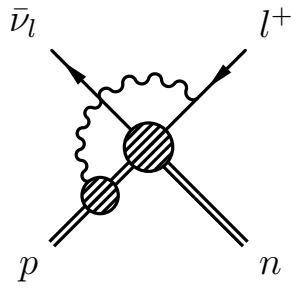

Figure 3.3: Virtual radiation correction to anti-neutrino proton scattering.

and we take the limit $m \ll E_\nu \ll M$ for Eq. (3.32).

Similarly, for anti-neutrino proton scattering, the virtual radiative correction is

$$\begin{aligned} i\mathcal{M}^{\bar{\nu}}_{vir} &= c_F \int \frac{d^dL}{(2\pi)^d} \bar{v}_{\bar{\nu}_l}(k)\gamma_\mu(1-\gamma^5)\frac{i}{\not{L}-\not{k}'-m+i0} v_{l^+}(k') iQ_l\gamma_\alpha \frac{-i}{L^2-\lambda^2+i0} \\ &\quad \otimes \bar{u}_n(p')\Gamma^\mu_h \frac{i}{-V\cdot L+i0} iQ_p V^\alpha u_p(p) \\ &= c_F \frac{\alpha}{4\pi}\left[\frac{1}{\epsilon}+2+\frac{5\pi^2}{3}+4\log\frac{\lambda}{m}\log\left(\frac{2V\cdot k'}{m}\right)-2\log^2\left(\frac{2V\cdot k'}{m}\right)\right. \\ &\quad \left.+4\log\left(\frac{2V\cdot k'}{m}\right)-2\log\left(\frac{2V\cdot k'}{\mu}\right)\right]\bar{v}_{\bar{\nu}_l}(k)\Gamma_l v_{l^+}(k')\otimes\bar{u}_n(p')\Gamma_h u_p(p)\,, \end{aligned} \tag{3.34}$$

where $V = p/M$, we neglect the imaginary part and $V\cdot k' = E_{\bar{\nu}} - Q^2/(2M)$.

Thus, similarly, the total of tree level and one-loop virtual correction to anti-neutrino proton scattering is

$$\begin{aligned} &\int d\Pi \sum |\mathcal{M}_{\bar{\nu}}(\mu)|^2_{tree}\left\{1+\frac{\alpha}{4\pi}\left[\frac{10\pi^2}{3}-4\log^2\left(\frac{2E_{\bar{\nu}}}{m}-\frac{Q^2}{mM}\right)\right.\right. \\ &\left.\left.+8\log\frac{\lambda}{m}\left[\log\left(\frac{2E_{\bar{\nu}}}{m}-\frac{Q^2}{mM}\right)-1\right]+4\log\left(\frac{2E_{\bar{\nu}}}{m}-\frac{Q^2}{mM}\right)-6\log\frac{m}{\mu}\right]\right\} \end{aligned} \tag{3.35}$$

where the tree level amplitude is the same as neutrino neutron scattering in the heavy nucleon limit,

$$\sum |\mathcal{M}_{\bar{\nu}}(\mu)|^2_{tree} = \frac{c_F^2}{2}128\left[c_V^2(\mu)+c_A^2(\mu)\right]M^2E^2_{\bar{\nu}}\left[1+\frac{c_A^2(\mu)-c_V^2(\mu)}{c_V^2(\mu)+c_A^2(\mu)}\frac{m^2+Q^2}{4E^2_{\bar{\nu}}}\right]. \tag{3.36}$$

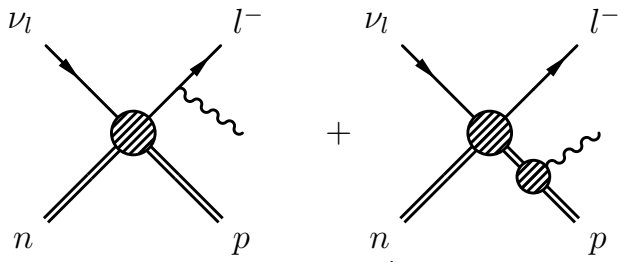

Figure 3.4: Real radiation correction to neutrino neutron scattering.

3.4 Real Radiative Correction

3.4.1 Real Radiation Amplitudes

We consider one real photon radiation correction to the tree level process, i.e. 2-to-3 process $\nu_l(k)+n(p) \to l^-(k')+p(p')+\gamma(k_\gamma)$ and $\bar{\nu}_l(k)+p(p) \to l^+(k')+n(p')+\gamma(k_\gamma)$. We will work in the heavy nucleon limit and neglect all $1/M$ order corrections.

For real radiation emission of neutrino neutron scattering, we have the following leading order diagrams:

$$\begin{aligned} i\mathcal{M}_\nu &= c_F \bar{u}_{l^-}(-ie)\not{\epsilon}^* \frac{i}{\not{k}' + \not{k}_\gamma - m}\Gamma_l u_\nu \otimes \bar{u}_p \Gamma_h u_n \\ &\quad + c_F \bar{u}_{l^-}\Gamma_l u_\nu \otimes \bar{u}_p(+ie)\not{\epsilon}^* \frac{i}{\not{p}' + \not{k}_\gamma - M}\Gamma_h u_n \,, \end{aligned} \tag{3.37}$$

where the polarization vector ϵ satisfies $\epsilon_\alpha \epsilon^*_\beta = -g_{\alpha\beta}$. In the limit $M \to \infty$, define $p'^\mu \equiv MV^\mu$ and we have

$$\frac{i}{\not{p}' + \not{k}_\gamma - M} = \frac{i(M\not{V} + \not{k}_\gamma + M)}{2MV \cdot k_\gamma} \to i\frac{1+\not{V}}{2V \cdot k_\gamma} \tag{3.38}$$

Thus, the amplitude becomes

$$i\mathcal{M}_\nu = ec_F \left[\bar{u}_{l^-}\not{\epsilon}^* \frac{\not{k}' + \not{k}_\gamma + m}{2k' \cdot k_\gamma}\Gamma_l u_\nu \otimes \bar{u}_p \Gamma_h u_n - \frac{V \cdot \epsilon^*}{V \cdot k_\gamma}\bar{u}_{l^-}\Gamma_l u_\nu \otimes \bar{u}_p \Gamma_h u_n \right] \tag{3.39}$$

Taking $\Gamma^\mu_l = \gamma^\mu(1-\gamma^5)$ and $\Gamma^\mu_h = c_V(\mu)\gamma^\mu + c_A(\mu)\gamma^\mu\gamma^5$, we have

$$\begin{aligned} \frac{1}{2}\sum_{spins}|\mathcal{M}_\nu|^2 = \frac{c_F^2}{2}128e^2M^2 \Bigg\{ & \left(c_V^2 + c_A^2\right)\cdot E_\nu^2 \Bigg[-\frac{1}{(V\cdot k_\gamma)^2} + \frac{2E_\nu}{V\cdot k_\gamma k'\cdot k_\gamma} \\ & + \frac{V\cdot k_\gamma}{E_\nu k'\cdot k_\gamma} - \frac{m^2}{(k'\cdot k_\gamma)^2} - \frac{2}{k'\cdot k_\gamma}\Bigg] + \frac{1}{2}\left(c_V^2 - c_A^2\right)\cdot\Bigg[\frac{k'\cdot k}{(V\cdot k_\gamma)^2} \\ & + \frac{k'\cdot k}{k'\cdot k_\gamma} + \frac{m^2(k'+k_\gamma)\cdot k}{(k'\cdot k_\gamma)^2} + \frac{E_\nu}{k_\gamma \cdot V} - 2\frac{E_\nu k'\cdot k}{V\cdot k_\gamma k'\cdot k_\gamma} - \frac{E_\nu k\cdot k_\gamma}{V\cdot k_\gamma k'\cdot k_\gamma}\Bigg]\Bigg\}. \end{aligned} \tag{3.40}$$

Similarly, for anti-neutrino proton scattering,

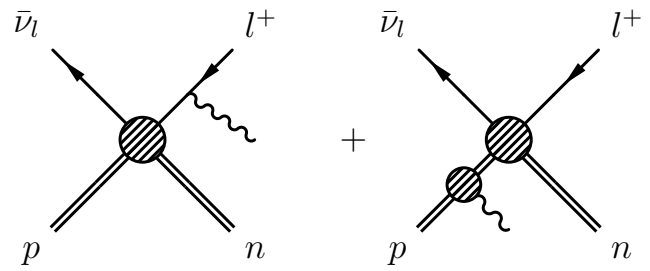

Figure 3.5: Real radiation correction to antineutrino proton scattering.

$$\begin{aligned} i\mathcal{M}_{\bar{\nu}} &= c_F \bar{v}_{\bar{\nu}} \Gamma_l \frac{i}{-\not{k}' - \not{k}_\gamma - m}(-ie)\not{\epsilon}^* v_{l^+} \otimes \bar{u}_n \Gamma_h u_p \\ &\quad + c_F \bar{v}_{\bar{\nu}} \Gamma_l v_{l^+} \otimes \bar{u}_n \Gamma_h \frac{i}{\not{p} - \not{k}_\gamma - M}(+ie)\not{\epsilon}^* u_n \end{aligned} \tag{3.41}$$

In the heavy nucleon mass limit, we also define the proton velocity to be V, then

$$i\mathcal{M}_{\bar{\nu}} = ec_F \left[-\bar{v}_{\bar{\nu}} \Gamma_l \frac{\not{k}' + \not{k}_\gamma - m}{2k' \cdot k_\gamma} \not{\epsilon}^* v_{l^+} \otimes \bar{u}_n \Gamma_h u_p + \frac{V \cdot \epsilon^*}{V \cdot k_\gamma} \bar{v}_{\bar{\nu}} \Gamma_l v_{l^+} \otimes \bar{u}_n \Gamma_h u_p \right] \tag{3.42}$$

Taking $\Gamma_l^\mu = \gamma^\mu(1-\gamma^5)$ and $\Gamma_h^\mu = c_V(\mu)\gamma^\mu + c_A(\mu)\gamma^\mu\gamma^5$, we have

$$\begin{aligned} \frac{1}{2}\sum_{spins} |\mathcal{M}_{\bar{\nu}}|^2 = \frac{c_F^2}{2} 128 e^2 M^2 \Bigg\{ & \left(c_V^2 + c_A^2\right) \cdot E_{\bar{\nu}}^2 \Bigg[-\frac{1}{(V \cdot k_\gamma)^2} + \frac{2E_{\bar{\nu}}}{V \cdot k_\gamma k' \cdot k_\gamma} \\ & + \frac{V \cdot k_\gamma}{E_{\bar{\nu}} k' \cdot k_\gamma} - \frac{m^2}{(k' \cdot k_\gamma)^2} - \frac{2}{k' \cdot k_\gamma} \Bigg] + \frac{1}{2}\left(c_V^2 - c_A^2\right) \cdot \Bigg[\frac{k' \cdot k}{(V \cdot k_\gamma)^2} \\ & + \frac{k' \cdot k}{k' \cdot k_\gamma} + \frac{m^2(k' + k_\gamma) \cdot k}{(k' \cdot k_\gamma)^2} + \frac{E_{\bar{\nu}}}{k_\gamma \cdot V} - 2\frac{E_{\bar{\nu}} k' \cdot k}{V \cdot k_\gamma k' \cdot k_\gamma} - \frac{E_{\bar{\nu}} k \cdot k_\gamma}{V \cdot k_\gamma k' \cdot k_\gamma} \Bigg] \Bigg\}. \end{aligned} \tag{3.43}$$

Note that the real radiative correction amplitude is the same in the heavy nucleon limit for both neutrino and antineutrino scattering processes when the incoming neutrino and antineutrino carry the same energy, outgoing (anti)leptons and photons have the same momenta.

3.4.2 Phase Space Integration for Real Radiation

Let us introduce a cut δ to do the phase space integration for the real radiation, where $\delta \ll E_\nu$.

For the integrals in the $c_V^2 + c_A^2$ part, we have

$$\int_0^\delta d\Pi\left[-E_\nu^2\frac{1}{(V\cdot k_\gamma)^2}\right] = -\frac{E_\nu^3}{2M(2\pi)^3}\left[-1+\log\frac{2\delta}{\lambda}\right] \tag{3.44}$$

$$\int_\delta^{E_\nu} d\Pi\left[-E_\nu^2\frac{1}{(V\cdot k_\gamma)^2}\right] = -\frac{E_\nu^3}{2M(2\pi)^3}\left[-1+\log\frac{E_\nu}{\delta}\right] \tag{3.45}$$

$$\int_0^\delta d\Pi\left[2E_\nu^3\frac{1}{(V\cdot k_\gamma)(k'\cdot k_\gamma)}\right] = \frac{2E_\nu^3}{2M(2\pi)^3}\left[-\frac{\pi^2}{12}-\frac{1}{2}\log^2\frac{2E_\nu}{m} + \log\frac{2\delta}{\lambda}\log\frac{2E_\nu}{m}\right] \tag{3.46}$$

$$\int_\delta^{E_\nu} d\Pi\left[2E_\nu^3\frac{1}{(V\cdot k_\gamma)(k'\cdot k_\gamma)}\right] = \frac{2E_\nu^3}{2M(2\pi)^3}\left[-\frac{\pi^2}{6}+\log\frac{E_\nu}{\delta}\log\frac{2E_\nu}{m}\right] \tag{3.47}$$

$$\int_0^\delta d\Pi\left[E_\nu\frac{V\cdot k_\gamma}{k'\cdot k_\gamma}\right] = \mathcal{O}\left(\frac{\delta^2}{E_\nu^2}\right) \tag{3.48}$$

$$\int_\delta^{E_\nu} d\Pi\left[E_\nu\frac{V\cdot k_\gamma}{k'\cdot k_\gamma}\right] = \frac{E_\nu^3}{2M(2\pi)^3}\left[-\frac{3}{4}+\frac{1}{2}\log\frac{2E_\nu}{m}\right] \tag{3.49}$$

$$\int_0^\delta d\Pi\left[-m^2E_\nu^2\frac{1}{(k'\cdot k_\gamma)^2}\right] = -\frac{E_\nu^3}{2M(2\pi)^3}\left[-\log\frac{2E_\nu}{m}+\log\frac{2\delta}{\lambda}\right] \tag{3.50}$$

$$\int_\delta^{E_\nu} d\Pi\left[-m^2E_\nu^2\frac{1}{(k'\cdot k_\gamma)^2}\right] = -\frac{E_\nu^3}{2M(2\pi)^3}\left[-1+\log\frac{E_\nu}{\delta}\right] \tag{3.51}$$

$$\int_0^\delta d\Pi\left[-2E_\nu^2\frac{1}{k'\cdot k_\gamma}\right] = \mathcal{O}\left(\frac{\delta}{E_\nu}\right) \tag{3.52}$$

$$\int_\delta^{E_\nu} d\Pi\left[-2E_\nu^2\frac{1}{k'\cdot k_\gamma}\right] = -2\frac{E_\nu^3}{2M(2\pi)^3}\left[-1+\log\frac{2E_\nu}{m}\right] \tag{3.53}$$

where the phase space in the heavy nucleon limit is

$$\begin{aligned}&\int\frac{d^3\mathbf{p}'}{(2\pi)^3 2E_{p'}}\int\frac{d^3\mathbf{k}'}{(2\pi)^3 2E_{k'}}\int\frac{d^3\mathbf{k}_\gamma}{(2\pi)^3 2E_{k_\gamma}}(2\pi)^4\delta^{(4)}(p'+k'+k_\gamma-p-k)\\ &=\int\frac{d^3\mathbf{k}'}{(2\pi)^3 2E_{k'}}\int\frac{d^3\mathbf{k}_\gamma}{(2\pi)^3 2E_{k_\gamma}}\frac{(2\pi)}{2M}\delta(E_{k'}+E_{k_\gamma}-E_\nu)\,,\end{aligned} \tag{3.54}$$

and the lower and upper limits in the integrals represent the energy range of the emitted photon. The general 2-to-3 phase space can be found in Appendix D.

For the integrals in the $(c_V^2-c_A^2)$ part, we can write them in terms of the integrals we have performed for the $(c_V^2+c_A^2)$ part, explicitly,

$$\int d\Pi\frac{k'\cdot k}{(V\cdot k_\gamma)^2} = \int d\Pi\frac{E_\nu^2}{(V\cdot k_\gamma)^2} - \int d\Pi\frac{E_\nu}{V\cdot k_\gamma} \tag{3.55}$$

$$\int d\Pi \frac{k'\cdot k}{k'\cdot k_\gamma} = \int d\Pi \frac{E_\nu^2}{k'\cdot k_\gamma} - \int d\Pi E_\nu \frac{V\cdot k_\gamma}{k'\cdot k_\gamma} \tag{3.56}$$

$$\begin{aligned}\int d\Pi \frac{m^2(k'+k_\gamma)\cdot k}{(k'\cdot k_\gamma)^2} &= \int d\Pi \frac{m^2 E_\nu^2}{(k'\cdot k_\gamma)^2} - \int d\Pi \frac{m^2 E_\nu^2 V\cdot k_\gamma}{(k'\cdot k_\gamma)^2} \\ &\quad + \int d\Pi \frac{m^2 E_\nu^2}{(k'\cdot k_\gamma)^2} - \int d\Pi \frac{m^2 E_\nu^2 V\cdot k'}{(k'\cdot k_\gamma)^2} \\ &= \int d\Pi \frac{m^2 E_\nu^2}{(k'\cdot k_\gamma)^2}\end{aligned} \tag{3.57}$$

$$\int d\Pi \frac{E_\nu}{k_\gamma\cdot V} = \int d\Pi \frac{E_\nu}{k_\gamma\cdot V} \tag{3.58}$$

$$-\int d\Pi \frac{2E_\nu k'\cdot k}{V\cdot k_\gamma k'\cdot k_\gamma} = -\int d\Pi \frac{2E_\nu^3}{V\cdot k_\gamma k'\cdot k_\gamma} + \int d\Pi \frac{2E_\nu^2}{k'\cdot k_\gamma} \tag{3.59}$$

$$-\int d\Pi \frac{E_\nu k\cdot k_\gamma}{V\cdot k_\gamma k'\cdot k_\gamma} = -\int d\Pi \frac{E_\nu^2}{k'\cdot k_\gamma} \tag{3.60}$$

The sum of the integrals in the $(c_V^2 - c_A^2)$ part, Eq. (3.55) to Eq. (3.60) is identical to that in the $(c_V^2 + c_A^2)$ part with a minus sign and we can write down the cross section for the process of one real photon emission as

$$\begin{aligned}\int \frac{d\Pi}{4E_\nu M}\frac{1}{2}\sum_{spins}|\mathcal{M}|^2 = \int \frac{d\Pi}{4E_\nu M}\frac{c_F^2}{2}128e^2M^2E_\nu^2\left(c_V^2+c_A^2\right)\left(1-\frac{1}{2}\frac{c_V^2-c_A^2}{c_V^2+c_A^2}\right) \\ \left[-\frac{1}{(V\cdot k_\gamma)^2}+\frac{2E_\nu}{V\cdot k_\gamma k'\cdot k_\gamma}+\frac{V\cdot k_\gamma}{E_\nu k'\cdot k_\gamma}-\frac{m^2}{(k'\cdot k_\gamma)^2}-\frac{2}{k'\cdot k_\gamma}\right].\end{aligned} \tag{3.61}$$

Summing over phase space integrals Eq. (3.45), Eq. (3.47), Eq. (3.49), Eq. (3.51) and Eq. (3.53), we obtain the total energetic real radiation with photon energy greater than δ

$$\int d\Pi \sum |\mathcal{M}|^2_{tree}\frac{\alpha}{4\pi}\left[13-\frac{4}{3}\pi^2+8\log\frac{2E_\nu}{\delta}\left(-1+\log\frac{2E_\nu}{m}\right)-6\log\frac{2E_\nu}{m}\right]. \tag{3.62}$$

The soft radiation comes from the terms with photon energy less than δ, corresponding to phase space integrals Eq. (3.44), Eq. (3.46), Eq. (3.48), Eq. (3.50) and Eq. (3.52), and their sum is

$$\int d\Pi \sum |\mathcal{M}|^2_{tree}\frac{\alpha}{\pi}\left[1-\frac{\pi^2}{6}-2\log\frac{2\delta}{\lambda}\left(1-\log\frac{2E_\nu}{m}\right)+\log\frac{2E_\nu}{m}-\log^2\frac{2E_\nu}{m}\right]. \tag{3.63}$$

It is also confirmed by the eikonal method calculation for the soft radiation,

$$\int_0^\delta d\Pi \sum |\mathcal{M}|^2_{soft} = \int_0^\delta d\Pi \sum |\mathcal{M}|^2_{tree}\int \frac{d^3\mathbf{k}_\gamma}{(2\pi)^3 2E_{k_\gamma}}\frac{1}{(k'\cdot k_\gamma)^2}\left[\mathbf{k}'^2-(\mathbf{k}'\cdot\hat{\mathbf{k}}_\gamma)^2\right]$$

$$= \int d\Pi \sum |\mathcal{M}|^2_{tree} \frac{e^2}{(4\pi)^2}(-4)\left[2\log\frac{2\delta}{\lambda}\left(1-\log\frac{2E_\nu}{m}\right)\right.$$
$$\left. -\log\frac{2E_\nu}{m}+\log^2\frac{2E_\nu}{m}+\frac{\pi^2}{6}-1\right], \tag{3.64}$$

where $\hat{\mathbf{k}}_\gamma \equiv \mathbf{k}_\gamma/\sqrt{{\mathbf{k}_\gamma}^2+\lambda^2}$.

The total real radiation result is

$$\int d\Pi \sum |\mathcal{M}|^2_{tree} \frac{\alpha}{4\pi}\left[17-2\pi^2-2\log\frac{2E_\nu}{m}-4\log^2\frac{2E_\nu}{m}\right.$$
$$\left. +8\log\frac{2E_\nu}{\lambda}\left(\log\frac{2E_\nu}{m}-1\right)\right]. \tag{3.65}$$

Summing up the virtual radiative correction Eq. (3.30) and real radiative correction Eq. (3.65), we obtain the total radiative corrected cross section in the heavy nucleon limit,

$$\sigma = \frac{1}{4E_\nu M}\int d\Pi \sum |\mathcal{M}|^2_{tree}\left[1+\frac{\alpha}{4\pi}\left(17+\frac{4}{3}\pi^2-6\log\frac{2E_\nu}{\mu}\right)\right]$$
$$= \sigma_{tree}\left[1+\frac{\alpha}{4\pi}\left(17+\frac{4}{3}\pi^2-6\log\frac{2E_\nu}{\mu}\right)\right], \tag{3.66}$$

where σ_{tree} is provided in Eq. (3.32).

Note that this result doesn't depend on the final state lepton mass, thus flavor-independent, which means the radiative correction effect doesn't affect the muon-neutrino oscillation result that is being measured as an inclusive observable in the experiments in the heavy nucleon limit with $m \ll E_\nu \ll M$ except for small mass power corrections of order m^2/E_ν^2. This is also a result of the Kinoshita-Lee-Nauenberg theorem [145, 146], which states that there is no mass singularity for inclusive QED scattering processes in the massless limit.

3.5 Sterman-Weinberg Cone Observable

We have computed inclusive observable in previous sections. Jet observables are another type of observables more common in high energy experiments. To study jet observables, We consider an observable defined by Sterman and Weinberg [147]. Define a cone along the outgoing lepton direction with half angle θ and assume that $(1-\beta)E_\nu$ is deposited within this cone, where $\theta \ll 1$, $\beta \ll 1$. There are three scenarios for possible photon emission, as analogs of those in [147]:

(a) one "hard" photon (energy $\geqslant \beta E_\nu$) being emitted within the cone;

(b) one "soft" photon (energy $\leqslant \beta E_\nu$) being emitted in or not in the cone;

(c) no photon emission (virtual process).

Senario (a): We can replace the cutoff δ in Section 3.4.2 by βE_ν and restrict the photon phase space integration within the cone, i.e. the angle between photon and outgoing lepton momenta ranges from $(0,\, \theta)$.

Collecting contribution from each term, we have

$$\int_{\beta E_\nu}^{E_\nu} d\Pi_{cone}\left[-\frac{1}{4}E_\nu^2\frac{1}{(V\cdot k)^2}\right] = -\frac{1}{4}\frac{E_\nu^3}{2M(2\pi)^3}\frac{\theta^2}{4}\left[-1-\log\beta\right] \tag{3.67}$$

$$\begin{aligned}\int_{\beta E_\nu}^{E_\nu} d\Pi_{cone}\left[\frac{1}{2}E_\nu^3\frac{1}{(V\cdot k)(p\cdot k)}\right] &= \frac{1}{4}\frac{E_\nu^3}{2M(2\pi)^3}\left[\frac{1}{2}\mathrm{Li}_2\left(-\eta^2\right) - \left(\tan^{-1}\eta\right)^2\right.\\ &\left. -\log\left(1+\eta^2\right)\log\beta + \frac{1}{4}\log^2\left(1+\eta^2\right)\right]\end{aligned} \tag{3.68}$$

$$\begin{aligned}\int_{\beta E_\nu}^{E_\nu} d\Pi_{cone}\left[\frac{1}{4}E_\nu\frac{V\cdot k}{p\cdot k}\right] &= \frac{1}{4}\frac{E_\nu^3}{2M(2\pi)^3}\left[-\frac{3-2\beta-\beta^2}{4} + \frac{\tan^{-1}\left[(1-\beta)\eta\right]}{\eta}\right.\\ &\left. +\frac{1}{4}\left(1-\beta^2-\frac{1}{\eta^2}\right)\log(1+\eta^2)\right]\end{aligned} \tag{3.69}$$

$$\begin{aligned}\int_{\beta E_\nu}^{E_\nu} d\Pi_{cone}\left[-\frac{1}{4}m^2E_\nu^2\frac{1}{(p\cdot k)^2}\right] &= -\frac{1}{4}\frac{E_\nu^3}{2M(2\pi)^3}\left[-(1-\beta) - \frac{\eta^2}{1+\eta^2}\log\beta\right.\\ &\left. -\frac{\log\left(1+(1-\beta)^2\eta^2\right)}{2(1+\eta^2)} + \frac{\tan^{-1}\left[(1-\beta)\eta\right]}{(1+\eta^2)\eta}\right]\end{aligned} \tag{3.70}$$

$$\begin{aligned}\int_{\beta E_\nu}^{E_\nu} d\Pi_{cone}\left[-\frac{1}{2}E_\nu^2\frac{1}{p\cdot k}\right] &= -\frac{1}{2}\frac{E_\nu^3}{2M(2\pi)^3}\left[-1+\beta + \frac{\tan^{-1}\left[(1-\beta)\eta\right]}{\eta}\right.\\ &\left. +\frac{1-\beta}{2}\log\left(1+(1-\beta)^2\eta^2\right)\right],\end{aligned} \tag{3.71}$$

where $\eta \equiv \theta E_\nu/m$, the phase space integrals for the $(c_V^2 - c_A^2)$ part terms are power terms of small angle θ and have been neglected.

The total energetic photon radiation in the cone is

$$\begin{aligned}\int d\Pi \sum |\mathcal{M}(\mu)|^2_{tree}\frac{\alpha}{4\pi}\left[9 - \frac{4(2+\eta^2)}{\eta(1+\eta^2)}\tan^{-1}\eta - 4\left(\tan^{-1}\eta\right)^2 + 4\frac{\eta^2}{1+\eta^2}\log\left(\frac{\Delta E}{E_\nu}\right)\right.\\ -3\log\left(1+\eta^2\right) - \frac{\log\left(1+\eta^2\right)}{\eta^2} + 2\frac{\log\left(1+\eta^2\right)}{1+\eta^2}\\ \left. -4\log\left(\frac{\Delta E}{E_\nu}\right)\log\left(1+\eta^2\right) + \log^2\left(1+\eta^2\right) + 2\mathrm{Li}_2(-\eta^2)\right].\end{aligned} \tag{3.72}$$

When $m \ll \theta E_\nu$, i.e. $\eta \gg 1$, the above results reduce to:

$$\int_{\beta E_\nu}^{E_\nu} d\Pi_{cone}\left[-\frac{1}{4}E_\nu^2\frac{1}{(V\cdot k)^2}\right] = -\frac{1}{4}\frac{E_\nu^3}{2M(2\pi)^3}\frac{\theta^2}{4}\left[-1-\log\beta\right] \tag{3.73}$$

$$\int_{\beta E_\nu}^{E_\nu} d\Pi_{cone}\left[\frac{1}{2}E_\nu^3\frac{1}{(V\cdot k)(p\cdot k)}\right] = \frac{1}{2}\frac{E_\nu^3}{2M(2\pi)^3}\left[-\frac{\pi^2}{6}-\log\beta\log\frac{\theta E_\nu}{m}\right] \tag{3.74}$$

$$\int_{\beta E_\nu}^{E_\nu} d\Pi_{cone}\left[\frac{1}{4}E_\nu\frac{V\cdot k}{p\cdot k}\right] = \frac{1}{4}\frac{E_\nu^3}{2M(2\pi)^3}\left[-\frac{3}{4}+\frac{1}{2}\log\frac{\theta E_\nu}{m}\right] \tag{3.75}$$

$$\int_{\beta E_\nu}^{E_\nu} d\Pi_{cone}\left[-\frac{1}{4}m^2E_\nu^2\frac{1}{(p\cdot k)^2}\right] = -\frac{1}{4}\frac{E_\nu^3}{2M(2\pi)^3}\left[-1-\log\beta\right] \tag{3.76}$$

$$\int_{\beta E_\nu}^{E_\nu} d\Pi_{cone}\left[-\frac{1}{2}E_\nu^2\frac{1}{p\cdot k}\right] = -\frac{1}{2}\frac{E_\nu^3}{2M(2\pi)^3}\left[-1+\log\frac{\theta E_\nu}{m}\right] \tag{3.77}$$

Scenario (b): We consider "soft" emission with photon energy less than βE_ν but without restriction of direction. Then we only need to replace δ in Sec. 3.4.2 by βE_ν, keeping the entire phase space and readily have,

$$\int_0^{\beta E_\nu} d\Pi\left[-\frac{1}{4}E_\nu^2\frac{1}{(V\cdot k)^2}\right] = -\frac{1}{4}\frac{E_\nu^3}{2M(2\pi)^3}\left[-1+\log\frac{2\beta E_\nu}{\lambda}\right] \tag{3.78}$$

$$\int_0^{\beta E_\nu} d\Pi\left[\frac{1}{2}E_\nu^3\frac{1}{(V\cdot k)(p\cdot k)}\right] = \frac{1}{2}\frac{E_\nu^3}{2M(2\pi)^3}\left[-\frac{\pi^2}{12}-\frac{1}{2}\log^2\frac{2E_\nu}{m} + \log\frac{2\beta E_\nu}{\lambda}\log\frac{2E_\nu}{m}\right] \tag{3.79}$$

$$\int_0^{\beta E_\nu} d\Pi\left[\frac{1}{4}E_\nu\frac{V\cdot k}{p\cdot k}\right] = \frac{1}{4}\frac{E_\nu^3}{2M(2\pi)^3}\left[\frac{1}{2}\beta^2\log\frac{2E_\nu}{m}\right] \tag{3.80}$$

$$\int_0^{\beta E_\nu} d\Pi\left[-\frac{1}{4}m^2E_\nu^2\frac{1}{(p\cdot k)^2}\right] = -\frac{1}{4}\frac{E_\nu^3}{2M(2\pi)^3}\left[\log\frac{\beta m}{\lambda}\right] \tag{3.81}$$

$$\int_0^{\beta E_\nu} d\Pi\left[-\frac{1}{2}E_\nu^2\frac{1}{p\cdot k}\right] = -\frac{1}{2}\frac{E_\nu^3}{2M(2\pi)^3}\left[\beta\log\frac{2E_\nu}{m}\right] \tag{3.82}$$

The sum of the above terms is the total soft emission

$$\int d\Pi\sum|\mathcal{M}(\mu)|^2_{tree}\frac{\alpha}{\pi}\left[1-\frac{\pi^2}{6}-2\log\frac{2\beta E_\nu}{\lambda}\left(1-\log\frac{2E_\nu}{m}\right)+\log\frac{2E_\nu}{m}-\log^2\frac{2E_\nu}{m}\right]. \tag{3.83}$$

Scenario (c): There is no real photon emission. The result is given by Eq.(3.24).

$$\int d\Pi \sum |\mathcal{M}(\mu)|^2_{tree} \frac{\alpha}{4\pi} \left[\frac{10\pi^2}{3} - 4\log^2 \frac{2E_\nu}{m} + 8\log\frac{\lambda}{m}\left(\log\frac{2E_\nu}{m} - 1\right) + 4\log\frac{2E_\nu}{m} - 6\log\frac{m}{\mu}\right], \tag{3.84}$$

The sum of hard real emission in the Sterman-Weinberg cone, soft real emission and virtual process is the total radiative correction cross section over tree level ratio is

$$\begin{aligned}\delta\sigma^{\rm SW} = \frac{\alpha}{\pi}\Bigg\{ & \frac{1}{2}\mathrm{Li}_2\left(-\eta^2\right) + \frac{1}{4}\ln^2\left(1+\eta^2\right) + \frac{1}{4}\left(\frac{2}{1+\eta^2} - \frac{1}{\eta^2} - 3\right)\ln\left(1+\eta^2\right) \\ & + \frac{3}{2}\ln\frac{\mu}{m} + \frac{13}{4} + \frac{2\pi^2}{3} - \left(\tan^{-1}\eta\right)^2 - \left(1 + \frac{1}{1+\eta^2}\right)\frac{\tan^{-1}\eta}{\eta} \\ & \left(\frac{\eta^2}{1+\eta^2} - 2 - \ln\left(1+\eta^2\right) + 2\ln\frac{2E_\nu}{m}\right)\ln\beta\Bigg\}. \end{aligned} \tag{3.85}$$

In the small mass limit, i.e. $\eta \gg 1$, it goes to

$$\delta\sigma^{\rm SW}_{m\to 0} = \frac{\alpha}{\pi}\left\{\frac{1}{4}\left(6\ln\frac{\mu}{2E_\nu} + \frac{4\pi^2}{3} + 13\right) - \frac{3}{4}\ln\frac{\theta^2}{4} - \left(1 + \ln\frac{\theta^2}{4}\right)\ln\beta\right\}. \tag{3.86}$$

In the small angle limit, i.e. $\eta \ll 1$, it goes to

$$\delta\sigma^{\rm SW}_{\theta\to 0} = \frac{\alpha}{\pi}\left\{2\left(\ln\frac{2E_\nu}{m} - 1\right)\ln\beta + \frac{3}{2}\ln\frac{\mu}{m} + 1 + \frac{2\pi^2}{3}\right\}. \tag{3.87}$$

3.6 Soft-Collinear Effective Theory

In light of the cone observable which is along a certain direction, we take the charged lepton direction to be $n^\mu = (1,0,0,1)$ and define another direction $\bar{n}^\mu = (1,0,0,-1)$. We have

$$n^2 = 0,\ \bar{n}^2 = 0,\ n\cdot\bar{n} = 2\,, \tag{3.88}$$

and we call $n-$direction collinear and $\bar{n}$-direction anticollinear.

A vector p^μ can be decomposed as

$$p^\mu = \frac{p\cdot\bar{n}}{2}n^\mu + \frac{p\cdot n}{2}\bar{n}^\mu + p^\mu_\perp\,, \tag{3.89}$$

where $p^\mu_\perp$ is the component perpendicular to n^μ and $\bar{n}^\mu$ directions.

In the basis of two light cone directions n, $\bar{n}$, and a perpendicular direction, we can write the components of a vector in this basis as

$$p^\mu = \left(p^-, p^+, |\mathbf{p}_\perp|\right) , \tag{3.90}$$

where $p^+ = p \cdot n$, $p^- = p \cdot \bar{n}$, $|\mathbf{p}_\perp|^2 = -p_\perp^2$ and $p^2 = p^+ p^- + p_\perp^2$.

Since we are studying the radiative corrections, we can decompose the radiated photon momentum into the above basis. For photon with different energy scales, it shows different scalings. A hard photon momentum scales as $p \sim E_\nu(1,\, 1,\, 1)$, a collinear photon with $p \sim E_\nu(\kappa,\, 1,\, \sqrt{\kappa})$ and a soft photon with $p \sim E_\nu(\kappa,\, \kappa,\, \kappa)$, where $\kappa \ll 1$ and $\kappa \sim O(m^2/\Lambda_{hard}^2)$, where Λ_{hard} is a hard scale in the problem. We still work in the heavy nucleon limit, where formally we have $m \ll E_\nu \ll M$.

The cross section can be factorized into a product of hard, collinear and soft functions, $\sigma \sim H(E_\nu/\mu) \cdot J(m/\mu, \theta, E_\nu/m) \cdot S(\Delta E/\mu, E_\nu/m)$ up to $O(\sqrt{\kappa})$, where ΔE is a photon energy threshold that could be resolved by the detector resolution and we regard photons with energy less than ΔE as soft photons, and θ is an angle parameter that describes the collinear jet's cone size.

We can construct an effective Lagrangian for collinear lepton, collinear photon and soft photon in QED systematically, which is similar to that for quarks and gluons in [9].

For a fermion $\psi(x)$ with a collinear scaling momentum p, we can decompose it into collinear and anticollinear components ξ_n and $\xi_{\bar{n}}$, and explicitly, we have

$$\xi_n = \frac{\not{n}\bar{\not{n}}}{4}\psi\,, \quad \xi_{\bar{n}} = \frac{\bar{\not{n}}\not{n}}{4}\psi\,. \tag{3.91}$$

Decompose the gauge field A into soft and collinear components A_s and A_n,

$$A^\mu = A_s^\mu + A_n^\mu\,. \tag{3.92}$$

Similar to the derivation in chapter 1 but with fermion mass in, the soft-collinear effective lagrangian is

$$\mathcal{L}_{sc} = \bar{\xi}_n \left[n \cdot iD_n + Qn \cdot A_s + \left(i\not{D}_n^\perp - m\right)(\bar{n} \cdot iD_n)^{-1}\left(i\not{D}_n^\perp + m\right)\right]\frac{\bar{\not{n}}}{2}\xi_n\,, \tag{3.93}$$

where $D_n^\mu = \partial_\mu - iQA_n^\mu$ is the collinear derivative and Q is the electric charge of the collinear fermion. The collinear fermion and collinear gauge boson interact gauge invariantly within this Lagrangian Eq. (3.93) with the Wilson line for collinear gauge fields [10, 148]

$$W_n(x) = \mathrm{P}\exp\left[-iQ\int_{-\infty}^{0} ds\bar{n} \cdot A_n(s\bar{n} + x)\right] , \tag{3.94}$$

where P denotes path-ordering for gauge fields from left to right with parameter s decreasing. Thus, $W_n^\dagger \xi_n$ is a gauge-invariant collinear fermion and $W_n^\dagger i D_n^\mu W_n$ is a gauge-invariant gauge field. The soft gauge field is an independent field interacting with the collinear fermion and doesn't play in a role in the collinear gauge invariance.

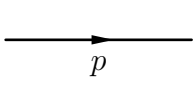

$$= i\frac{\not{\bar{n}}}{2}\frac{\bar{n}\cdot p}{(n\cdot p)(\bar{n}\cdot p)+p_\perp^2-m^2+i\epsilon}$$

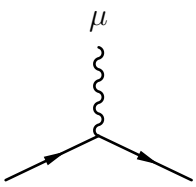

$$= iQ\frac{\not{\bar{n}}}{2}n_\mu$$

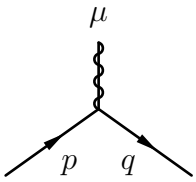

$$= iQ\left[n_\mu+\gamma_\mu^\perp\frac{(\not{p}_\perp+m)}{\bar{n}\cdot p}+\frac{(\not{q}_\perp-m)}{\bar{n}\cdot q}\gamma_\mu^\perp-\frac{(\not{q}_\perp-m)(\not{p}_\perp+m)}{(\bar{n}\cdot p)(\bar{n}\cdot q)}\bar{n}_\mu\right]\frac{\not{\bar{n}}}{2}$$

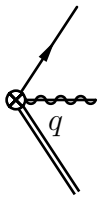

$$= iQ\frac{\bar{n}^\mu}{\bar{n}\cdot q}$$

Figure 3.6: From above to below, collinear fermion propagator, soft photon coupled to collinear fermion vertex, collinear photon coupled to collinear fermion vertex, effective current from heavy fermion to collinear fermion with collinear photon.

Radiative corrections to collinear fields involve the Feyman rules in Fig. 3.6.

Soft radiation will be treated in heavy particle effective field theory as in eq. (3.19) and Feynman rules are given in Fig. 3.7.

In the following, we will compute soft function and jet function using these two effective field theories, at α order.

3.7 Soft Function

We first consider soft virtual radiative correction diagram Fig. 3.8 for neutrino neutron scattering, treating nucleons and charged lepton as heavy particles, and making use

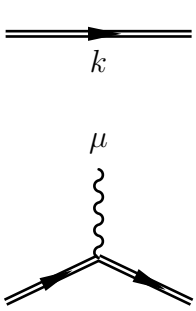

Figure 3.7: From above to below, heavy particle propagator with V being the velocity of the heavy particle and k is a dynamical momentum, soft photon coupled to heavy particle vertex with Q being the electric charge of the heavy particle.

of Feynman rules in Fig. 3.7.

The amplitude is

$$
\begin{aligned}
i\mathcal{M}^{vir}_{\nu,\,soft} &= \int \frac{d^dL}{(2\pi)^d} \bar{u}_{l^-}(k') iQ_l \frac{ik'_\alpha}{k'\cdot(-L)+i0}\gamma_\mu(1-\gamma^5)u_{\nu_l}(k)\frac{-i}{L^2-\lambda^2} \\
&\quad \otimes \bar{u}_p(p') iQ_p V^\alpha \frac{i}{V\cdot L + i0}\Gamma_h^\mu u_n(p) \\
&= c_F\frac{\alpha}{4\pi}\left[-\frac{2}{\epsilon}\log\left(\frac{2V\cdot k'}{m}\right) - 4\log\left(\frac{2V\cdot k'}{m}\right)\log\frac{\mu}{\lambda}\right]\bar{u}_{l^-}(k')\Gamma_l u_{\nu_l}(k) \\
&\quad \otimes \bar{u}_p(p')\Gamma_h u_n(p) \\
&= c_F\frac{\alpha}{4\pi}\left[-\frac{2}{\epsilon}\log\left(\frac{2E_\nu}{m}-\frac{m}{M}\right) - 4\log\left(\frac{2E_\nu}{m}-\frac{m}{M}\right)\log\frac{\mu}{\lambda}\right]\bar{u}_{l^-}(k')\Gamma_l u_{\nu_l}(k) \\
&\quad \otimes \bar{u}_p(p')\Gamma_h u_n(p)\,, \qquad (3.95)
\end{aligned}
$$

where $V = p'/M$, $V\cdot k' = E_\nu - m^2/(2M)$ in the heavy nucleon limit.

The field strength renormalization factors for the soft virtual radiative correction diagram are

$$
Z_l^s = Z_p^s = 1 + \frac{\alpha}{4\pi}\left(\frac{2}{\epsilon} + 2\log\frac{\mu^2}{\lambda^2}\right). \qquad (3.96)
$$

The interference of the virtual one loop diagram with tree level diagram gives the radiative correction to the tree level neutrino neutron scattering cross section,

$$
\int d\Pi \sum |\mathcal{M}_\nu(\mu)|^2_{tree}\frac{\alpha}{\pi}\left\{\log\frac{\mu^2}{\lambda^2}\left[1-\log\left(\frac{2E_\nu}{m}-\frac{m}{M}\right)\right]\right\}. \qquad (3.97)
$$

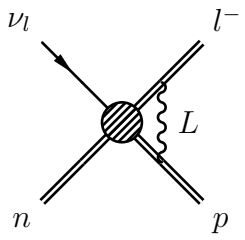

Figure 3.8: Soft virtual radiative correction to the neutrino neutron scattering.

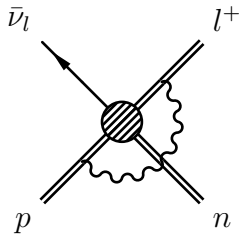

Figure 3.9: Soft virtual radiative correction to the anti-neutrino proton scattering.

Similarly for anti-neutrino proton scattering, the soft virtual radiative correction shown in Fig. 3.9 is

$$\begin{aligned} i\mathcal{M}^{\bar{\nu}}_{vir} &= c_F \int \frac{d^dL}{(2\pi)^d} \bar{v}_{\bar{\nu}_l}(k)\gamma_\mu(1-\gamma^5)\frac{-ik'_\alpha}{k'\cdot(-L)+i0}v_{l^+}(k')iQ_l\gamma_\alpha\frac{-i}{L^2-\lambda^2+i0} \\ &\quad \otimes \bar{u}_n(p')\Gamma^\mu_h\frac{i}{-V\cdot L+i0}iQ_pV^\alpha u_p(p) \\ &= c_F\frac{\alpha}{4\pi}\left[-\frac{2}{\epsilon}\log\left(\frac{2V\cdot k'}{m}\right)-4\log\left(\frac{2V\cdot k'}{m}\right)\log\frac{\mu}{\lambda}\right]\bar{v}_{\bar{\nu}_l}(k)\Gamma_l v_{l^+}(k') \\ &\quad \otimes \bar{u}_n(p')\Gamma_h u_p(p)\,, \end{aligned} \tag{3.98}$$

where $V = p/M$ and $V\cdot k' = E_{\bar{\nu}} - Q^2/(2M)$.

The interference of the virtual one loop diagram with tree level diagram gives the radiative correction to the tree level anti-neutrino proton cross section,

$$\int d\Pi \sum |\mathcal{M}_{\bar{\nu}}(\mu)|^2_{tree}\frac{\alpha}{\pi}\left\{\log\frac{\mu^2}{\lambda^2}\left[1-\log\left(\frac{2E_{\bar{\nu}}}{m}-\frac{Q^2}{2mM}\right)\right]\right\}. \tag{3.99}$$

The soft real radiative correction to neutrino neutron scattering consists of real emissions from both charged lepton and charged nucleon as in Fig. 3.10.

The amplitude of photon emission from the lepton line is

$$i\mathcal{M}^{real}_{\nu,ls} = e\frac{\epsilon\cdot k'}{k_\gamma\cdot k'}\bar{u}_{l^-}(k')\Gamma_l u_{\nu_l}(k)\otimes\bar{u}_p(p')\Gamma_h u_n(p) \tag{3.100}$$

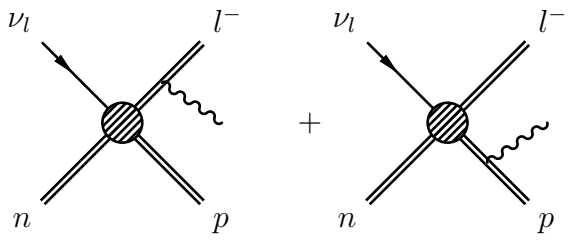

Figure 3.10: Soft photon emissions from charged lepton and charged nucleon.

The amplitude of photon emission from the hadron line is

$$i\mathcal{M}^{real}_{\nu,\,hs} = -e\frac{\epsilon\cdot V}{k_\gamma\cdot V}\bar{u}_{l^-}(k')\Gamma_l u_{\nu_l}(k)\otimes\bar{u}_p(p')\Gamma_h u_n(p) \tag{3.101}$$

The total amplitude of real soft photon emission is

$$i\mathcal{M}^{real}_{\nu,\,s} = e\left(\frac{\epsilon\cdot k'}{k_\gamma\cdot k'}-\frac{\epsilon\cdot V}{k_\gamma\cdot V}\right)\bar{u}_{l^-}(k')\Gamma_l u_{\nu_l}(k)\otimes\bar{u}_p(p')\Gamma_h u_n(p) \tag{3.102}$$

$$\int d\Pi|\mathcal{M}^{real}_{\nu,\,s}|^2 = \int d\Pi\int_{k^0_\gamma\leqslant\Delta E}\frac{d^3\mathbf{k}_\gamma}{(2\pi)^3}\frac{1}{2k^0_\gamma}\left[-e^2\left(\frac{V^\mu}{k_\gamma\cdot V}-\frac{V'^\mu}{k_\gamma\cdot V'}\right)^2\right]|\mathcal{M}_\nu|^2_{tree}\,, \tag{3.103}$$

where $V = p'/M$ and $V' = k'/m$.

The integral is, c.f. [149]

$$\begin{aligned}&\int_{k^0_\gamma\leqslant\Delta E}\frac{d^3\mathbf{k}_\gamma}{(2\pi)^3}\frac{1}{2k^0_\gamma}\left(\frac{V^\mu}{k_\gamma\cdot V}-\frac{V'^\mu}{k_\gamma\cdot V'}\right)^2\\ &=\frac{1}{4\pi^2}\left\{2\log\left(\frac{2\Delta E}{\lambda}\right)\Big[wf(w)-1\Big]+G(w,V^0,V'^0)\right\},\end{aligned} \tag{3.104}$$

where $w = V\cdot V'$, $k^0_\gamma = \sqrt{\mathbf{k}^2_\gamma+\lambda^2}$,

$$\begin{aligned}f(w) &= \frac{1}{\sqrt{w^2-1}}\log(w_+),\\ G(w,V^0,V'^0) &= \frac{V^0}{\sqrt{(V^0)^2-1}}\log V^0_+ + \frac{V'^0}{\sqrt{(V'^0)^2-1}}\log V'^0_+\\ &\quad+\frac{w}{\sqrt{w^2-1}}\left[\log^2 V^0_+ - \log^2 V'^0_+ + \mathrm{Li}_2\left(1-\frac{V^0_+}{\sqrt{w^2-1}}\left(w_+V^0-V'^0\right)\right)\right.\\ &\quad+\mathrm{Li}_2\left(1-\frac{V^0_-}{\sqrt{w^2-1}}\left(w_+V^0-V'^0\right)\right)\\ &\quad\left.-\mathrm{Li}_2\left(1-\frac{V'^0_+}{\sqrt{w^2-1}}\left(V^0-w_-V'^0\right)\right)\right.\end{aligned}$$

$$- \mathrm{Li}_2\left(1 - \frac{V'^0_-}{\sqrt{w^2-1}}\left(V^0 - w_- V'^0\right)\right)\Bigg], \tag{3.105}$$

and for any quantity $x > 0$, we define

$$x_\pm = x \pm \sqrt{x^2-1}\,. \tag{3.106}$$

The kinematics yield

$$\begin{aligned} V^0 &= 1 + \frac{Q^2}{2M^2}\,, \\ V'^0 &= \frac{E_\nu}{m} - \frac{Q^2}{2mM}\,, \\ w &= \frac{E_\nu}{m} - \frac{m}{2M}\,. \end{aligned} \tag{3.107}$$

In the heavy nucleon limit, neglecting all $1/M$ terms, $V^0 \to 1$, $V'^0 \to E_\nu/m$ and $w \to E_\nu/m$, and the soft real radiative correction to the tree level neutrino neutron scattering is,

$$\begin{aligned} \int d\Pi |\mathcal{M}^{real}_{\nu,\,s}|^2 = \int d\Pi |\mathcal{M}_\nu|^2_{tree} \frac{\alpha}{\pi}\Bigg[1 - \frac{\pi^2}{6} + \log\frac{2E_\nu}{m} - \log^2\frac{2E_\nu}{m} \\ - 2\log\frac{2\Delta E}{\lambda}\left(1 - \log\frac{2E_\nu}{m}\right)\Bigg]. \end{aligned} \tag{3.108}$$

Similarly, the soft real radiation for anti-neutrino proton scattering is shown in Fig. 3.11 and the result is

$$\begin{aligned} \int d\Pi |\mathcal{M}^{real}_{\bar\nu,\,s}|^2 &= \int d\Pi \int_{k^0_\gamma \leqslant \Delta E} \frac{d^3\mathbf{k}_\gamma}{(2\pi)^3}\frac{1}{2k^0_\gamma}\left[-e^2\left(\frac{V^\mu}{k_\gamma\cdot V} - \frac{V'^\mu}{k_\gamma\cdot V'}\right)^2\right]|\mathcal{M}_{\bar\nu}|^2_{tree} \\ &= -\int d\Pi \frac{\alpha}{\pi}\left\{2\log\left(\frac{2\Delta E}{\lambda}\right)\Big[wf(w) - 1\Big] + G(w, V^0, V'^0)\right\}|\mathcal{M}_{\bar\nu}|^2_{tree}\,, \end{aligned} \tag{3.109}$$

where $V = p/M$ and $V' = k'/m$.

Explicitly, the kinematics are

$$\begin{aligned} V^0 &= 1, \\ V'^0 &= \frac{E_{\bar\nu}}{m} - \frac{Q^2}{2mM}, \\ w &= \frac{E_{\bar\nu}}{m} - \frac{Q^2}{2mM}\,. \end{aligned} \tag{3.110}$$

In the heavy nucleon limit, neglecting all $1/M$ terms, $V^0 \to 1$, $V'^0 \to E_\nu/m$ and $w \to E_\nu/m$, and the soft real radiative correction to the tree level anti-neutrino

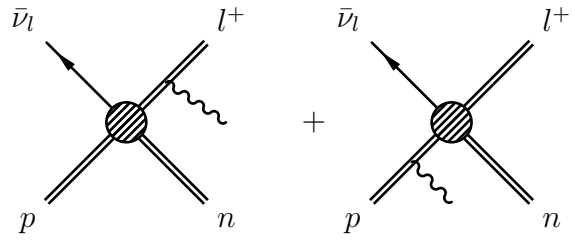

Figure 3.11: Soft photon emissions from charged lepton and charged nucleon.

proton scattering is,

$$\int d\Pi |\mathcal{M}^{real}_{\bar{\nu},\,s}|^2 = \int d\Pi |\mathcal{M}_{\bar{\nu}}|^2_{tree} \frac{\alpha}{\pi}\left[1 - \frac{\pi^2}{6} + \log\frac{2E_{\bar{\nu}}}{m} - \log^2\frac{2E_{\bar{\nu}}}{m} - 2\log\frac{2\Delta E}{\lambda}\left(1 - \log\frac{2E_{\bar{\nu}}}{m}\right)\right]. \tag{3.111}$$

Combining virtual and real emission, the total soft-radiative corrected cross section called soft function in the heavy nucleon limit is

$$\begin{aligned} S &= \int \frac{d\Pi}{4E_\nu M}\left[1 + \frac{\alpha}{\pi}\log\frac{\mu^2}{\lambda^2}\left(1 - \log\frac{2E_\nu}{m}\right)\right]\sum|\mathcal{M}(\mu)|^2_{tree} + \int \frac{d\Pi}{4E_\nu M}\frac{\alpha}{\pi}\left[1 - \frac{\pi^2}{6}\right. \\ &\quad \left. + \log\frac{2E_\nu}{m} - \log^2\frac{2E_\nu}{m} - 2\log\frac{2\Delta E}{\lambda}\left(1 - \log\frac{2E_\nu}{m}\right)\right]\sum|\mathcal{M}|^2_{tree} \\ &= \int \frac{d\Pi}{4E_\nu M}\left\{1 + \frac{\alpha}{\pi}\left[1 - \frac{\pi^2}{6} + \log\frac{2E_\nu}{m} - \log^2\frac{2E_\nu}{m}\right.\right. \\ &\quad \left.\left. + 2\log\left(\frac{\mu}{2\Delta E}\right)\left(1 - \log\frac{2E_\nu}{m}\right)\right]\right\}\sum|\mathcal{M}(\mu)|^2_{tree}\,. \end{aligned} \tag{3.112}$$

3.8 Jet Function

The collinear virtual radiative correction is depicted in Fig. 3.12 and the amplitude is

$$\begin{aligned} i\mathcal{M}^{vir}_c &= \int \frac{d^dL}{(2\pi)^d}\bar{u}_{l^-}(k')iQ_l\Big[n_\mu + \gamma^\perp_\mu\frac{\not{L}_\perp + m}{\bar{n}\cdot L} + \frac{\not{k}'_\perp - m}{\bar{n}\cdot k'}\gamma^\perp_\mu - \frac{\not{k}'_\perp - m}{\bar{n}\cdot k'}\frac{\not{L}_\perp + m}{\bar{n}\cdot L}\bar{n}_\mu\Big] \\ &\cdot\frac{\bar{n}\!\!\!/}{2}i\frac{n\!\!\!/}{2}\frac{\bar{n}\cdot L}{L^2 - m^2}Q_p\frac{\bar{n}^\mu}{\bar{n}\cdot(L - k')}\gamma_\alpha(1 - \gamma^5)u_{\nu_l}(k)\otimes\bar{u}_p(p')\Gamma_h u_n(p)\cdot\frac{-i}{(L - k')^2 - \lambda^2} \\ &= \frac{\alpha}{4\pi}\left[\frac{1}{\epsilon^2} + \frac{2}{\epsilon}\left(1 + \log\frac{\mu}{m}\right) + 4 + \frac{\pi^2}{12} + 4\log\frac{\mu}{m} + 2\log^2\frac{\mu}{m}\right]\bar{u}_{l^-}(k')\Gamma_l u_{\nu_l}(k) \end{aligned}$$

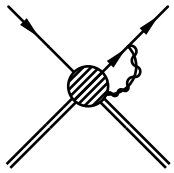

Figure 3.12: Collinear virtual radiative correction to neutrino neutron scattering.

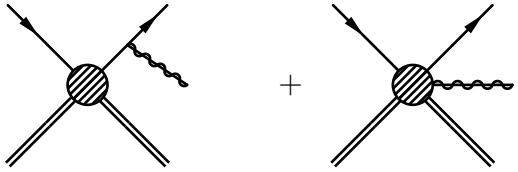

Figure 3.13: One real collinear photon emission from neutrino neutron scattering.

$$\otimes \bar{u}_p(p')\Gamma_h u_n(p)\,. \tag{3.113}$$

Collinear diagram field strength renormalization factor is

$$Z_l^c = 1 + \frac{\alpha}{4\pi}\left(-\frac{3}{\epsilon} - 4 - 6\log\frac{\mu}{m}\right). \tag{3.114}$$

The interference with the tree level diagram gives the leading order collinear virtual radiative correction

$$J_v = \int \frac{d\Pi}{4E_\nu M}\frac{\alpha}{\pi}\left[1 + \frac{\pi^2}{24} + \frac{1}{2}\log\frac{\mu}{m} + \log^2\frac{\mu}{m}\right]\sum |\mathcal{M}(\mu)|^2_{tree}\,, \tag{3.115}$$

where we have subtracted the $1/\epsilon^2$ pole, which will be canceled by that from hard function and the $1/\epsilon$ pole is canceled by coefficients c_V and c_A.

The real collinear radiation involves the two diagrams in Fig. 3.13. The amplitude for collinear emission from charged lepton is

$$\begin{aligned} i\mathcal{M}^{real}_{lc} = e\bar{u}_{l^-}(k')\Bigg[& n\cdot\epsilon + \not{\epsilon}^{\perp}\frac{\not{k}'^{\perp} + \not{k}'^{\perp}_{\gamma} + m}{\bar{n}\cdot(k'+k_\gamma)} + \frac{\not{k}'^{\perp} - m}{\bar{n}\cdot k'}\not{\epsilon}^{\perp} \\ & - \frac{(\not{k}'^{\perp} - m)(\not{k}'^{\perp} + \not{k}^{\perp}_{\gamma} + m)}{\bar{n}\cdot(k'+k_\gamma)\bar{n}\cdot k'}\bar{n}\cdot\epsilon\Bigg]\frac{\bar{n}\cdot(k'+k_\gamma)}{(k'+k_\gamma)^2 - m^2}\Gamma_l u_{\nu_l}(k) \\ & \otimes \bar{u}_p(p')\Gamma_h u_n(p)\,. \end{aligned} \tag{3.116}$$

The amplitude for collinear emission from heavy-to-light effective operator is

$$i\mathcal{M}^{real}_{HLc} = -e\frac{\bar{n}\cdot\epsilon}{\bar{n}\cdot k_\gamma}\bar{u}_{l^-}(k')\Gamma_l u_{\nu_l}(k)\otimes\bar{u}_p(p')\Gamma_h u_n(p)\,. \tag{3.117}$$

$$|\mathcal{M}_{lc}^{real}+\mathcal{M}_{HLc}^{real}|^2=\frac{e^2}{k'\cdot k_\gamma}\left[\frac{k_\gamma\cdot\bar{n}}{k'\cdot\bar{n}}\Big(1-\frac{m^2}{k'\cdot k_\gamma}\Big)-\frac{m^2}{k'\cdot k_\gamma}+2\frac{k'\cdot\bar{n}}{k_\gamma\cdot\bar{n}}+2\right]$$
$$\sum|\ \bar{u}_{l^-}\Gamma_l u_{\nu_l}\otimes\bar{u}_p\Gamma_h u_n\ |^2\,, \tag{3.118}$$

where the outgoing lepton carries a fraction $k'\cdot\bar{n}/(k'\cdot\bar{n}+k_\gamma\cdot\bar{n})$ of the total electromagnetic energy which is the energy of the tree level lepton.

The jet function is

$$\begin{aligned}J=&\int\frac{d\Pi}{4E_\nu M}\left\{1+\frac{\alpha}{\pi}\left[1+\frac{\pi^2}{24}+\frac{1}{2}\log\frac{\mu}{m}+\log^2\frac{\mu}{m}\right]\right\}\sum|\mathcal{M}(\mu)|^2_{tree}\\&+\int\frac{d\Pi}{4E_\nu M}\frac{4\pi\alpha}{k'\cdot k_\gamma}\left[\frac{k_\gamma\cdot\bar{n}}{k'\cdot\bar{n}}\Big(1-\frac{m^2}{k'\cdot k_\gamma}\Big)-\frac{m^2}{k'\cdot k_\gamma}+2\frac{k'\cdot\bar{n}}{k_\gamma\cdot\bar{n}}+2\right]\\&\frac{k'\cdot\bar{n}}{k'\cdot\bar{n}+k_\gamma\cdot\bar{n}}\sum|\mathcal{M}(\mu)|^2_{tree}\,,\end{aligned}\tag{3.119}$$

where if we specify the phase space as emitted energetic photon (energy greater than a threshold ΔE) within a cone relative to the charged lepton with cone angle θ, it reduces to

$$\begin{aligned}J=&\int d\Pi\Bigg\{1+\frac{\alpha}{\pi}\left[1+\frac{\pi^2}{24}+\frac{1}{2}\log\frac{\mu}{m}+\log^2\frac{\mu}{m}\right]\\&+\frac{\alpha}{4\pi}\Bigg[9-\frac{4(2+\eta^2)}{\eta(1+\eta^2)}\tan^{-1}\eta-4\left(\tan^{-1}\eta\right)^2+4\frac{\eta^2}{1+\eta^2}\log\left(\frac{\Delta E}{E_\nu-Q^2/(2M)}\right)\\&-3\log\left(1+\eta^2\right)-\frac{\log\left(1+\eta^2\right)}{\eta^2}+2\frac{\log\left(1+\eta^2\right)}{1+\eta^2}+\log^2\left(1+\eta^2\right)\\&-4\log\left(\frac{\Delta E}{E_\nu-Q^2/(2M)}\right)\log\left(1+\eta^2\right)+2\mathrm{Li}_2(-\eta^2)\Bigg]\Bigg\}\sum|\mathcal{M}(\mu)|^2_{tree}\,,\end{aligned}\tag{3.120}$$

where $\eta=\theta[E_\nu-Q^2/(2M)]/m$. Note that the terms involving ΔE are soft limit terms of this jet function, and we could subtract them, moving them to soft function. However, we will not differentiate collinear and soft scales in this problem or evolve from one scale to another. It is no difference keeping them here in the jet function.

For anti-neutrino proton scattering, the format of jet function is the same and we just replace E_ν by $E_{\bar{\nu}}$ and tree level amplitude by anti-neutrino process tree level amplitude in Eq. (3.120).

3.9 Hard Function

The hard function describes hard photon contributions and depends on the hadronic physics, which requires the knowledge of a full theory. It is related to the matching coefficient when we match the full theory to the soft-collinear effective theory.

The one-loop diagram Fig. 3.2 computed in the full theory has an amplitude result c.f. Eq. (3.20)

$$i\mathcal{M}_{full} = c_F \frac{\alpha}{4\pi}\left[\frac{1}{\epsilon} + 2 + \frac{5\pi^2}{3} + 4\log\frac{\lambda}{m}\log\left(\frac{2E_\nu}{m} - \frac{m}{M}\right) - 2\log^2\left(\frac{2E_\nu}{m} - \frac{m}{M}\right)\right.$$
$$\left. +4\log\left(\frac{2E_\nu}{m} - \frac{m}{M}\right) - 2\log\left(\frac{2E_\nu}{\mu} - \frac{m^2}{\mu M}\right)\right]\bar{u}_l(k')\Gamma_l u_{l_\nu}(k)\otimes\bar{u}_p(p')\Gamma_h u_n(p)\,. \tag{3.121}$$

Field strength renormalization factors are

$$Z_l = 1 + \frac{\alpha}{4\pi}\left(-\frac{1}{\epsilon} + 2\log\frac{m^2}{\lambda^2} + \log\frac{m^2}{\mu^2} - 4\right), \tag{3.122}$$

and

$$Z_p = 1 + \frac{\alpha}{4\pi}\left(\frac{2}{\epsilon} + 2\log\frac{\mu^2}{\lambda^2}\right). \tag{3.123}$$

By doing one-loop matching, we obtain

$$\begin{aligned}
&\delta c\cdot\mathcal{M}_{tree}\\
&= \sqrt{Z_l Z_p}\mathcal{M}_{tree} + \mathcal{M}^{full}_{loop} - \left[\sqrt{Z^s_l Z^s_p}\mathcal{M}_{tree} + \mathcal{M}^s_{loop} + \sqrt{Z^c_l}\mathcal{M}_{tree} + \mathcal{M}^c_{loop}\right]\\
&= \mathcal{M}^{full}_{loop} - \mathcal{M}^s_{loop} - \mathcal{M}^c_{loop}\,,
\end{aligned} \tag{3.124}$$

where $\delta c \equiv c - 1$ and c is the matching coefficient.

Explicitly, we use eq. (3.121) to subtract eq. (3.95) and eq. (3.113) and obtain

$$\delta c = \frac{\alpha}{4\pi}\left[-2 + \frac{19\pi^2}{12} + 2\log\left(\frac{2E_\nu}{\mu} - \frac{m^2}{\mu M}\right) - 2\log^2\left(\frac{2E_\nu}{\mu} - \frac{m^2}{\mu M}\right)\right], \tag{3.125}$$

where we subtracted the $1/\epsilon^2$ pole which cancels that from the jet function and $1/\epsilon$ is canceled by poles in coefficients c_V and c_A.

The neutrino neutron scattering hard function is given by

$$\begin{aligned}
H^\nu(\mu) &= \int \frac{d\Pi}{4E_\nu M}|c|^2|\mathcal{M}_\nu(\mu)|^2_{tree}\\
&= \int \frac{d\Pi}{4E_\nu M}\left(1 + 2\delta c\right)|\mathcal{M}_\nu(\mu)|^2_{tree}\,.
\end{aligned} \tag{3.126}$$

The anti-neutrino proton scattering hard function is

$$H^{\bar\nu}(\mu) = \int \frac{d\Pi}{4E_{\bar\nu}M}|\mathcal{M}_{\bar\nu}(\mu)|^2_{tree}\left\{1 + \frac{\alpha}{2\pi}\left[-2 + \frac{19\pi^2}{12} + 2\log\left(\frac{2E_{\bar\nu}}{\mu} - \frac{Q^2}{\mu M}\right)\right.\right.$$
$$\left.\left. - 2\log^2\left(\frac{2E_{\bar\nu}}{\mu} - \frac{Q^2}{\mu M}\right)\right]\right\}. \tag{3.127}$$

3.10 Hard Function Resummation

Hard function has large double logarithms such as $\log^2(E_\nu/\mu)$ at a low energy scale $\mu \sim m_e$, while soft and collinear functions have large logarithms at high energy scale about the neutrino energy scale E_ν. In order to avoid large logarithms, we evolve the hard function from high energy scale to low energy scale and the product of hard, soft and collinear function at low energy scale has controlled logarithms perturbatively, which yields a reliable cross section.

The hard function evolves as

$$\frac{d}{d\log\mu}H(\mu) = 2\Gamma_{\rm cusp}H(\mu)\,, \tag{3.128}$$

where the cusp anomalous dimension is given by [149–151]

$$\Gamma_{\rm cusp} = -\gamma_{\rm cusp}(\alpha)\log\left(\frac{M\mu}{-2p'\cdot k'}\right) + \gamma^h(\alpha) + \gamma^\psi(\alpha)\,, \tag{3.129}$$

and $\gamma_{\rm cusp}$ is massless cusp anomalous dimension function, γ^h is massive one-particle anomalous dimension, γ^ψ is massless one-particle anomalous dimension and explicitly,

$$\gamma_{\rm cusp}(\alpha) = \sum_{n=0}^{\infty}\left(\frac{\alpha}{4\pi}\right)^{n+1}\gamma_n^{\rm cusp}, \quad \gamma_0^{\rm cusp} = 4, \quad \gamma_1^{\rm cusp} = -\frac{80}{9}n_f\,, \tag{3.130}$$

$$\gamma^h(\alpha) = \sum_{n=0}^{\infty}\left(\frac{\alpha}{4\pi}\right)^{n+1}\gamma_n^{h}, \quad \gamma_0^{h} = -2, \quad \gamma_1^{h} = \frac{40}{9}n_f\,, \tag{3.131}$$

$$\begin{aligned}\gamma^\psi(\alpha) &= \sum_{n=0}^{\infty}\left(\frac{\alpha}{4\pi}\right)^{n+1}\gamma_n^{\psi}, \quad \gamma_0^{\psi} = -3,\\ \gamma_1^{\psi} &= -\frac{3}{2} + 2\pi^2 - 24\zeta_3 + n_f(\frac{130}{27} + \frac{2}{3}\pi^2)\,.\end{aligned} \tag{3.132}$$

Explicitly,

$$\begin{aligned}\Gamma_{\rm cusp} = \frac{\alpha}{\pi}\left[\log\left(\frac{2m_l w}{\mu}\right) - \frac{5}{4}\right] + \frac{\alpha^2}{864\pi^2}\Bigg[&-81 + 108\pi^2 - 1296\zeta_3\\ &+n_f\left(500 + 36\pi^2 - 480\log\left(\frac{2m_l w}{\mu}\right)\right)\Bigg]\end{aligned} \tag{3.133}$$

where m_l denotes the charged lepton mass with l-flavor, in the heavy nucleon limit $m_l w = E_\nu$ for neutrino neutron scattering and $m_l w = E_\nu - Q^2/(2M)$ for anti-neutrino proton scattering, and the relation between onshell and $\overline{\rm MS}$ coupling is

$$\alpha \equiv \alpha(\mu) = \alpha_0\left[1 + \sum_{n=0}^{\infty} z_n\left(\frac{\alpha_0}{4\pi}\right)^{n+1}\right]\,. \tag{3.134}$$

The solution of Eq. (3.128) is

$$\log\frac{H(\mu_l)}{H(\mu_h)} = -\frac{\gamma_0}{\beta_0}\left[\log\frac{\alpha_0(\mu_l)}{\alpha_0(\mu_h)}+...\right] - \frac{\gamma_0^{\rm cusp}}{2\beta_0}\Bigg\{\log\frac{(2m_l w)^2}{\mu_h^2}\log\frac{\alpha_0(\mu_l)}{\alpha_0(\mu_h)}$$
$$+\frac{1}{\beta_0}\Bigg[\frac{4\pi}{\alpha_0(\mu_h)}\left(-1+\frac{\alpha_0(\mu_h)}{\alpha_0(\mu_l)}+\log\frac{\alpha_0(\mu_l)}{\alpha_0(\mu_h)}\right)+\left(\frac{\gamma_1^{\rm cusp}}{\gamma_0^{\rm cusp}}-\frac{\beta_1}{\beta_0}\right)\left(\log\frac{\alpha_0(\mu_h)}{\alpha_0(\mu_l)}+\frac{\alpha_0(\mu_l)}{\alpha_0(\mu_h)}$$
$$-1\right)-\frac{\beta_1}{2\beta_0}\log^2\frac{\alpha_0(\mu_l)}{\alpha_0(\mu_h)}\Bigg]+...\Bigg\}, \tag{3.135}$$

where "..." denotes power suppressed terms, $\gamma_0 \equiv \gamma_0^h + \gamma_0^\psi$, β_0 and β_1 are defined by the QED beta function

$$\frac{d\alpha}{d\log\mu} = -2\alpha\sum_{n=0}^{\infty}\beta_n\left(\frac{\alpha}{4\pi}\right)^{n+1},$$
$$\beta_0 = -\frac{4}{3}n_f, \quad \beta_1 = -4n_f\,. \tag{3.136}$$

For electron-flavor neutrino scattering, final state charged lepton is electron. We consider muon mass, hadronic scale are much heavier than electron mass and can be integrated out. The only dynamical fermion for computing coupling $\alpha(\mu)$ is electron and the light flavor number $n_f = 1$, in $d = 4$ dimensions we have

$$z_0 = \frac{8}{3}\log\frac{\mu}{m}, \quad z_1 = \frac{64}{9}\log^2\frac{\mu}{m}+8\log\frac{\mu}{m}+15\,. \tag{3.137}$$

Explicitly, the solution of eq.(3.128) is

$$\begin{aligned}\log\frac{H(\mu_l)}{H(\mu_h)} &= \frac{\alpha_0}{4\pi}\left[-\log^2\frac{\mu_l^2}{\mu_h^2}+\log\frac{\mu_l^2}{\mu_h^2}\left(2\log\frac{(2m_l w)^2}{\mu_h^2}-5\right)\right]\\ &+\left(\frac{\alpha_0}{4\pi}\right)^2\left[\frac{4}{9}\log^3\frac{\mu_l^2}{\mu_h^2}+\frac{4}{3}\log^2\frac{\mu_l^2}{\mu_h^2}\log\left(\frac{m^2\mu_h^2}{\mu_l^2(2m_l w)^2}\right)+\frac{50}{9}\log^2\frac{\mu_l^2}{\mu_h^2}+...\right]\\ &+\left(\frac{\alpha_0}{4\pi}\right)^3\left[\frac{88}{27}\log^4\frac{\mu_l^2}{\mu_h^2}+...\right],\end{aligned} \tag{3.138}$$

where we do the power counting considering large logarithm $\alpha\log^2(\mu_h^2/\mu_l^2)\sim 1$ and "..." denotes the terms with order higher than α^1, which are numerically suppressed and can be ignored.

For muon-flavor neutrino scattering, the final state charged lepton is muon. The dynamical fermions in the loop are electron and muon, and heavier particles have been integrated out. In this case, $n_f = 2$, and coupling $\alpha(\mu)$ is

$$\alpha \equiv \alpha(\mu) = \alpha_0\left[1+\sum_{n=0}^{\infty}z_n\left(\frac{\alpha}{4\pi}\right)^{n+1}\right],$$

$$z_0 = \frac{8}{3}\log\frac{\mu^2}{m_e m_\mu},$$
$$z_1 = \frac{64}{9}\left(\log^2\frac{\mu}{m_e} + \log^2\frac{\mu}{m_\mu}\right) + 8\log\frac{\mu^2}{m_e m_\mu} + 30\,. \tag{3.139}$$

The running for muon hard function is

$$\begin{aligned}\log\frac{H(\mu_l)}{H(\mu_h)} &= \frac{\alpha_0}{4\pi}\left[-\log^2\frac{\mu_l^2}{\mu_h^2} + \log\frac{\mu_l^2}{\mu_h^2}\left(2\log\frac{(2m_l w)^2}{\mu_h^2} - 5\right)\right] \\ &\quad + \left(\frac{\alpha_0}{4\pi}\right)^2\left[-\frac{16}{9}\log^3\frac{\mu_l^2}{\mu_h^2} + \frac{8}{3}\log^2\frac{\mu_l^2}{\mu_h^2}\left(\log\frac{\mu_l^2}{m_e m_\mu} + \frac{5}{3}\right) + ...\right] \\ &\quad + \left(\frac{\alpha_0}{4\pi}\right)^3\left[\frac{16}{27}\log^4\frac{\mu_l^2}{\mu_h^2} + ...\right]. \end{aligned} \tag{3.140}$$

Conversely, we could evolve soft and jet functions to high energy scales by renormalization group running to obtain the resummed cross section. The soft function evolves as

$$\frac{d}{d\log\mu}S(\mu) = 2\Gamma_S S(\mu)\,, \tag{3.141}$$

where the cusp anomalous dimension for soft function to α^2 order is [149]

$$\Gamma_S = \left[\frac{\alpha}{\pi} + \left(\frac{\alpha}{4\pi}\right)^2\frac{80}{9}n_f\right]\left[1 - \frac{w}{\sqrt{w^2-1}}\log\left(w + \sqrt{w^2-1}\right)\right]. \tag{3.142}$$

The virtual jet function evolves as

$$\frac{d}{d\log\mu}J_v(\mu) = 2\Gamma_J J_v(\mu)\,, \tag{3.143}$$

where the cusp anomalous dimension for virtual jet function to α^2 order is

$$\begin{aligned}\Gamma_J &= -\Gamma_{\rm cusp} - \Gamma_S \\ &= \frac{\alpha}{\pi}\left[\frac{1}{4} + \log\left(\frac{\mu}{2wm_l}\right) + \log\left(w + \sqrt{w^2-1}\right)\frac{w}{\sqrt{w^2-1}}\right] \\ &\quad + \left(\frac{\alpha}{4\pi}\right)^2\left\{-\frac{3}{2} + 2\pi^2 - 24\zeta_3 + n_f\left[\frac{10}{27} + \frac{2}{3}\pi^2 + \frac{80}{9}\log\frac{\mu}{2wm_l}\right.\right. \\ &\quad \left.\left. + \frac{80}{9}\log\left(w + \sqrt{w^2-1}\right)\frac{w}{\sqrt{w^2-1}}\right]\right\}. \end{aligned} \tag{3.144}$$

3.11 Collinear Real Radiation Resummation

Besides the double large logarithms from the difference between hard scale and soft scale, there are also double large logarithms from real collinear terms which is manifested in Eq. (3.86). Thus, we need to sum all double large logarithms from all orders in perturbation theory.

3.11.1 Multiple Collinear Photons Emission Summation

In the massless charged lepton limit, we could work out the leading logarithms of collinear photons radiation by the splitting method. First, consider one collinear photon emission case, if the outgoing lepton carries a fraction of the total electromagnetic energy $(1-z)$ and the collinear photon carries the other fraction z, then Eq. (3.118) becomes

$$|\mathcal{M}|^2 = \frac{e^2}{z(1-z)E_{p'}^2\left[1-(1-\frac{m^2}{2(1-z)^2E_{p'}^2})\cos\theta\right]}\left[2\frac{1-z}{z}+2+\frac{z}{1-z}\right]$$
$$\cdot(1-z)|\mathcal{M}|^2_{tree}\,, \tag{3.145}$$

and

$$\int d\Pi|\mathcal{M}|^2 = \frac{e^2}{8\pi^2}\int_{z_{min}}^{z_{max}} dz\left[\frac{1+(1-z)^2}{z}\right]\int_{\cos\theta}^{1}\frac{d\cos\theta}{\left[1-(1-\frac{m^2}{2(1-z)^2E_{p'}^2})\cos\theta\right]}$$
$$\cdot\int d\Pi|\mathcal{M}|^2_{tree}\,, \tag{3.146}$$

where the phase space derivation can be found in Appendix D.

For a jet with cone size θ, and we have integration limits $z_{min}=\Delta E/E_\nu$, $z_{max}=1-m/E_\nu$, then

$$\sigma(\nu n\to lp\gamma) = \frac{2\alpha}{\pi}\left[\log\left(\frac{E_\nu}{\Delta E}\right)\log\left(\frac{\theta E_\nu}{m}\right)-\frac{3}{4}\log\left(\frac{\theta E_\nu}{m}\right)+\frac{5}{8}-\frac{\pi^2}{6}\right]$$
$$\cdot\sigma(\nu n\to lp), \tag{3.147}$$

and we compare it with the accurate result of this real collinear radiation, i.e. the sum of Eq. (3.74), Eq. (3.75), Eq. (3.76) and Eq. (3.77)

$$\sigma(\nu n\to lp\gamma) = \frac{2\alpha}{\pi}\left[\log\left(\frac{E_\nu}{\Delta E}\right)\log\left(\frac{\theta E_\nu}{m}\right)-\frac{3}{4}\log\left(\frac{\theta E_\nu}{m}\right)-\frac{1}{2}\log\left(\frac{E_\nu}{\Delta E}\right)\right.$$
$$\left.+\frac{9}{8}-\frac{\pi^2}{6}\right]\cdot\sigma(\nu n\to lp). \tag{3.148}$$

The massless limit splitting treatment result Eq. (3.147) produces the correct leading double logarithm as in Eq. (3.148) when we set the Sterman-Weinberg observable parameter β to be $\Delta E/E_\nu$. However, it loses subleading logarithm terms such as $\log(E_\nu/\Delta E)$, but they are suppressed compared to the leading double logarithms. It is reasonable and computationally economic to sum only the leading double logarithms using the splitting treatment, where we consider the virtual fermions are approximately on-shell compared to the radiated photons' transverse momenta [133] about θE_ν and for multiple collinear photon radiation process we have

$$\sigma(\nu n\to lpN\gamma) = \left\{\frac{\alpha}{2\pi}\int dz\left[\frac{1+(1-z)^2}{z}\right]\int_{\cos\theta}^{1}\frac{d\cos\theta}{\left[1-(1-\frac{m^2}{2(1-z)^2E_{p'}^2})\cos\theta\right]}\right\}^N$$

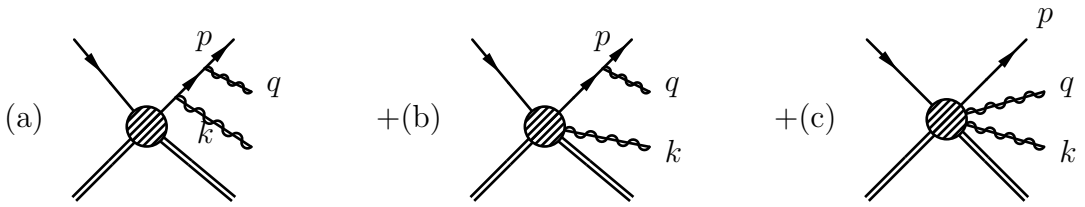

Figure 3.14: Two collinear photons emission diagrams.

$$\cdot\sigma(\nu n \to lp)\,. \tag{3.149}$$

When the inner photon electron cone angle is wider than the outer one, which is equivalent to the condition that the virtual fermion is on-shell compared to the first photon it emits since the transverse momentum integration is equivalent to the cone angle integration, the N-cone angle integration becomes

$$\int_{\cos\theta_1}^{1} d\cos\theta_1 \int_{\cos\theta_2}^{1} d\cos\theta_2 ... \int_{\cos\theta_{N-1}}^{1} d\cos\theta_N\,, \tag{3.150}$$

where $\theta = \theta_1 \gg \theta_2 ...$, then it gives a factor of $1/N!$.

The leading logarithm from N-collinear photons radiation Eq. (3.149) is

$$\frac{1}{N!}\left[\frac{2\alpha}{\pi}\log\left(\frac{E_\nu}{\Delta E}\right)\log\left(\frac{\theta E_\nu}{m}\right)\right]^N\,. \tag{3.151}$$

When we sum over all collinear photons leading logarithms, we get an exponential

$$\sum_{N=0}^{\infty}\sigma(\nu n \to lpN\gamma) = \exp\left\{\frac{2\alpha}{\pi}\log\left(\frac{E_\nu}{\Delta E}\right)\log\left(\frac{\theta E_\nu}{m}\right)\right\}\sigma(\nu n \to lp) \tag{3.152}$$

We explicitly compute two collinear photons radiation using SCET Feynman rules and show it confirms the exponentiation result. The two collinear photons radiation diagrams are shown in Fig. 3.14.

The diagrams are evaluated by soft-collinear effective theory Feynman rules and explicitly they are

$$\begin{aligned}
(a) = {}& \bar{u}_l i(-e)\left[n\cdot\epsilon_1^* + \not{\epsilon}_1^{*\perp}\frac{\not{p}_\perp + \not{q}_\perp + m}{\bar{n}\cdot(p+q)} + \frac{\not{p}_\perp - m}{\bar{n}\cdot p}\not{\epsilon}_1^{*\perp} - \frac{\not{p}_\perp - m}{\bar{n}\cdot p}\cdot\frac{\not{p}_\perp + \not{q}_\perp + m}{\bar{n}\cdot(p+q)}\right.\\
&\left.\cdot(\bar{n}\cdot\epsilon_1^*)\right]\frac{\not{\bar{n}}}{2}i\frac{\not{p}}{2}\frac{\bar{n}\cdot(p+q)}{(p+q)^2 - m^2 + i0}\cdot i(-e)\left[n\cdot\epsilon_2^* + \not{\epsilon}_2^{*\perp}\frac{\not{p}_\perp + \not{q}_\perp + \not{k}_\perp + m}{\bar{n}\cdot(p+q+k)}\right.\\
&+\left.\frac{\not{p}_\perp + \not{q}_\perp - m}{\bar{n}\cdot(p+q)}\not{\epsilon}_2^{*\perp} - \frac{\not{p}_\perp + \not{q}_\perp - m}{\bar{n}\cdot(p+q)}\cdot\frac{\not{p}_\perp + \not{q}_\perp + \not{k}_\perp + m}{\bar{n}\cdot(p+q+k)}\bar{n}\cdot\epsilon_2^*\right]\frac{\not{\bar{n}}}{2}\\
&\cdot i\frac{\not{p}}{2}\frac{\bar{n}\cdot(p+q+k)}{(p+q+k)^2 - m^2 + i0}\Gamma^l u_\nu \otimes \bar{u}_p\Gamma^h u_n\,,
\end{aligned} \tag{3.153}$$

$$
\begin{aligned}
(b) = \bar{u}_l i(-e)\Bigg[& n\cdot\epsilon_1^* + \not{\epsilon}_1^{*\perp}\frac{\not{p}_\perp + \not{q}_\perp + m}{\bar{n}\cdot(p+q)} + \frac{\not{p}_\perp - m}{\bar{n}\cdot p}\not{\epsilon}_1^{*\perp} - \frac{\not{p}_\perp - m}{\bar{n}\cdot p}\cdot\frac{\not{p}_\perp + \not{q}_\perp + m}{\bar{n}\cdot(p+q)} \\
& \cdot(\bar{n}\cdot\epsilon_1^*)\Bigg]\frac{\not{\bar{n}}}{2} i\frac{\not{p}}{2}\frac{\bar{n}\cdot(p+q)}{(p+q)^2 - m^2 + i0}(-e)\frac{\bar{n}\cdot\epsilon_2^*}{\bar{n}\cdot k}\Gamma^l u_\nu \otimes \bar{u}_p\Gamma^h u_n \\
& + \bar{u}_l(-e)\frac{\bar{n}\cdot\epsilon_1^*}{\bar{n}\cdot q} i(-e)\Bigg[n\cdot\epsilon_2^* + \not{\epsilon}_2^{*\perp}\frac{\not{p}_\perp + \not{q}_\perp + \not{k}_\perp + m}{\bar{n}\cdot(p+q+k)} + \frac{\not{p}_\perp + \not{q}_\perp - m}{\bar{n}\cdot(p+q)}\not{\epsilon}_2^{*\perp} \\
& - \frac{\not{p}_\perp + \not{q}_\perp - m}{\bar{n}\cdot(p+q)}\cdot\frac{\not{p}_\perp + \not{q}_\perp + \not{k}_\perp + m}{\bar{n}\cdot(p+q+k)}\bar{n}\cdot\epsilon_2^*\Bigg]\frac{\not{\bar{n}}}{2}\cdot i\frac{\not{p}}{2}\frac{\bar{n}\cdot(p+q+k)}{(p+q+k)^2 - m^2 + i0}\Gamma^l u_\nu \\
& \otimes \bar{u}_p\Gamma^h u_n\,, \qquad (3.154)
\end{aligned}
$$

$$
(c) = e^2(\bar{n}\cdot\epsilon_2^*)(\bar{n}\cdot\epsilon_1^*)\left[\frac{1}{\bar{n}\cdot k}\frac{1}{\bar{n}\cdot(q+k)} + \frac{1}{\bar{n}\cdot q}\frac{1}{\bar{n}\cdot(q+k)}\right]\bar{u}_l\Gamma^l u_\nu \otimes \bar{u}_p\Gamma^h u_n\,. \qquad (3.155)
$$

The momenta of collinear fermions and photons are denoted as

$$
\begin{aligned}
p &= (1-y)(p+q) && (3.156)\\
q &= y(p+q) + q_\perp && (3.157)\\
p+q &= (1-z)(p+q+k) \equiv (1-z)p' && (3.158)\\
k &= z(p+q+k) + k_\perp = zp' + k_\perp\,, && (3.159)
\end{aligned}
$$

with z and y are splitting fractions.

The sum of amplitude squared is

$$
\begin{aligned}
\sum \mid (a)+(b)+(c) \mid^2 = e^4 \sum \mid \bar{u}_l\Gamma_l u_{\nu_l} \otimes \bar{u}_p\Gamma_h u_n \mid^2_{tree} & \left[\frac{1+(1-y)^2}{2y}\frac{1}{(1-z)z}\right. \\
\cdot\Bigg\{ & -\frac{z^3}{(p\cdot k + p\cdot q + q\cdot k)^2} + \frac{1-z}{p\cdot q}\Bigg[\frac{2(1-z)}{p\cdot k + p\cdot q + q\cdot k} + \frac{z^2}{p\cdot k + p\cdot q + q\cdot k} \\
& \cdot\left(1 - \frac{p\cdot q}{p\cdot k + p\cdot q + q\cdot k}\right)\Bigg]\Bigg\} + \frac{1}{2z(1-z)}\frac{m^2}{(p\cdot q)^2}\frac{1}{p\cdot k + p\cdot q + q\cdot k}\Bigg\{\Bigg[z^3 \\
& - \frac{z(1-z)\Big[(1-y)^2+1\Big]}{y}\Bigg]\frac{p\cdot q}{p\cdot k + p\cdot q + q\cdot k} - (1-z)\Bigg[2(1-z) + z^2\Bigg(1 \\
& \left. - \frac{p\cdot q}{p\cdot k + p\cdot q + q\cdot k}\Bigg)\Bigg]\Bigg\} + \frac{m^4}{2(p\cdot q)^2}\cdot\frac{1}{p\cdot k + p\cdot q + q\cdot k}\right]. \qquad (3.160)
\end{aligned}
$$

In the massless charged lepton limit and considering the transverse momentum of the second emission is much smaller than the first one (i.e. the outgoing lepton is onshell, while the intermediate lepton is less on-shell, also see argument in Peskin and Schroder [133] Eq.(17.108) and surrounding discussion), which is $p\cdot q \ll k\cdot(p+q)$ here explicitly, we have

$$
\sigma(\nu n \to l p\gamma\gamma) = \int d\Pi \sum |(a)+(b)+(c)|^2
$$

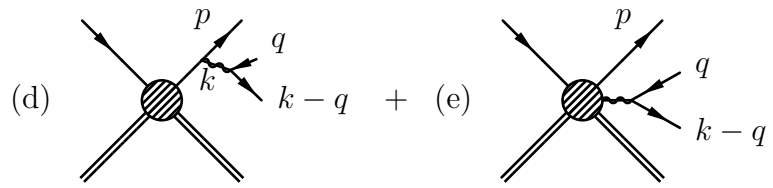

Figure 3.15: Electron-positron pair production process.

$$= \frac{1}{2}\left(\frac{\alpha}{2\pi}\right)^2 \int \frac{d\cos\theta'}{1-(1-\frac{m^2}{2(1-z)^2(1-y)^2E_\nu^2})\cos\theta'} \frac{d\cos\theta}{1-(1-\frac{m^2}{2(1-z)^2E_\nu^2})\cos\theta} dydz$$
$$\left[\frac{1+(1-y)^2}{y}\frac{1+(1-z)^2}{z}\right]\cdot\sigma(\nu n\to lp)\,, \tag{3.161}$$

which renders a leading logarithm

$$\frac{1}{2}\left(\frac{2\alpha}{\pi}\right)^2 \log^2\left(\frac{E_\nu}{\Delta E}\right)\log^2\left(\frac{\theta E_\nu}{m}\right), \tag{3.162}$$

and numerically is of $O(1)$ contribution.

3.11.2 Collinear Pair Production Summation

Lastly, we estimate another higher order process, the e^+e^- pair production, which is shown in Fig. 3.15.

$$(d) = \bar{u}_l i(-e)\left[n_\mu + \gamma_\mu^\perp \frac{(\not p_\perp + \not k_\perp + m)}{\bar n\cdot(p+k)}\frac{(\not p_\perp - m)}{\bar n\cdot p}\gamma_\mu^\perp - \frac{(\not p_\perp - m)(\not p_\perp + \not k_\perp + m)}{\bar n\cdot(p+k)\bar n\cdot p}\bar n_\mu\right]$$
$$\frac{\bar{\not n}}{2} i\frac{\not n}{2}\frac{\bar n\cdot(p+k)}{2p\cdot k}\gamma^\alpha(1-\gamma^5)u_\nu \otimes \frac{-i}{k^2-\lambda^2}\bar u_e i(-e)\left[n^\mu + \gamma^{\mu\perp}\frac{\not q_\perp - m}{\bar n\cdot q}\right.$$
$$\left. + \frac{(\not k_\perp - \not q_\perp - m)}{\bar n\cdot(k-q)}\gamma^{\mu\perp} - \frac{(\not k_\perp - \not q_\perp - m)(\not q_\perp - m)}{\bar n\cdot(k-q)\bar n\cdot q}\bar n^\mu\right]\frac{\bar{\not n}}{2} v_{e^+}\otimes\bar u_p\Gamma_h u_n\,. \tag{3.163}$$

$$(e) = \bar u_l\gamma^\alpha(1-\gamma^5)u_\nu(-e)\frac{\bar n_\mu}{\bar n\cdot k}\otimes\frac{-i}{k^2-\lambda^2}\bar u_e i(-e)\left[n^\mu + \gamma^{\mu\perp}\frac{\not q_\perp - m}{\bar n\cdot q}\right.$$
$$\left. + \frac{(\not k_\perp - \not q_\perp - m)}{\bar n\cdot(k-q)}\gamma^{\mu\perp} - \frac{(\not k_\perp - \not q_\perp - m)(\not q_\perp - m)}{\bar n\cdot(k-q)\bar n\cdot q}\bar n^\mu\right]\frac{\bar{\not n}}{2} v_{e^+}\otimes\bar u_p\Gamma_h u_n\,. \tag{3.164}$$

We define the following relations for momenta by splitting parameters x and z.

$$p' = p + k \tag{3.165}$$
$$p = xp' \tag{3.166}$$

$$
\begin{aligned}
k &= (1-x)p' + k_\perp && (3.167)\\
q &= zk && (3.168)\\
q' &= (1-z)k + q'_\perp && (3.169)
\end{aligned}
$$

up to order $O(m/E_{p'})$ corrections.

In the massless charged lepton limit, the amplitude squared is

$$
\begin{aligned}
\sum |\ (d) + (e)\ |^2 &= \left[E_{p'}^2 x(1-x)(1-\cos\theta)\right]^{-1}\left[E_k^2 z(1-z)(1-\cos\theta')\right]^{-1}\\
&\quad \cdot \frac{1}{1-x}\left\{(1+x^2)\left[(1-z)^2+z^2\right] + 4x(1-z)z\right\}\\
&\quad \cdot \sum |\ \bar{u}_l \Gamma_l u_{\nu_l} \otimes \bar{u}_p \Gamma_h u_n\ |^2 \qquad (3.170)
\end{aligned}
$$

The cross section of pair production is

$$
\begin{aligned}
\sigma(\nu n \to l p e^+ e^-) = \left(\frac{\alpha}{2\pi}\right)^2 \int \frac{d\cos\theta'}{1-(1-\frac{m^2}{2z^2(1-x)^2E_\nu^2})\cos\theta'} d(1-z)\Bigg\{\left[(1-z)^2+z^2\right]\\
+ \frac{4x(1-z)z}{1+x^2}\Bigg\}\int dx \frac{1+x^2}{1-x}\int \frac{d\cos\theta}{1-(1-\frac{m^2}{2x^2E_\nu^2})\cos\theta}\cdot\sigma(\nu n\to lp)\,. \qquad (3.171)
\end{aligned}
$$

The leading logarithm is

$$
\left(\frac{2\alpha}{\pi}\right)^2 \log\left(\frac{E_\nu}{\Delta E}\right)\log^2\left(\frac{\theta E_\nu}{m}\right), \qquad (3.172)
$$

which is numerically $O(\alpha^{1/2})$ and suppressed compared to the two collinear photons emission leading logarithm $O(\alpha^0) \sim O(1)$ contribution. Therefore, we neglect pair production contributions in the jet resummation.

3.12 Jet Observable Cross Sections

3.12.1 Electron and Muon Observables

Let us consider a jet observable which is defined as in Sec. 3.5. The total cross section including energetic photon in the cone and collinear virtual photon emission which is captured by jet function $J(\mu)$, soft photon inside and outside of the cone and virtual soft photon emission captured by soft function $S(\mu)$, and energetic virtual photon emission captured by hard function $H(\mu)$, is proportional to

$$
H(\mu)J(\mu)S(\mu)\,, \qquad (3.173)
$$

where H is taken from Eq. (3.126), J taken from Eq. (3.120), and S taken from Eq. (3.112).

Table 3.1: A table of parameters taken for neutrino nucleon scattering jet observable.

c_V	c_A	E_ν (GeV)	θ (Degree)	ΔE (MeV)
1	-1.27	$(0.5, 1)$	10	20

Hard function $H(\mu)$ contains double logarithms $\log^2(E_\nu/\mu)$, jet function $J(\mu)$ contains double logarithms $\log(E_\nu/\Delta E)\log(\theta E_\nu/m)$, $\log^2(m/\mu)$ and soft function $S(\mu)$ contains double logarithms $\log(\Delta E/\mu)\log(E_\nu/m)$, $\log^2(E_\nu/m)$. In the massless limit, the mass divergences in soft function and jet function cancel, and this jet observable only contains double logarithm $\log(E_\nu/\Delta E)\log\theta$, see Eq. (3.86) .

However, they live at different energy scales, varying renormalization scale μ for the product of the three functions Eq. (3.173) directly from soft scale to hard scale would yield large perturbative uncertainty. In order to obtain a cross section with a higher precision, we use renormalization group evolution to bring the hard function down to a low scale μ_l, the soft and collinear scale $\Delta E \sim \theta E_\nu$. Then the product of the resummed hard function with jet and soft function at low scale μ_l does not suffer large logarithms, yielding a cross section with small perturbative uncertainty. Explicitly,

$$H(\mu_l)J(\mu_l)S(\mu_l) = H(M)\frac{H(\mu_h)}{H(M)}\frac{H(\mu_l)}{H(\mu_h)}J(\mu_l)S(\mu_l)\,, \tag{3.174}$$

where we first bring the hard function from a scale M to a high scale $\mu_h \sim E_\nu$, and from the high scale μ_h to a low scale μ_l using the hard function ratio between different scales Eq. (3.138) for e-flavor and Eq. (3.140) for mu-flavor. We also exponentiate jet function by Eq. (3.152) for real collinear photons resummation. The soft function does not have large logarithms numerically from real soft photon emission at this low scale μ_l.

We take $c_V(\mu_l) = 1$, $c_A(\mu_l)$=-1.27 and the jet cone size θ to be 10°, soft photon threshold ΔE to be 20 MeV and the incoming (anti)neutrino energy ranging from 0.5 to 1 GeV for quasi-elastic process for relevant experiments such as T2K [80] and DUNE [84], all tabulated in Table 3.1.

For electron-flavor cross section, we use Eq. (3.138) to evolve the hard function from heavy mass scale M to a hard scale μ_h and then evolve from μ_h scale to a low scale μ_l, where we take $E_\nu/\sqrt{2} \leqslant \mu_h \leqslant \sqrt{2}E_\nu$, and $\mathrm{Min}(\theta E_\nu, \Delta E)/\sqrt{2} \leqslant \mu_l \leqslant \sqrt{2}\mathrm{Max}(\theta E_\nu, \Delta E)$.

For muon-flavor cross section, we use Eq. (3.140) to evolve the hard function from heavy mass scale M to a hard scale μ_h and then evolve from μ_h scale to a low scale μ_l, where we take $E_\nu/\sqrt{2} \leqslant \mu_h \leqslant \sqrt{2}E_\nu$, and $\mathrm{Min}(m_\mu, \Delta E)/\sqrt{2} \leqslant \mu_l \leqslant \sqrt{2}\mathrm{Max}(m_\mu, \Delta E)$. In experiments, the muons can be separately measured from their energetic photon radiation. So the muon-flavor process final state observable is the cross section in Eq. (3.173) with the jet function $J(\mu)$ being replaced by the virtual jet function $J_v(\mu)$ in Eq. (3.115).

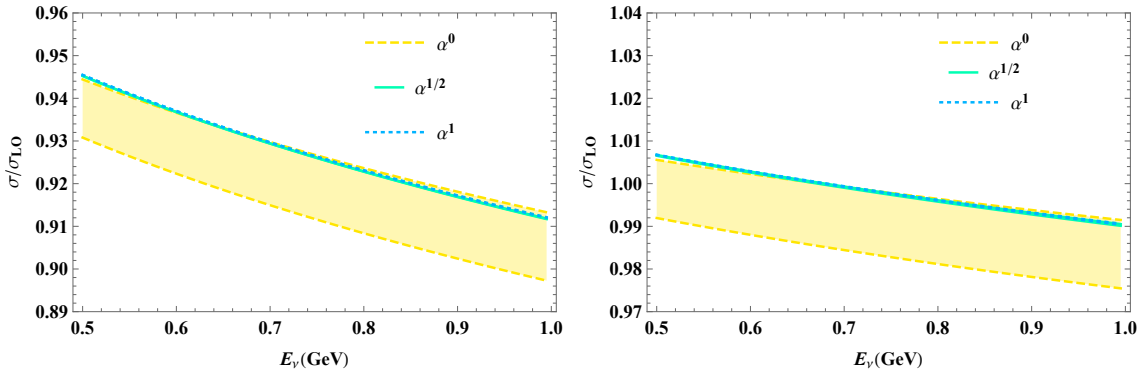

Figure 3.16: Left: Comparison of resummed and unresummed soft radiatively corrected cross section over tree level cross section ratios for electron-flavor process. Right: Comparison of resummed and unresummed soft radiatively corrected cross section over tree level cross section ratios for muon-flavor process. Yellow dashed line is unresummed result, green solid line is resummed to $O(\alpha^{1/2})$ and blue dotted line is resummed to $O(\alpha^1)$. The bands show uncertainties from varying the scales as described in the text.

3.12.2 Resummation Effect

To show the convergence of resummation, we compute the ratio of cross section with one virtual photon radiative correction and one soft real photon over the tree level cross section, as a function of the incoming (anti)neutrino energy E_ν. When we evolve the hard function from a high scale to a low scale, we use different orders of large logarithms power counting in the evolution equation Eq. (3.138). We compare the resummed results at $O(\alpha^{1/2})$ and $O(\alpha^1)$ with unresummed result (denoted by $O(\alpha^0)$) in Fig. 3.16 for incoming neutrino energy range (0.5, 1) GeV. Explicitly, the observable is proportional to HJ_vS, where H is taken from Eq. (3.126), S is from Eq. (3.112) with $\Delta E = 20$ MeV being taken for relevant neutrino experiments., and J_v is the virtual part of jet function Eq. (3.120),

$$J_v = \left\{1 + \frac{\alpha}{\pi}\left[1 + \frac{\pi^2}{24} + \frac{1}{2}\log\frac{\mu}{m} + \log^2\frac{\mu}{m}\right]\right\}\left(\int d\Pi \sum |\mathcal{M}(\mu)|^2\right)_{tree} . \quad (3.175)$$

We see that the $O(\alpha^{1/2})$ result already converges well, and $O(\alpha^1)$ result has almost the same upper and lower bound on top of it. The resummed calculations vary renormalization scales at the soft scale from $\Delta E/\sqrt{2}$ to $\sqrt{2}\Delta E$, while the unresummed result varies scale from soft scale ΔE to hard scale E_ν.

3.12.3 Jet Observable Cross Sections in the Heavy Nucleon Limit

Neglecting lepton mass power corrections compared to nucleon mass M and neutrino energy E_ν in the heavy nucleon limit, the resummed to $O(\alpha^1)$ jet observable total cross section for different incoming neutrino energies has been plotted in Fig. 3.17 and it is the same for both neutrino neutron scattering and anti-neutrino proton scattering.

We resum the Eq. (3.173) to obtain a jet observable cross section and show its ratio by tree level cross section. The difference of radiative correction to electron-flavor and muon-flavor scatterings is presented by the ratio of the two observables cross sections, and they share the same tree level cross section in this limit, shown in Fig. 3.18. We list the ratios with their perturbative uncertainties for neutrino energies at 0.55 GeV, 0.75 GeV and 0.95 GeV in Table 3.2.

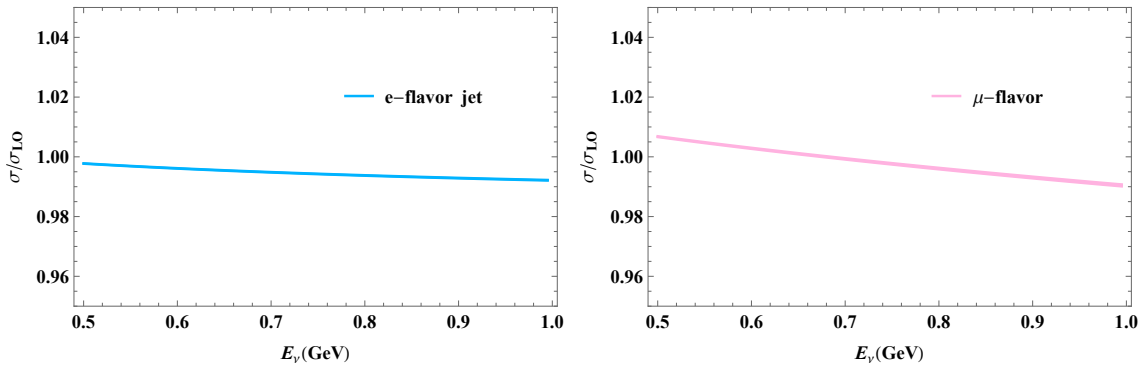

Figure 3.17: The resummed jet observable is shown by the ratio of jet cross section over tree level cross section. Left: electron-flavor process. Right: muon-flavor process.

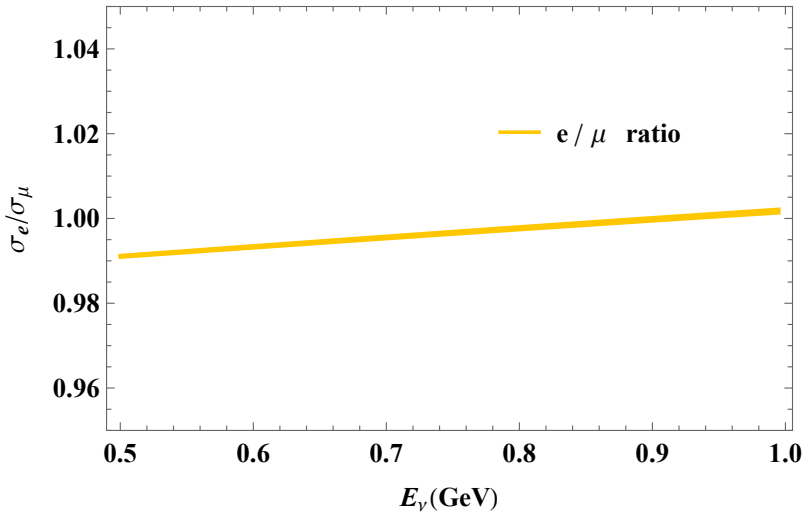

Figure 3.18: Ratio of electron-flavor jet cross section over muon-flavor cross section.

Table 3.2: A table of e-flavor and μ-flavor observable cross section ratios at the heavy nucleon limit $m \ll E_\nu \ll M$, neglecting all power corrections, with perturbative uncertainty in parentheses for last digit.

E_ν (GeV)	0.55	0.75	0.95
σ_e/σ_μ	0.9922(1)	0.9966(2)	1.0009(3)

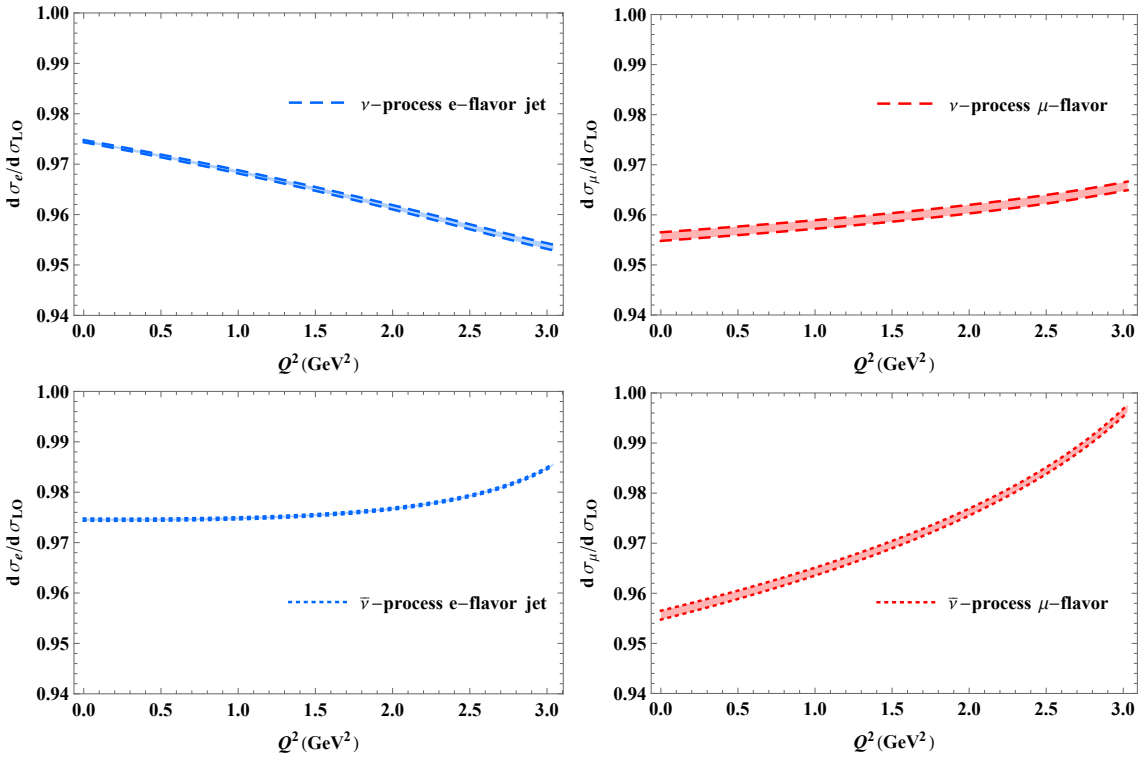

Figure 3.19: Left: Ratio of electron jet differential cross section over tree level differential cross section. Right: Ratio of muon observable differential cross section over tree level differential cross section. Upper: Ratios for neutrino neutron scattering process. Lower: Ratios for anti-neutrino proton scattering process.

The ratio of electron flavor jet and muon flavor cross sections determines the muon-neutrino oscillation net result. We find the difference of these two observables is below $\sim 1\%$ in the energy range 0.5 GeV to 1 GeV in the heavy nucleon limit.

3.12.4 Differential Cross Sections

Since the ratio of different flavor jet observables does not depend on the hard function, which is flavor-independent and will cancel out, let us compute the ratio using a more physical tree level model with the universal soft function derived S^ℓ from Eq. (3.97), Eq. (3.99), Eq. (3.103), Eq. (3.109) for ℓ-flavor lepton, and jet function J^ℓ from Eq. (3.120) for ℓ-flavor lepton. Specifically, the ratio is

$$\frac{d\sigma^e/dQ^2}{d\sigma^\mu/dQ^2} = \frac{d\left[H_{tree}S^e(\mu_h)J^e(\mu_h)\right]/dQ^2}{d\left[H_{tree}S^\mu(\mu_h)J_v^\mu(\mu_h)\right]/dQ^2}\,, \tag{3.176}$$

where we neglect α order hard function, since it is the same for e-flavor and μ-flavor processes and numerically small at μ_h. The uncertainty of this procedure will be controlled by varying μ_h from $E_\nu/\sqrt{2}$ to $\sqrt{2}E_\nu$.

The jet and soft functions suffer large logarithms at μ_h and we use renormalization group evolution to bring the low energy soft and jet functions (free of large logarithms)

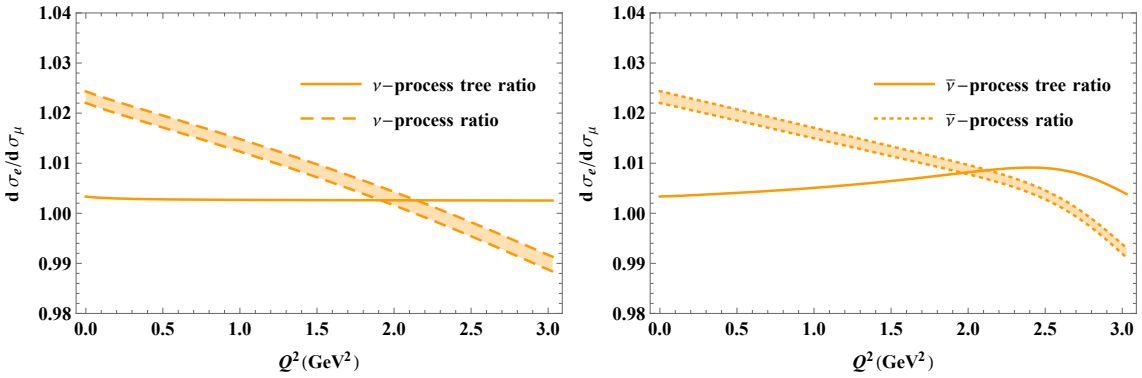

Figure 3.20: Ratio of electron jet differential cross section over muon observable differential cross section. Left: Ratios for neutrino neutron scattering process. Right: Ratios for anti-neutrino proton scattering process.

to high energy scale,

$$S^e(\mu_h)J^e(\mu_h) = \frac{H(\mu_l)}{H(\mu_h)}S^e(\mu_l)J^e(\mu_l)\,, \tag{3.177}$$

with $H(\mu_l)/H(\mu_h)$ for electron-flavor taken from exponentiation of Eq. (3.138), electron flavor real radiation jet function exponentiated by Eq. (3.152) and

$$S^\mu(\mu_h)J^\mu_v(\mu_h) = \frac{H(\mu_l)}{H(\mu_h)}S^\mu(\mu_l)J^\mu_v(\mu_l)\,, \tag{3.178}$$

with $H(\mu_l)/H(\mu_h)$ for muon-flavor taken from exponentiation of Eq. (3.140).

Explicitly, we use a phenomenological dipole form factor tree level model,

$$\Gamma^\mu_h \;=\; \gamma^\mu F_1^V(q^2) + i\frac{\sigma^{\mu\nu}q_\nu}{2M}F_2^V(q^2) + \gamma^\mu\gamma^5 F_A(q^2) + \frac{q^\mu\gamma^5}{M}F_P(q^2)\,, \tag{3.179}$$

where

$$F_1^V(q^2) = F_1^p(q^2) - F_1^n(q^2) \tag{3.180}$$

$$F_2^V(q^2) = F_2^p(q^2) - F_2^n(q^2) \tag{3.181}$$

$$F_A(q^2) = \frac{g_A}{\left(1-\frac{q^2}{\Lambda_A^2}\right)^2} \tag{3.182}$$

$$F_P(q^2) = 2\frac{M^2}{m_\pi^2 - q^2}F_A(q^2)\,, \tag{3.183}$$

and

$$F_1^N(q^2) = \frac{G_E^N(q^2) - \frac{q^2}{4M^2}G_M^N(q^2)}{1-\frac{q^2}{4M^2}}\,, \quad F_2^N(q^2) = \frac{G_M^N(q^2) - G_E^N(q^2)}{1-\frac{q^2}{4M^2}}\,, \tag{3.184}$$

$$G_E^N(q^2) = \frac{G_E^N(0)}{\left(1-\frac{q^2}{\Lambda^2}\right)^2}\,, \quad G_M^N(q^2) = \frac{G_M^N(0)}{\left(1-\frac{q^2}{\Lambda^2}\right)^2}\,, \tag{3.185}$$

Table 3.3: A table of integrated e-flavor and μ-flavor observable cross section ratios including radiative corrected cross section ratios and tree level ratios with dipole form factors tree level model, with perturbative uncertainty in parentheses for last digit.

E_ν (GeV)	$\sigma_{e^-}/\sigma_{\mu^-}$	$\sigma^{\rm LO}_{e^-}/\sigma^{\rm LO}_{\mu^-}$	$\sigma_{e^+}/\sigma_{\mu^+}$	$\sigma^{\rm LO}_{e^+}/\sigma^{\rm LO}_{\mu^+}$
0.6	1.0141(6)	1.0246	1.0119(7)	1.0202
1	1.0059(8)	1.0088	1.0094(8)	1.0096
2	1.018(2)	1.0032	1.021(2)	1.0039

Table 3.4: A table of integrated e-flavor and μ-flavor observable cross section ratios including radiative corrected cross section ratios and tree level ratios in the heavy nucleon limit with lepton mass power corrections, with perturbative uncertainty in parentheses for last digit.

E_ν (GeV)	σ_e/σ_μ	$\sigma^{\rm LO}_e/\sigma^{\rm LO}_\mu$
0.6	1.010(3)	1.016
1	1.008(3)	1.006
2	1.020(3)	1.001

$$G_E^p(0)=1\,,\quad G_E^n(0)=\frac{\langle r_E^2\rangle q^2/6}{1-4.6\frac{q^2}{4M^2}}\,,\langle r_E^2\rangle=-0.1161\,\mathrm{fm}^2\,, \tag{3.186}$$

$$G_M^p(0)=\mu_p=2.793\,,\quad G_M^n(0)=\mu_n=-1.913\,, \tag{3.187}$$

$$M=(939.57+938.27)/2\,\mathrm{MeV}\,,\quad m_\pi=139.57\,\mathrm{MeV}\,, \tag{3.188}$$

$$\Lambda_A^2=1\,\mathrm{GeV}^2\,,\quad \Lambda^2=0.71\,\mathrm{GeV}^2\,,\quad g_A=-1.27\,, \tag{3.189}$$

where the parameters are taken from Ref. [152].

We plot the ratio $\frac{d\sigma}{dQ^2}/\frac{d\sigma_{\rm LO}}{dQ^2}$ between radiative corrected differential cross section over leading order differential cross section in Fig. 3.19, where the leading order cross section is the tree level cross section with hadronic model Eq. (3.179). The ratio of electron jet differential cross section over muon observable differential cross section is shown in Fig. 3.20. The tree level ratio of electron-flavor process over muon-flavor process also varies with momentum transfer Q^2, which is shown in Fig. 3.20 as a solid line for comparison with the radiative corrected results, the bands. Neutrino energy is taken at $E_\nu = 2$ GeV, cone size $\theta = 10^\circ$ and soft energy threshold $\Delta E = 20$ MeV.

We compute the integrated cross sections from these differential cross sections, still for the cone size $\theta = 10^\circ$ and soft energy threshold $\Delta E = 20$ MeV but for a few different energies $E_\nu = 0.6$, 1, 2 GeV, tabulated in Table 3.3.

We also compute the integrated cross sections from the differential cross sections in the heavy nucleon limit, with tree level cross section taken from Eq. (3.32) and all lepton mass power corrections in the endpoints $Q^2_{\rm min}$, $Q^2_{\rm max}$ retained. The results are listed in Table 3.4. We find that the lepton mass power correction m^2/E_ν^2 at tree level can be as large as percent level for small neutrino energy. However, if we subtract the tree level ratio from the radiative corrected ratio, the pure radiative correction

agrees with that in Table 3.2, which has a tree level ratio identical to 1. The difference between Table 3.4 and Table 3.2 represents the lepton mass power correction effects.

3.13 Conclusion

We have applied factorization theorem and soft-collinear effective field theory to investigate the radiative correction to the neutrino nucleon elastic charged current scattering. The soft function and jet function do not depend on hadronic physics, but are flavor dependent via different charged leptons' masses. For a jet observable, the hard function relies on hadronic physics but will be canceled when we consider the ratio of electron and muon neutrino charged current elastic scattering cross sections since it is flavor-independent.

To determine the neutrino oscillation signal in the long baseline experiments, the ratio between electron and muon flavor neutrinos interaction cross sections in the detector is needed. For jet-like observables, it could be computed perturbatively, insensitive to hadronic physics. For jet-like observables, e-flavor observable contains double logarithm $\log(E_\nu/\Delta E)\log\theta$ and does not suffer lepton mass logarithm, while μ-flavor observable exhibits lepton mass logarithm $\log(E_\nu/m)\log(E_\nu/\Delta E)$. In the heavy nucleon limit, the ratio of electron and muon jet observables is about 0.99 to 1 for incoming neutrino energy range from 0.5 GeV to 1 GeV. For physical tree level processes, the radiative corrected jet observable differential cross sections ratio has been computed and the integrated cross section ratio is about 1.01 to 1.02 for incoming neutrino energy range from 0.6 GeV to 2 GeV. The ratio being close to 1 is the accidental cancellation between e-flavor and μ-flavor different double logarithms with similar numerical values. For an inclusive observable, radiative correction contributes equally to electron and muon flavor processes in the heavy nucleon limit, causing no effect except lepton mass power corrections.

Appendix A Feynman Rules for HWET

We list relevant Feynman rules of heavy wimp effective theory Eq. (2.1) after electroweak symmetry breaking.

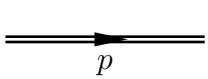

$$= \frac{i}{p \cdot v - \delta m + i0}$$

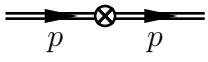

$$= \frac{-i}{2M} \frac{p^2 - (p \cdot v)^2}{(p \cdot v - \delta m + i0)^2}$$

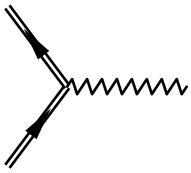

$$= i \frac{g_2}{\sqrt{2}} \tilde{T}^\pm v_\mu$$

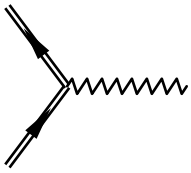

$$= i \frac{g_2}{\cos\theta_W} \left(\tilde{T}^3 - Q \sin^2\theta_W \right) v_\mu$$

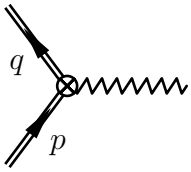

$$= \frac{i}{2M} \frac{g_2}{\sqrt{2}} \tilde{T}^\pm \left[(p_\mu + q_\mu) - v \cdot (p+q) v_\mu \right]$$

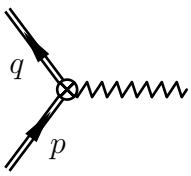

$$= \frac{i}{2M} \frac{g_2}{\cos\theta_W} \left(\tilde{T}^3 - Q \sin^2\theta_W \right) \left[(p_\mu + q_\mu) - v \cdot (p+q) v_\mu \right]$$

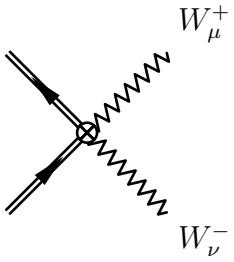

$$= \frac{ig_2^2}{2M}\frac{1}{2}\left(\tilde{T}^+\tilde{T}^- + \tilde{T}^-\tilde{T}^+\right)(g_{\mu\nu} - v_\mu v_\nu)$$

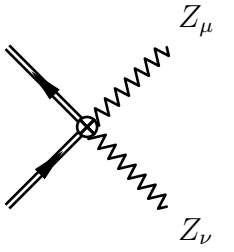

$$= \frac{ig_2^2}{2M}\frac{1}{\cos^2\theta_W}\left(\tilde{T}^3 - Q\sin^2\theta_W\right)^2(g_{\mu\nu} - v_\mu v_\nu)$$

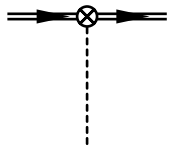

$$= i\tfrac{v}{M}\tilde{c}_H$$

Appendix B QCD β-function and Quark Mass Anomalous Dimension

The n_f-flavor QCD theory has a β-function expansion in α_s series as follows, c.f. Ref. [73],

$$\frac{\beta}{g} = \frac{d\log g}{d\log\mu} = -\sum_{n=0}^{\infty}\beta_n\left(\frac{\alpha_s}{4\pi}\right)^{n+1}\,, \tag{B.1}$$

where

$$\begin{aligned}
\beta_0 &= 11 - \frac{2}{3}n_f\,,\\
\beta_1 &= 102 - \frac{38}{3}n_f\,,\\
\beta_2 &= \frac{2857}{2} - \frac{5033}{18}n_f + \frac{325}{54}n_f^2\,,\\
\beta_3 &= \frac{149753}{6} + 3564\,\zeta(3) - \left(\frac{1078361}{162} + \frac{6508}{27}\,\zeta(3)\right)n_f\\
&\quad + \left(\frac{50065}{162} + \frac{6472}{81}\,\zeta(3)\right)n_f^2 + \frac{1093}{729}n_f^3\,.
\end{aligned} \tag{B.2}$$

The quark mass anomalous dimension is expanded as, c.f. Ref. [73],

$$\gamma_m = \frac{d\log m_q}{d\log\mu} = -\sum_{n=0}^{\infty}\gamma_n^m\left(\frac{\alpha_s}{4\pi}\right)^{n+1}\,, \tag{B.3}$$

where

$$\begin{aligned}
\gamma_0^m &= 8\,,\\
\gamma_1^m &= \frac{404}{3} - \frac{40}{9}n_f\,,\\
\gamma_2^m &= 2498 - \left(\frac{4432}{27} + \frac{320}{3}\,\zeta(3)\right)n_f - \frac{280}{81}n_f^2\,,\\
\gamma_3^m &= \frac{4603055}{81} + \frac{271360}{27}\,\zeta(3) - 17600\,\zeta(5) + \Bigg(-\frac{183446}{27} - \frac{68384}{9}\,\zeta(3) + 1760\,\zeta(4)\\
&\quad + \frac{36800}{9}\,\zeta(5)\Bigg)n_f + \left(\frac{10484}{243} + \frac{1600}{9}\,\zeta(3) - \frac{320}{3}\,\zeta(4)\right)n_f^2\\
&\quad + \left(-\frac{664}{243} + \frac{128}{27}\,\zeta(3)\right)n_f^3\,.
\end{aligned} \tag{B.4}$$

Appendix C Field Strength Renormalization in SCET

Figure C.1: QED self-energy diagram for a massive fermion.

For a relativistic QED massive fermion, the one-loop self-energy diagram Fig. C.1 yields

$$\begin{aligned} -i\Sigma_2(p) &= (-ie)^2 \int \frac{d^dL}{(2\pi)^d} \frac{\gamma^\mu(\not{p}+\not{L}+m)\gamma_\mu}{[(p+L)^2-m^2+i0]\,(L^2-\lambda^2+i0)} \\ &= -e^2 \int_0^1 dx \int \frac{d^dl}{(2\pi)^d} \frac{\gamma^\mu \not{l} \gamma_\mu + (1-x)(2-d)\not{p} + md}{(l^2-\Delta)^2}\,, \end{aligned} \tag{C.1}$$

where $\Delta = (x^2-x)p^2 + xm^2 + (1-x)\lambda^2$ and $d = 4-2\epsilon$.

$$\begin{aligned} \left.\frac{d\Sigma_2(p)}{d\not{p}}\right|_{\not{p}=m} &= -ie^2 \int_0^1 dx \int \frac{d^dl}{(2\pi)^d} \left[\frac{(1-x)(2-d)}{(l^2-\Delta)^2} \right. \\ &\left. -4m^2 \frac{[(1-x)(2-d)+d]}{(l^2-\Delta)^3}(x^2-x) \right] \Bigg|_{\not{p}=m} \\ &= \frac{\alpha}{4\pi} \left[\left(-\frac{1}{\epsilon} - 2 + \log\frac{m^2}{\mu^2} \right) - 2\left(1 + \log\frac{\lambda^2}{m^2} \right) \right] \\ &= \frac{\alpha}{4\pi} \left[-\frac{1}{\epsilon} - 4 + 2\log\frac{m^2}{\lambda^2} + \log\frac{m^2}{\mu^2} \right], \end{aligned} \tag{C.2}$$

where we have used the bare coupling and renormalized $\overline{MS}$ coupling relation

$$\frac{e_{bare}^2}{4\pi}(4\pi)^\epsilon e^{-\gamma_E \epsilon} = \alpha_{bare} = \mu^{2\epsilon}\alpha \left[1 + \sum_{n=0}^{\infty} \left(\frac{\alpha}{4\pi} \right)^{n+1} \right]. \tag{C.3}$$

Therefore, the field strength renormalization for a relativistic QED particle is

$$Z_l = 1 + \frac{\alpha}{4\pi} \left(-\frac{1}{\epsilon} + 2\log\frac{m^2}{\lambda^2} + \log\frac{m^2}{\mu^2} - 4 \right). \tag{C.4}$$

For a heavy non-relativistic QED (NRQED) particle, the one-loop self-energy diagram Fig. C.2 yields

$$-i\Sigma_2(p) = -e^2 \int \frac{d^dL}{(2\pi)^d} \frac{\gamma^\mu(\not{v}+1)\gamma_\mu}{[M(v^2-1)+2v\cdot L+i0]\,(L^2-\lambda^2+i0)}$$

Figure C.2: QED self-energy diagram for a heavy particle.

$$= -e^2 \int_0^\infty ds \int \frac{d^d L}{(2\pi)^d} \frac{\gamma^\mu (\not{p} + 1)\gamma_\mu}{(l^2 - \Delta)^2}\,, \tag{C.5}$$

where $p = Mv$ and $\Delta = v^2 s^2 + sM(1 - v^2) + \lambda^2$.

$$\begin{aligned}
\left.\frac{d\Sigma_2(p)}{Md\not{p}}\right|_{\not{p}=1} &= -i\frac{e^2}{M}\int_0^\infty ds \int \frac{d^d l}{(2\pi)^d}\left[\frac{2-d}{(l^2-\Delta)^2} + \frac{8(s^2 - sM)}{(l^3 - \Delta)^3}\right]\Bigg|_{\not{p}=1} \\
&= \frac{e^2}{(4\pi)^{2-\epsilon}} 4\Gamma(1+\epsilon)\int_0^\infty ds \frac{s}{(s^2+\lambda^2)^{1+\epsilon}} \\
&= \frac{\alpha}{4\pi}\left(\frac{2}{\epsilon} + 2\log\frac{\mu^2}{\lambda^2}\right)\,.
\end{aligned} \tag{C.6}$$

Therefore, the field strength renormalization for a heavy NRQED particle is

$$Z_h = 1 + \frac{\alpha}{4\pi}\left(\frac{2}{\epsilon} + 2\log\frac{\mu^2}{\lambda^2}\right)\,. \tag{C.7}$$

For the soft function calculation in the SCET, we treat the fermion heavy and the field strength renormalization for it is the same as NRQED result

$$Z_l^s = Z_p^s = 1 + \frac{\alpha}{4\pi}\left(\frac{2}{\epsilon} + 2\log\frac{\mu^2}{\lambda^2}\right)\,. \tag{C.8}$$

Figure C.3: QED self-energy diagram for a collinear fermion.

For a collinear fermion in the SCET, we have the one-loop self-energy diagram

$$-i\Sigma_2(p) = \int \frac{d^d L}{(2\pi)^d} i(-e)\left[n_\mu + \gamma_\mu^\perp \frac{\not{L}_\perp + \not{p}_\perp + m}{\bar{n}\cdot(L+p)} + \frac{\not{p}_\perp - m}{\bar{n}\cdot p}\gamma_\mu^\perp\right.$$

$$+\frac{(\not{p}_\perp - m)(\not{L}_\perp + \not{p}_\perp + m)}{\bar{n}\cdot(L+p)\bar{n}\cdot p}\bar{n}_\mu\Bigg]\frac{\not{\bar{n}}}{2}\frac{-i}{L^2-\lambda^2+i0}i\frac{\not{n}}{2}\frac{\bar{n}\cdot(L+p)}{(L+p)^2-m^2+i0}$$
$$\cdot i(-e)\left[n^\mu+\gamma^{\mu\perp}\frac{\not{p}_\perp+m}{\bar{n}\cdot p}+\frac{\not{L}_\perp+\not{p}_\perp-m}{\bar{n}\cdot(L+p)}\gamma^{\mu\perp}+\frac{(\not{L}_\perp+\not{p}_\perp-m)(\not{p}_\perp+m)}{\bar{n}\cdot(L+p)\bar{n}\cdot p}\bar{n}^\mu\right]$$
$$\cdot\frac{\not{\bar{n}}}{2}$$
$$=-e^2\frac{\not{\bar{n}}}{2}\Bigg\{(d-2)\frac{L^2-(n\cdot L)(\bar{n}\cdot L)-m^2}{(L^2-m^2)(L-p)^2(\bar{n}\cdot L)}+(d-2)\frac{p^2-(n\cdot p)(\bar{n}\cdot p)-m^2}{(L^2-m^2)(L-p)^2(\bar{n}\cdot p)^2}$$
$$\cdot\bar{n}\cdot L+\frac{(4-2d)\left[L\cdot p-\frac{1}{2}(n\cdot p)(\bar{n}\cdot L)-\frac{1}{2}(n\cdot L)(\bar{n}\cdot p)\right]+2dm^2}{(L^2-m^2)(L-p)^2(\bar{n}\cdot p)}\Bigg\} \tag{C.9}$$

The definition of field strength renormalization factor Z_2 is

$$\frac{i}{\frac{\not{\bar{n}}}{2}\frac{p^2-m^2}{\bar{n}\cdot p}-\Sigma_2(p)}=\frac{iZ_2}{\frac{\not{\bar{n}}}{2}\frac{p^2-m^2}{\bar{n}\cdot p}}\,, \tag{C.10}$$

and

$$Z_2=\left[1-\frac{\not{n}}{2}\frac{\bar{n}\cdot p}{p^2-m^2}\Sigma_2(p)\right]^{-1} \tag{C.11}$$

$$\left.\frac{d\left(\bar{n}\cdot p\Sigma_2(p)\right)}{dp^2}\right|_{p^2=m^2}=-\frac{\not{\bar{n}}}{2}\frac{e^2}{(4\pi)^{2-\epsilon}}\Gamma(\epsilon)\Bigg[-(d-2)(n\cdot p)(\bar{n}\cdot p)I_2+(d-2)\big[I_1$$
$$-(n\cdot p)(\bar{n}\cdot p)I_2\big]+(4-2d)I_1+(4-2d)\left[m^2-(n\cdot p)(\bar{n}\cdot p)\right]I_2+2dm^2I_3\Bigg]$$
$$=-\frac{\not{\bar{n}}}{2}\frac{\alpha}{4\pi}\left(\frac{3}{\epsilon}+4+6\log\frac{\mu}{m}\right)\,, \tag{C.12}$$

where

$$I_1=\int_0^1 dx x(1-x)^{-2\epsilon}m^{-2\epsilon}=m^{-2\epsilon}\left(\frac{1}{2}+\frac{3}{2}\epsilon\right)\,, \tag{C.13}$$
$$I_2=\int_0^1 dx(-\epsilon)x(x^2-x)\left[(1-x)^2m^2\right]^{-1-\epsilon}=-m^{-2\epsilon-2}\left(\frac{1}{2}+\frac{3}{2}\epsilon\right)\,, \tag{C.14}$$
$$I_3=\int_0^1 dx(-\epsilon)(x^2-x)\left[(1-x)^2m^2\right]^{-1-\epsilon}=-m^{-2\epsilon-2}\left(\frac{1}{2}+\epsilon\right)\,. \tag{C.15}$$

At one-loop order, the collinear field strength renormalization factor is

$$Z_l^c=1-\frac{\alpha}{4\pi}\left(\frac{3}{\epsilon}+4+6\log\frac{\mu}{m}\right)\,, \tag{C.16}$$

where we appplied $\bar{\xi}_n\not{n}\not{\bar{n}}\xi_n/4=\bar{\xi}_n\xi_n$ for a collinear field ξ_n.

Appendix D Phase Space Integration

D.1 Tree Level Phase Space Integration

The tree level process is

$$\begin{aligned}\nu_l(k) + n(p) &\to l^-(k') + p(p')\,,\\ \bar{\nu}_l(k) + p(p) &\to l^+(k') + n(p')\,.\end{aligned} \tag{D.1}$$

The phase space of 2-to-2 process is

$$\int d\Pi = \int \frac{d^3\mathbf{p}'}{(2\pi)^3 2E_{p'}} \int \frac{d^3\mathbf{k}'}{(2\pi)^3 2E_{k'}} (2\pi)^4 \delta^{(4)}(p' + k' - p - k)\,. \tag{D.2}$$

We define the momentum transfer $q = p' - p$, in the laboratory frame for fixed nucleon target, $dp' = dq$, $E_{p'} = M - \frac{q^2}{2M}$, $q^0 = -\frac{q^2}{2M}$ and we have

$$\begin{aligned}\int d\Pi &= \int \frac{d^3\mathbf{q}}{(2\pi)^3 2E_{p'}} \int \frac{d^3\mathbf{k}'}{(2\pi)^3 2E_{k'}} (2\pi)^4 \delta(E_\nu - E_{k'} + \frac{q^2}{2M}) \delta^{(3)}(\mathbf{k}' + \mathbf{q} - \mathbf{k})\\ &= \int \frac{d^3\mathbf{q}}{(2\pi)^3 2E_{p'}} \frac{2\pi}{2E_{k'}} \delta(E_\nu - E_{k'} + \frac{q^2}{2M})\\ &= \int \frac{|\mathbf{q}|^2 d|\mathbf{q}| d\cos\alpha \delta\left(E_\nu - \sqrt{E_\nu^2 - 2E_\nu|\mathbf{q}|\cos\alpha + |\mathbf{q}|^2 + m_l^2} + \frac{q^2}{2M}\right)}{2\pi \cdot 2\left(E_\nu + \frac{q^2}{2M}\right) \cdot 2\left(M - \frac{q^2}{2M}\right)}\\ &= \int \frac{|\mathbf{q}| d|\mathbf{q}|}{8\pi E_\nu \left(M - \frac{q^2}{2M}\right)}\\ &= \int \frac{d|q^2|}{16\pi E_\nu M}\,,\end{aligned} \tag{D.3}$$

where α is the angle between vector $\mathbf{q}$ and $\mathbf{k}'$, and m_l is the final lepton mass.

D.2 Collinear Phase Space Integration

We define momentum of each particle as

$$\nu(p_\nu) + n(p_n) \to p(P) + e(p) + \gamma(k) \tag{D.4}$$

The three-final-states phase space is defined as

$$\begin{aligned}\int d\Pi \;=\; &\int \frac{d^3\mathbf{P}}{(2\pi)^3 2E_P} \int \frac{d^3\mathbf{k}}{(2\pi)^3 2E_k} \int \frac{d^3\mathbf{p}}{(2\pi)^3 2E_p} (2\pi)^4 \delta(E_P + E_p + E_k - E_\nu - E_n)\\ &\delta^{(3)}(\mathbf{P} + \mathbf{p} + \mathbf{k} - \mathbf{p}_\nu - \mathbf{p_n})\end{aligned} \tag{D.5}$$

In the collinear limit, call the sum of electron and photon momenta p', and introduce a splitting ratio z so that

$$p' \equiv p + k \tag{D.6}$$

where

$$|\mathbf{p}| \simeq (1-z)E_{p'} \tag{D.7}$$
$$|\mathbf{k}| \simeq zE_{p'} \tag{D.8}$$

up to order $O(m/E_{p'})$ corrections.

Then the phase space of electron contains (choosing the direction of $\mathbf{p}$ to be the $\hat{z}$-axis in the spherical coordinate)

$$\begin{aligned} d^3\mathbf{p} &= |\mathbf{p}|^2 d|\mathbf{p}| d\Omega \\ &= (1-z)^2|\mathbf{p}'|^2 d\Big[(1-z)|\mathbf{p}'|\Big] d\Omega \\ &= (1-z)^3|\mathbf{p}'|^2 d|\mathbf{p}'| d\Omega - (1-z)^2|\mathbf{p}'|^3 dz d\Omega \end{aligned} \tag{D.9}$$

The phase space of photon contains (photon has a relative angle θ to $\hat{z}$-axis, which causes a perpendicular momentum $\mathbf{k}_\perp$.)

$$\begin{aligned} d^3\mathbf{k} &= dk^{\hat{z}} d^2\mathbf{k}_\perp \\ &= d\Big(z|\mathbf{p}'|\Big) d^2\mathbf{k}_\perp \\ &= z d|\mathbf{p}'| d^2\mathbf{k}_\perp + |\mathbf{p}'| dz d^2\mathbf{k}_\perp \end{aligned} \tag{D.10}$$

where $d^2\mathbf{k}_\perp = E_k^2 d\cos\theta d\phi$ is the area element of a small disk perpendicular to $\hat{z}$-axis.

Then we combine the phase space of electron and photon Eq.(D.9) and Eq.(D.10) (considering wedge product property $dx_i \wedge dx_j = -dx_j \wedge dx_i$)

$$\begin{aligned} \frac{d^3\mathbf{p} d^3\mathbf{k}}{2E_p 2E_k} &= \frac{\Big[(1-z)^3 + z(1-z)^2\Big]|\mathbf{p}'|^3 d|\mathbf{p}'| d\Omega dz d^2\mathbf{k}_\perp}{2E_p 2E_k} \\ &= \frac{\Big[(1-z)^3 + z(1-z)^2\Big]|\mathbf{p}'|^3 E_k^2 d|\mathbf{p}'| d\Omega dz d\cos\theta d\phi}{2E_p 2E_k} \\ &= \left[\frac{|\mathbf{p}'|^2}{2E_{p'}} d|\mathbf{p}'| d\Omega\right] E_{p'}^2 z(1-z) dz d\cos\theta \cdot \pi \\ &= \frac{d^3\mathbf{p}'}{2E_{p'}} E_{p'}^2 z(1-z) dz d\cos\theta \cdot \pi \end{aligned} \tag{D.11}$$

$$\tag{D.12}$$

The original phase space Eq.(D.5) becomes

$$\begin{aligned} \int d\Pi &= \int \frac{d^3\mathbf{P}}{(2\pi)^3 2E_P} \frac{d^3\mathbf{p}'}{2E_{p'}(2\pi)^6} E_{p'}^2 z(1-z) dz d\cos\theta \cdot \pi \cdot (2\pi)^4 \delta(E_P + E'_p - E_\nu - E_n) \\ &\quad \delta^{(3)}(\mathbf{P} + \mathbf{p}' - \mathbf{p}_\nu - \mathbf{p_n}) \end{aligned}$$

$$= \left[\int \frac{d^3\mathbf{P}}{(2\pi)^3 2E_P} \int \frac{d^3\mathbf{p}'}{(2\pi)^3 2E_{p'}} (2\pi)^4 \delta(E_P + E'_p - E_\nu - E_n) \delta^{(3)}(\mathbf{P} + \mathbf{p}' - \mathbf{p}_\nu - \mathbf{p_n}) \right]$$
$$\cdot \int \frac{\pi z(1-z) E_{p'}^2 dz d\cos\theta}{(2\pi)^3} \tag{D.13}$$

where we recognize the phase space in the bracket [...] is exactly the 2-to-2 phase space.

Bibliography

[1] G. Bertone, D. Hooper, and J. Silk, Phys. Rept. **405**, 279 (2005), arXiv:hep-ph/0404175 .

[2] M. C. Gonzalez-Garcia and Y. Nir, Rev. Mod. Phys. **75**, 345 (2003), arXiv:hep-ph/0202058 .

[3] P. A. Zyla *et al.* (Particle Data Group), PTEP **2020**, 083C01 (2020).

[4] W. E. Caswell and G. P. Lepage, Phys. Lett. B **167**, 437 (1986).

[5] N. Isgur and M. B. Wise, Phys. Lett. B **232**, 113 (1989).

[6] E. Eichten and B. R. Hill, Phys. Lett. B **234**, 511 (1990).

[7] H. Georgi, Phys. Lett. B **240**, 447 (1990).

[8] C. W. Bauer, S. Fleming, and M. E. Luke, Phys. Rev. D **63**, 014006 (2000), arXiv:hep-ph/0005275 .

[9] C. W. Bauer, S. Fleming, D. Pirjol, and I. W. Stewart, Phys. Rev. D **63**, 114020 (2001), arXiv:hep-ph/0011336 .

[10] C. W. Bauer and I. W. Stewart, Phys. Lett. B **516**, 134 (2001), arXiv:hep-ph/0107001 .

[11] C. W. Bauer, D. Pirjol, and I. W. Stewart, Phys. Rev. D **65**, 054022 (2002), arXiv:hep-ph/0109045 .

[12] C. W. Bauer, S. Fleming, D. Pirjol, I. Z. Rothstein, and I. W. Stewart, Phys. Rev. D **66**, 014017 (2002), arXiv:hep-ph/0202088 .

[13] M. Beneke, A. P. Chapovsky, M. Diehl, and T. Feldmann, Nucl. Phys. B **643**, 431 (2002), arXiv:hep-ph/0206152 .

[14] T. Becher, R. J. Hill, and M. Neubert, Phys. Rev. D **69**, 054017 (2004), arXiv:hep-ph/0308122 .

[15] T. Becher, R. J. Hill, and M. Neubert, Phys. Rev. D **72**, 094017 (2005), arXiv:hep-ph/0503263 .

[16] T. Becher, M. Neubert, and G. Xu, JHEP **07**, 030 (2008), arXiv:0710.0680 [hep-ph] .

[17] T. Becher and M. Neubert, Eur. Phys. J. C **71**, 1665 (2011), arXiv:1007.4005 [hep-ph] .

[18] I. W. Stewart, F. J. Tackmann, and W. J. Waalewijn, Phys. Rev. D **81**, 094035 (2010), arXiv:0910.0467 [hep-ph] .

[19] J.-y. Chiu, F. Golf, R. Kelley, and A. V. Manohar, Phys. Rev. Lett. **100**, 021802 (2008), arXiv:0709.2377 [hep-ph] .

[20] A. Fuhrer, A. V. Manohar, and W. J. Waalewijn, Phys. Rev. D **84**, 013007 (2011), arXiv:1011.1505 [hep-ph] .

[21] M. Bauer, T. Cohen, R. J. Hill, and M. P. Solon, JHEP **01**, 099 (2015), arXiv:1409.7392 [hep-ph] .

[22] R. K. Ellis, H. Georgi, M. Machacek, H. D. Politzer, and G. G. Ross, Nucl. Phys. B **152**, 285 (1979).

[23] S. B. Libby and G. F. Sterman, Phys. Rev. D **18**, 3252 (1978).

[24] A. H. Mueller, Phys. Rept. **73**, 237 (1981).

[25] J. C. Collins and D. E. Soper, Nucl. Phys. B **193**, 381 (1981), [Erratum: Nucl.Phys.B 213, 545 (1983)].

[26] J. C. Collins, D. E. Soper, and G. F. Sterman, Phys. Lett. B **109**, 388 (1982).

[27] J. C. Collins, D. E. Soper, and G. F. Sterman, Nucl. Phys. B **261**, 104 (1985).

[28] J. C. Collins, D. E. Soper, and G. F. Sterman, Adv. Ser. Direct. High Energy Phys. **5**, 1 (1989), arXiv:hep-ph/0409313 .

[29] F. Zwicky, Helvetica Physica Acta **6**, 110 (1933).

[30] V. C. Rubin, D. Burstein, W. K. Ford, Jr., and N. Thonnard, Astrophys. J. **289**, 81 (1985).

[31] J. A. Tyson, G. P. Kochanski, and I. P. Dell'Antonio, Astrophys. J. Lett. **498**, L107 (1998), arXiv:astro-ph/9801193 .

[32] N. Inada *et al.* (SDSS), Nature **426**, 810 (2003), arXiv:astro-ph/0312427 .

[33] M. J. Jee *et al.*, Astrophys. J. **661**, 728 (2007), arXiv:0705.2171 [astro-ph] .

[34] D. Clowe, M. Bradac, A. H. Gonzalez, M. Markevitch, S. W. Randall, C. Jones, and D. Zaritsky, Astrophys. J. Lett. **648**, L109 (2006), arXiv:astro-ph/0608407 .

[35] M. Milgrom, Astrophys. J. **270**, 384 (1983).

[36] N. Aghanim *et al.* (Planck), Astron. Astrophys. **641**, A6 (2020), arXiv:1807.06209 [astro-ph.CO] .

[37] J. L. Feng, Ann. Rev. Astron. Astrophys. **48**, 495 (2010), arXiv:1003.0904 [astro-ph.CO] .

[38] T. Lin, PoS **333**, 009 (2019), arXiv:1904.07915 [hep-ph] .

[39] S. Profumo, L. Giani, and O. F. Piattella, Universe **5**, 213 (2019), arXiv:1910.05610 [hep-ph] .

[40] B. W. Lee and S. Weinberg, Phys. Rev. Lett. **39**, 165 (1977).

[41] J. E. Gunn, B. W. Lee, I. Lerche, D. N. Schramm, and G. Steigman, Astrophys. J. **223**, 1015 (1978).

[42] G. Steigman, C. L. Sarazin, H. Quintana, and J. Faulkner, Astron. J. **83**, 1050 (1978).

[43] J. R. Ellis, J. S. Hagelin, D. V. Nanopoulos, K. A. Olive, and M. Srednicki, *Particle physics and cosmology: Dark matter*, Nucl. Phys. **B238**, 453 (1984).

[44] M. W. Goodman and E. Witten, Phys. Rev. **D31**, 3059 (1985).

[45] H. Goldberg, Phys. Rev. Lett. **50**, 1419 (1983).

[46] J. Bramante, N. Desai, P. Fox, A. Martin, B. Ostdiek, and T. Plehn, Phys. Rev. **D93**, 063525 (2016), arXiv:1510.03460 [hep-ph] .

[47] G. Arcadi, M. Dutra, P. Ghosh, M. Lindner, Y. Mambrini, M. Pierre, S. Profumo, and F. S. Queiroz, Eur. Phys. J. **C78**, 203 (2018), arXiv:1703.07364 [hep-ph] .

[48] L. Roszkowski, E. M. Sessolo, and S. Trojanowski, Rept. Prog. Phys. **81**, 066201 (2018), arXiv:1707.06277 [hep-ph] .

[49] G. Jungman, M. Kamionkowski, and K. Griest, Phys. Rept. **267**, 195 (1996), arXiv:hep-ph/9506380 [hep-ph] .

[50] D. Abercrombie *et al.*, Phys. Dark Univ. **27**, 100371 (2020), arXiv:1507.00966 [hep-ex] .

[51] L. Oakes *et al.* (Fermi-LAT, HAWC, H.E.S.S., MAGIC, VERITAS), PoS **ICRC2019**, 012 (2021), arXiv:1909.06310 [astro-ph.HE] .

[52] R. Abbasi *et al.* (IceCube), (2012), arXiv:1210.3557 [hep-ex] .

[53] S. Adrian-Martinez *et al.* (ANTARES), JCAP **11**, 032 (2013), arXiv:1302.6516 [astro-ph.HE] .

[54] T. Tanaka *et al.* (Super-Kamiokande), Astrophys. J. **742**, 78 (2011), arXiv:1108.3384 [astro-ph.HE] .

[55] M. N. Mazziotta, A. Cuoco, P. De La Torre Luque, F. Loparco, and D. Serini (Fermi-LAT), PoS **ICRC2019**, 531 (2020).

[56] E. Aprile *et al.* (XENON), JCAP **1604**, 027 (2016), arXiv:1512.07501 [physics.ins-det] .

[57] D. S. Akerib *et al.* (LZ), (2015), arXiv:1509.02910 [physics.ins-det] .

[58] P. A. Amaudruz *et al.* (DEAP-3600), Phys. Rev. Lett. **121**, 071801 (2018), arXiv:1707.08042 [astro-ph.CO] .

[59] X. Cui *et al.* (PandaX-II), Phys. Rev. Lett. **119**, 181302 (2017), arXiv:1708.06917 [astro-ph.CO] .

[60] R. Agnese *et al.* (SuperCDMS), Phys. Rev. Lett. **120**, 061802 (2018), arXiv:1708.08869 [hep-ex] .

[61] Q. Arnaud *et al.* (EDELWEISS), Phys. Rev. D **97**, 022003 (2018), arXiv:1707.04308 [physics.ins-det] .

[62] A. H. Abdelhameed *et al.* (CRESST), Phys. Rev. D **100**, 102002 (2019), arXiv:1904.00498 [astro-ph.CO] .

[63] R. Agnese *et al.* (SuperCDMS), Phys. Rev. Lett. **121**, 051301 (2018), [Erratum: Phys.Rev.Lett. 122, 069901 (2019)], arXiv:1804.10697 [hep-ex] .

[64] H. Jiang *et al.* (CDEX), Phys. Rev. Lett. **120**, 241301 (2018), arXiv:1802.09016 [hep-ex] .

[65] P. Agnes *et al.* (DarkSide), Phys. Rev. D **98**, 102006 (2018), arXiv:1802.07198 [astro-ph.CO] .

[66] M. Tanabashi *et al.* (Particle Data Group), Phys. Rev. **D98**, 030001 (2018).

[67] A. Canepa, T. Han, and X. Wang, Ann. Rev. Nucl. Part. Sci. **70**, 425 (2020), arXiv:2003.05450 [hep-ph] .

[68] *Searches for electroweak production of supersymmetric particles with compressed mass spectra in* $\sqrt{s} = 13$ *TeV pp collisions with the ATLAS detector*, Tech. Rep. ATLAS-CONF-2019-014 (CERN, Geneva, 2019).

[69] L. Longo (ATLAS Collaboration), *Searches for charginos and neutralinos in ATLAS*, Tech. Rep. ATL-PHYS-PROC-2019-077 (CERN, Geneva, 2019).

[70] M. Cirelli, N. Fornengo, and A. Strumia, Nucl. Phys. B **753**, 178 (2006), arXiv:hep-ph/0512090 .

[71] R. J. Hill and M. P. Solon, Phys. Lett. **B707**, 539 (2012), arXiv:1111.0016 [hep-ph] .

[72] R. J. Hill and M. P. Solon, Phys. Rev. **D91**, 043504 (2015), arXiv:1401.3339 [hep-ph] .

[73] R. J. Hill and M. P. Solon, Phys. Rev. **D91**, 043505 (2015), arXiv:1409.8290 [hep-ph] .

[74] Y. Fukuda *et al.* (Super-Kamiokande), Phys. Rev. Lett. **81**, 1562 (1998), arXiv:hep-ex/9807003 .

[75] Q. R. Ahmad *et al.* (SNO), Phys. Rev. Lett. **89**, 011301 (2002), arXiv:nucl-ex/0204008 .

[76] Z. Maki, M. Nakagawa, and S. Sakata, Prog. Theor. Phys. **28**, 870 (1962).

[77] B. Pontecorvo, Zh. Eksp. Teor. Fiz. **34**, 247 (1957).

[78] P. Adamson *et al.* (MINOS), Phys. Rev. Lett. **110**, 171801 (2013), arXiv:1301.4581 [hep-ex] .

[79] M. Antonello *et al.* (ICARUS), Eur. Phys. J. C **73**, 2599 (2013), arXiv:1307.4699 [hep-ex] .

[80] K. Abe *et al.* (T2K), Phys. Rev. Lett. **112**, 061802 (2014), arXiv:1311.4750 [hep-ex] .

[81] N. Agafonova *et al.* (OPERA), Phys. Rev. Lett. **120**, 211801 (2018), [Erratum: Phys.Rev.Lett. 121, 139901 (2018)], arXiv:1804.04912 [hep-ex] .

[82] P. Adamson *et al.* (NOvA), Phys. Rev. Lett. **116**, 151806 (2016), arXiv:1601.05022 [hep-ex] .

[83] K. Abe *et al.* (Hyper-Kamiokande Proto-), PTEP **2015**, 053C02 (2015), arXiv:1502.05199 [hep-ex] .

[84] B. Abi *et al.* (DUNE), (2018), arXiv:1807.10334 [physics.ins-det] .

[85] K. Eguchi *et al.* (KamLAND), Phys. Rev. Lett. **90**, 021802 (2003), arXiv:hep-ex/0212021 .

[86] F. P. An *et al.* (Daya Bay), Phys. Rev. Lett. **115**, 111802 (2015), arXiv:1505.03456 [hep-ex] .

[87] S.-B. Kim, Nucl. Part. Phys. Proc. **265-266**, 93 (2015), arXiv:1412.2199 [hep-ex] .

[88] Y. Abe *et al.* (Double Chooz), JHEP **01**, 163 (2016), arXiv:1510.08937 [hep-ex] .

[89] F. An *et al.* (JUNO), J. Phys. G **43**, 030401 (2016), arXiv:1507.05613 [physics.ins-det] .

[90] N. Cabibbo, Phys. Rev. Lett. **10**, 531 (1963).

[91] M. Kobayashi and T. Maskawa, Progress of Theoretical Physics **49**, 652 (1973), https://academic.oup.com/ptp/article-pdf/49/2/652/5257692/49-2-652.pdf .

[92] S. M. Bilenky, J. Hosek, and S. T. Petcov, Phys. Lett. B **94**, 495 (1980).

[93] M. Doi, T. Kotani, H. Nishiura, K. Okuda, and E. Takasugi, Phys. Lett. B **102**, 323 (1981).

[94] J. Schechter and J. W. F. Valle, Phys. Rev. D **23**, 1666 (1981).

[95] P. Langacker, S. T. Petcov, G. Steigman, and S. Toshev, Nucl. Phys. B **282**, 589 (1987).

[96] N. Okamura, Prog. Theor. Phys. **114**, 1045 (2006), arXiv:hep-ph/0411388 .

[97] H. Nunokawa, S. J. Parke, and R. Zukanovich Funchal, Phys. Rev. D **72**, 013009 (2005), arXiv:hep-ph/0503283 .

[98] K. Abe *et al.* (Super-Kamiokande), Phys. Rev. D **97**, 072001 (2018), arXiv:1710.09126 [hep-ex] .

[99] M. Freund, Phys. Rev. D **64**, 053003 (2001), arXiv:hep-ph/0103300 .

[100] E. P. Wigner, Annals Math. **40**, 149 (1939).

[101] J. Heinonen, R. J. Hill, and M. P. Solon, Phys. Rev. D **86**, 094020 (2012), arXiv:1208.0601 [hep-ph] .

[102] R. J. Hill and M. P. Solon, Phys. Rev. Lett. **112**, 211602 (2014), arXiv:1309.4092 [hep-ph] .

[103] J. Hisano, K. Ishiwata, N. Nagata, and T. Takesako, JHEP **07**, 005 (2011), arXiv:1104.0228 [hep-ph] .

[104] E. Aprile *et al.* (XENON), Phys. Rev. Lett. **121**, 111302 (2018), arXiv:1805.12562 [astro-ph.CO] .

[105] J. Liu, X. Chen, and X. Ji, Nature Phys. **13**, 212 (2017), arXiv:1709.00688 [astro-ph.CO] .

[106] J. Billard, L. Strigari, and E. Figueroa-Feliciano, Phys. Rev. **D89**, 023524 (2014), arXiv:1307.5458 [hep-ph] .

[107] C.-Y. Chen, R. J. Hill, M. P. Solon, and A. M. Wijangco, Phys. Lett. **B781**, 473 (2018), arXiv:1801.08551 [hep-ph] .

[108] M. Hoferichter, P. Klos, J. Menndez, and A. Schwenk, Phys. Rev. **D99**, 055031 (2019), arXiv:1812.05617 [hep-ph] .

[109] M. Hoferichter, P. Klos, J. Menndez, and A. Schwenk, Phys. Rev. **D94**, 063505 (2016), arXiv:1605.08043 [hep-ph] .

[110] N. Nagata and S. Shirai, JHEP **01**, 029 (2015), arXiv:1410.4549 [hep-ph] .

[111] R. Krall and M. Reece, Chin. Phys. **C42**, 043105 (2018), arXiv:1705.04843 [hep-ph] .

[112] A. Delgado, A. Martin, and M. Quirs, Phys. Rev. **D99**, 075015 (2019), arXiv:1812.08019 [hep-ph] .

[113] T. Cohen, J. Kearney, A. Pierce, and D. Tucker-Smith, Phys. Rev. **D85**, 075003 (2012), arXiv:1109.2604 [hep-ph] .

[114] W. Chao, G.-J. Ding, X.-G. He, and M. Ramsey-Musolf, JHEP **08**, 058 (2019), arXiv:1812.07829 [hep-ph] .

[115] A. Berlin, D. S. Robertson, M. P. Solon, and K. M. Zurek, Phys. Rev. **D93**, 095008 (2016), arXiv:1511.05964 [hep-ph] .

[116] J. Bramante, P. J. Fox, G. D. Kribs, and A. Martin, Phys. Rev. **D94**, 115026 (2016), arXiv:1608.02662 [hep-ph] .

[117] V. A. Novikov, M. A. Shifman, A. I. Vainshtein, and V. I. Zakharov, Fortsch. Phys. **32**, 585 (1984).

[118] R. J. Crewther, Phys. Rev. Lett. **28**, 1421 (1972).

[119] M. S. Chanowitz and J. R. Ellis, Phys. Lett. B **40**, 397 (1972).

[120] J. C. Collins, A. Duncan, and S. D. Joglekar, Phys. Rev. D **16**, 438 (1977).

[121] K. G. Chetyrkin, B. A. Kniehl, and M. Steinhauser, Nucl. Phys. B **510**, 61 (1998), arXiv:hep-ph/9708255 .

[122] S. Aoki *et al.* (Flavour Lattice Averaging Group), (2019), arXiv:1902.08191 [hep-lat] .

[123] S. Durr *et al.*, Phys. Rev. **D85**, 014509 (2012), [Erratum: Phys. Rev.D93,no.3,039905(2016)], arXiv:1109.4265 [hep-lat] .

[124] Y.-B. Yang, A. Alexandru, T. Draper, J. Liang, and K.-F. Liu (xQCD), Phys. Rev. **D94**, 054503 (2016), arXiv:1511.09089 [hep-lat] .

[125] S. Durr *et al.*, Phys. Rev. Lett. **116**, 172001 (2016), arXiv:1510.08013 [hep-lat] .

[126] W. Freeman and D. Toussaint (MILC), Phys. Rev. **D88**, 054503 (2013), arXiv:1204.3866 [hep-lat] .

[127] P. Junnarkar and A. Walker-Loud, Phys. Rev. **D87**, 114510 (2013), arXiv:1301.1114 [hep-lat] .

[128] M. Hoferichter, J. Ruiz de Elvira, B. Kubis, and U.-G. Meiner, Phys. Rev. Lett. **115**, 092301 (2015), arXiv:1506.04142 [hep-ph] .

[129] J. Ruiz de Elvira, M. Hoferichter, B. Kubis, and U.-G. Meiner, J. Phys. **G45**, 024001 (2018), arXiv:1706.01465 [hep-ph] .

[130] J. M. Alarcon, J. Martin Camalich, and J. A. Oller, Phys. Rev. **D85**, 051503 (2012), arXiv:1110.3797 [hep-ph] .

[131] J. Gasser and H. Leutwyler, Phys. Rept. **87**, 77 (1982).

[132] A. D. Martin, W. J. Stirling, R. S. Thorne, and G. Watt, Eur. Phys. J. **C63**, 189 (2009), arXiv:0901.0002 [hep-ph] .

[133] M. E. Peskin and D. V. Schroeder, *An Introduction to quantum field theory* (Addison-Wesley, Reading, USA, 1995).

[134] D. S. Akerib *et al.* (LUX), Phys. Rev. Lett. **118**, 021303 (2017), arXiv:1608.07648 [astro-ph.CO] .

[135] R. H. Helm, Phys. Rev. **104**, 1466 (1956).

[136] J. D. Lewin and P. F. Smith, Astropart. Phys. **6**, 87 (1996).

[137] J. Engel, Phys. Lett. B **264**, 114 (1991).

[138] V. Cirigliano, M. L. Graesser, and G. Ovanesyan, JHEP **10**, 025 (2012), arXiv:1205.2695 [hep-ph] .

[139] C. Krber, A. Nogga, and J. de Vries, Phys. Rev. **C96**, 035805 (2017), arXiv:1704.01150 [hep-ph] .

[140] J. Hisano, K. Ishiwata, and N. Nagata, JHEP **06**, 097 (2015), arXiv:1504.00915 [hep-ph] .

[141] M. Day and K. S. McFarland, Phys. Rev. D **86**, 053003 (2012), arXiv:1206.6745 [hep-ph] .

[142] F. Akbar, M. Rafi Alam, M. Sajjad Athar, S. Chauhan, S. K. Singh, and F. Zaidi, Int. J. Mod. Phys. E **24**, 1550079 (2015), arXiv:1506.02355 [nucl-th] .

[143] O. Tomalak, Q. Chen, R. J. Hill, and K. S. McFarland, (2021), arXiv:2105.07939 [hep-ph] .

[144] C. Llewellyn Smith, Phys. Rept. **3**, 261 (1972).

[145] T. Kinoshita, J. Math. Phys. **3**, 650 (1962).

[146] T. D. Lee and M. Nauenberg, Phys. Rev. **133**, B1549 (1964).

[147] G. F. Sterman and S. Weinberg, Phys. Rev. Lett. **39**, 1436 (1977).

[148] R. J. Hill and M. Neubert, Nucl. Phys. B **657**, 229 (2003), arXiv:hep-ph/0211018 .

[149] R. J. Hill, Phys. Rev. D **95**, 013001 (2017), arXiv:1605.02613 [hep-ph] .

[150] T. Becher and M. Neubert, JHEP **06**, 081 (2009), [Erratum: JHEP 11, 024 (2013)], arXiv:0903.1126 [hep-ph] .

[151] T. Becher and M. Neubert, Phys. Rev. Lett. **102**, 162001 (2009), [Erratum: Phys.Rev.Lett. 111, 199905 (2013)], arXiv:0901.0722 [hep-ph] .

[152] C. Andreopoulos, C. Barry, S. Dytman, H. Gallagher, T. Golan, R. Hatcher, G. Perdue, and J. Yarba, (2015), arXiv:1510.05494 [hep-ph] .

Vita

Qing Chen

Education

- 2015 - present, Ph.D. candidate of Physics, University of Kentucky
- 2011 - 2014, M.S. Astrophysics, University of Science and Technology of China
- 2007 - 2011, B.S. Physics, University of Science and Technology of China

Professional Positions

- 2020 Spring - present, Graduate Research Assistant and Teaching Assistant, University of Kentucky
- 2018 Fall - 2020 Fall, Graduate Research Assistant, University of Kentucky
- 2015 Fall - 2018 Spring, Graduate Teaching Assistant, University of Kentucky
- 2011 Fall - 2013 Spring, Graduate Teaching Assistant, University of Science and Technology of China

Publications

- [1] Oleksandr Tomalak, Qing Chen, Richard J. Hill, and Kevin S. McFarland, QED radiative corrections to neutrino-nucleon elastic scattering. arXiv: 2105.07939
- [2] Qing Chen and Richard J. Hill, Direct detection rate of heavy Higgsino-like and Wino-like dark matter, Phys. Lett. B 804 (2020) 135364,

  arXiv:1912.07795
- [3] Yang Zhang, Qing Chen and Shu-Guang Wu, Field theory of the correlation function of mass density fluctuations for self-gravitating systems, Res. Astron. Astrophys. 19 (2019) 4, 053
- [4]Yang Zhang and Qing Chen, Field equation of the correlation function of mass-density fluctuations for self-gravitating systems, Astron. Astrophys. 581 (2015) A53, arXiv:1408.5237